Universidad de Valladolid

eSDUVa
Escuela de Doctorado Universidad de Valladolid

PROGRAMA DE DOCTORADO EN
INVESTIGACION BIOMEDICA

TESIS DOCTORAL:

Use of Kv1.3 channel blockers for the prevention of restenosis in human vessels: Mechanisms and outcomes in diabetic patients

Presentada por Marycarmen Arévalo Martínez
para optar al grado de
Doctora por la Universidad de Valladolid

Dirigida por:
Dra. María Teresa Pérez García
Dra. Pilar Cidad Velasco

Financiación

Este trabajo ha sido realizado con los siguientes proyectos de investigación:

- **Los canales iónicos del músculo liso como dianas terapéuticas en el remodelado vascular (BFU2013-45867-R).**

Entidad financiadora: Ministerio de Economía y Competitividad (Programa Estatal I+D+i)

Duración: 2014 - 2016

Investigador Responsable: José Ramón López López, María Teresa Pérez García.

- **Los canales iónicos del músculo liso como marcadores, dianas y efectores en el remodelado vascular (BFU2016-75360-R).**

Entidad financiadora: Ministerio de Ciencia e Innovación

Duración: 2016 - 2020

Investigador Responsable: José Ramón López López, María Teresa Pérez García.

- **Nuevas terapias farmacológicas y génicas para la prevención y tratamiento de enfermedades vasculares oclusivas (VA114P17).**

Entidad financiadora: Junta de Castilla y León (JCyL), Consejería de Educación

Duración: 2017 - 2019

Investigador Responsable: María Teresa Pérez García.

Además, esta tesis se ha realizado con las siguientes ayudas económicas destinadas al contrato predoctoral, ayudas a estancias y cursos:

- **Contratos predoctorales UVa 2015**

Duración: 2016 - 2020.

Titulo proyecto: Canales de potasio Kv1.3 como dianas terapéuticas para prevenir la restenosis vascular.

- **MOVILIDAD DOCTORANDOS UVa 2017**

Movilidad de doctorandos, ayudas para estancias breves en el desarrollo de tesis doctorales. Convocatoria 2018.

Duración: Mayo 2018 – Julio 2018

Lugar: Lund University, Suecia.

- **ERASMUS +**

Prácticas en modalidad abierta convocatoria de fecha 3 de mayo de 2018

Duración: Mayo 2018 – Julio 2018

Lugar: Lund University, Suecia.

- **MOVILIDAD DE DOCTORANDOS UVa 2019**

Ayuda por la asistencia a cursos, congresos y jornadas relevantes en el desarrollo de tesis doctorales 2019.

Curso: workshop on surgical techniques in the laboratory mouse, Jackson Laboratories. (Beca Howard Hughes Medical Institute)

Duración: Junio 2019

Lugar: Sorbonne Université, Francia.

Divulgación científica

Publicación en revistas

Arévalo-Martínez M, Cidad P, García-Mateo N, Moreno-Estar S, Serna J, Fernández M, Swärd K, Simarro M, de la Fuente MA, López-López JR & Pérez-García MT (2019). Myocardin-Dependent Kv1.5 Channel Expression Prevents Phenotypic Modulation of Human Vessels in Organ Culture. Arterioscler Thromb Vasc Biol; DOI: 10.1161/ATVBAHA.119.313492.

Comunicación en Congresos

- **The Smooth Muscle Conference 2019 (FASEB)**

Kv1.5 downregulation triggers phenotypic modulation in human vessels. M. Teresa Pérez-García, **Marycarmen Arévalo-Martínez**, Sara Moreno-Estar, Esperanza Alonso, Julia Serna, Miguel A de la Fuente, Pilar Cidad and José R López-López. 2019, 14-19 julio, Florida (USA).

- **Reunión española de Canales Iónicos RECI VII**

Regulation of Kv1.3 to Kv1.5 ratio modulates vascular smooth muscle cell proliferation in human vessels. **Marycarmen Arévalo-Martínez**, Sara Moreno, Nadia García-Mateo, Miguel A de la Fuente, Beatriz Merino, Esperanza Alonso, Mireia Fernández, Pilar Cidad, José R López-López and M. Teresa Pérez-García. 2019, 15-17 mayo, Caceres (España). Participación con póster.

- **Europhysiology 2018, London, UK**

Kv1.3 channel blockers as therapeutical agents against intimal hyperplasia: New evidences in human arteries from diabetic patients. **Marycarmen Arévalo-Martínez,** Nadia García-Mateo, Miguel A de la Fuente, Esperanza Alonso, Mireia Fernández, José R López-López, M. Teresa Pérez-García and Pilar Cidad,2018, 14-16 septiembre, Londres (Reino Unido). Participación con póster.

- **Reunión española de Canales Iónicos. RECI VI**

Characterization of the effect of Kv1.3 channel blockers on vascular remodeling in human vessels. **Arévalo-Martínez M**., García-Mateo N., de la Fuente M.A., Alonso E., Fernández M., López-López J.R., Pérez-García M.T. and Cidad P**.,** 2017, 6-8 septiembre, Santiago de Compostela (España). Participación con poster.

- **12th International Symposium on Resistance Arteries (ISRA), Manchester UK,**

Characterization of an intimal hyperplasia model in mice with vascular risk factors **M. Arévalo-Martínez,** E. Alonso, I. Cózar, JR López-López, M. T. Pérez-García and P Cidad**,**2017, 3-6 Septiembre, Journal of Vascular Research 54 (Suppl2) p21, B20. Participación con póster, premio al mejor póster.

- **Experimental Biology Chicago 2017**

Kv1.3 and Kv1.5 Channels as Novel Targets for the Prevention of Restenosis in Human Vessels **M T Perez-Garcia , M Arevalo-Martinez, MA de la Fuente, M Simarro, E Alonso; JR Lopez-Lopez and Pilar Cidad,** 2017, 22-26 Abril, FASEB J 31(1) Supplement, pos1015.4. Participación con póster.

- **Smooth Muscle, FASEB Science Research Conferences,**

Characterization of the effect of Kv1.3 channel blockers on intimal hyperplasia in human vessel in organ culture, **M. Arévalo-Martínez, E. Alonso, JR López-López, MT Pérez-García and P. Cidad,** 2016, Julio 17-22, Lisboa, Portugal, Participación con póster.

Divulgación de la investigación

- 3MT-EsDUVa Octubre de 2016
- Actividad de difusión de la investigación del concurso 3MT en Centros de Enseñanza Secundaria de Valladolid. Marzo 2017
- Concurso Three-Minute Thesis 2017
- Concurso Three-Minute Thesis 2018
- Concurso Three-Minute Thesis 2019

Abstract

Vascular smooth muscle cells (VSMCs) can undergo phenotypic modulation (PM) to a dedifferentiated state, which contributes to angiogenesis and vessel repair. PM is triggered by vascular surgeries such as those directed to unclog obstructed vessels. However, an excessive VSMC migration and proliferation drives intimal hyperplasia (IH) leading to restenosis. This situation is even worse in patients with background diseases like type 2 diabetes mellitus (T2DM). T2DM patients have more aggressive forms of vascular disease and worse outcomes, with exacerbated restenosis after vascular surgery.

We have previously demonstrated that an increased functional expression of the potassium channel Kv1.3 contributes to PM in several models of VSMCs, as Kv1.3 blockers inhibit VSMCs migration and proliferation. In addition, we found that Kv1.3 increased activity upon PM is a consequence of Kv1.5 downregulation, so that the changes in Kv1.3 to Kv1.5 ratio can define VSMCs phenotype.

Objective: Here, we sought to explore the efficacy of Kv1.3 inhibition for the prevention of remodeling in human vessels and the mechanism linking the switch of Kv1.3/Kv1.5 ratio to PM. In addition, we investigated if the augmented remodeling observed in T2DM vessels is associated to an increased Kv1.3 activity, in order to determine if the use of Kv1.3 blockers could improve the outcomes of vascular surgery these vulnerable groups.

Approach: Vascular remodeling was explored in vessel rings in organ culture obtained from human mammary artery (hMA), human saphenous vein (hSV) and human renal artery (hRA) samples. Vessels were incubated for 2 weeks in organ culture. We studied the effects of Kv1.3 blockers (PAP-1, margatoxin), or Kv1.5 overexpression on IH development. In addition, primary VSMCs culture were used to explore the effects of these maneuvers on migration and proliferation.

An *in-vivo* model of vascular disease was developed by feeding hypertensive mice with high fact diet (BPH/HFD). These mice developed obesity, glucose intolerance, insulin resistance and hypertension. Carotid ligation was used to get an *in-vivo* model of IH in control (BPH) and diseased (BPH/HFD) vessels.

IH in both, human and mouse vessel samples was explored with hystomorphometric analysis of 7-μm sections stained with Masson trichrome. In addition, we studied gene and miRNA expression by qPCR and protein expression by western blot and immunohistochemistry.

Results: Kv1.3 blockade prevented IH induced by 20% FBS in our *in-vitro* intimal hyperplasia model by inhibiting proliferation, migration, and extracellular matrix secretion. The effects of Kv1.3 blockers were reproduced by Kv1.5 overexpression, being both effects non-additive.

Myocardin knock-down in human vessels in organ culture reduced Kv1.5 expression and induced IH, while Kv1.5 overexpression inhibited IH without affecting myocardin expression. Moreover, myocardin overexpression upregulated Kv1.5 expression in VSMCs.

When human samples were categorized as T2DM or non-T2DM, we found that T2DM vessels showed increased IH in organ culture. Also, T2DM VSMCs had higher rates of proliferation and migration than non-T2DM cells. We observed a higher expression of Kv1.3 in T2DM vessels, and consequently PAP-1 was more efficient preventing vascular remodeling in T2DM vessels. Differences in T2DM samples persisted in VSMCs cultures, suggesting a metabolic memory of those cells. We carried out a miRNA PCR array to explore the contribution of miRNAs to T2DM epigenetic signature in human VSMCs. We focused on miR-126, which was upregulated in T2DM VSMC in proliferative phenotype. miR-126 overexpression in non-T2DM increased migration and proliferation rate, but had no effect on T2DM VSMCs.

Finally, in our BPH/HFD animal model, we found increased expression of Kv1.3 in VSMCs and an increased vascular remodeling upon carotid ligation compared to control (BPH) mice. Treatment with PAP-1 prevented IH upon carotid ligation in both groups, and decreased obesity and improved insulin sensitivity in BPH/HFD.

Conclusions: Our data indicated that Kv1.5 channel is a myocardin-regulated gene in human VSMCs. Kv1.5 downregulation upon PM leaves Kv1.3 as the dominant Kv1 channel expressed, increasing Kv1.3 functional contribution to dedifferentiated phenotype. Kv1.3 channel blockade prevents vascular remodeling of human vessels in organ culture by inhibiting VSMCs proliferation, migration and extracellular matrix secretion, and Kv1.5 overexpression also inhibits vascular remodeling by occluding the K1.3 channel effects.

Kv1.3 blockade is more efficient in T2DM vessels reducing IH in organ culture than in those from non-T2DM patients, as T2DM vessels show higher expression of Kv1.3 channels and increased remodeling. Epigenetic changes in VSMC from T2DM associated to differences in miRNA profile.

Our data indicated that the increase of miR-126 in T2DM VSMCs cultures contributes to the metabolic memory of these cells.

BPH/HFD is an animal model that parallels the characteristics of T2DM human vessels: increased Kv1.3 channel expression and vascular remodeling. Kv1.3 blockers not only showed higher efficiency in the prevention of IH in diseased vessels compared to healthy vessels, but also ameliorate metabolic risk factors in the BPH/HFD model.

Abbreviations

AAV	Adeno-associated viral vectors
AUC	Area under the curve
BCL2	B cell lymphoma 2
BKCa	High conductance-KCa
BP	Blood pressure
BPH	Blood Pressure High
BPN	Blood Pressure Normal
CABG	Coronary artery bypass grafting
CNN1	Calponin
COLMAH	COLección de Muestras Arteriales Humanas
CRISPR	Clustered regularly interspaced short palindromic repits
C_T	Threshold cycle
DAB	3,3'-Diaminobenzidine
DAG	Diacylglycerol
DPO	Diphenyl-iodinium
ECM	Extracellular matrix
ECs	Endothelial cells
EdU	5-Ethynyl-2´-deoxyuridine
ELR	Elastin like recombinamer
eNOS	Endothelial nitric oxide synthase
ERK	Extracellular regulated kinases
EVL	Everolimus
FBS	Fetal bovine serum,
FFPE	Formalin fixed paraffin embedded
FOXO3	Forkhead box O3,
GPCRs	G protein coupled receptors
hCA	human coronary artery
HFD	High-fat diet
hMA	human mammary artery ,
hRA	human renal artery
HRP	Horseradish peroxidase
hSV	human saphenous vein
I/M ratio	Intima /Media ratio
IGF-1	Insulin-like growth factor-1
IGF-IR	IGF-I receptor
IH	Intimal hyperplasia
IP3	Inositol-1,4,5-trisphosphate
ipGTT	Intraperitoneal glucose tolerance test
ipITT	Intraperitoneal insulin tolerance test
IR:	Insulin receptor
IRS-1	Insulin receptor substrate-1
K2P	two pore domain K channels
K_{Ca}	Calcium activated K channels
K_{IR}	inward rectifier K channels,
Kv	Voltage gated K channels
Lv-	Lentiviral vector
Lv-ccMYOCD	Lentiviral myocardin knock-down
MAPK	Mitogen-activated protein kinase
MgTx	Margatoxin
MHCII	Myosin heavy chain II
miRNAs	Micro-RNAs
MLCK	myosin light chain kinase
MLCP	myosin light chain phosphatase
MRTF-A/B	Myocardin-related transcription factors A and B,
mTOR	mammalian Target Of Rapamycin
MYOCD	Myocardin
NTC	No template control
PAP-1	5-(4-phenoxybutoxy) psoralen
PBS	Phosphate Buffered Saline

Abbreviations

PDGF-BB	Platelet-derived growth factor–BB,
PI3K	Phosphatidylinositol 3-kinase
PLC	Phospholipase C
PM	Phenotypic modulation
pre-miRNA	precursor-miRNA
pri-miRNA	primary-miRNA
PTA	Percutaneous transluminal angioplasty
PTEN	Phosphatase and tensin homolog
RISC	RNA-induced silencing complex
ROCK	Rho-kinase
ROCs	Receptor operated channels
RT	Reverse transcription
SM	Smooth muscle
SM22α	Smooth muscle protein 22-alpha
SMCs	Smooth muscle cells
SPRED1	Sprouty-related protein
SRF	Serum response factor
T2DM	Type 2 Diabetes mellitus
TKR	Tyrosine kinase receptors
TRP	Transient receptor potential channels
VDCCs	Voltage-dependent Ca2+ channels.
V_M	Membrane potential
VRF	Vascular risk factors
VSMCs	Vascular smooth muscle cells

Index

Index

Abstract vii

Abbreviations xiii

Introduction 1

- 1. Cardiovascular system 3
  - 1.1. The blood vessels 3
- 2. Vascular smooth muscle cells (VSMC) 4
  - 2.1. VSMC Contraction 5
  - 2.2. Ion channels of VSMCs 9
- 3. VSMC Phenotypic modulation (PM). 11
  - 3.1. Regulation of VSMC contractile genes expression 13
  - 3.2. Growth factors and cytokines and signaling pathways. 15
  - 3.3. MicroRNAs (miRNAs). 21
  - 3.4. Ion channels in VSMC phenotypic modulation 26
- 4. Phenotypic modulation and intimal hyperplasia 29
  - 4.1. Mechanisms of intimal hyperplasia 30
  - 4.2. Restenosis after angioplasty. 31
  - 4.3. Bypass grafting occlusion. 32
  - 4.4. Transplant vasculopathy. 34
  - 4.5. Experimental in vivo models of intimal hyperplasia. 35
- 5. Vascular diseases as risk factors for intimal hyperplasia 36
  - 5.1. Diabetes 37
  - 5.2. Insulin resistance 38
  - 5.3. Hypertension 39
  - 5.4. Obesity 40
  - 5.5. Metabolic syndrome 40

Hypothesis 43

Objectives 47

Materials and Methods 51

Index

1. Experimental samples and animal models 53
    1.1. Human samples 53
    1.2. Animal models 55
2. Tools 60
    2.1. Pharmacological treatments 60
    2.2. Viral vectors production and transduction 61
    2.3. microRNAs Mimics and VSMC transfection 66
3. Histological techniques and morphometric studies 67
    3.1. Paraffin embedding and sectioning of tissue. 67
    3.2. Masson trichrome stain. 68
    3.3. Hoechst Stain. 69
    3.4. Morphometric analysis 70
4. RNA expression analysis by quantitative PCR 72
    4.1. mRNA extraction 72
    4.2. microRNA isolation. 73
    4.3 Reverse Transcription 74
    4.4. Quantitative PCR 75
    4.5. miRNA PCR array 80
5. Protein expression 81
    5.1. Western Blot 81
    5.2. Immunofluorescence 83
    5.3. Immunohistochemistry. 83
    5.4. Antibodies 83
6. Functional studies 84
    6.1. Proliferation studies 84
    6.2. Migration studies 85
    6.3. Electrophysiological studies 87
7. Statistical analyses 89

Results 91
1. Kv1.3 blockade and phenotypic modulation of human vessels 93
    1.1. Characterization of the human vessel organ culture model 93
    1.2. Effect of Kv1.3 blockers on FBS-induced IH 95
    1.3. Effects of Kv1.3 blockade on the functional characteristics of dedifferentiated VSMCs. 96
2. Mechanisms linking Kv1.3/Kv1.5 ratio to phenotypic modulation 100
    2.1. Regulation of the expression of Kv1.3 and Kv1.5 channels upon phenotypic modulation 100
    2.2. Effects of manipulating Kv1.3/Kv1.5 expression 103
    2.3. Myocardin as mediator of Kv1.5 effects on PM 109
3. Expression and functional contribution of Kv1.3 to PM in diseased vessels 114
    3.1. Effect of Kv1.3 blockers inhibiting phenotypic modulation in T2DM patients 114
    3.2. Differential miRNA expression profile in T2DM vessels 121
    3.3. Role of Kv1.3 in IH in a cardiovascular risk mice model. 129
Discussion 143
1. Contribution of Kv1.3 channel to IH in human vessels 145
2. Kv1.5 as a novel myocardin-regulated contractile marker 149
    2.1. Mechanisms of Kv1.5 antiproliferative effects 151
    2.2. Mechanisms of Kv1.3-pro-proliferative effects 153
3. Effect of Kv1.3 blockers on remodeling in T2DM 154
    3.1. Effect of Kv1.3 blockers in T2DM vessels 155
    3.2. Signaling pathways affected by T2DM in VSMCs 156
4. T2DM-associated miRNA profile in VSMCs: miR-126 158
    4.1. miRNA profile in T2DM vessels 159
    4.2. miR-126 role in vascular diseases and T2DM 160
5. Vascular remodeling in T2DM-like animal models 164
    5.1. Development of a VRF mouse model. 164

5.2. Effects of Kv1.3 blockers in remodeling in mice models.........165

Conclusions 169

References 175

Resumen..189

Annex..197

Introduction

1. Cardiovascular system

The cardiovascular system is formed by the heart, blood vessels and blood. The main function of the cardiovascular system is supply blood to all tissues, which transports oxygen, and nutrients to the cells and takes away metabolic waste. In addition, the cardiovascular system also participates in homeostatic functions, contributing to blood pressure regulation, transporting hormones, participating in temperature regulation and taking part in other homeostatic adjustments in response to physiological of pathological stimuli (Noble, 2005).

1.1. The blood vessels

The blood vessels constitute a close circuit of conducts that are disposed as a network in order to irrigate all tissues and organ of the body.

The heart pumps the blood to the aorta (major circulation) and pulmonary (minor circulation) artery from the left and right ventricle respectively. The aorta and pulmonary artery are elastic arteries that carry the blood away from the heart. The elastic arteries ramify to muscular arteries, arterioles and then capillaries, where the exchange of substances takes place. The capillaries converge in venulas and veins, and the blood circulation finish with the cava vein (major circulation) returning to the right atrium and pulmonary vein (minor circulation) to the left atrium (Noble, 2005; Levick, 2013).

1.1.a. The vascular wall

The structure of the blood vessels varies to adapt to their specific functional roles. Nevertheless, with the exception of the capillary vessels, whose wall is formed by a single layer of endothelial cells (ECs) placed on a basal membrane, the vessels wall has a conserved structure formed by three layers: tunica intima, tunica media and tunica adventitia (Figure I1).

- ***Tunica intima*** is the inner layer or endothelium, formed by a single layer of simple squamous epithelium cells, the ECs, the basal laminal and the sub-endothelial layer of connective tissue. The internal elastic lamina which separates the tunica intima from the tunica media.
- ***Tunica media*** is the intermediate layer of the vessel wall, composed mainly of one or several vascular smooth muscle cells (VSMCs) layers arranged circumferentially. This media layer is thicker in arteries than

in veins. The external elastic lamina separates the tunica media from the tunica adventitia.

- ***Tunica adventitia*** is outer layer, consisting on collagen and elastic tissue, which functions as support for the vessels. In the case of large vessels contains even small vessels, the so called *vasa vasorum*, literally "vessels of vessels"(Ross & Pawlina, 2007).

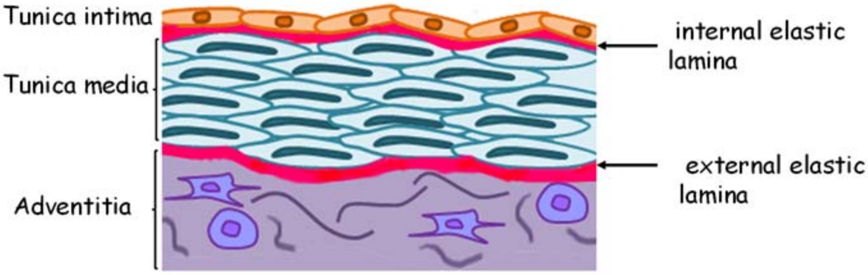

Figure I1. Cartoon illustrating the structure of the vascular wall with the different layers.

2. Vascular smooth muscle cells (VSMC)

VSMCs are fusiform or spindle-shaped cells around 20–60 µm long by 4 µm wide. These cells are the principal component of the tunica media of vascular vessels. They are arranged in a helical pattern around the vessels lumen, in such a way that changes in their state of contraction, which will modify cells length, will regulate vessels diameter and consequently blood flow (Levick, 2013).

The principal function of VSMCs is to accomplish contraction. For this purpose, VSMCS express the necessary receptors, ion channels, signal transduction proteins, calcium regulatory protein and of course, smooth muscle (SM) contractile genes. (Wamhoff *et al.*, 2006).These genes, also known as contractile markers such as myosin heavy chain 2, SM22-alpha, smooth muscle alpha-actin, calponin-1 or smoothelin are proteins involved in the contractile machinery (Thiriet, 2013). Most VSMCs from adult animals show a differentiated, contractile phenotype, but they have also a remarkable degree of plasticity (see below). Contractile VSMC do not migrate or proliferate, and show very low rate of synthesis of extracellular matrix components.

2.1. VSMC Contraction

During contraction, VSMCs can shorten to less than half of their maximal length in the relaxed state, (Figure I2), and in this way they decrease lumen ratio and regulate blood flow. It is interesting to point out that VSMC are always in a partially contracted state (known as basal tone). Therefore, when vasoconstriction is required, VSMCs increased this basal state rather than start a contraction de novo. Conversely, vasodilation is achieved via reduction of the basal tone of VSMCs, with the consequent increase of cell length and vessel diameter (Levick, 2013).

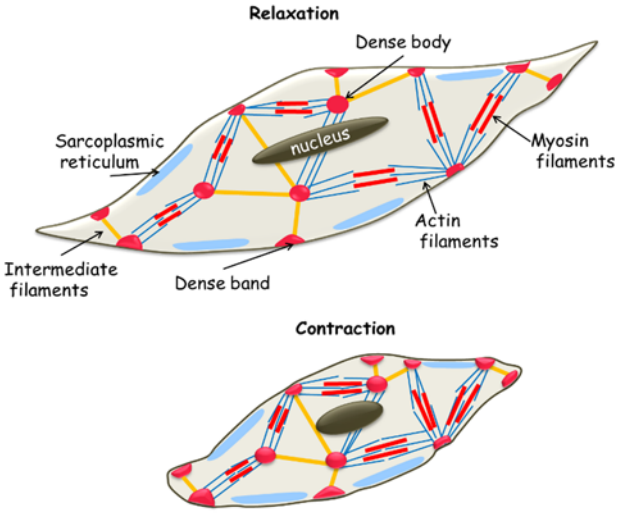

Figure I2. Scheme showing the structures required for VSMC contraction. Contraction of VSMCs leads to activation of the cross-bridge cycle, so that actin filaments slide over myosin filaments, shortening the cell. The shape of the nucleus follows the shape of the cell.

Structures of particular importance for VSMC contraction include the contractile elements, the Ca^{2+} stores and the intercellular junctions. The basic contractile unit in VSMC is a sarcomere-like structure formed by myosin filament (thick filaments) that interdigitates with actin filaments (thin filaments, Figure I2).

The ***thick filaments*** are composed of myosin molecules, formed by two myosin heavy chains and two myosin light chains. The heavy chain forms the body of the thick filament and the light chains are the mobile part of the myosin filament. The myosin isoform differs from the cardiac and skeletal muscle myosin in that it needs to get phosphorylated to start the contraction (Levick, 2013).

The ***thin filaments*** are composed of α-actin molecules. A-actin is a monomeric, globular protein that in solution tends to aggregate in filaments. The actin filament forms a double helical filament, with a groove between the two helixes which is the docking place for Ca^{2+}-dependent regulatory proteins such as caldesmon and calponin (Thiriet, 2013).

The actin filaments are rooted in “dense bands” located on the inner surface of the cell membrane and in “dense bodies” located in the cytoplasm (Figure I2). The dense bands and dense bodies, which are composed of alpha-actinin, are not aligned; instead they are randomly located. In addition to thick and thin filaments, there is a third type of filament important for the contractile unit: the ***intermediate filaments***, composed of desmin and vimentin, which connect various dense bands and dense bodies, making possible that the VSMC contract as a whole (Levick, 2013).

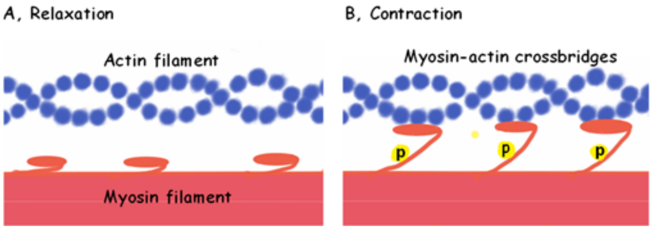

Figure I3. **A**, schematic myosin and actin filament during relaxation. **B**, myosin-actin cross bridges during contraction.

The contraction starts with a rise of cytoplasmic Ca^{2+}. Four Ca^{2+} ions binds with calmodulin, forming the Ca^{2+}-calmodulin complex. This complex activates the myosin light chain kinase (MLCK), which phosphorylates the myosin light chain (the mobile part of the myosin thick filament). The phosphorylated myosin is then able to interact with actin molecules (Figure I3), creating cross-bridges that allow the shortening and force generation of the VSMCs (Levick, 2013).

The duration of the contraction is determined by the balance of MLCK activity and myosin light chain phosphatase (MLCP) activity. MLCP is an enzyme that dephosphorylates myosin and it is also regulated by intracellular [Ca^{2+}], but in the opposite way to MLCK, so that it became more activated when [Ca^{2+}] decreases. More MLCK activity means contraction and more MLCP activity means relaxation. In this way, the increase [Ca^{2+}] leads to activation of MLCK and contraction, with a concomitant decrease of MLCP activity. When the [Ca^{2+}] decreases, there is a decline in the MLCK activity together with an increase in the MLCP, which releases the cross-bridges leading to relaxation. The tight regulation via intracellular Ca^{2+} levels of the number of phosphorylated cross-bridges is a special feature of smooth muscle contraction, which makes especially relevant the control of intracellular calcium. In this way, the $[Ca^{2+}]$ determines the number of phosphorylated cross-bridges, which in turn defines the speed of contraction (Levick, 2013).

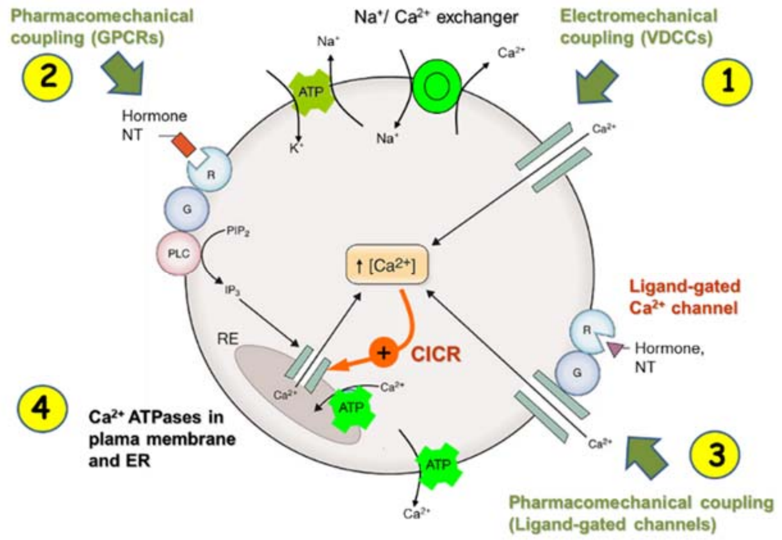
Pharmacomechanical coupling (GPCRs)
2
Na+/ Ca2+ exchanger
Na+
Ca2+
ATP
K+
Na+
Electromechanical coupling (VDCCs)
1
Ca2+
Hormone
NT
R
G
PLC
PIP2
IP3
↑ [Ca2+]
RE
+
CICR
Ligand-gated Ca2+ channel
R
Hormone,
NT
G
Ca2+
Ca2+
ATP
Ca2+
4
Ca2+ ATPases in plama membrane and ER
ATP
Ca2+
3
Pharmacomechanical coupling (Ligand-gated channels)

Figure I4. Summary of the mechanisms controlling $[Ca^{2+}]_i$ in VSMCs. The increase of $[Ca^{2+}]_i$ could be due to Ca^{2+} influx through VDCC (electromechanically coupling, 1 in the diagram), activation of Ca^{2+} release via GPCRs (pharmacomechanical coupling, 2) or Ca^{2+} influx through ligand gated channels (another kind of pharmacomechanical coupling, 3). Finally, there are several mechanism for Ca^{2+} efflux (mainly Ca^{2+} pumps, number 4, and also Na/Ca exchanger) to regulate $[Ca^{2+}]_i$. Modified from Berne and Levy, see text for more details.

Both the entry of extracellular Ca^{2+} and the Ca^{2+} release from the sarcoplasmic reticulum can lead to the increase of cytosolic $[Ca^{2+}]$ needed for initiate contraction. These changes can occur both with and without changes in membrane potential. The processes are named electromechanical coupling and pharmacomechanical coupling, respectively (Mohrman & Heller, 2006) (Figure I5).

Electromechanical coupling means that depolarization of the membrane potential increases the open probability of the voltage-dependent Ca^{2+} channels (VDCCs). The influx of Ca^{2+} acts as second messenger to activate Ca^{2+} channels in the sarcoplasmic reticulum, known as ryanodine receptors, in a process known as calcium-induced calcium release (CICR, Figure I5) (Mohrman & Heller, 2006).

In addition, hormones and neurotransmitters can induce contraction without the activation of voltage-dependent channels and in some cases even without changes in membrane potential. This is termed pharmacomechanical coupling (Figure I5).

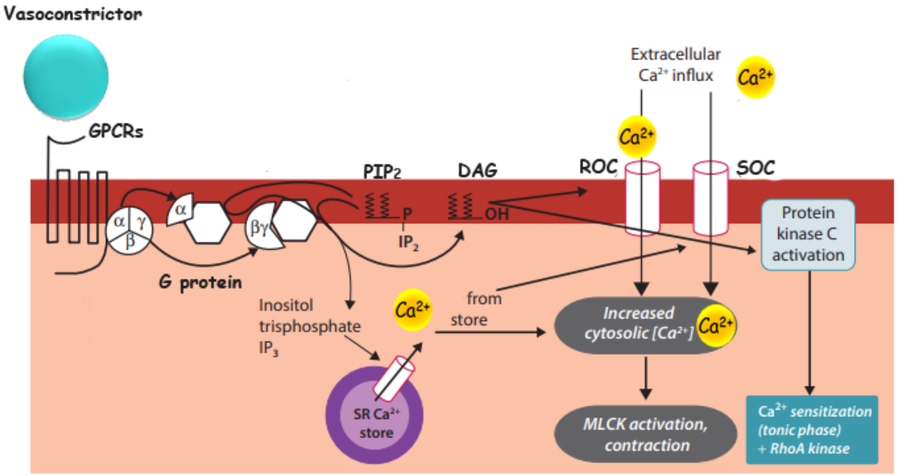
Vasoconstrictor
GPCRs
α
γ
β
α
βγ
G protein
PIP2
P
IP_2
DAG
OH
Extracellular Ca^{2+} influx
Ca^{2+}
Ca^{2+}
ROC
SOC
Protein kinase C activation
Inositol trisphosphate IP_3
Ca^{2+}
from store
Increased cytosolic $[Ca^{2+}]$
Ca^{2+}
SR Ca^{2+} store
MLCK activation, contraction
Ca^{2+} sensitization (tonic phase) + RhoA kinase

Figure I5. Pharmacomechanical coupling (Levick, 2013).

Classic vasoconstrictors, such as endothelin-1, angiotensin II, norepinephrine, or vasopressin act through G protein coupled receptors (GPCRs) coupled to G-proteins of the G_q/G_{11}, G_{12}/G_{13}, and G_i families. G_q/G_{11} link these receptors to the activation of phospholipase C (PLC), leading to the formation of inositol-1,4,5-trisphosphate (IP3) and diacylglycerol (DAG). IP3 activates receptors located on the sarcoplasmic reticulum leading to Ca^{2+} release and a transient increase in $[Ca^{2+}]_i$. Since the reticulum is relatively poorly developed in VSMCs, tonic vasoconstriction also requires extracellular Ca^{2+} entry. There is good evidence that the Ca^{2+} influx from the extracellular space is mainly mediated by DAG-activated, receptor operated channels (ROCs), which belong to the transient receptor potential (TRP) channels family (Koeppen *et al.*, 2018).

Most GPCRs are also able to regulate myosin light chain phosphorylation and dephosphorylation by a mechanism involving changes in calcium sensitivity of the contractile machinery. This pathway is mediated by the small GTP-binding protein RhoA. After activation, RhoA stimulates Rho-kinase (ROCK) which then phosphorylates and inactivates MLCP, increased the number of phosphorylated cross-bridges which promotes further VSMC contraction. The ROCK-mediated enhancement of smooth muscle contraction is a Ca^{2+} sensitization mechanism that occurs in the absence of significant changes in $[Ca^{2+}]_i$ (Somlyo & Somlyo, 2003). In most cases the G-proteins G_{12}/G_{13} link receptors to the Rho/ROCK pathway in VSMCs. In addition, G_q/G_{11} can activate RhoA indirectly (Althoff & Offermanns, 2015).

Most vasoconstrictor receptors are coupled to both G_q/G_{11} and G_{12}/G_{13}. Also, some GPCRs are coupled to the G_i family of G proteins, which may contribute to the pro-contractile activity of their ligands by releasing βγ-subunits resulting in the activation of PLC or by inhibiting adenylyl cyclase leading to a decrease in intracellular cAMP levels (Althoff & Offermanns, 2015).

Relaxation is initiated by a decrease in $[Ca^{2+}]_i$ as a consequence of Ca^{2+} uptake by the sarcoplasmic reticulum (by the sarcoplasmic reticulum Ca^{2+}pump) and Ca^{2+} extrusion by the plasma membrane Ca^{2+} pump and the Na^+-Ca^{2+} exchanger (Somlyo & Avril, 1994, see Figure I5).

2.2. Ion channels of VSMCs

As reviewed above, intracellular $[Ca^{2+}]$ is pivotal for regulation VSMCs contraction. Even though calcium release from sarcoplasmic reticulum is important for the onset of agonist induced response, a sustained entry of extracellular Ca^{2+} is needed to maintain basal tone (Siegel *et al.*, 1991). This sustained Ca^{2+} entry is very dependent on resting membrane potential of VSMCs. Membrane potential is the net result of the activity of a number of active and passive ion transport mechanisms in the cell membrane.

The vascular smooth muscle sarcolemma has at least four types of K^+ conducting channels, four types of Ca^{2+} conducting channels, and one type of Cl^- conducting channel (Jackson, 2000). Among Ca^{2+} conducting channels we found voltage-dependent calcium channels (VDCC) that are highly selective for Ca^{2+}, and TRP channels, that are Ca^{2+} permeable non-selective cation-conducting channels with very diverse functions and modulation. VDCC, and in particular L-type Ca2+ channels are the predominant Ca^{2+} channels in contractile VSMC.

Potassium selective channels are the most diverse group of ion channels, encoded by at least 70 mammalian genes and expressed as more than 100 principal pore forming or principal subunits (α subunits). They can produced a very diverse set of functional complexes by alternative splicing, heteromultimeric assembly of different pore-forming subunits and co-assembly with different modulatory auxiliary subunits (Coetzee *et al.*, 1999; Wickenden, 2002). K^+ channels play a role in the regulation of arterial tone and in the control of cell proliferation. Moreover, changes in K+ channels expression have been described in association with the phenotypic switch of VSMCs (Neylon, 2002).

K+ channels are gated by different stimuli and have different structures. Based on their structure K^+ channels are classified into 4 subgroups (Figure I6). This classification roughly correlates with their functional characterization based on their physiological properties: voltage gated (Kv), calcium activated (K_{Ca}), inward rectifier (K_{IR}), and two pore domain channels (K_{2P}). Among those, Kv and high conductance-K_{Ca} (BK_{Ca}) channels are present in basically all vascular myocytes, and have an important role in modulating contractile responses and basal tone (Nelson & Quayle, 1995).

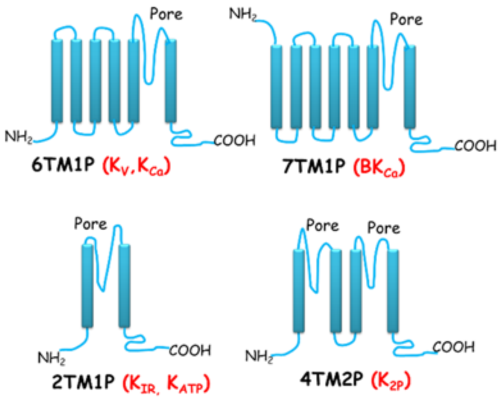

Figure I6. Structural classification of potassium channels, based on the number of transmembrane regions (TM) and the number of pore regions (P). Within each group, there are one or more subfamilies, which are defined according to their functional properties (with the names in red in the figure). See text for more details.

K_{ca} channels are activated by elevations in intracellular Ca^{2+}, by depolarization or by vasodilators that increase intracellular levels of cAMP or cGMP. (Ledoux *et al.*, 2006) The activation of these channels prevent excessive Ca^{2+} entry and promote muscle relaxation. They are classified by their relative conductances into large (BK_{Ca}, hSlo or MaxiK channels), intermediate (IK) and small (SK) conductance subfamilies. Excluding BK_{Ca} channels, all K_{ca} channels are formed by 6 transmembrane and 1 pore domains, **6TM1P** α subunits. However BK_{Ca} have an additional T0 transmembrane domain, **7TM1P**, which determines an extracellular topology for N-terminus (Wallner *et al.*, 1996).

Kv channels activated in response to depolarizing influence, hence contributing to membrane repolarization. Kv channels are relevant players in the control of myogenic tone, acting as an effective brake controlling depolarization-mediated influx of Ca^{2+} through VDCCs (Plane *et al.*, 2005). These channels are tetrameric structures consisting of four pore-forming α subunits. Each α subunit is formed by 6 transmembrane and 1 pore domains, **6TM1P**. They have a voltage-sensing transmembrane domain (the S4 region), and intracellular amino and carboxyl terminus that can participate in cell signaling via protein-protein interactions (Tykocki *et al.*, 2017).The Kv tetrameric structure can be formed from four identical α subunits The functional Kv channels can be formed as homotetrameric structures with four identical α subunits, or as heteromultimers of two or more different α subunits. In this case, only α subunits from the same subfamily can heteromultimerize, so that for instance Kv1 heteromultimers will be formed by combinations of different Kv1.x subunits (Wickenden, 2002).

Native Kv1 channels are commonly presented as heteromultimers rather than homomultimers. For instance, (Plane *et al.*, 2005) have stated that heteromultimers conformed by Kv1.2, Kv1.5 and Kv1.6 contribute to the myogenic control in resistance arteries, and each α subunits give specific features such as the presence of Kv1.6 slow inactivation of the channel, or that Kv1.5 presence decrease sensitivity for 4-aminopyridine(Kv1 blocker). Renal artery is characterized for having Kv1.2/Kv1.4 heteromultimers in which Kv1.4 gives fast inactivation to the channel that correlates with the number of Kv1.4 α subunits in the heteromultimer (Po *et al.*, 1993; Fergus *et al.*, 2003; Plane *et al.*, 2005). Thus, heteromultimers have different and unique pharmacologic and kinetics properties according to the Kv1 α subunit components. Together with alternative splicing and association with other modulatory subunits, Kv channel heteromultimerization contributes to the large diversity and complexity of native Kv currents. Kv channels will be further described in greater detail.

3. VSMC Phenotypic modulation (PM).

The main function of the smooth muscle cells of the blood vessels wall (VSMC) is that of contractility, effected by a highly organized cytoskeleton with defined F-actin filaments and expression of smooth muscle-specific contractile proteins (Alexander & Owens, 2012). In response to local cues, VSMCs can switch to a dedifferentiated phenotype, in which VSMC can migrate and proliferate and exhibit a diffuse, loose F-actin network concomitant with a loss of contractile proteins. This process is known as phenotypic switch or phenotypic modulation (PM, Figure I7). In healthy vessels, phenotypic switching is fully reversible, and VSMC alternate between these states according to environmental signals (Owens *et al.*, 2004). This inherent plasticity of VSMC permits switching to proliferative and secretory phenotypes which are essential during vascular development, repair and adaptation, but also contribute to progression of vascular diseases such as atherosclerosis, restenosis after angioplasty and bypass graft failure. PM can be trigger by different stimuli, such as mechanical, chemical or humoral factors.

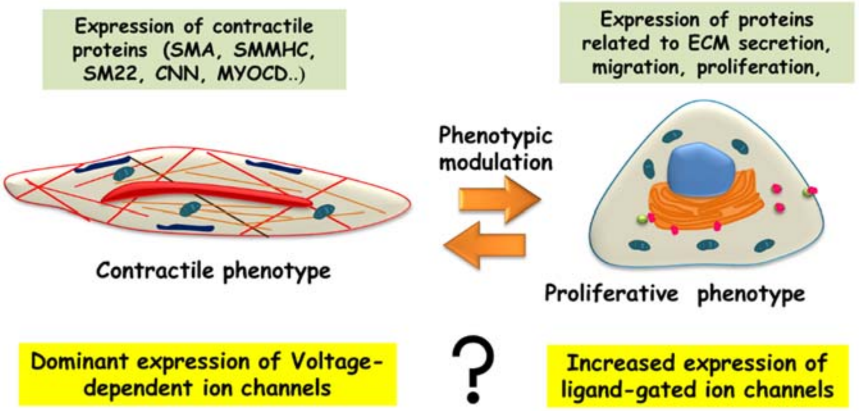
Expression of contractile proteins (SMA, SMMHC, SM22, CNN, MYOCD..)
Expression of proteins related to ECM secretion, migration, proliferation,
Phenotypic modulation
Contractile phenotype
Proliferative phenotype
Dominant expression of Voltage-dependent ion channels
?
Increased expression of ligand-gated ion channels

Figure I7. Phenotypic modulation .of VSMC is a reversible process. Changes in several set of proteins are well characterized, and also changes in many different ion channels have been proposed. According to some authors, contractile VSMC require more voltage-gated channels to regulate vascular tone whereas proliferating VSMC need more ligand (Ca^{2+} or second-messenger) gated channels.

The mechanisms that regulate the phenotypic modulation of VSMC are complex and not fully understood. Each VSMC phenotype is characterized by a clear and well defined set of physiological properties that require the functional expression of different genes and proteins. In this regard, several proteins have been described as specific markers of the contractile smooth muscle (SM), such as SM-α actin, SM myosin heavy chain, h1-caponin, SM22α and smoothelin (Rovner *et al.*, 1986; Owens *et al.*, 2004). Not surprisingly, all this proteins are in one way or another related with the contractile apparatus and are downregulated during PM when the contractile function disappears in favor of the acquisition of new functional characteristic such as a high rate of proliferation or a synthetic or migratory activity. In the case of the proliferative phenotype, its characterization is less clear, as there are not specific markers of this stage, which is usually defined by the loss of contractile markers.

However, proliferation is not exclusive of the proliferative phenotype, since differentiated (contractile) cells are also capable of proliferate, although at a very low rate. Evidence of this is found during late embryogenesis and postnatal development when VSMCs are known to have an extremely high rate of proliferation while exhibiting a high expression of multiple VSMC differentiation markers. Conversely, VSMCs within advanced atherosclerotic lesions show a very low rate of proliferation that approaches that of fully differentiated VSMC but are also highly phenotypically modulated (O'Brien *et al.*, 1993). These observations suggest that contractile and dedifferentiated phenotypes represent the extreme cases of a continuum of possible phenotypes that can be seen in the VSMC of the vessel wall, with many intermediate phenotypes. These intermediate phenotypes result in part from the different environmental signals, which determine the degree of VSMC dedifferentiation. For instance, during vessel formation, VSMCs present a phenotype with contractile properties but at the same time show higher proliferation rates, necessary for the vessel formation (Bhattacharyya *et al.*, 2014). It has been proposed that cell morphology and organization may regulate differentiation of VSMCs and subsequent function, as differentiated VSMC phenotype can be induced in culture by micropatterning to control VSMC morphology (Chang *et al.*, 2014). Another example is provided by the effect of the matrix composition in the phenotype of VSMC in culture (Morla & Mogford, 2000). They found that PM differs when VSMCs are seeded in fibronectin or laminin matrix. VSMCs cultured on laminin or in micro-patterned cultured systems present an intermediate phenotype, showing similar migration rates but less proliferation rates and less ERK activity than VSMCs seeded in fibronectin, which show a more dedifferentiated phenotype. It is plausible that these intermediate phenotypes serve different functions in the blood vessel, such as during injury, hypertension, humoral or immunological responses among others.

3.1. Regulation of VSMC contractile genes expression

The serum response factor (SRF) is a transcription factor that regulates most of SM contractile genes. SRF binds as a dimer to a CArG box located within the promotor region of the regulated gene. CArG box is a DNA consensus sequence CC(A/T)6 GG that is present within nearly all of the SM genes. However, SRF is an ubiquitously expressed protein that also regulates the expression of other genes, such as growth factor inducible genes (MacK, 2011). In fact, the requirement of SRF for expression of growth factor-inducible and muscle-specific genes is paradoxical since growth factor signaling represses muscle gene expression.(Wang *et al.*, 2001). The explanation for this paradox is that SRF-dependent transcription is controlled to a large extend by SRF interactions with additional transcription factors or coactivators, which provide tissue-specificity to the mechanism. In VSMC, the relevant cofactor is myocardin (MYOCD), a SRF-coactivator that positively regulates cardiac and SM contractile genes. (Wang *et al.*, 2001). Two-Myocardin SRF complexes can induce transcriptional activity (Figure I8), providing a mechanism for cooperative activation of SM genes by SRF-myocardin complexes (Wang *et al.*, 2003). Of interest, SM genes have at least two CArG boxes whereas growth factor-inducible genes (like c-fos) have only one CArG box (Miano, 2003).

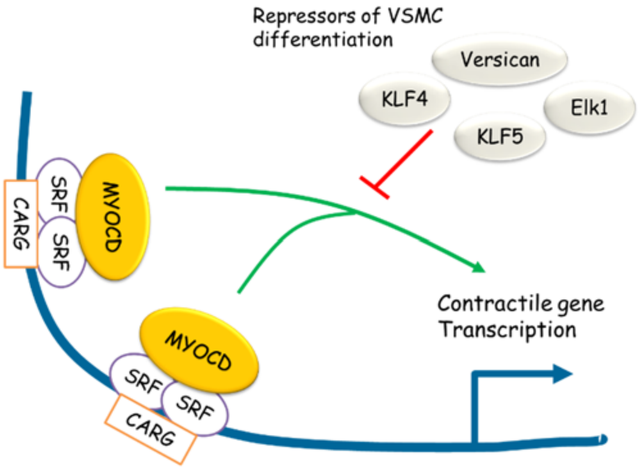
Repressors of VSMC differentiation
Versican
KLF4
Elk1
KLF5
CARG
SRF
SRF
MYOCD
Contractile gene Transcription
MYOCD
SRF
SRF
CARG

Figure I8. VSMC contractile gene expression involves binding of two myocardin-SRF-CArG Box ternary complex. Activation of SM genes can be inhibited by several repressors such as Kruppel-like factor 4 and 5 (KLF4, KLF5). Modified from (Davis-Dusenbery *et al.*, 2011).

Even though myocardin is expressed both in cardiac and smooth muscle cells.(Wamhoff *et al.*, 2006), its activity is more specific for SM gene expression, because cardiac muscle gene expression requires other cofactors in addition to myocardin. In fact, myocardin transfected fibroblasts can activate SM gene expression in these non-muscle cells via its association with SRF (Chen *et al.*, 2002; Wang *et al.*, 2003). However, it cannot induce cardiac genes) expression due to the absence of essential cardiac cofactors (Wang *et al.*, 2003).

Two myocardin-related transcription factors (MRTFs), MRTF-A and MRTF-B, have been identified that have transcriptional properties similar to those of myocardin. Although the MRTFs are expressed more ubiquitously, both are strongly expressed in SMC (MacK, 2011). MRTF-A is also an effective activator of SM gene expression when transfected in non-muscle cells in vitro. However it is unclear why SM genes are not expressed in many of the cell types that express MRTF-A in vivo. Thought MRTF-B shares high homology with myocardin and MRTF-A in the SRF biding region, it is ineffective in activating smooth muscle gene expression in non-muscle cells (Wang *et al.*, 2003).

Although it has been well demonstrated that PM of VSMC contributes to the occurrence and progression of many proliferative vascular diseases, little is known about the details and the molecular mechanisms involved. Growing evidence suggests that variety of molecules including microRNAs, cytokines and biochemical factors, membrane receptors, ion channels, cytoskeleton and extracellular matrix play important roles in controlling VSMC phenotype (Zhang *et al.*, 2016). We will next review some of these elements.

3.2. Growth factors and cytokines and signaling pathways.

Numerous biochemical factors and its membrane receptors such as platelet-derived growth factor–BB (PDGF-BB), insulin-like growth factor-1 (IGF-1), transforming growth factor (TGF-beta), all-trans retinoic acid, bone morphogenetic proteins, angiotensin II and insulin can exert an influence on VSMC phenotype. (Zhang *et al.*, 2016). Among those, the contribution of PDGF-BB and IGF-1 or insulin are among the most relevant in physiological conditions and the best characterized. All these factors exert their cellular effects by binding to, and activating, structurally related tyrosine kinase receptors (RTKs; (Krauss, 2014)).

RTKs have a ligand binding domain on the extracellular side, a transmembrane portion composed of a single α-helical element, and a cytosolic part with a conserved TK domain. (Figure I9). Most RTKs are monomeric in the absence of ligand, and ligand binding triggers their association into dimers or higher oligomers. One exception are the insulin and IGF-1 receptors, which exist as preformed dimers comprising two extracellular α-chains and two membrane-spanning β-chains. Ligand-induced activation activated the TK domain, most often via autophosphorylation at Tyrosine (Tyr) residues. These P-Tyr formed at the receptor serve as docking sites for downstream effector proteins that harbor P-Tyr specific interaction domains, such as SH2, P-Tyr-binding (PTB) and C2 domains. In addition, downstream effectors can be Tyr-phosphorylated by the activated RTK to transmit the signal further.

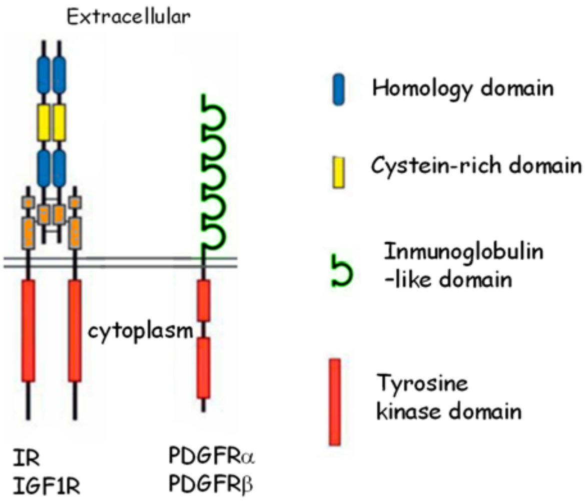

Figure I9. Domain organization of tyrosine kinase receptors: PDGFR(platelet-derived growth factor receptor); IR (insulin receptor); and IGF1R (insulin-like-growth factor 1 receptor) Scheme modified from (Krauss, 2014).

In general, ligand-induced activation of the TK activity serves to recruit a multitude of effector proteins into RTKs signaling. Two ways of recruiting the effectors have been identified:

a) An SH2 or PTB domain of the effector binds to P-Tyr on the RTKs, linking the effector directly to the RTKs; and
b) Adapter or scaffolding protein serves to recruit the effector to the RTKs for further signal transmission. These adaptors bind via SH2 or PTB domains to the activated RTKs; the adapter is then Tyr-phosphorylated by the RTKs, after which its P-Tyr residues serve to guide SH2-domain-containing effectors to the receptor. Important adaptors in RTKs signaling are the insulin receptor substrate-1 (IRS-1), Grb2 and Gab proteins, which interact with downstream effectors to organize larger signaling complexes at the activated receptor. In this way, RTKs can become part of large signaling networks.

Examples of downstream effectors of RTKs include phosphatidylinositol 3-kinase (PI3K), phospholipase Cγ (PLCγ), small GTPases such as Ras protein, mitogen-activated protein kinase (MAPK), non-RTKs such as Src kinase, and protein-Tyr phosphatases. Signaling by RTKs is tightly regulated via positive and negative feedbacks, inhibitors, ubiquitination, endocytosis, and trafficking. (Krauss, 2014). Two of the best characterized effectors in VSMCs are MAPK and PI3K pathways (Figure I10).

3.2.a. MAPK pathway

The MAPK (mitogen-activated protein kinase) pathways are involved in directing cellular responses to a diverse array of stimuli, such as mitogens, osmotic stress, heat shock and pro-inflammatory cytokines. They regulate cell functions including proliferation, gene expression, differentiation, mitosis, cell survival, and apoptosis (Pearson *et al.*, 2001).

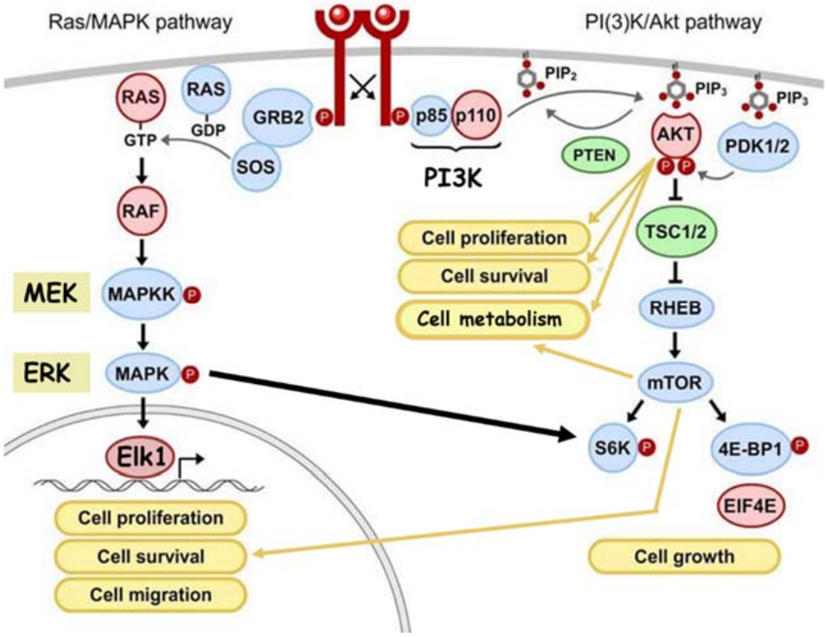
Ras/MAPK pathway
PI(3)K/Akt pathway
RAS
RAS
GDP
GTP
GRB2
P
P
p85
p110
PI3K
SOS
PIP2
PIP3
PIP3
AKT
PTEN
PDK1/2
P
P
RAF
MEK
MAPKK
P
ERK
MAPK
P
TSC1/2
Cell proliferation
Cell survival
Cell metabolism
RHEB
mTOR
S6K
P
4E-BP1
P
EIF4E
Elk1
Cell proliferation
Cell survival
Cell migration
Cell growth

Figure I10. A simplified view of some of the elements of two relevant RTK-activated pathways in VSMCs, which contribute to cell proliferation, cell survival, cell growth and other relevant metabolic functions. There are many interactions between these pathways, which are not represented un the scheme. Adapted from (Haglund *et al.*, 2007).

MAPK pathways uses a cascade of three protein kinases to transduce extracellular and intracellular signals down to the level of transcription. The three protein kinases of typical MAPK pathways are organized as functional units, often with the aid of scaffold proteins. The protein kinases at the bottom of the cascade, the MAPKs or ERKs (extracellular regulated kinases), are activated by the MEKs, also named MAPK kinases (MAPKK). The MEKs are phosphorylated and activated by the kinases at the top of the cascade, the MEK kinases (MEKKs) or MAPKK kinases (MAPKKKs).

ERKs deliver signals both to nuclear and cytoplasmic substrates. The activation of ERKs by MEKs promotes their dimerization and the ERK dimers can translocate into the nucleus to phosphorylate and activate various transcription factors. An example of a nuclear substrate is the transcription factor Elk-1, which is positively regulated via the ERK pathway.

An important cytoplasmic substrate of ERK1/2 proteins is the ribosomal S6 kinase (S6K), also termed MAPK-activated protein kinase 1. A number of cellular functions have been proposed for S6K, including the phosphorylation of transcription factors such as CREB and NFkB, as well as the stimulation of protein synthesis (Krauss, 2014).

3.2. b. PI3K pathway

PI3K catalyzes the phosphorylation of various phosphatidylinositol (PI) derivatives. The products of the reaction, such as PIP3, serve as membrane-localized second messengers that help to localize various signaling proteins to membranes. The major downstream effector of PI3K is the protein kinase AKT, also known as protein kinase B (PKB). The PIP3 formed by PI3K kinase binds to AKT and other PKs, inducing their membrane association and activation. Major processes regulated by AKT signaling include:

1. Stimulation of protein synthesis and cell growth: This effect is mediated by a complex signaling cascade involving the protein kinases TSC and mTOR (mammalian Target Of Rapamycin).
2. Promotion of cell survival and inhibition of apoptosis: Among the substrates of AKT kinase involved in these functions are cell cycle regulators (p27, p21, cyclin D1), transcriptional regulators such as NFkB or the pro-apoptotic protein Bad. This is why deregulation of the AKT pathway is frequently associated with the development of cancer.
3. Regulation of cellular metabolism: Insulin activates PI3K/AKT pathway, which mediates many of the metabolic effects of insulin, including glucose transport, lipid metabolism and protein synthesis (Krauss, 2014).

3.2. c. PDGF

PDGF-BB is considered the most powerful and efficient inhibitor of VSMC differentiation (Zhang *et al.*, 2016). PDGF strongly stimulates phenotypic switch by enhancing VSMC proliferation and migration and downregulating VSMC differentiation marker gene expression through multiple and partially overlapping mechanisms (MacK, 2011).

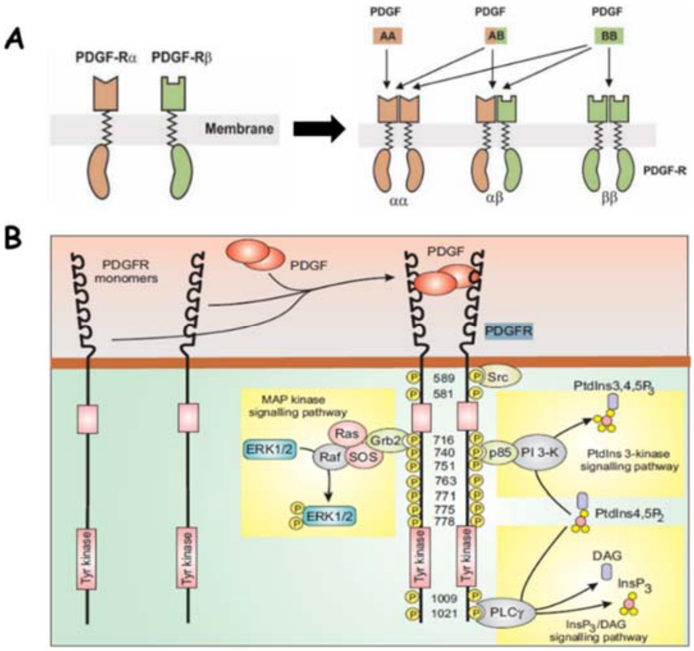
A
PDGF-Rα
PDGF-Rβ
Membrane
PDGF
AA
PDGF
AB
PDGF
BB
αα
αβ
ββ
PDGF-R
B
PDGFR monomers
PDGF
PDGF
PDGFR
589
581
Src
MAP kinase signalling pathway
Ras
Grb2
ERK1/2
Raf
SOS
ERK1/2
716
740
751
763
771
775
778
p85
PI 3-K
PtdIns3,4,5P3
PtdIns 3-kinase signalling pathway
PtdIns4,5P2
DAG
InsP3
Tyr kinase
Tyr kinase
Tyr kinase
Tyr kinase
1009
1021
PLCγ
InsP3/DAG signalling pathway

Figure I11. A. Heterodimerization of PDGF receptors. (a) There are α and β subtypes of platelet-derived growth factor receptor (PDGFR); these are induced by ligand binding to form homodimers and heterodimers; (b) Platelet derived growth factor (PDGF) is a dimeric growth factor, composed of chains A and/or B. The protein may exist as a homodimer (AA, BB) or a heterodimer (AB). The AA homodimer of PDGF binds to the αα dimer of PDGF-R, AB binds to the αα and αβ types, and BB binds all three combinations (Krauss, 2014). **B**. Activation of the PDGFRs triggers MAPK, PI3K/Akt and PLCγ pathways (Berridge, 2014).

PDGF-BB exerts its cellular effects by binding to, and activating, two structurally related RTKs, PDGFα and PDGFβ receptors, (Figure I11, A) which results in receptor dimerization and autophosphorylation. (Heldin & Westermark, 1999). Because there are differences between α- and β-receptors in their binding specificity of PDGF-BB and in the signals they transduce, their expression determines the cell responses to PDGF-BB stimulation. The classical target cells for PDGF-BB, fibroblasts and SMCs, express both α- and β-receptors, but generally higher levels of β-receptors. Other cell types such as human platelets express only α-receptors, whereas other cell types, such as mouse capillary ECs express only β-receptors.(Heldin & Westermark, 1999). Upon PDGF receptor activation, the P-Tyr residues provide docking sites for various signaling components to generate multiple output pathways (Figure I11), including ERK, PI3K/AKT and PLCγ pathways (Berridge, 2014).

3.2.d. Insulin and Insulin-like growth factor (IGF-1)

IGF-1 is an anabolic hormone mainly synthesized in the liver and locally expressed in peripheral tissues under the control of pituitary GH, within a negative feedback loop system. IGF-1 is a pleiotropic factor, which is found in the circulation (endocrine IGF-1) and is also produced locally in ECs and VSMCs from arteries (Beneit *et al.*, 2016). Insulin is an IGF-1 related peptide hormone, secreted by the beta cell in the pancreatic islets.

The insulin and IGF-1 signaling is mediated by hormone interaction with the insulin receptor (IR) and the IGF-I receptor (IGF-IR), both members of the RTK family. Both receptors are expressed at the cellular surface as preformed disulfide-linked dimers in α2β2 configuration. The extracellular α subunit of each hemireceptor contains the ligand binding sites, while β subunits include a large cytoplasmic region with tyrosine kinase activity. Because of the high degree of homology of the two receptors, hybrid receptors formed by IR and IGF-IR hemireceptors are also found in cells co-expressing IR and IGF-IR (Beneit *et al.*, 2016).

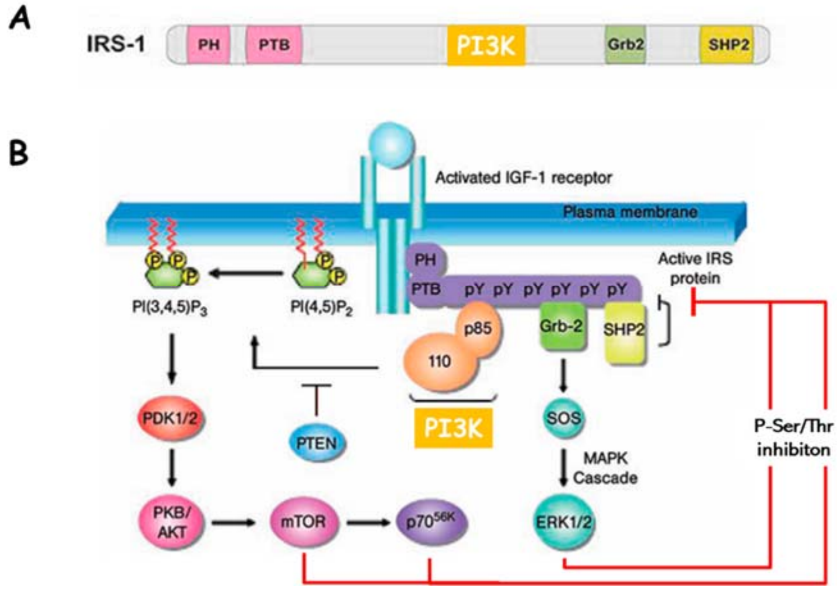
A
IRS-1
PH
PTB
PI3K
Grb2
SHP2
B
Activated IGF-1 receptor
Plasma membrane
P
PI(3,4,5)P3
PI(4,5)P2
PH
PTB
pY pY pY pY pY pY
Active IRS protein
p85
110
Grb-2
SHP2
PDK1/2
PTEN
PI3K
SOS
MAPK Cascade
P-Ser/Thr inhibiton
PKB/ AKT
mTOR
p70S6K
ERK1/2

Figure I12. A, schematic of the IRS protein, showing the docking site for several relevant downstream effectors**. B**, IR/IGF1R activation is mediated by IRS-1 activation via P-Tyr (pY), but several of the downstream effectors can in turn lead to activation of P-Ser/Thr, inhibiting pY, representing a feedback regulatory mechanism (modified from (Krauss, 2014))**.**

The IR and IGF1-R rely entirely on adaptors of the IRS family (especially IRS-1) for the recruitment of downstream signaling molecules. It is a major task of the IRS-1 to shape insulin and IGF-1 signaling in response to multiple micro-environmental stimuli (Figure I12).

IRS protein presents a set of P-Tyr sites at the C-terminal part that act as on/off switches to recruit the downstream effectors (Figure I12 B). There are approximately 20 potential P-Tyr sites on IRS-1, and these serve to bind to SH2 domains of the downstream effectors. Activation of IR or IGF1R stimulates IRS protein binding to P-Tyr residues of the receptor. Subsequently the IRS protein is phosphorylated by the activated receptor at multiple Tyr residues, which then serve as attachment points for sequential effector molecules. One of the best-characterized downstream effectors of IRS proteins is PI3K, which in turn activates AKT kinase (see above).

Another distinct feature of IRS proteins is the presence of multiple serine/threonine phosphorylation (P-Ser/Thr) sites. The P-Ser/Thr of IRS-proteins alters their capacity to be P-Tyr, inhibiting IR and IGF-1R signaling. For instance, P-Ser/Thr in the vicinity of Tyr-phosphorylation sites impedes binding of the SH2 domains of downstream effectors, thus inhibiting insulin signaling, which can lead to insulin resistance. Among these protein kinases responsible for phosphorylation of Ser/Thr there are mediators of insulin action, such as mTOR, S6 kinase, MAPK and PKC-δ; these kinases negatively regulate IRS proteins upon prolonged insulin stimulation, representing a negative-feedback regulatory mechanism.

Overall, IRS proteins illustrate in an impressive manner the multiplicity of signals that converge on and are distributed further from a seemingly simple signaling intermediate. The large number of distinct Tyr- and Ser/Thr phosphorylation sites that can be used by incoming signals in a specific fashion enables the IRS proteins to be sensitive not only to many internal and external stimuli but also to the triggering of distinct biological responses (Krauss, 2014).

3.3. MicroRNAs (miRNAs).

miRNAs are small non-coding RNAs, with an average 22 nucleotides in length that modulate gene expression, and are generally inhibitory, as they bind to their target genes mRNA and repress their expression via inhibition of RNA translation or mRNA degradation (Figure I13).

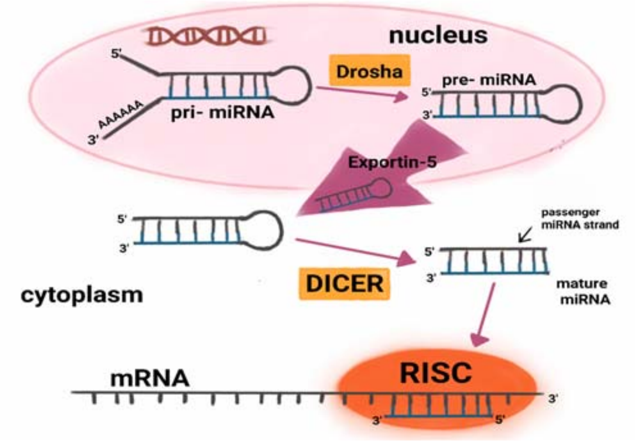
nucleus
5'
AAAAAA
3'
pri- miRNA
Drosha
pre- miRNA
5'
3'
Exportin-5
5'
3'
passenger miRNA strand
5'
3'
mature miRNA
cytoplasm
DICER
mRNA
RISC
3'
3'
5'

Figure I13. miRNA biogenesis, from the precursors pri-miRNA and pre-miRNA in the nucleus to the mature cytoplasmic form of miRNA, that can incorporate to RISC complex to inhibit the expression of its target genes (see text for details).

miRNA are transcribed as long capped and poly-adenylated primary-miRNAs (pri-miRNA). This pri-miRNA is cleaved by the RNase III enzyme Drosha, generating a precursor-miRNA (pre-miRNA), a 60-100 nt hairpin structure. Next, the pre-miRNA leaves the nucleus and is cleaved by DICER, leading to a mature miRNA molecule. This molecule is a short (usually 20 to 24-bp) double-stranded RNA (dsRNA) with two overhanging nucleotides at the 3' ends. Mature miRNA is loaded into a large protein complex named RNA-induced silencing complex (RISC) which presents the guide strand to its target mRNAs while the passenger miRNA strand is degraded. The RNA-induced silencing complex promotes association of miRNA with the specific regions in the target genes (usually in the 3' untranslated region) to inhibit protein expression (Davis-Dusenbery *et al.*, 2011).

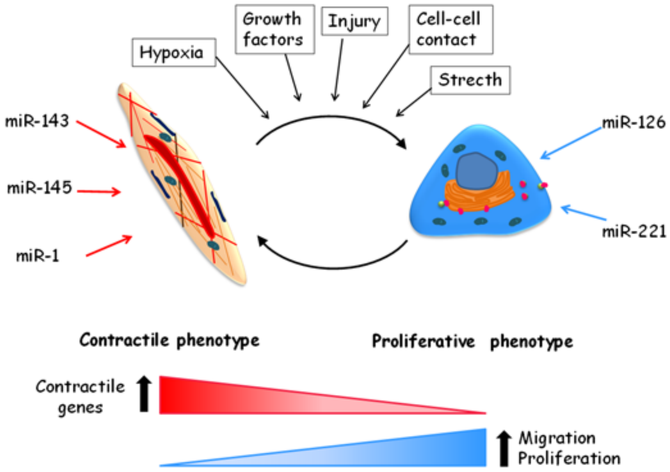
Hypoxia
Growth factors
Injury
Cell-cell contact
Strecth
miR-143
miR-145
miR-1
miR-126
miR-221
Contractile phenotype
Proliferative phenotype
Contractile genes
Migration Proliferation

Figure I14. Regulation of VSMC phenotype by miRNAs, modified from (Davis-Dusenbery, Wu, & Hata, 2011), see text for more details.

An important role of miRNAs in the regulation of proliferation and VSMC differentiation has been demonstrated through experiments with SM-Dicer knockout mice. These mice show extensive internal hemorrhage and embryonic lethality due to reduced cellular proliferation, decreased medial thickness and nearly abolished contractile force of the vessels (Davis-Dusenbery *et al.*, 2011). These results suggest that miRNAs are essential not only for the differentiation of VSMCs during early development but also for the maintenance of VSMCs in the adult. In fact, there is a long list of miRNAs that have been shown to play relevant roles in VSMC phenotypic modulation (either activating or inhibiting it Table I1) (Davis-Dusenbery *et al.*, 2011). Among miRNA relevant for to PM, it is known that miRNAs mir143, mir145 and mir1 promote the contractile phenotype while mir221 and mir126 associated with the dedifferentiated phenotype (Figure I14). For other miRNAs involved in this process, such as mir21, the available data is contradictory.

Contractile phenotype		**Proliferative phenotype**	
miRNAs	**Target Genes**	**miRNAs**	**Target Genes**
miR-1	Pim1	miR-21	PTEN, Bcl-2
miR-15/16	YAP	miR-24	Trb3
miR-21	PDCD4	miR-26a	SMAD1
miR-132	LRRFIP-1	miR-31	CREG
miR-133	Sp-1	miR-96	Trb3
miR-142-3p	DOCK6	miR-142-5p	BTG3
miR-143	Elk-1, Versican, PKC-e , PDGF-Ra	miR-146a	KLF4
miR-145	ACE, KLF4/5, CamkIId, MYOCD, Fascin	miR-208	p21
miR-153	IGF-1R	miR-221	p27 (Kip1)
miR-195	Cdc42, CCND1, FGF1	miR-222	p57
miR-203	Ab11, p63	miR-223	Mef2c, RhoB
miR-204	SHP2		
miR-223	IGF-1R		
miR-424/322	Calumenin, CCND1		
miR-490-3p	PAPP-A		
miR-638	NOR1		
miR-663	JunB		
Let-7d	KRAS		

Table I1. miRNAs related to VSMC phenotypic modulation (Zhang *et al.*, 2016).

3.3.a. miR-143 and miR-145

miR-143 and miR-145 are very well characterized in the vasculature and are known as critical regulators of VSMC differentiation. They express together forming a small cluster and show abundant expression in vascular wall and in freshly isolated VSMCs, being downregulated in neointimal lesions. miR-145 targets and inhibits the two transcription factors Kruppel-like factor 4 and 5. (KLF4, KLF5), which inhibit myocardin expression. In addition, miR-143 promotes myocardin actions by repressing ELK-1, a transcription factor who competes with myocardin for its docking with SRF (Albinsson & Sessa, 2011; Kasza, 2013; Zhang *et al.*, 2016).

Unlike VSMC specific Dicer-KO mice, miR-143/145-KO animals are viable through adulthood, suggesting that additional miRNAs are required to provide robust control of VSMC differentiation during development and in response to cellular stimuli (Albinsson & Sessa, 2011).

3.3.b. miR-1

miR-1 expression is induced by myocardin in VSMC, and mediates the inhibitory effects of myocardin on VSMC proliferation via down-regulation of Pim-1, a gene encoding an oncogenic Ser/Thr kinase. Pim-1 is required for injury-induced neointima formation and VSMC proliferation (Chen *et al.*, 2011). miR-1 also targets KLF4. The observation that both miR-1 and miR-145 repress KLF4 during VSMC differentiation indicates that repression of inhibitory pathways by multiple miRNAs is critical for VSMC differentiation (Davis-Dusenbery *et al.*, 2011).

3.3.c. miR-21

miR-21 can induce both VSMC proliferation and differentiation (Albinsson & Sessa, 2011). Increased expression of miR-21 induces proliferation and reduces apoptosis by targeting phosphatase and tensin homolog (PTEN) and increases the expression of B cell lymphoma 2 (BCL2) (Ji *et al.*, 2007). PTEN blocks PI3K signaling by inhibiting PIP3 dependent processes such as the membrane recruitment and activation of AKT, therefore inhibiting cell survival, growth, and proliferation (Hopkins *et al.*, 2014). The BCL-2 family of proteins, is the key regulatory cascade governing mitochondrial apoptosis, acting itself as an anti-apoptotic protein (Davids, 2017).

However, VSMC stimulation with some growth factors such as transforming growth factor beta (TGF-b) induce contractile phenotype in VSMCs mediated by miR-21. In this case, miR-21 increases expression of SM markers (Davis *et al.*, 2008). The dual action of miR-21 in promoting both differentiation and proliferation suggest that its sets of target genes depends on the cellular context (Davis-Dusenbery *et al.*, 2011).

3.3.d. miR-221

Mature miR-221 exerts multiple effects on the phenotype of VSMCs, including increased proliferation and migration and reduced expression of SM genes. miR-221 promotes proliferation through the repression of the cyclin-dependent kinase inhibitor p27Kipl. Overexpression of miR-221 is accompanied by reduction of myocardin expression. The mechanism by which miR-221 increase migration is still unknown (Davis-Dusenbery *et al.*, 2011).

3.3.e. miR-126

miR126 is a miRNA highly expressed in ECs that modulates vascular development, vascular integrity and angiogenesis.(Zhou *et al.*, 2013). In fact, miR126 KO animals show leaky vessels, hemorrhaging and partial embryonic lethality, due to loss of vascular integrity (Fish *et al.*, 2008; Wang *et al.*, 2008).

miR-126 promotes vascular endothelial growth factor (VEGF) signaling by targeting the Sprouty-related protein SPRED1 and PI3K regulatory subunit 2 (PIK3R2/p85-β). SPRED1 and PIK3R2 negatively regulate growth factor signaling via independent mechanisms. SPRED1 functions by inhibiting growth factor-induced activation of the MAPK pathway while PIK3R2 is thought to negatively regulate the activity of PI3K (Fish *et al.*, 2008).

miRNAs can be packaged in membranous vesicles that change in numbers, cellular origin, and composition depending on the disease state. Accumulating evidence support the notion that these vesicles (exosomes) are not just by-products resulting from cell activation or apoptosis. Instead, they constitute a novel type of cell–cell mechanism of communication (Zampetaki *et al.*, 2010). In the case of miR126, it has been proposed that it serves as a paracrine mediator secreted by the ECs to act on VSMC, where it modulates gene expression and function towards proliferative phenotype. miR-126 regulates VSMC gene expression by targeting Forkhead box O3 (FOXO3), BCL2 and IRS-1 mRNAs (Zhou *et al.*, 2013).

miR-126 has a modulatory role in vascular pathogenesis as its expression is increased after angioplasty in rat carotid artery and intimal hyperplasia in mouse carotid artery after ligation (Zhou *et al.*, 2013). In agreement with this, miR-126 KO-induced mice shows a decreased neointima formation. Thus miR-126 contributes to IH and VSMCs dedifferentiation despite showing some beneficial effects on endothelial functions (Zhou *et al.*, 2013).

Loss of miR-126 is consistently associated with Diabetes mellitus. The miR-126 content in exosomes is reduced in a glucose-dependent fashion. Because these particles can be transferred to other cell types, low plasma levels might result in reduced delivery of miR-126 to monocytes, contributing to VEGF resistance and endothelial dysfunction and elevating the risk of symptomatic and subclinical peripheral artery disease (Zampetaki *et al.*, 2010).

3.4. Ion channels in VSMC phenotypic modulation

As described in the previous sections, the phenotypic switch of VSMCs implies a profound change in the physiological capabilities of the cells. The most evident changes are the loss of the contractile ability, the activation of the proliferative machinery and the acquisition of migratory competence. While a substantial amount of work has been devoted to study the factors that promote this process, focusing mainly in the transcriptional regulation of contractile proteins, the characterization of the changes in expression of other pro-proliferative or pro-migratory proteins such as ion channels or pumps is relative scant. Expression of ion channels in the contractile phenotype is particularly suited to control membrane potential and Ca^{2+} entry to activate contraction (Wamhoff *et al.*, 2006). Conversely, expression of ion channels in the proliferative phenotype changes to accommodate the new status of the cell, facilitating proliferation, migration and/or secretory functions (House *et al.*, 2008; López-López *et al.*, 2018).

Initial events in the phenotypic switch include a significant loss of BK_{Ca} and VDCCs, and gain of the intermediate conductance Ca^{2+}-dependent channels (IK) and the Ca^{2+} entry through TRPC (transient receptor potential canonical) channels (Neylon, 2002; Köhler *et al.*, 2003). Both, IK and TRPC channels are essentially voltage-independent, so that the role of membrane potential becomes very different in both phenotypes. In the contractile phenotype, depolarization opens VDCC channels, promoting Ca^{2+} influx for contraction, and the increase of Ca^{2+} activates BK_{Ca} channels allowing repolarization. Conversely, in proliferative phenotype, changes in $[Ca^{2+}]_i$ activate IK channels, which enable membrane hyperpolarization. This hyperpolarization increases the driving force for

Ca^{2+} influx through TRPC1, STIM1, and Orai1 which is required to activate proliferation and migration (Beech, 2007; López-López *et al.*, 2018).

3.4.a. Kv1.3 channels and VSMC phenotypic switch

Previous work from our lab (Cidad *et al.*, 2010) have studied the ion channels pattern expression in VSMCs through exploring the relative expression of 87 ion channel genes in mouse femoral artery in contractile and two proliferative VSMC models: an *in-vivo* model of intimal hyperplasia, and an *in-vitro* model using cultured VSMCs. This study stated that only two genes were overexpressed in both proliferative models: Kv1.3 (KCNA3) and its accessory subunit Kvβ2 (KCNAB2) (Figure I15).

Moreover, the upregulation of Kv1.3 mRNA expression correlated with an increased functional expression of Kv1.3 channel proteins. Electrophysiological studies in proliferative VSMCs showed an increased functional expression of Kv1.3. In addition, selective blockers of Kv1.3 such as PAP-1 or margatoxin (MgTx) inhibited VSMCs migration and proliferation (Cidad et al., 2010).

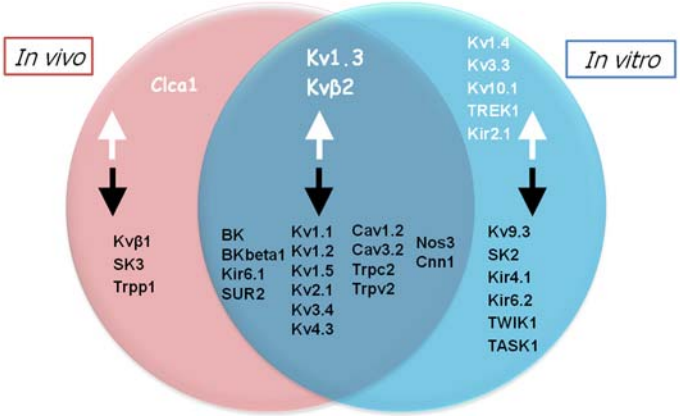

Figure I15. Venn diagram shows genes exhibiting significant change expression in proliferative VSMCs compared to contractile cells from mouse endoluminal lesion samples (*in vivo*) and in cultured VSMCs *(in vitro)* (Cidad et al, 2010).

Interestingly, Kv1.3 increased expression paralleled an enormous decrease of Kv1.5 (Figure I16). Kv1.5 is the most abundantly expressed Kv1 channel in contractile VSMC while Kv1.3 channel is the main Kv1 channel in proliferative phenotype (Cidad *et al.*, 2012). Of interest, the switch from quiescence to activation and proliferation in several nonvascular preparations in which Kv1.3 is upregulated is often accompanied by the decrease in Kv1.5 channels. Altogether, a very attractive hypothesis to explain and understand PM is that the control of

Kv1.3/Kv1.5 ratio (and not simply Kv1.3 upregulation) could be what determines the phenotypic switch of VSMCs.

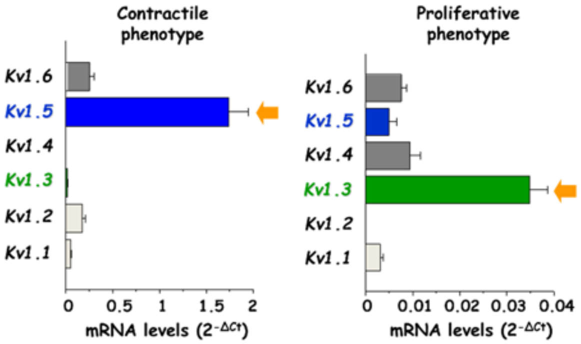

Figure I16. mRNA levels of all the members of the Kv1 family of voltage-dependent K channels in contractile and proliferative VSMC from mouse femoral arteries are expressed as 2 $^{-\Delta Ct}$, normalized to the endogenous control RPL18. (Modified from Cidad P., et al., 2012).

The same pattern expression of Kv1.3 and Kv1.5 has been observed in different vascular beds including from mice and human vessels, (Figure I17), so it can be concluded that the Kv1.3 to Kv1.5 ratio can be used to define VSMC phenotype (Cidad *et al.*, 2015).

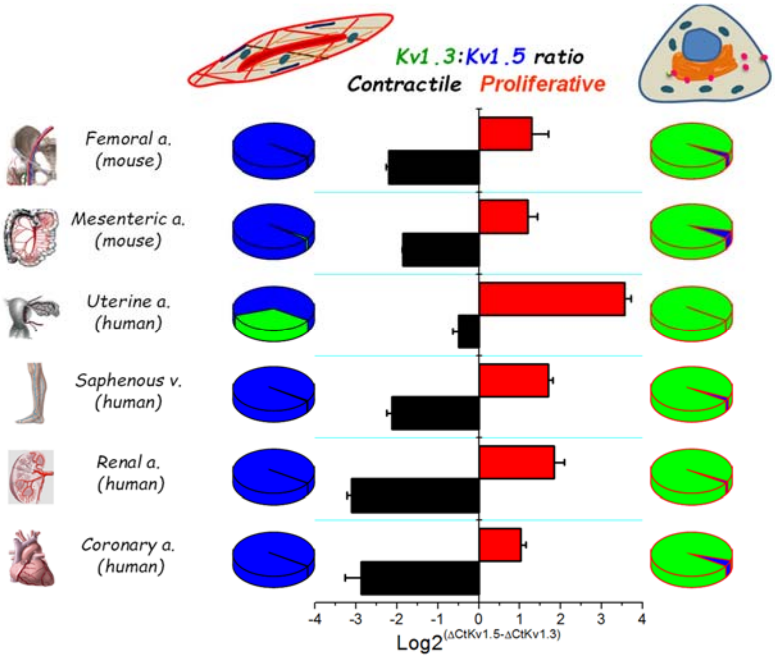

Figure I17. Kv1.3 and Kv1.5 mRNA pattern expression in different human and mouse vascular beds. The pie charts show the relative abundance of Kv1.5 (blue) and Kv1.3 (green) in contractile and proliferative VSMC from the indicated vascular beds. The bars plot shows the Kv1.3/Kv1.5 ratio in a log scale, in contractile (black bars) and proliferative (red bars) VSMCs. Modified from (Cidad *et al.*, 2012) (Pilar Cidad et al., 2015).

3.4.b. Molecular mechanisms linking Kv1.3 to proliferation

Kv1.3 overexpression in HEK293 cells increase proliferation, and the use of selective Kv1.3 blockers inhibit this increase (Cidad *et al.*, 2012). Several evidences indicate that the effect of Kv1.3 on proliferation is not dependent on Kv1.3-induced changes in membrane potential (Cidad *et al.*, 2012). Characterization of the molecular mechanisms involved using Kv1.3 mutants indicated that overexpression in HEK293 cells of a non-conducting Kv1.3 mutant (Kv1.3 WF), induces cell proliferation at the same rate as WT Kv1.3, while a voltage-insensitive Kv1.3 mutant does not induce proliferation (Cidad *et al.*, 2012). Additional mutagenesis experiments demonstrated that the molecular determinants for Kv1.3-induced proliferation are located at the carboxyl terminal domain, where the point mutation to Alanine of two individual residues (Tyr-447 and Ser-459) abolished the effect of Kv1.3 in proliferation (Jiménez-Pérez *et al.*, 2016). The proposed mechanism suggests that voltage-induced conformational changes of Kv1.3 channel regulate the accessibility of Tyr-447 and Ser-459 phosphorylation sites, which in turn are substrates of MEK-ERK. Thus, activation of Kv1.3 channel provide docking sites for potentiation MEK/ERK signaling pathway activity (Figure I18) (Jiménez-Pérez et al., 2016).

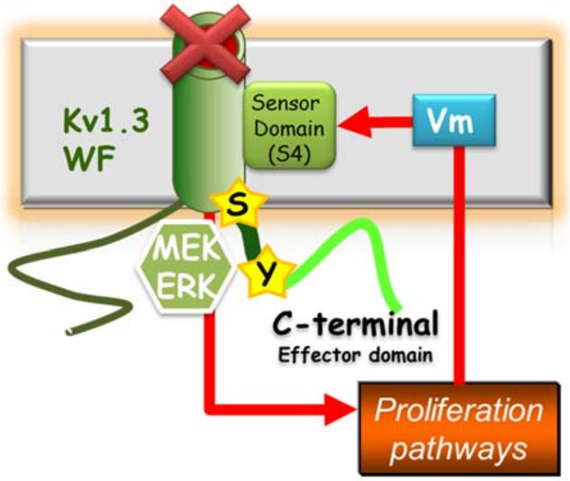

Figure I18. Proposed mechanism for Kv1.3 induced proliferation using HEK cells overexpression of Kv1.3 mutant channels. Activation of Kv1.3-induced proliferation requires the C-terminal domain of the channel, and at least two phosphorylatable residues (Ser-459 and Tyr--477), which became accesible upon voltage-dependent comformational change of the channel and can activate MEK/ERK signaling pathways to promote proliferation (Jiménez-Pérez *et al.*, 2016).

4. Phenotypic modulation and intimal hyperplasia

Vascular remodeling defines the structural changes in blood vessel geometry that occur in response to long-term physiologic alterations in blood flow or in response to vessel wall injury. The process of remodeling, which can be initially an adaptive response to long-term hemodynamic alterations, may eventually become maladaptive, leading to impaired vascular function. Vascular remodeling associates with several common cardiovascular disorders such as hypertension, atherosclerosis, and restenosis after angioplasty or coronary bypass. Although the underlying pathophysiological processes are complex, a common and essential feature of all of them is abnormal VSMC proliferation, migration and extracellular matrix secretion (Bagmet, 2002). Here we will focus on the restenosis produced after vascular surgery, due to intimal hyperplasia.

4.1. Mechanisms of intimal hyperplasia

Intimal hyperplasia (IH), also known as accelerated atherosclerosis, is the main limiting factor for the long-term success of vascular interventions such as coronary revascularization and solid-organ transplants (Ip *et al.*, 1990). Intimal hyperplasic lesions are the pathological lesion underlying the restenosis after angioplasty, the bypass grafting occlusion and the transplant vasculopathy.

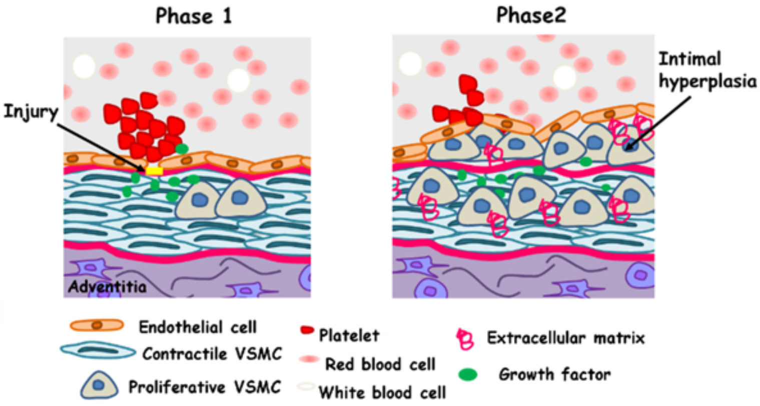
Phase 1
Phase2
Injury
Adventitia
Intimal hyperplasia
Endothelial cell
Contractile VSMC
Proliferative VSMC
Platelet
Red blood cell
White blood cell
Extracellular matrix
Growth factor

Figure I19. Scheme of the two phases of intimal hyperplasia formation described in the text.

In all these cases, vascular injury activates the vessel repair mechanism in a process that can be divided in two phases (see Figure I19):

1) Thrombosis and inflammation. Endothelial lesion leads to platelets aggregation and thrombus formation, initiating the release of growth factors like PDGF and other molecules. These molecules trigger the VSMC phenotypic modulation which lead the next phase,

2) VSMC migration, proliferation and extracellular matrix secretion. These processes culminate in a fibro-cellular mass composed of secreted glycoproteins, dedifferentiated VSMCs and local inflammation, forming the intimal hyperplasic lesion (Dhalla *et al.*, 2011).

4.2. Restenosis after angioplasty.

Angioplasty, also known as percutaneous transluminal angioplasty (PTA), is a minimally invasive endovascular procedure used to widen narrowed or obstructed arteries using a deflated balloon that when inflated at the obstruction site forces expansion of the blood vessel and the surrounding muscular wall, allowing an improved blood flow. A stent may be inserted at the time of ballooning to ensure the vessel remains open, and the balloon is then deflated and withdrawn. This technique has the advantage of lower risk compared to other surgical techniques (Vlodaver *et al.*, 2012), but has a higher incidence of restenosis, even with the use of stents, anti-thrombotic and/or anti-proliferative drugs. Nowadays, drug-eluting stent (containing mTOR inhibitors) are used to prevent IH. However the anti-proliferative effect of mTOR also affects re-endothelization, delaying arterial healing and favoring stent thrombosis. Clearly, there is a need from improved treatments against IH, as all these complications have a high socio-economic impact. Coronary PTA is one of the most common interventions for the treatment of coronary artery disease.

4.2.a. Structure of coronary arteries

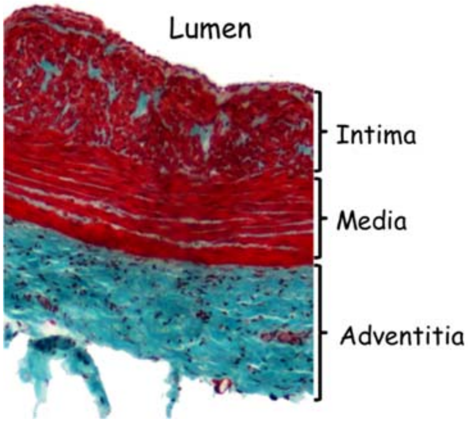

Figure I20. Masson trichrome stain of a pig coronary artery, indicating the layers.

Coronary arteries supplies oxygenated blood to the heart as they lie on the surface of the heart in the epicardium surrounded by adipose tissue. (Ross & Pawlina, 2007). Coronary arteries are medium-sized muscular arteries, with walls usually thicker than those of comparable arteries on the upper o lower limbs because of the large amounts of circular VSMC layers in the tunica media. The subendothelial layer of the tunica intima of younger people is inconspicuous, but it progressively thickens by increasing amounts of VSMCs and fibroelastic tissue with aging. The internal elastic membrane is well developed, although it may be fragmented, duplicated, or focally lost in older individuals. The “loose” consistency of the tunica adventitia is reinforced by longitudinal bundles of collagen fibers that allow for continuous changes of the vascular diameter. Atherosclerotic changes in coronary arteries that restrict blood flow and oxygen supply to cardiac muscle lead to ischemic heart disease (Ross & Pawlina, 2007).

4.3. Bypass grafting occlusion.

When angioplasty is not possible, revascularization with vein grafts is standard surgical therapy for occlusive arterial diseases. This technique is known as coronary artery bypass grafting (CABG, Figure I21). Most patients undergoing CABG have the so called three-vessel disease (left, right and circumflex coronary arteries (Vlodaver *et al.*, 2012). Autologous saphenous vein grafts and mammary artery are used in the majority of graft procedures. Though arterial grafts exhibit superior patency rate, saphenous vein is most commonly used as it is easier to harvest, and its length allows for making of multiple grafts. However, up to 50% of these grafts will be occluded during the first decade after surgery, as a result of IH which is exacerbated due to hemodynamic changes (Onuki *et al.*, 2008).

.

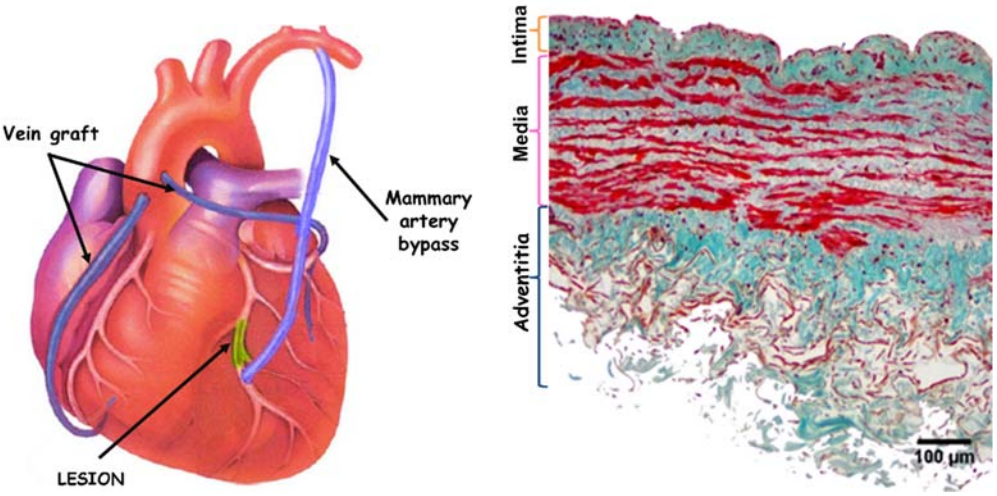

Figure I21. Scheme of CABG using both vein grafts and internal mammary artery grafts (left). The right panels shows a section of a human saphenous vein with Masson trichrome stain.

Neointimal graft-wall thickening is an adaptive reaction that provides hemodynamics stability to the graft but leads to up-regulated expression of growth factors, cytokines, and adhesion molecules by the VSMCs. In addition to the pro-inflammatory behavior of neointimal VSMCs, there is dysfunction of the overlying endothelium (Mann *et al.*, 1999). Intimal hyperplasia can be further complicated by the concomitant development of atherosclerosis and thrombosis (Murphy & Angelini, 2004). At present, there are not effective pharmacological interventions for preventing graft occlusion (Onuki *et al.*, 2008).

4.3. a. Structure of saphenous vein

The greater saphenous vein remains the primary source of free grafts. If it is absent or inadequate, the lesser saphenous vein can be used. The main advantages of the vein graft include that it provides excellent blood flow to the target arteries due to its lower flow resistance. The disadvantage of vein graft is its poor long-term patency rate. On average about 50% grafts would develop significant atherosclerotic disease and/or stenosis in 10 years. (Vlodaver *et al.*, 2012).

The great saphenous vein is a long subcutaneous vein of the lower limb that originates in the foot and drains into the femoral vein just below the inguinal ligament. This vein is considered as a muscular vein because of the presence of an unusual amount of smooth muscle. In addition to the thick circular arrangement of VSMCs in its tunica media, the great saphenous vein possesses numerous longitudinal VSMC bundles in the intima and in the well-developed adventitia (red labelling in the Mason trichrome in Figure I21). A thin, poorly developed internal elastic membrane separates the tunica intima from the media (Ross & Pawlina, 2007).

4.3. b. Structure of mammary artery

Arterial grafts for CABG can use mammary, radial, gastroepiploic, inferior epigastric or splenic arteries. All are conduit arteries, being the mammary artery the most suitable graft, as it shows superior long-term results due to its anatomic and functional properties. Mammary artery is a muscular artery with a well-formed internal elastic laminae, more developed than in other conduit arteries of similar size. This elastic structure favors higher long-term patency and less incidence of atherosclerosis and occlusion rate.(He, 1999). However, patients with multiple-vessel disease may lack sufficient arterial conduits for grafting (Solanes *et al.*, 2004).

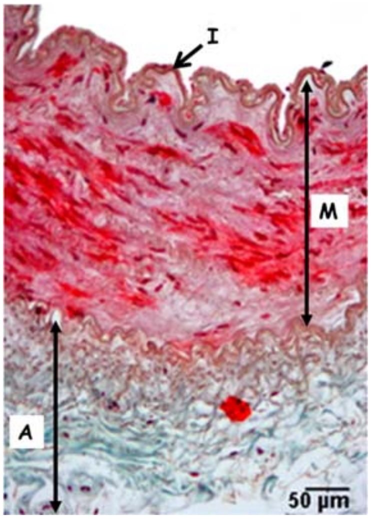

Figure I22. Human mammary artery, labeling intima, media and adventitia layers (I,M,A).

The mammary artery originates from the subclavian artery. The tunica intima consists of an endothelial lining with its basal lamina, a sparse subendotelial layer of connective tissue and a prominent internal elastic membrane Figure I22. The thickness of the tunica intima varies with age and other factors. In young children, it is very thin. In young adults, the tunica intima accounts for about one-sixth of the total wall thickness. In older adults, the tunica intima may be expanded by lipid deposits, often in the form of irregular "fatty streaks."

The tunica media is composed of VSMC arranged in a spiral fashion, elastic material and collagen fibers. The tunica adventitia is mainly composed of collagen fibers. However, a concentration of elastic material immediately adjacent to the tunica media is often present, constituting the external elastic membrane (Ross & Pawlina, 2007).

4.4. Transplant vasculopathy.

Although major improvements have been made in the prevention and treatment of acute transplant rejection, accelerated post-organ allograft vasculopathy still limits the long-term success of heart or renal transplantation (Schmauss & Weis, 2008). Transplant vasculopathy manifests as a unique and unusually aggressive form of arterial disease that differs from traditional atherosclerosis. It is believed to be caused by immunologic mechanisms that combine with non-immunologic factors to cause endothelial injury, resulting in SM proliferation and intimal thickening. This IH leads to vessel obstruction and allograft failure (Aranda Jr. & Hill, 2000).

In contrast with the other restenosis mentioned before (restenosis after angioplasty, bypass grafting occlusion), in transplant vasculopathy there is interaction between immunological and non-immunological factors, and for many years it was attributed only to immunological factors. However, immunosuppressive therapies have not reduced the incidence of the restenosis. On the contrary, the incidence of IH augmented with some immunosuppressors like cyclosporine (Dhaliwal & Thohan, 2006). In-vivo studies using MMF (mofetilmicofenolato), a drug that combines immunosuppressive with antiproliferative actions, provides superior protection compared to other immunosuppressive drugs (Gibson & Hayden, 2007). The diffuse characteristic of transplant vasculopathy limits the use of revascularization procedures.

4.5. Experimental in vivo models of intimal hyperplasia.

Several diverse strategies have been explored to prevent restenosis after angioplasty, bypass grafting occlusion and transplant vasculopathy. These include pharmacological agents, cytostatic drugs, sheaths, internal stents, drug eluting stents, gene transfer, and cell therapy with stem/progenitor cells. Prevention of IH, however, has proven elusive despite many trials and still represents a major clinical problem that needs to be urgently resolved.

Animal models are a crucial means of testing new potential alternative treatments. It is difficult, if not impossible, to study the complexity of the extra- and intra-cellular mechanisms underlying IH formation and associated vasculopathy in man. Thus, animal models are an essential pre-clinical means of studying the pathophysiology of restenosis following vascular surgery procedures (Jeremy & Thomas, 2010).

Mice models. Mice are attractive experimental models. They are inexpensive, easy to maintain, available as purebred lines, and amenable to most surgical interventions (Mehta *et al.*, 1996). The most commonly used procedures to induce arterial injury in mice are carotid artery ligation with cessation of blood flow and mechanically-induced denudation of endothelium in the carotid or the femoral arteries. Both procedures result in IH after two to three weeks (Hui, 2008). Although these are more representative models of angioplasty rather than bypass grafting, they are still relevant to the latter, since IH is a common denominator event in both scenarios (Jeremy & Thomas, 2010).

In the arterial ligation model, blood flow in the common carotid artery is disrupted by ligation. This is a model originally described by Kumar and Lindner (Kumar & Lindner, 1997), in which there is a complete disruption of blood flow in the common carotid artery by ligation near the bifurcation, thus causing the lumen to decrease to ≈20% of its original size. Because the ligated vessel was still subject to arterial blood pressure, pulsation persisted in these vessels, and the hemodynamic changes associated to the loss of laminar flow activate formation of neointima. Two mechanisms contribute to luminal narrowing in this model: one was by neointima formation and the other by constriction of the vessel diameter, which initially represents a vasoactive response of the endothelium but at 2-4 weeks becomes a fixed change in the vessel wall structure. Thrombus formation is not observed with this technique, as the endothelium is not injured. (Kumar & Lindner, 1997). One advantage of this model is its reproducibility due to the ease of operation. However, the disadvantage of this model is that it does not resemble the physiological setting of some vascular interventions such as PCA. It has been reported that the mechanism responsible for neointimal formation due to arterial ligation may be different from neointimal formation due to endothelial denudation (Hui, 2008).

A ***mechanically-induced endothelial denudation*** model was initially developed by Lindner and colleagues by passing a flexible guide wire through the carotid artery three times (Lindner *et al.*, 1993). The removal of the EC layer results in the covering of the denuded surface with a platelet monolayer and the activation of the underlying medial VSMCs. Neointimal formation is typically observed within 2 weeks after injury. The advantage of this experimental procedure is its resemblance to angioplasty and its maintenance of normal blood flow. The disadvantage of this procedure is the relatively challenging operational procedure, which leads to difficulty in achieving reproducible results. In many instances, insertion and passage of the guide wire through the vessel wall results in tearing and disruption of the elastic lamina, thus causing exuberant VSMC response (Hui, 2008).

Porcine models. In spite of their size and expense of maintenance, these models have proven useful in all aspects of vascular research owing to their considerable physiological, morphological and histological similarity to humans. The animal's size becomes an advantage in the evaluation of diagnostic and surgical procedures prior to their application in human, as in the case of novel drug-eluting stents implanted in coronary arteries (Mehta *et al.*, 1996). Also, because of its size, arterial type (muscular artery) and ease of surgical access, the porcine femoral artery is a good model to study arterial transplant vasculopathy (Solanes *et al.*, 2005).

5. Vascular diseases as risk factors for intimal hyperplasia

As mentioned, most often IH lesions will be taking place in already diseased vessel, with the underlying pathologies determining evolution and prognosis. For that reason, it is necessary to consider some of the pathologies that represent vascular risk factors and how they can affect the development of vascular disease and the response to treatment. We will define briefly some of the most common pathologies associated to increased cardiovascular risk.

5.1. Diabetes

Diabetes is a chronic disease characterized by impaired glucose intake by cells leading to hyperglycemia, as a consequence of either impaired insulin formation (type1, T1DM) or insulin resistance (type 2, T2DM). In the last decades, according to the World Health Organization, diabetes prevalence had risen from 108 million in 1980 to 422 million in 2014.

Diabetes confers a substantially increased risk for cardiovascular morbidity and mortality. Even with a good blood glucose control, diabetic patients have poorer cardiovascular outcomes than nondiabetic individuals. T2DM exacerbates traditional, modifiable risk factors for vascular disease; each additional risk factor caused a greater, incremental rise in risk among individuals with diabetes than those without (Vlodaver *et al.*, 2012). Adults with T2DM but without known cardiac disease have a similar risk of a cardiovascular event as nondiabetic adults with a history of a prior myocardial infarct. Although these risks can be substantially reduced by controlling risk factors, less than 10% of patients with diabetes reach their glucose, blood pressure, and cholesterol targets.

Hyperglycemia contributes to cardiovascular risk in patients with diabetes, but this is not the only factor affecting cardiovascular diseases. In fact, while large clinical trials have shown that early glycemic control can retard microvascular disease (neuropathy, retinopathy and nephropathy) in T2DM (Brown *et al.*, 2010), macrovascular complications persist particularly in patients with active coronary heart disease (Skyler *et al.*, 2009). Undiagnosed or uncontrolled hyperglycemia can leave an early imprint on vascular cells, the so called “legacy effect” or “metabolic memory” (Cooper, 2009).

The metabolic memory refers to alterations induced by hyperglycemia that remains after blood glucose normalization. Many different mechanisms have been proposed as involved in the metabolic memory, including oxidative stress, non-enzymatic glycation of proteins, epigenomic changes and chronic inflammation.

At early stages of diabetes, hyperglycemia increase oxidative stress and advanced glycation products (AGEs) which are responsible of vascular damage. After that, a persistent respiratory chain protein glycation and DNA damage in the mitochondria could generate a hyperglycemia-independent vicious cycle in which oxidative stress s self-supporting and AGEs increase this process. Also, inflammatory processes induced by receptor biding of AGEs or oxidative stress induce changes in the composition and structure of the extracellular matrix (fibrosis). In addition, hyperglycemia can induce change of epigenetic which include histone modifications, DNA methylation and miRNA alterations, mainly through the involvement of inflammatory genes. All of these modifications might persist over time after the normalization of the glucose levels, which explain the long-term harmful effect of metabolic memory (Prattichizzo *et al.*, 2016; Testa *et al.*, 2017; Cavalli & Heard, 2019).

Clinical data unequivocally illustrate the harmful nature of metabolic memory, leading to research into the underlying mechanisms that define the T2DM epigenetic signature (Skyler *et al.*, 2009; Intine & Sarras, 2012; Reaven *et al.*, 2019).However, significant knowledge gaps exist concerning the precise molecular and biochemical mechanisms involved and hence the optimal strategies to prevent or ameliorate macrovascular disease in this vulnerable population.

5.2. Insulin resistance

Insulin is produced by the pancreas in response to hyperglycemia and stimulates glucose use in various tissues. In the skeletal muscle and adipose tissue, insulin stimulates glucose uptake by translocation of the GLUT4 glucose transporter to the cell surface. In the skeletal muscle and liver, insulin stimulates the synthesis of glycogen from glucose and inhibits glycogenolysis. In the liver, insulin also decreases hepatic gluconeogenesis, preventing an influx of more glucose into the bloodstream. In adipose tissue, insulin inhibits fat breakdown, or lipolysis, and stimulates glucose uptake. The net effect of all of these changes is to increase glucose uptake and increase the conversion of glucose into the storage molecules, glycogen or fat. Insulin resistance occurs when there is a decrease in the responsiveness of peripheral tissues (skeletal muscle, fat and liver) to the effects of insulin, and circulating glucose levels remain high. Insulin resistance is a powerful predictor of T2DM, and hyperinsulinemia is a surrogate marker for insulin resistance.

Physiological insulin signaling occurs following the binding of insulin to the insulin receptor that results in activation of two parallel pathways: the PI3K pathway and the MAPK pathway. The effects of these pathways are tissue specific. For example, in vascular ECs, PI3K/AKT activates endothelial nitric oxide synthase (eNOS), while MAPK activation induces VSMC growth and proliferation. In skeletal muscle and adipose tissue, PI3K/AKT stimulates membrane translocation of GLUT4, increasing glucose uptake (Johnstone & Veves, 2005).

Insulin resistance associates with impaired PI3K/AKT signaling, whereas MAPK pathway is not affected, leading to an imbalance between these two parallel pathways. Inhibition of the PI3K/AKT pathway leads to endothelial dysfunction, while MAPK pathway is hyperactive leading to increased mitogenic stimulus to VSMCs. These effects on ECs predispose to atherosclerosis.(Huang, 2009), but the direct effects on VSMC are not well characterized.

5.3. Hypertension

Hypertension is defined as a persistently elevated systolic blood pressure ≥140 mmHg and a diastolic blood pressure ≥90 mmHg or both, although several categories of high blood pressure are typified (O’Shea *et al.*, 2017). In most patients with hypertension, no clear etiology is identified, this is referred to as essential hypertension, which accounts for ~ 90–95% of all cases of hypertension. A complex interaction between genetic predisposition and environmental factors predisposed to essential hypertension. The genetic inheritance is polygenic, and may only find full expression when combined with environmental factors, including obesity, high alcohol and/or salt intake, insulin resistance, aging, sedentary lifestyle, and stress among others (O’Shea *et al.*, 2017).

Hypertension is the major risk factor for premature cardiovascular disease, morbidity and mortality. There is a linear relationship between the blood pressure value and the risk of cardiovascular, cerebrovascular, peripheral vascular and kidney disease, so that rising blood pressure confers risk, even at pressures below the population average.(O’Shea *et al.*, 2017). Furthermore, studies using hypertensive mice reveal that they develop more IH after femoral artery injury (Cidad *et al.*, 2014).

5.4. Obesity

Obesity is a major risk factor for a number of chronic diseases, including diabetes, cardiovascular diseases and cancer (WHO). Visceral obesity causes a decrease in insulin-mediated glucose uptake that is related to insulin resistance. Obesity alters the levels of several adipokines secreted by adipose tissue, increasing the levels of some pro-inflammatory adipokines such as TNFα and IL-6, which contribute to insulin resistance and vascular dysfunction, and decreasing the levels of protective adipokines such as adiponectin. In addition to these adipokines, free fatty acids released from visceral fat, and other bioactive lipid intermediates act together to impair the PI3K/AKT pathway and increase oxidative stress (Huang, 2009).

5.5. Metabolic syndrome

Metabolic syndrome is a constellation of interrelated risk factors that directly promote the development of atherosclerotic cardiovascular disease (Grundy *et al.*, 2005). These metabolic alterations include glucose intolerance, insulin resistance, central obesity, dyslipidemia and hypertension, all well documented risk factors for cardiovascular disease. These conditions co-occur in an individual more often than might be expected by chance (Eckel *et al.*, 2005). In addition, patients with metabolic syndrome also are at increased risk for developing T2DM.

The TableI2 summarizes four of the most commonly used definitions of metabolic syndrome. In the first definitions, developed by the World Health Organization (WHO) and the European Group for the Study of Insulin Resistance (EGIR) hyperinsulinemia or insulin resistance are absolute requirements for metabolic syndrome. The definition of the National Cholesterol Education Program Adult Treatment Panel III (NCEP ATPIII) has no absolute requirements and the International Diabetes Foundation (IDF) requires central obesity (Huang, 2009).

All agree on the essential components: glucose intolerance, obesity, hypertension and atherogenic dyslipidemia (Eckel *et al.*, 2005) (Grundy *et al.*, 2005). Moreover, individuals with these characteristics commonly manifest a pro-thrombotic and a pro-inflammatory state as well.

	NCEP ATP III(2005)	**WHO (1998)**	**EGiR (1990)**	**IDF(2005)**
Absolutely required	none	Insulin resistance	Hyperinsulinemia	Central obesity
Criteria	Any 3 of the 5 criteria below	Insulin resistance or diabetes plus 2 of the 5 criteria below	Hyperinsulinema, plus 2 of the 4 criteria below	Obesity, plus 2 of the 4 criteria below
Obesity	Waist circumference >40 inches (M), >35 inches (F)	Waist/hip ratio: >0.90(M), >0.85 (F) or BMI >30Kg/m2	Waist circumference >94cm(M), > 0.80cm (F)	Waist circumference >94cm(M), > 0.80cm (F)
Hyperglycemia	Fasting glucose >100 mg/dl	Insulin resistance already required	Insulin resistance already required	Fasting glucose >100 mg/dl
Dyslipidemia	TG >150 mg/dl	TG >150 mg/dl or HDL-C <35 mg/dl(M), <39 mg/dl(F)	TG >177 mg/dl or HDL-C <39 mg/dl	TG >150 mg/dl
Dyslipidemia (second criteria)	HDL cholesterol: <40 mg/dl(M), <50 mg/dl (F)			HDL cholesterol: <40 mg/dl(M), <50 mg/dl (F)
Hypertension	>130 mmHG systolic or >85 mmHg diastolic	>140/90 mmHg	>140/90 mmHg	>130 mmHG systolic or >85 mmHg diastolic
Other criteria		Microalbuminuria		

Table I2. Definitions of metabolic syndrome taken from (Paul L. Huang 2009).

Hypothesis

On the basis of our previous data, we concluded that the increased functional contribution of Kv1.3 is an essential element for phenotypic modulation of VSMCs. Kv1.3 blockers can prevent VSMC migration and proliferation *in vitro* and also the development of intimal hyperplasic lesions after vascular surgery *in vivo* in a mouse model of femoral artery lesion. However, the contribution of Kv1.3 to intimal hyperplasic lesions in human arteries has not been directly explored.

Hypothesis 1: ***We postulate that Kv1.3 blockers will be also capable to prevent intimal hyperplasic lesions in human vessels in organ culture***.

Previous work from our laboratory has established that changes in the expression of Kv channels couple to phenotypic modulation, so that the Kv1.3 to Kv1.5 ratio is a landmark of the VSMC phenotype. While we and others have demonstrated that Kv1.3 induces proliferative pathways in VSMCs, the exact role of Kv1.5 in the phenotypic modulation of VSMC remains unknown. Kv1.5 could have a direct effect inhibiting proliferation or could be occluding Kv1.3 pro-proliferative signals. Regardless of the mechanism.

Hypothesis 2. ***We postulate that Kv1.5 channel is a contractile marker whose overexpression can prevent phenotypic modulation.***

Intimal hyperplasia is the main long-term success limiting factor for vascular surgeries, and can be exacerbated by underlying diseases such as diabetes and metabolic syndrome. While Kv1.3 blockers have proven their efficacy inhibiting these lesions in healthy vessels of animal models of vascular lesion, their effects in diseased vessels from patients with additional risk factors are unexplored. Notably, genetic or pharmacological blockade of Kv1.3 channels exhibit anti-inflammatory, and immunomodulatory effects and improves the metabolic profile in animal models.

Hypothesis 3. ***We propose that the use of Kv1.3 blockers for the prevention of intimal hyperplasia in cardiovascular patients with coexisting diseases could have additional advantages by having beneficial effects on the associated risk factors***.

Objectives

The main goal of this thesis is to explore the mechanism linking the switch in Kv1.3/Kv1.5 ratio to phenotypic modulation and the efficacy of Kv1.3 inhibition for the prevention of intimal hyperplasia in human vessels. In addition, we will extend this study to characterize the Kv1.3/Kv1.5 ratio in vessels with underlying diseases, such as hypertension, diabetes or metabolic syndrome, in order to determine if the use of Kv1.3 blockers could improve the outcomes of vascular surgery in these vulnerable groups. The specific objectives of the work will be:

1. To characterize the effects of Kv1.3 blockade in the phenotypic modulation of human vessels in organ culture, to determine their effects on the proliferative, secretory and migratory properties of dedifferentiated VSMCs.
2. To explore the mechanisms linking the changes in the Kv1.3 to Kv1.5 ratio to the phenotypic modulation of human VSMCs. We will accomplish this using complementary approaches to analyze:
    a. The regulation of the expression of these channels upon phenotypic modulation.
    b. The effects of manipulating their expression on the remodeling both in whole vessels and in isolated VSMCs.
    c. The role of myocardin as a link between changes in channel expression and phenotypic modulation.
3. To investigate the changes in the expression and the functional contribution of Kv1.3 to the phenotypic modulation in diseased vessels. To carry out this objective, we will analyze:
    a. The effect of Kv1.3 blockers in the prevention of phenotypic modulation in vessels and VSMCs from type 2 diabetic patients.
    b. The differential miRNA expression profile in mammary arteries and VSMCs from diabetic patients, and their contribution to increased vascular remodeling.
    c. The characterization of intimal hyperplasia in a mice model of associated cardiovascular risk factors (hyperglycemia, insulin resistance, obesity and hypertension), and the effect of Kv1.3 blockers to prevent remodeling in this model.

Materials and Methods

1. Experimental samples and animal models

1.1. Human samples

Human mammary arteries (hMA), human saphenous veins (hSV) and human renal arteries (hRA) belonging to the COLMAH collection (**COL**ección de **M**uestras **A**rteriales **H**umanas;) were obtained from donors undergoing heart bypass surgery (for hMA and hSV) or nephrectomy surgery (for hRA) with the written informed consent obtained from each participant. The sample collection and the study were approved by the Hospital Ethics Committee according to the standards of the Helsinki Declaration. Information regarding COLMAH can be found at https://www.redheracles.net/plataformas/coleccion-muestras-arteriales-humanas.html. The vessels were collected in culture medium (DMEM/F-12 with HEPES Buffer) and used in the next 24 hours. An associated anonymized data file with relevant medical antecedents was also gathered with each sample.

Vessels were used for organ culture, primary VSMCs culture or saved in RNAlater (Invitrogen) for RNA and protein isolation (Figure M1).

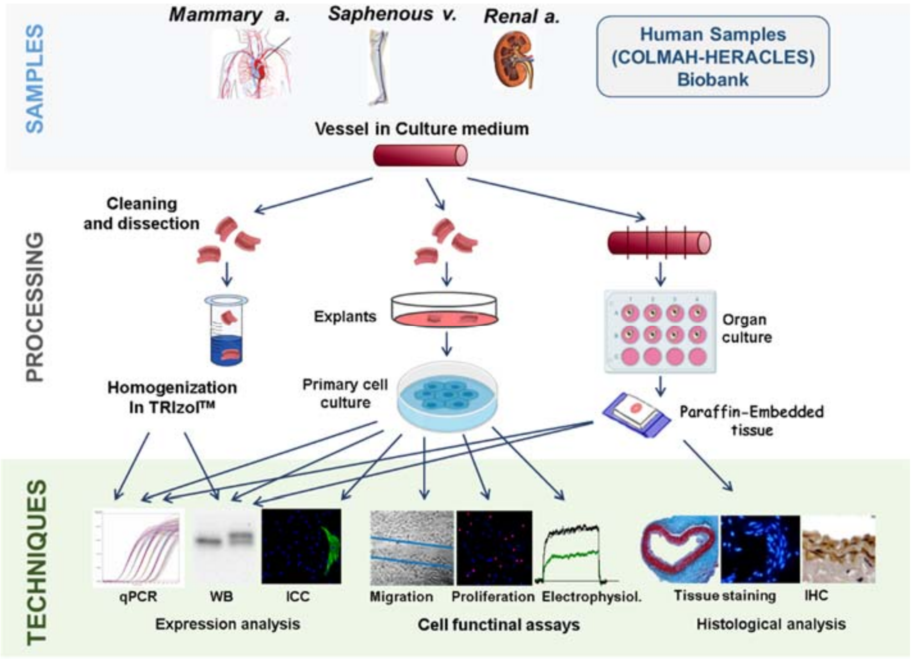
SAMPLES
Mammary a.
Saphenous v.
Renal a.
Human Samples (COLMAH-HERACLES) Biobank
Vessel in Culture medium
PROCESSING
Cleaning and dissection
Homogenization In TRIzol™
Explants
Primary cell culture
Organ culture
Paraffin-Embedded tissue
TECHNIQUES
qPCR
WB
ICC
Expression analysis
Migration
Proliferation
Electrophysiol.
Cell functinal assays
Tissue staining
IHC
Histological analysis

Figure M1. Workflow used for the human vascular samples arriving in our laboratory.

1.1.a. Primary VSMCs cultures

Primary cultures of VSMCs were obtained from explants of vessels and maintained as previously described (Miguel-Velado *et al.*, 2005). Briefly, after peeling off the adventitia layer, the endothelial layer was mechanically scraped, and the remaining media layer was cut into small fragments (1-3 mm). Explants were washed several times with sterile PBS in a laminar flow cabinet and then placed in 35 mm Petri dishes coated with Cultrex® Basement Membrane Matrix (Trevigen) and incubated in Minimal Essential Medium (MEM, Gibco) supplemented with 20% fetal bovine serum (FBS), 100 U/ml penicillin, 100 U/ml streptomycin, 5 µg/ml fungizone and 2 mM L-glutamine, at 37C in a 5% CO2 humidified atmosphere. The explants were placed close to each other to facilitate paracrine stimulation among them. Migration and proliferation of VSMCs from explants was visible within 1-2 weeks.

Once VSMCs had surrounded the explants and reached a high confluence, we moved the explants aside and plated VSMCs in a new dish. To do so, after removing the medium, the petri dish was washed with PBS at RT, then we added trypsin EDTA solution (200 mg/l, Lonza) to cover the cells. After 30 seconds at 37 ºC cells were mechanically resuspended with a pipette and the same volume of serum-containing medium was added to inactivate the enzyme. Then the medium was centrifuged at 180 g for 4 minutes, the supernatant was discarded and the pellet was resuspended in maintenance SMC P-STIM medium (MEM culture medium with 10% FBS, 5µg/ml insulin, 1 ng/ml bFGF, 5 ng/ml EGF, 100 U/ml penicillin, 100 U/ml streptomycin, 0.25 µg/ml fungizone and 2 mM L-glutamine). Cells were then plated ensuring a uniform distribution. From this moment on, every time VSMCs reached 80-90% confluence, they were split and seeded again at 30-50% confluence. VSMC cultures could be subjected to 7 to 10 passages without showing morphological changes.

1.1.b. Organ culture of blood vessels

For organ culture experiments, hMA and hSV were carefully cleaned of surrounding adipose and connective tissue in Tyrode solution (in mM: 140 NaCl, 5KCl, 2 $CaCl_2$, 1.1 $MgCl_2$, 5 Glucose and10 Hepes, at pH 7.4). Then vessels were cut in 5 mm-wide rings that were incubated at 37ºC in a 5% CO2 humidified atmosphere in MEM with 2mM L-Glutamine, 200 U/ml penicillin, 200 U/ml streptomycin and 0.5 µg/ml fungizone with the indicated treatments (see Figure M2). 20%FBS was used to induce intimal hyperplasia (positive control) while FBS-free medium (0%FBS) was used as negative control. The experimental conditions include the addition pharmacological agents such as the Kv1.3 blockers PAP-1 (5-(4-phenoxybutoxy) psoralen) or Margatoxin (MgTx), or the mTOR blocker Everolimus (EVL), or the infection with viral vectors overexpressing or knocking down some of the target proteins under study. Positive and negative controls were always included, and sequential sections of the same artery were used for the different experimental conditions.

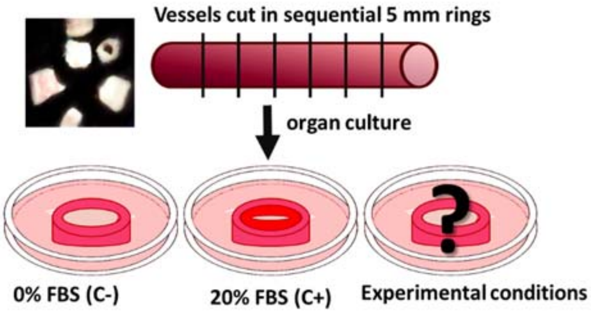

Figure M2. Scheme of the experimental design for human vessels in organ culture.
C- = Negative control;
C+ = positive control

The media was changed every 2 days, and after 2 weeks in organ culture, the rings were washed with PBS (Phosphate Buffered Saline, Lonza) and either fixed with 4% formaldehyde (Sigma) for histomorphometric analysis or saved in RNAlater for expression studies (mRNA, microRNA and/or protein expression).

1.2. Animal models

1.2.a. Mouse model of essential hypertension

All animal procedures were approved by the Institutional care and Use Committee of the University of Valladolid and are in accordance with the European Community guiding principles with respect to the care and use of animals (Directive 2010/63/UE).

The hypertensive mice BPH (Blood Pressure High) and their normotensive controls BPN (Blood Pressure Normal) obtained from Jackson Laboratories (Jackson Laboratories, Bar Harbor, ME, USA) were maintained by inbreeding crossing and housed under controlled conditions and free access to water and food.

The BPH strain was phenotypically selected from crossbreeding of eight different mouse strains, the BPN strain shares a comparable genetic background as it was derived from the unselected control mice maintained throughout the selection process (Schlager & Sides, 1997). BPH mice showed a significantly higher mean BP which was associated with a faster heart rate, higher heart weight, left ventricular mass, kidney weight and hematocrit. BPH mice also showed lower levels of renin, aldosterone and angiotensin and a shorter lifespan compared to PBN strain (Schlager, 1981; Schlager & Sides, 1997).

1.2. b. Mouse model of vascular risk factors

To obtain a mice model with vascular risk factors (VRF), BPH mice were fed with a high-fat diet (HFD, Research Diets Inc.) containing in % of Kcal: 60 from fat, 20 from protein and 20 from carbohydrate.

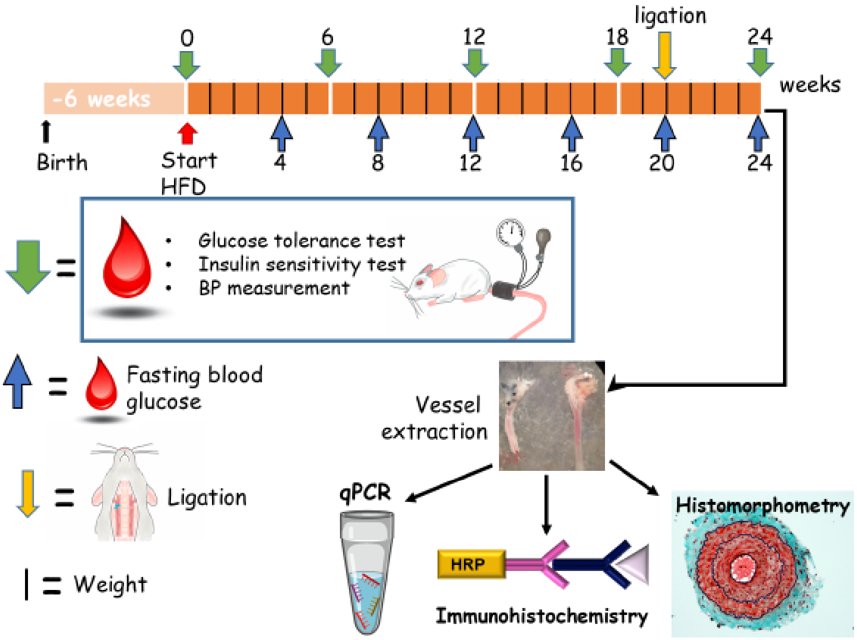
ligation
0
6
12
18
24
weeks
-6 weeks
Birth
Start HFD
4
8
12
16
20
24
=
Glucose tolerance test
Insulin sensitivity test
BP measurement
=
Fasting blood glucose
=
Ligation
= Weight
Vessel extraction
qPCR
HRP
Immunohistochemistry
Histomorphometry

Figure M3. Schematic workflow used to monitor the development of a vascular risk factors animal model.

6 weeks old BPH mice were fed with standard (SD) or HFD for 12 or 24 weeks, and several physiological variables and metabolic parameters were register at fixed times (as depicted in Figure M3). Mice were weighed once a week, fasting blood glucose was measured once a month and blood pressure, glucose and insulin tolerance were tested every 6 weeks. Food was weighted every twice a day to calculate the food intake of each group.

The study of the evolution of all the parameters explored indicated that in our experimental setting the effects of HFD were maximal at week 12, and no further changes could be obtained from there to week 24. For this reason, subsequent experiments were carried out with a 12 week HFD treatment, and in this case the carotid ligation was carried out at week 8.

Blood pressure measurements

Blood pressure (BP) was measured in awake animals using the CODA® High Throughput System (Kent Scientific Corporation), a mouse tail-cuff system design for noninvasive blood pressure measurements.

The system uses a cuff placed on the tail of the animal to occlude the blow flow, so that upon deflation of the cuff systolic and diastolic blood pressures are measured by determining the speed of changes in tail blood volume using a volume pressure recording (VPR) sensor. The VPR measures simultaneously six parameters: systolic blood pressure, diastolic blood pressure, mean blood pressure, heart pulse rate, tail blood volume and tail blood flow.

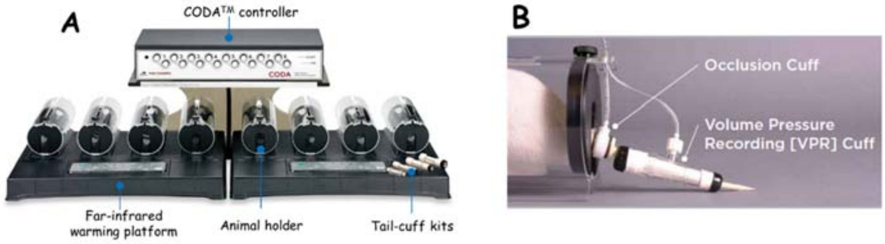
A
CODA™ controller
Far-infrared warming platform
Animal holder
Tail-cuff kits
B
Occlusion Cuff
Volume Pressure Recording [VPR] Cuff

Figure M4. CODA® High Throughput Noninvasive Blood Pressure System (A) and mouse tail with occlusion cuff and the VPR cuff setup (B).

Briefly, the mice were placed in the holder in a warming platform and the tails were cuffed with the VPR sensor and the occlusion cuff (Figure M4). Animals were acclimated to 32-35°C during 15 min before measurements. Sessions of data acquisition were carried out daily during 4-6 consecutive days at the same hour to reduce animal stress and ensure reliable data. Each session consisted of 40 cycles of an inflating step to a maximum occlusion pressure of 250 mmHg followed by a deflating step of 15 s. The first 5 cycles were used for acclimation and were not included for the analysis. Values of 15 µl were fixed as the minimum tail volume for data acquisition. Mice were first trained at least 2 days prior to data acquisition, as we found that this was enough to ensure reliable and reproducible measurements from session to session.

Metabolic parameters

Blood glucose levels were determining using the glucometer Contour®XT (Bayer) from a drop of blood from the mouse nicked tail. Blood glucose was obtained under fasting (16 h) conditions Glucose concentration was measured in mg/dl.

Intraperitoneal glucose tolerance test (ipGTT) was performed to measure the clearance of a glucose load. Mice were fasted overnight and injected intraperitoneally with glucose (25% D-Glucose in 0-9% NaCl solution, Merck) at a dose of 2 g/Kg body weight. Blood glucose levels were determined before (t=0) and 20, 40, 60 and 120 min after glucose challenge. Blood glucose levels were plotted as a function of time and the area under the curve (AUC) was calculated relative to the fasted glucose concentrations (Villa-Pérez *et al.*, 2017).

Intraperitoneal insulin tolerance test (ipITT) was performed to evaluate the insulin action. The test evaluates insulin sensitivity by monitoring the time course of endogenous blood glucose decrease and recovery in response to an injection of human insulin. Glucose clearance rate reflects the action of insulin in periphery tissues, determining the insulin sensitivity. Mice in non-fasting conditions were injected intraperitoneally with human insulin (Gibco) at a dose of 1 U/Kg body weight. Blood glucose levels was monitored before (t=0) and 20, 40, 60 and 90 minutes after injection. Blood glucose levels were presented as percentage of basal glucose concentration and depicted as a function of time, and also de the AUC was calculated as describe above (Vinué & González-navarro, 2015; Villa-Pérez *et al.*, 2017).

1.2.c. Mouse model of vascular lesion: Carotid artery ligation

In order to obtain an animal model of IH with VRF, we performed carotid artery ligation in BPH mice fed with HFD. In this model (Kumar & Lindner, 1997) there is a blood flow cessation in the common carotid artery by ligation near the bifurcation.

After cleaning and disinfecting the surgery area and material, mice were anesthetized with isoflurane, an inhalant general anesthesia. Isoflurane was administrated using SomnoSuite® Low Flow Anesthesia system (Kentscientific) at dose: 2% induction and 1-2% maintenance (Plumb, 2008) with a flow rate 500 ml/min and 45 ml/min respectively. The eyes were lubricated during the surgery with eye drops to avoid drying of the cornea. The fur was removed from the ventral region of the neck and the skin was disinfected with 0.5% chlorhexidine. With the animal in dorsal recumbence with the head positioned near to the surgeon, a 10 mm incision was made in the midline of the ventral neck which exposed the salivary glands. The right carotid artery (RCA) was exposed by blunt dissection. Two 6-0 silk sutures were passed under the RCA with the help of 2 Moria forceps and were firmly tied with two surgeon´s knots at the distal portion near the carotid bifurcation. Finally, the dissected tissue was repositioned, and the skin was closed with continuous suture using vycril 8-0.

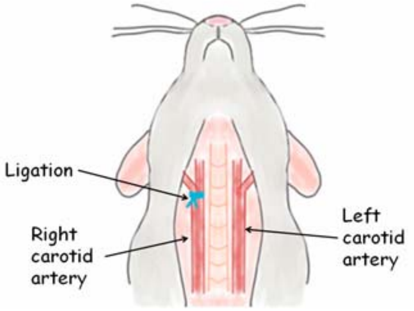

Figure M5. Cartoon of the procedure of carotid artery ligation, showing the ligation of right carotid artery distal to the bicufcation to obtain an *in vivo* model of IH. Contralateral artery was used as control.

In addition, ligated mice received a 4 weeks treatment with the Kv1.3 blocker PAP-1, using either a systemic drug delivery or local application. For the systemic treatment, we used an osmotic minipump (model 2004, Alzet), containing either PAP-1 (50 µg/Kg/day) or vehicle (PEG-35 castor oil,25% in H_2O, Kolliphor® EL, Sigma). The minipump was implanted subcutaneously in the dorsal region of the neck. For the local treatment, we used an hydrogel formed "*in-situ*" by catalyst free click reactions between two elastin like recombinamers (ELR): an azide group and an activated alkyne as cyclooctine group. The control-ELR or PAP-1-ELR containing gels were applied surrounding the ligated artery.

During the postsurgical period, mice were kept warm until they recovery from anesthesia and ibuprofen (20 mg/100 ml in the drinking water), was administered for 3 days. In addition, the mice were daily observed and weighted once a week.

Four weeks after the surgery the ligated animals were euthanized in CO_2 chamber.to collect tissue. Right (ligated) and left (control) carotid arteries were harvested and fixated overnight in 4% formaldehyde to perform histological techniques and explore histomorphometric changes produced by the carotid ligation. Additionally, mesenteric arteries were saved in RNAlater and used for gene expression studies (qPCR).

2. Tools

2.1. Pharmacological treatments

PAP-1. 5- (4- phenoxybutoxy)psoralen (Sigma) is a selective Kv1.3 blocker. PAP-1 was designed by using Psora-4 , a Kv1.x blocker compound obtained from the plant Ruda or *Ruta graveolens*, as template to create a Kv1.3 channel selective blocker (Schmitz *et al.*, 2005). They described that two PAP-1 molecules interact with one channel molecule, and that PAP-1 binds to the C-Type inactivated state of Kv1.3 at the S4-S5 linker and the pore loop (Schmitz *et al.*, 2005; Zimin *et al.*, 2009; Jorgensen *et al.*, 2015). We also know that PAP-1 blocks Kv1.3 channel in a use-dependent manner with an EC50 of 2 nM. This EC50 represents a selectivity for Kv1.3 ranging between 23-fold and 125-fold over all the other members of the Kv1 subfamily (Schmitz *et al.*, 2005). PAP-1 was reconstituted in DMSO at 10 mM and stored at -20ºC, 1 mM working aliquots were kept at 4 ºC for 1-2 weeks and it was used at a final concentration of 100 nM.

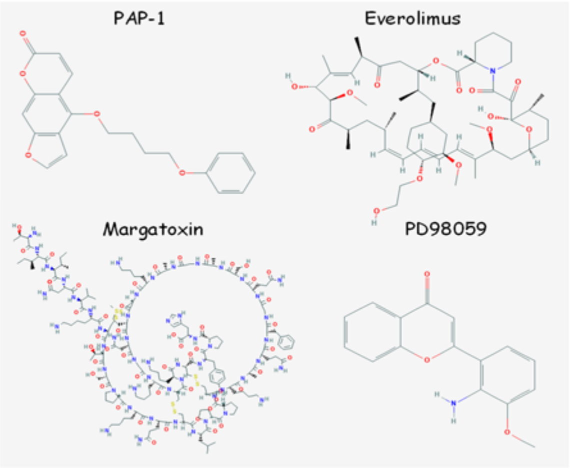

Figure M6. Chemical structures of PAP-1, everolimus, MgTx and PD98059 blockers.Taken from National Center for Biotechnology Information. PubChem Database.

Margatoxin (MgTx) (Alomone) is a toxin obtained from the scorpion *Centruroides margaritatus,* which has been characterized as a Kv1.3 inhibitor. MgTx is a 39- peptide membrane-impermeable with high specificity to block Kv1.3 channel by binding its Lys35 residue to the Kv.13 pore and stabilizing it with a salt bridge between margatoxin-Lys28 and Kv1.3-Asp449. (Garcia-Calvo *et al.*, 1993; Chen & Chung, 2014). Specificity for Kv1.3 of MgTx was also confirmed in mitral cells of Kv1.3 null mice (Fadool *et al.*, 2004). MgTx suppress mitral cell current in wild animals but do not affect the currents from Kv1.3 null mice. MgTx was obtained lyophilized and reconstituted in PBS at 2 µM, stored at -20ºC and used at 10nM.

Everolimus (EVL) (Sigma) is a synthetic macrocyclic lactone derived from rapamycin (also known as sirolimus), a compound isolated from *Streptomyces hygroscopicus* found on the island Rapa Nui. Everolimus is an inhibitor of mTOR complex I (mTORC-1), thus inhibiting several crucial cellular functions including: protein synthesis, regulation of angiogenesis, lipid biosynthesis, cell growth and cell-cycle progression. Everolimus was reconstituted in DMSO at 10 mM, stored at -20ºC and used at working concentrations of 0.01 to 1 nM.

PD98059. 2-(2-amino-3-methoxyphenyl)-4H-1-Benzopyran-4-one (Tocris Bioscience) is a cell permeable inhibitor of MEK1/2. It binds to the inactive form of MEK1/2 thereby preventing its activation by upstream kinases. PD98059 was reconstituted at 25mM in DMSO, stored at -20ºC and used at 20 µM.

2.2. Viral vectors production and transduction

Viral vectors are an excellent tool for gene transfer in primary cell cultures and tissues, where conventional transfection methods show very low efficiencies. In addition to their high efficiency for gene delivery, the use of viral vectors ensures long-term expression because they can penetrate into the cell nucleus (Ibraheem *et al.*, 2014). Two different types of viral vectors were used in this study, to perform overexpression or knockdown studies both in tissues and in VSMC cultures.

2.2.a. Adeno-associated virus (AAV) production

Adeno-associated viruses (AAV) are naturally replicant-defective parvoviruses that requires several factor for productive infection. They can infect both dividing and non-diving cells of a broad range of mammalian cells and can induce long-term expression of our gene of interest (Ibraheem *et al.*, 2014).

AAV were produced using AAV Helper-Free System (Agilent Technologies) according to manufacturer´s instructions. This kit contains the three necessary plasmids for AAV serotype 2(which has affinity to VSMCs) particles production:

1) The **pAAV-RC vecto**r that contains the rep and cap genes, encoding replication and viral capsid structural proteins, respectively,

2) The **pHelper vector** that contains a subset of adenovirus genes: VA, E2A and E4 necessary for high-titer AAV production,

These two vectors supply all the factors required for AAV replication and packaging in the AAV-293 cells, which stably express the adenovirus E1 required for AAV particles production,

3) The **pAAV-MCS vector**, the ITR/MCS containing vector where the DNA of interest is subcloned in the multiple cloning site (MCS).

Plasmids expressing the full-length Kv1.5 and Kv1.3 channels as a fusion protein with fluorescent tags (Kv1.5-EGFP and Kv1.3-Cherry) as well as some mutant channels such as the Kv1.3 pore mutant WF-Kv1.3-EGFP, or the phosphorylation defective mutant Y2-Kv1.3-Cherry have been previously described. (Cidad *et al.*, 2012; Jiménez-Pérez *et al.*, 2016), Control plasmids coding for EGFP or Cherry inserts alone were used as a controls. All inserts of the above plasmids were digested with the appropriate restriction enzymes and further subcloned into the pAAV-MCS.

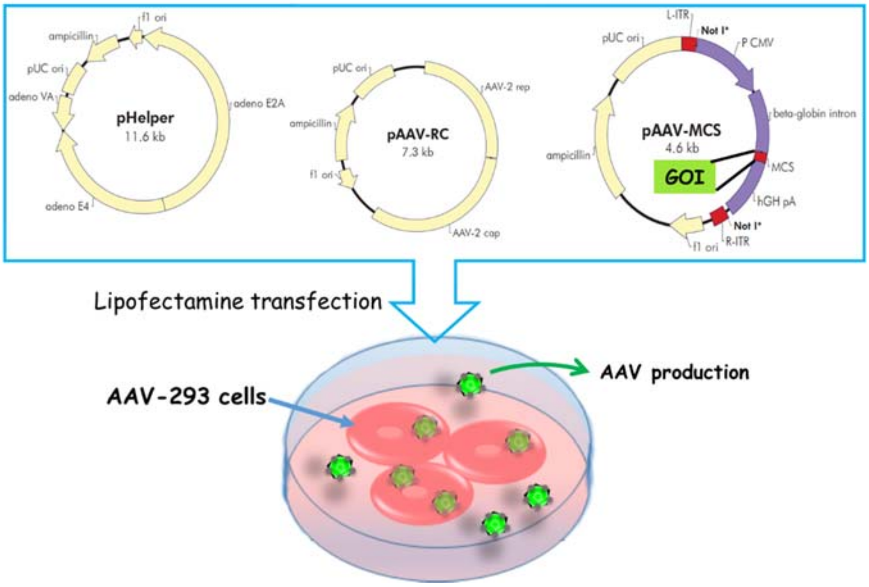
f1 ori
ampicillin
pUC ori
adeno VA
pHelper
11.6 kb
adeno E2A
adeno E4
pUC ori
AAV-2 rep
ampicillin
pAAV-RC
7.3 kb
f1 ori
AAV-2 cap
L-ITR
Not I*
pUC ori
P CMV
beta-globin intron
pAAV-MCS
4.6 kb
ampicillin
GOI
MCS
hGH pA
Not I*
f1 ori
R-ITR
Lipofectamine transfection
AAV-293 cells
AAV production

Figure M7. AAV production graphic scheme. Packaging cells were transfected with the three plasmids of the AAV Helper Free System required to produce viral vectors: The GOI (gene of interest) was subcloned in the indicated plasmid AAV particles were harvested 72 hour after transfection.

Viral particles were produced by co-transfecting AAV-293 cells (Agilent) with the pAAV-MCS vector with the gene of interest, the pAAV-RC and pHelper vectors (1:1:1), using Lipofectamine 2000 (Invitrogen) in a 1:3 ratio, following manufacturer's instructions. After overnight transfection, medium was changed to fresh10%FBS MEM. Viral particles are present in both intact cells and the growth medium, therefore 72 hours post-transfection both cells and medium were collected in a 15 ml conical tube and subjected to four rounds of 10 mins freeze/thaw (dry ice/ 37 ºC bath). Then, the tube was centrifuged (10 minutes at 10000 g) and the supernatant containing the viral particles was aliquoted and stored at -80ºC (Matsushita *et al.*, 1998).

Viral titration was performed to calculate the quantity of viral particles in our AAV stock. First, we isolated the viral DNA with PureLink™ Viral RNA/DNA Mini Kit (Invitrogen) as manufacture recommendations. Briefly, 50 µl of AAV particles were lysed with proteinase K to isolate DNA. The DNA was stored at -80°C or immediately used for titration. Titration was done by qPCR with the primers targeting the ITRs regions (Aurnhammer *et al.*, 2012): FW-ITR primer: 5´-GGAACCCCTAGTGATGGAGTT-3´ and REV-ITR primer: 5´-CGGCCTCAGTGAGCGA-3´ with the Power SYBR® Green Master Mix (ThermoFisher Scientific) . The qPCR reaction was carried out in a Rotor-Gene 3000 (Corbett Research) thermocycler with the following protocol: 15 min at 95 ºC followed of 40 cycles of 95 ºC 15s - 60 ºC 20s - 72 ºC 20s.

To estimate the titer our virus stock, a standard curve was generated with serially diluted standards of the pAAV-MCS vector (1:100, 1:1000, 1:10000, 1:100000). The number of copies of vector were calculated with the online calculator of URI Genomics and Sequencing Center (https://web.uri.edu/gsc/dsdna-calculator/).

The standard curve resulted in a linear fit between Ct and concentration of the dilutions. The extrapolation of the Ct from our virus stock to the standard curve showed the virus titers were in the range of 10^8-10^{10} viral particles per microliter.

2.2.b. Lentivirus production for overexpressing Kv1.5 channels

Lentiviral particles production was carried out using the system provided by Addgene, which consists of three different plasmids

1) **psPAX2**, the packing plasmid which contains Gag, Pol, Rev and Tat genes;

2) **pMD2.G**, the envelope plasmid, that encodes for the envelope glycoprotein VSV-G;

3) **pSin-EF2-Sox2_Pur**, the transfer vector, which contains the DNA of our gene of interest and the flanking long terminal repeats (LTRs). This plasmid

has a large deletion in the 3'LTR that makes the virus replicant incompetent, ensuring the safety of this system of gene delivery.

Lentivirus transfer plasmid to overexpress Kv1.5 channels as a fusion protein with GFP (Lv-Kv1.5) or GFP as an infection control, where previously constructed in the laboratory (Jiménez Pérez, 2015, see Figure M8).

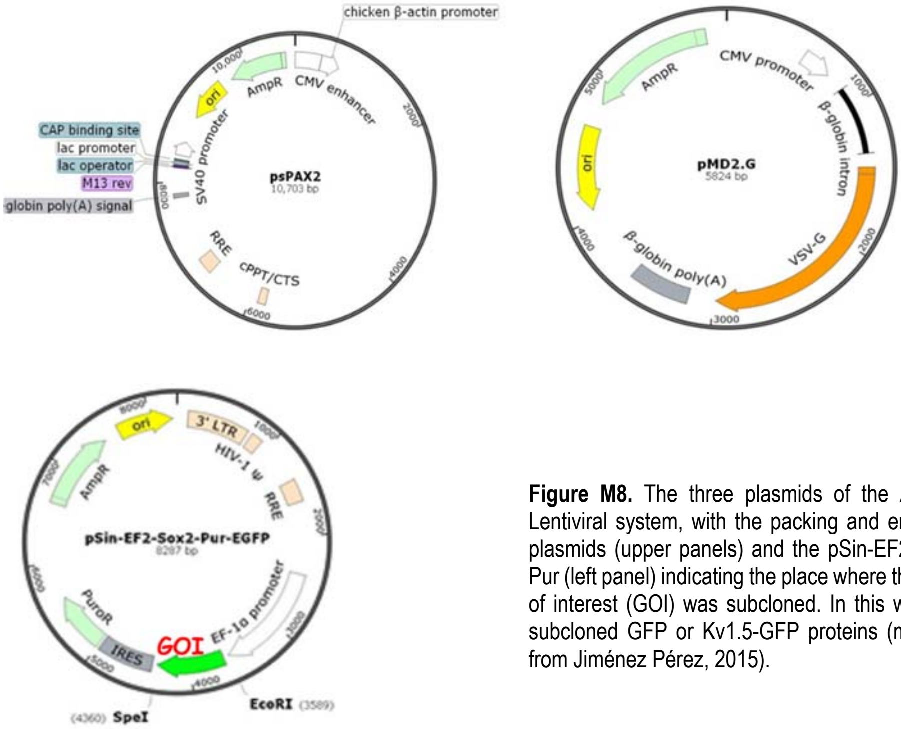
chicken β-actin promoter
CAP binding site
lac promoter
lac operator
M13 rev
globin poly(A) signal
10,000
ori
AmpR
CMV enhancer
2000
SV40 promoter
8000
psPAX2
10,703 bp
RRE
cPPT/CTS
4000
6000
CMV promoter
1000
AmpR
5000
β-globin intron
ori
pMD2.G
5824 bp
4000
β-globin poly(A)
VSV-G
2000
3000
8000
ori
3' LTR
1000
HIV-1 ψ
7000
AmpR
RRE
2000
pSin-EF2-Sox2-Pur-EGFP
8287 bp
6000
EF-1α promoter
PuroR
3000
GOI
IRES
5000
4000
EcoRI (3589)
(4360) SpeI

Figure M8. The three plasmids of the Adgene Lentiviral system, with the packing and envelope plasmids (upper panels) and the pSin-EF2-Sox2-Pur (left panel) indicating the place where the gene of interest (GOI) was subcloned. In this work we subcloned GFP or Kv1.5-GFP proteins (modified from Jiménez Pérez, 2015).

2.2.c. Lentivirus production for knocking down myocardin

We also produced viral particles for the construction of the myocardin knock-down (Lv-ccMYOCD) using the CRISPR (clustered regularly interspaced short palindromic repits)-Cas9 technology. In this case the lentiCRISPR-v2 plasmid (a gift from Feng Zhang, Addgene plasmid #52961) was used as transfer gene. This vector expresses a single guide RNA (gRNA) under the hU6 promoter and the WT Cas9 nuclease under the EFS promoter (Sanjana *et al.*, 2014).

We modified this vector replacing the unique hU6-gRNA cloning site cassette with an insert containing 2 gRNAs cloning sites under independent U6 promoters. Target sequences in myocardin exons 1 (with 5' overhang

BsmBI digestion sites) and 10 (with 5’ overhang BsaI digestion sites) were selected with the software tool CRISPOR (http://crispor.org/) (Haeussler *et al.*, 2016):

gRNA myocardin Exon 1: CACC-GAACTTTGCTCCTAATCAGCA
gRNA myocardin Exon 10: CACC-GTGGTAGAAGCCGTTGGACA

Both gRNA shows high specificity and efficiency score, with no other target sequences in the genome. The lentiCRISPR-v2 plasmid, expressing a single sgRNA was also used to create 2 other Myocardin knockdown vectors, targeting only exon 1 (CRISPR-1) or exon 10 (CRISPR-10), as controls for off target effects of Lv-ccMYOCD. sgRNA sequences and plasmids were confirmed by Sanger sequencing.

As in the case of AAV vectors, lentiviral particles were produced by co-transfecting HEK293FT cells with the transfer lentiviral plasmid with the gene or sequences of interest, the packing vector psPAX2 and the envelop plasmid pMD2.G (in a ration 2:1.5:1) using Lipofectamine 2000 (in 1:3 ratio, as described in AAV production). Culture medium with viral particles was collected 48 (store at -20ºC) and 72 hours after transfection. From the collected medium, after filtration and centrifugation a pellet containing the viral particles is obtained, resuspended in albumin, kept at 4 ºC overnight and store at -80ºC in small aliquots until use.

Lentivirus particles titration was performed by qPCR with the primers targeting the LTRs sequences: FW-LTR primer: 5´-TGGGAGCTCTCTGGCTAACT-3´ and REV-LTR primer: 5´-GACGGGCACACACTACTTGA-3´. The standard curve was generated using dilutions with known concentration of pSin-EF2-Soux2-Pur vector. Stock virus titers were between 10^6 and 10^8 viral particles per microliter.

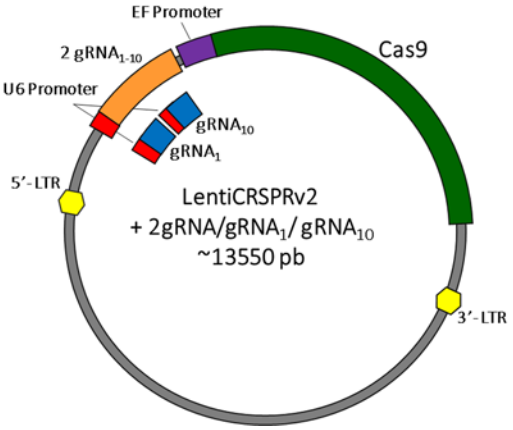

Figure M9. The lentiCRISPR v2 transfer vector used to produce viral particles to Knock-down myocardin. Three different vectors were constructed, one with two guide RNAs against two different myocardin exons 1 and 10 (sequence in orange) and two other vectors with each individual guide RNA (in blue gRNA1 and gRNA10).

2.2.d. Viral transduction of cultured VSMCs and vessels

VSMC in culture were transduced with a multiplicity of infection (MOI) of approximately 500 viral particles per cell in the case of AAV and with a MOI of around 30-50 for lentivirus. Briefly viral particles were added to 80% confluent VSMC and incubated during 4 hours in Opti-MEM medium (Invitrogen), followed by 48 hours incubation in complete medium. Afterwards, cells were used for proliferation, migration and electrophysiological studies for 3 passages at most. Efficiency of viral infection was monitored by the expression of the reporter protein which was routinely over 75-90%.

Human vessels in organ culture were transduced with 10^8-10^9 viral particles for AAV and 10^7-10^8 for lentivirus per vessel ring in a 2 cm^2 well. Viral particles were added to the vessel in 100 µl of OptiMEM in the presence of 10 µg/ml protamine (10µg/ml). After 4 hours of incubation, 200 µl of complete medium was added to the vessels and were incubated for 96 hours. Arterial rings were kept in culture medium with the indicated treatments for 2 weeks.

2.3. microRNAs Mimics and VSMC transfection

To study the effect of miRNAs on VSMCs phenotype and functions, we used miRNA mimics. The miRNA mimics are small double-stranded RNAs (with a guide strand identical to the mature miRNA) that mimic endogenous miRNAs and enable functional studies by upregulating their activity.

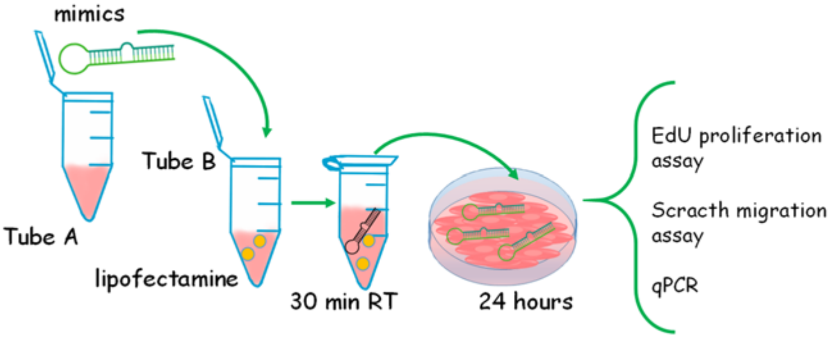

Figure M10. Diagram of the protocol used for miRNA mimics transfections.

The mirVana^{TM} miRNA mimics (Ambion) were used to study mir126 (hsa-miR-126-3p (MH12841, Ambion)) function. Both mir126 mimic and mimic negative control were stored at 50 µM in RNase free water at -20C.

Cultured VSMCs at 80-90% confluence were transfected with 10 nM of miR-126 mimic or mimic negative control (C-) using lipofectamine following manufacter's instructions. Briefly, a tube A containing the miRNA mimic in 500ul Opti-MEM was combined with a tube B with 0.83 ul of lipofectamine in 500 ul Opti-MEM. The mixture was incubated 30 minutes at RT before adding the transfection mix to the VSMCs. After 24 hours of incubation cells were used for expression and functional studies.

3. Histological techniques and morphometric studies

The analysis of the vascular remodeling both in human vessels in organ culture or in mice vessels after the different in vivo experiments was carried out using a set of histological techniques.

3.1. Paraffin embedding and sectioning of tissue

To preserve the vessel structure after harvesting the vessels samples, the mice arteries or the human vessels rings were fixed with 4% formaldehyde overnight in PBS at 4°C, washed with PBS and stored in 70% ethanol to proceed with the paraffin-embedding process.

All this processing was carried out with an automated tissue processor Microm STP120 (ThermoFisher Scientific) and consisted in three main steps:

1) Dehydration replacing water for ethanol: 1 hour in 75% ethanol, 1 hour in 90% ethanol, 1 hour in 96% ethanol and 1 hour in absolute ethanol (3 times);

2) Clearing with Xylene to remove ethanol: 1 hour, 2 times) and

3) Paraffin incubations in which paraffin supplanting the xylene: (2 hours, 2 times).

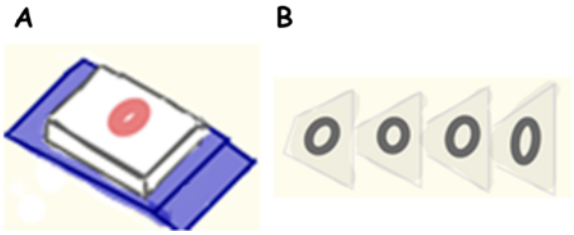

Figure M11. Formalin-fixated-paraffin-embedded (FFPE) (A) tissue block were used to generate 7 µm-thick cross sections (B) of vessels used to perform Masson thrichrome stain, Hoechst stain or immuhistochemistry. FFPE tissue block were also used to obtain RNA.

Next, we used the modular embedding center Microm EC350 (Thermo Scientific) to obtain the formalin fixated paraffin embedded (FFPE) tissue (Figure M11 A). This step is very important because we had to position properly the vessel so that we can make transversal section of the vessel necessary for the histomorphometric analysis.

The 7 μm-thick sections of transverse cross-sections of the vascular vessels (Figure M11 B) were obtained with the rotary microtom Microm HM340E (ThermoFisher Scientific) placed over poli-L-lysine coated slides (ThermoFisher Scientific) and stored at room temperature.

Before starting any stain or immunohistochemistry, we needed to deparaffinize and hydrate the sections on the slides. The deparaffinization consisted in two xylene incubations for 5 minutes. Then, the sections were hydrated by incubations of 5 minutes in absolute ethanol (twice), 5 minutes in 96% ethanol (twice) and 5 minutes in 70% ethanol (twice). Finally the sections were washed in distilled water for 5 minutes.

3.2. Masson trichrome stain.

Masson trichrome stain was used extensively for the analysis of vascular remodeling and IH development in the vessel samples. This technique provides a good characterization of the vessel architecture, as it allows to differentiate muscular tissue (red), nuclei (black) and collagen and connective tissue (green).

The sections were deparaffinized and hydrated as previously described before. Then, the slides were incubated in Bouin's solution (Pancreac) for 48 hours at room temperature, as fixative that increases the intensity of the stain. Next, the slides were washed with running tap water and distilled H_2O and continued with the staining:

1) The nuclei were stained with iron hematoxylin (Sigma-Aldrich) for 30 minutes.

2) Staining of the cytoplasm with Biebrich scarlert-acid fuchsin solution incubation for 20 minutes. This solution is a mixture of 90 ml of 1% Biebrich scarlet in distilled water (Sigma B6008) plus10 ml of 1% acid fuchsin in distilled water (Sigma F8129) and 1 ml glacial acetic acid (MERCK). After washing with H_2O, the slides were incubated 8 minutes in 5% Phosphotungstic acid (Sigma P4006).

3) Staining of the collagen fibers. This third stain, Light Green, was prepared using 2 gr of Light Green SF Yellowish, (Sigma L1886-25), 1 ml

acetic acid (MERCK) and 100 ml of distilled water. The sections were incubated for 2 minutes.

Finally after and incubation in 1% of acetic acid for3 minutes to preserve the tissues, the samples were dehydrated and the coverslips mounted with Eukitt® (Kindler) mounting medium. An example of Masson trichrome stain in a human mammary is shown in Figure M12, with the nuclei in black, the VSMC from the media in red and collagen fibers in green.

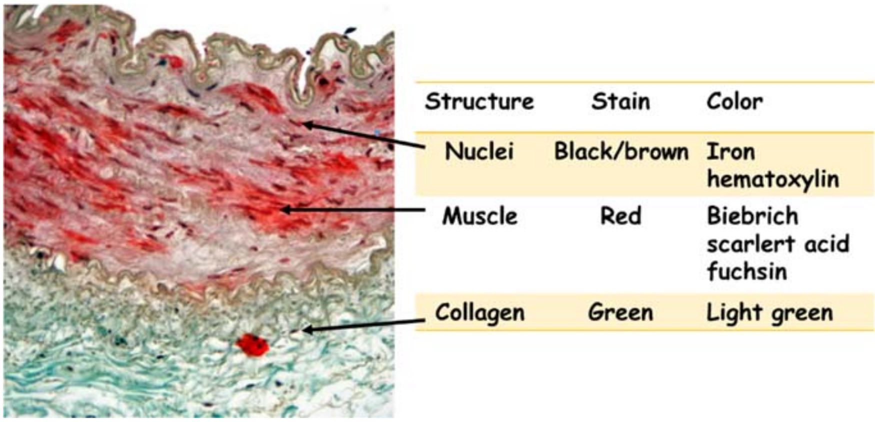

Structure	Stain	Color
Nuclei	Black/brown	Iron hematoxylin
Muscle	Red	Biebrich scarlert acid fuchsin
Collagen	Green	Light green

Figure M12. Human mammary artery stained with Masson trichrome stain. The table indicated the color and the structure stained with each dye.

3.3. Hoechst Stain.

To detect the nuclei in organ culture, we used the nuclear dye Hoechst that binds to the minor groove of the double-stranded DNA. The bounded dye is excited with UV light and emits blue fluorescence. This stain enabled us to analyze the number and the shape of the nuclei (Figure M13).

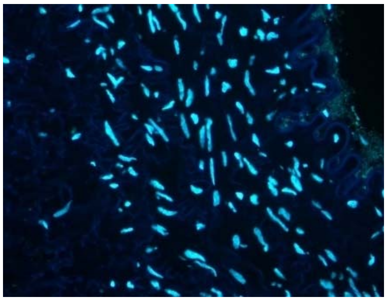

Figure M13. Microphotograph of a mouse carotid artery labelled with Hoechst, The elongated nuclei correspond to VSMC from the tunica media.

Samples were deparaffinized and hydrated as indicated before. Then, the sections were incubated with Hoechst 3334 (Life Technologies) at

1:2000 dilution in PBs for 30 minutes. After 3 PBS washes, the coverslip were mounted with 50% glycerol in distilled water and stored 4ºC.

3.4. Morphometric analysis

To analyze the morphology and vascular remodeling of the vessels, microphotographs were acquired from a Nikon Eclipse 90i microscope using a Nikon CCD camera. Images of 4 different sections for each sample were taken with the 4x (NA=0.13), the 10x (NA=0.3) or the 20x (NA=0.5) objectives. Fluorescence images where taken with the filters: UV-2A for blue, B-2A for green and G-2A for red (Nikon). Images were analyzed using the Image J (Fiji) software to study the parameters described next.

3.4.a. Analysis of vascular remodeling

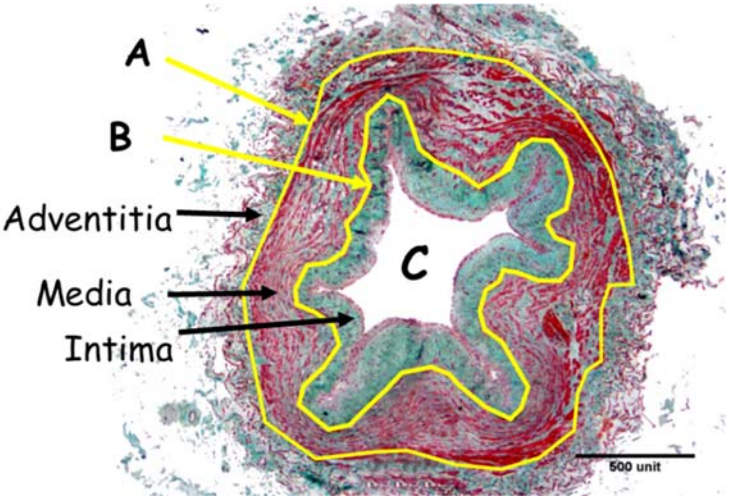

Figure M14. Section of a human saphenous vein The external (A) and internal (B) elastic laminas are labelled in yellow, and C indicates the lumen area. The three layers of the vessel are also indicated. Scale bar =500μm See text for more details.

Vessel sections stained with Masson trichrome were used for this analysis. This stained allows to identify the three layers (tunica intima, media and adventitia) which are limited by the internal (B) and external elastic laminae (A, Figure M14).

We measured the luminal area (C_a, limited by the outer border of the intima layer), the intimal area (B_a, limited by the internal elastic lamina and the outer border of the intima layer), the vessel area (A_a, limited by the external elastic area) and the perimeter of the external elastic lamina (A_p). Using these measurements we obtained the parameters shown in Table M1. Some of them (such as I/M ratio and % stenosis) are common descriptors, to define vascular remodeling and quantify IH (Cidad *et al.*, 2014; Roque *et al.*, 2000).

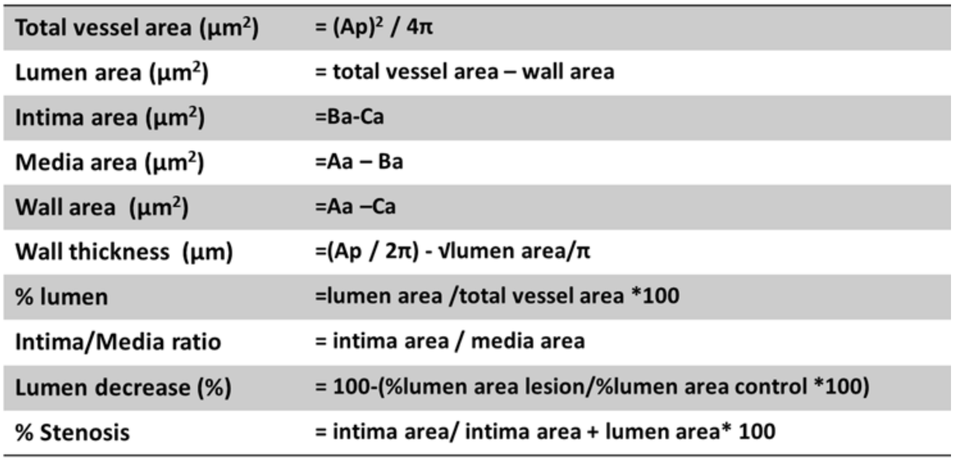

Total vessel area (μm^2)	**= $(Ap)^2 / 4\pi$**
Lumen area (μm^2)	**= total vessel area – wall area**
Intima area (μm^2)	**=Ba-Ca**
Media area (μm^2)	**=Aa – Ba**
Wall area (μm^2)	**=Aa –Ca**
Wall thickness (μm)	**=$(Ap / 2\pi)$ - √lumen area/π**
% lumen	**=lumen area /total vessel area *100**
Intima/Media ratio	**= intima area / media area**
Lumen decrease (%)	**= 100-(%lumen area lesion/%lumen area control *100)**
% Stenosis	**= intima area/ intima area + lumen area* 100**

Table M1. Parameters used to evaluate vascular remodeling and intimal hyperplasia.

We calculated the total vessel area using the perimeter of the external elastic lamina to correct the fact that the vessels might be collapsed. This collapse can be prevented by perfusion fixation. This approach could not be performed in human vessels. In mice vessels we did by cardiac puncture, however the perfusion did not always reached the arteries under study.

3.4.b. Elastin analysis

Elastin fibers emit green autofluorescence when excited with blue light. Thus, we took advantage of this characteristic and measured the quantity and the organization of the elastin in the arteries using the green channel of the microphotographs. We selected the tunica media of the artery to obtain the Integrated Density in Fiji ImageJ. Using the *RawIntDen*, which is the sum of the values of the green pixels in the image, divided by the area of the selection we could represent the quantity of elastin by μm^2. (elastin labelling/μm^2).

3.4.c. Nuclei analysis

Nuclei labeling with Hoechst allowed us to perform two different analysis:

1- Proliferation studies, by counting the number of nuclei from a section of the wall vessel (including tunica intima and media) of a fixed width (225.18 μm in human vessels or 122.40 μm in mice vessels). We counted the nuclei in four different areas for each sample, selecting one in each quadrant of the whole vessel section as depicted in Figure M15. The total number of nuclei was used to determine proliferation rate.

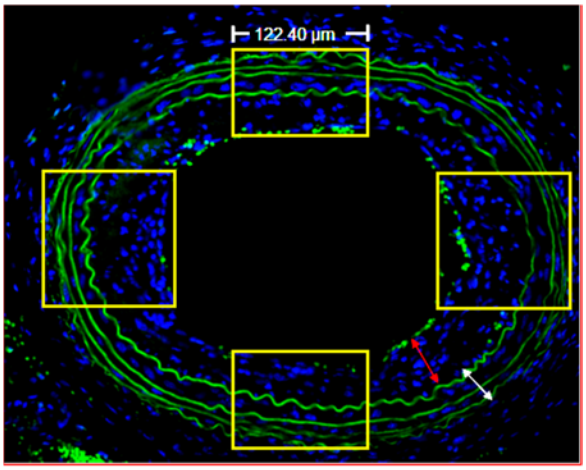

Figure M15. Cross section of a mouse carotid artery with nuclei stained with Hoechst (blue), showing elastin autofluorescence (green). The yellow box represents the sections of the wall vessel used for counting the number of nuclei from the tunica intima (red arrow) and tunica media (white arrow). The number of nuclei per section was obtained from the average of 4 different measurements, one for each quadrant.

2- Characterization the VSMC nuclei shape as a surrogate of the VSMC cell shape. VSMCs are usually fusiform and present elongated nuclei shape. If basal contraction is increased, VSMCs and their nuclei become more rounded, but this also happens in dedifferentiated, proliferating cells. We use the shape descriptors provided by Fiji software, specifically the aspect ratio (AR) that represents major axis / minor axis of a selected area. AR equals to1 indicates a perfectly rounded shape while increasing values of AR means an elongating shape. We performed AR measurement in ten nuclei from 4 different sections for each sample.

4. RNA expression analysis by quantitative PCR

To explore mRNA gene expression and miRNA expression quantitative PCR (qPCR) was performed. The protocol consisted in several consecutive steps including RNA isolation, reverse transcription to synthetize complementary DNA (cDNA) and real-time PCR to quantify expression.

4.1. mRNA extraction

For cultured VSMCs we removed the medium, washed once with PBS 1X and cells were lysed adding 1 ml TRIzol® (Ambion) at 4 ºC.

For vessel segments, tissue were first homogenized in tubes containing ceramic beads (Precellys kit CK28) and TRIzol® using the Precellys®24 homogenizer (two cycles of 5000 rpm for 15 seconds). After homogenization the debris was eliminated by centrifugation at 12000 g for 3 minutes at 4ºC.

For tissues in FFPE blocks, to extract the tissue embedded in the paraffin, we cut the blocks in small pieces and incubated with xylene at 50ºC (twice). Then, the tissue was washed with 100% ethanol and left air dry for 20 minutes. Homogenization was performed with protease K (500 µg/ml) for 45 minutes at 55ºC.

After homogenization and/or lysis, samples were incubated 5 minutes at room temperature with TRIzol® to allow complete lysis and dissociation of the nucleoproteins complex. Chloroform was added to separate the sample in three phases: 1) the aqueous or upper phase containing the RNA, 2) the interphase with DNA and 3) the organic phase which was saved for protein extraction. For FFPE samples, we added 10 µg glycogen (Invitrogen) to the aqueous phase as a carrier to increase recovery of RNA. Next, isopropanol was added to the aqueous phase to precipitated RNA, the RNA pellet was washed with 75% ethanol an finally, the RNA was resuspended in RNase free water, incubated at 60ºC for 5 minutes and stored at – 80ºC.

4.2. microRNA isolation.

For microRNA isolation, we used the miRNeasy Mini Kit (Qiagen) following the manufactor's instruction. This kit enables purification of total RNA, including small RNA from 18 nucleotides and upwards. Briefly, tissue samples were homogenized and cell lysed with 700 µl of TRIzol® as previously described. Chloroform was added to obtain the aqueous phase containing total RNA, 100% ethanol was added and the solution was passed through an RNeasy mini column, the RNA binding to the column was washed and finally collected with RNase-free water and stored at - 80ºC.

In all cases, RNA quantification and quality verification was performed by measurements of optical density at 260 and 280 nm in the spectrophotometer (NanoDrop™ 1000, Thermo Scientific). RNA concentration was calculated using the Lambert-Beer Law, which correlates absorbance to concentration: A=E*b*c, where A is the measured absorbance (or optical density in absorbance units), E is the molar absorptivity coefficient (in M^{-1} cm^{-1}), b is the sample thickness (in cm) and c is the analyte concentration (in mol/L). To measure nucleic acids concentration the equation is rearranged to c=A*e/b, were is e is a standard coefficient which is 40 ng*cm/ul for RNA and b=1 cm.

The RNA quality was assessed with the ratio of absorbance at 260nm and 280 nm, a ratio ~2.0 is accepted as “pure RNA” and lower values indicates contamination by protein or phenolic compounds.

4.3 Reverse Transcription

The reverse transcription (RT) reaction was used to obtain cDNA from previously quantified and purified RNA samples. The cDNA synthesis reaction was slightly different when looking at mRNA or microRNA expression. In all cases, we used 200 to 500 ng of RNA to synthesize cDNA.

For mRNA expression, RT was performed with 500 ng of RNA in a thermal cycler Rotor-Gene 3000 (Corbett Research) programmed with the protocol indicated in Figure M16, using Moloney Murine Leukemia Virus Reverse Transcriptase (M-MLV RT) (2.5 u/µl), Random Hexamers (2.5 µM), RNAse inhibitor (1 u/µl), PCR buffer (1X), MgCl2. (5 mM) and a mixture of dNTPs (4 mM) in a final volume of 20-60 µl. All reagents were purchased from ThermoFisher Scientific.

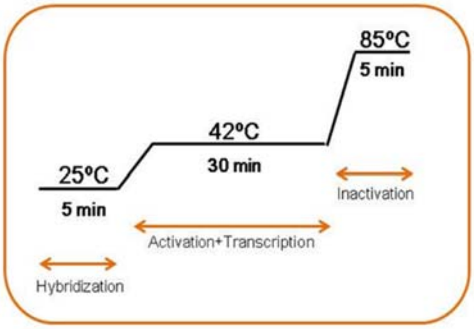

Figure M16. Reverse Transcription protocol.

The cDNA produced with random hexamers keeps the proportion of RNA present in the reaction, including ribosomal RNA. (Biermann, 2004). cDNA was stored at -20°C.

For miRNA expression, it was necessary to perform a RT that ensured the cDNA synthesis and further detection and quantification of small RNA molecules, so that we used the miScript II RT kit (Qiagen).

The kit includes two different buffers: HiSpec and Hi-Flex Buffer. In RT with HiSpec Buffer mature miRNA is polyadenylated by a poly(A) polimerase and converted into cDNA with oligo-dT priming. The oligo-dT primers have a 3’ degenerate anchor and a universal tag sequence on the 5’ end, allowing amplification of mature miRNA in the real-time PCR (Figure M17).

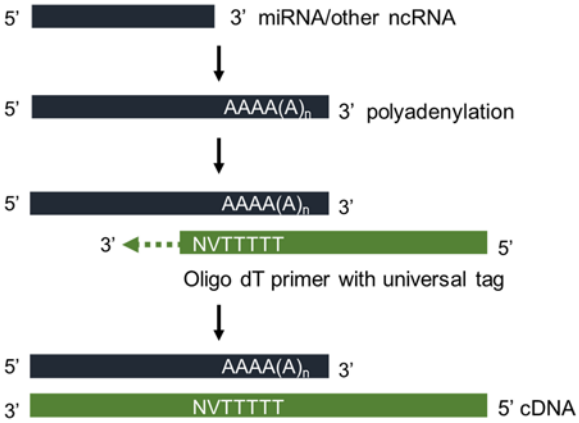

Figure M17. Conversion of mature miRNA into cDNA with the miScript II RT kit. Mature miRNAs are polyadenylated by poly(A) polimerase and reverse transcribed into cDNA using oligo-dT primers with an universal tag. Those steps are performed in the same tube and ensures that miSript Primer Assays do not detect genomic DNA.

The HiFlex Buffer includes both the oligo-dT and random primers, so miRNA, pre-miRNA and mRNAs (all RNA species) can be converted in cDNA and can be further detected. The HiSpec buffer was used when the cDNA was destined to the miRNA qPCR array or miRNA qPCR, while the HiFlex buffer was used when the cDNA would be used for pre-miRNA, miRNA and mRNA expression studies.

The RT mix reaction includes: 200-500 ng RNA, 1X RT buffer, 1XmiScript RT mix, 1X miSript nucleics mix and RNAse-free water up to 20 µl. The reaction was incubated at 37ºC for 1 hour, followed by 5 minutes at 95ºC to inactive the RT enzyme. The samples were diluted in 60-120 µl of RNase-free water and stored at -20°C.

4.4. Quantitative PCR

Finally, cDNA was used as a template for amplification through qPCR to obtain the mRNA expression of the genes of interest. We employed two different qPCR assays: for mRNA expression studies we used TaqMan assays and for miRNA and pre-miRNA expression SYBR green was employed.

4.4.a. qPCR with TaqMan® probes

TaqMan® Gene Expression Assays (Applied Biosystems) were used to explore mRNA gene expression. TaqMan assays are characterized of being highly specific as they contain a probe recognizing a DNA sequence within the fragment to be amplified by the primers. The probe has a fluorophore in 5’ and a quencher in 3’ whose emission and absorption spectra respectively overlap. When the probe is free, the signal emitted by the reporter is absorbed by the quencher and no fluorescence is detected. But when the probe binds its target cDNA (annealing), the 5’-3’ exonuclease activity of the Taq polymerase degrades it so that the reporter emits fluorescence which can be detected.

For the qPCR reaction, 1X Maxima Probe qPCR Mix (ThermoFisher Scientific) was mixed with 1 µl of the TaqMan assay (two primers and the probe), the cDNA sample (1 or 2 µl) and nuclease-free water up to 20 µl. A no template control (NTC) was always included with samples, with all reagents but cDNA. For TaqMan® probes the protocol was: 15 minutes at 95 ºC (enzyme activation), followed by 40 cycles of 15 seconds at 95 ºC (DNA denaturation) and 60 seconds at 60 ºC (annealing and elongation). At the end of each cycle the signal emitted by the fluorophore is measured (see Figure M18). The TaqMan assays used are listed in the Table M2.

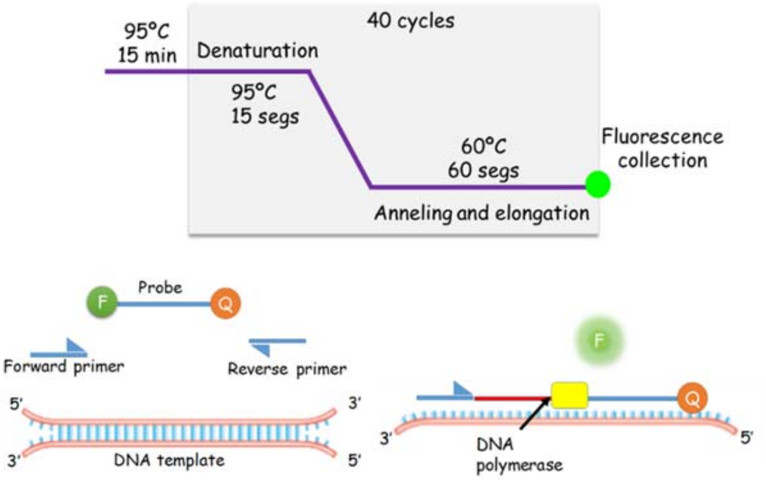
95°C
15 min
40 cycles
Denaturation
95°C
15 segs
60°C
60 segs
Fluorescence collection
Anneling and elongation
Probe
F
Q
Forward primer
Reverse primer
5'
3'
3'
5'
DNA template
F
Q
3'
5'
DNA polymerase

.**Figure M18.** TaqMan qPCR protocol and TaqMan principle.

4.4.b. qPCR with SYBRGreen

SYBR Green qPCR was used for detection of mature miRNA and precursor miRNA. SYBR Green is a fluorescent dye that binds to double-stranded DNA molecules intercalating between the DNA bases. The fluorescence emitted when it is bounded to dsDNA is measured at the end of each PCR cycle and it is proportional to the amount of DNA amplified.

For mature miRNA detection, we used the miScript SYBR® Green PCR kit (Qiagen) to prepare the PCR reaction mix that includes 5µl SYBR Green PCR Master Mix, 1 µl of universal primer (reverse primer), 1 µl of miScript Primer Assay (forward primer, the miRNA specific primer), 3 µl of cDNA prepared with HiSpec buffer or HiFlex Buffer and nuclease-free water up to 10 µl. For precursor-miRNA quantification, we also used the miScript SYBR® Green PCR master mix, but using the the miScript Precursor Assay (Qiagen).The precursor assay consists of the primers targeting the stem-loop sequence of the precursor miRNA under study, which allows quantification of both primary miRNA (pri-miRNA) and precursor miRNA (pre-miRNA).

Gene Name	Protein	Assay ID (Applied Biosystem)
AKT2	AKT2	Hs01086099_m1
CNN1	Calponin	Hs00154543_m1
COL1A1	Collagen I	Hs00164004_m1
COL3A1	Collagen III	Hs00943809_m1
COL8A1	Collagen VIII	Hs00156669_m1
IRS1	Insulin Receptor Substrate	Hs00178563_m1
KCNA1	Kv1.1	Hs00264798_s1
KCNA2	Kv1.2	Hs00270656_s1
KCNA3	Kv1.3	Hs00704943_s1
KCNA4	Kv1.4	Hs00937357_s1
KCNA5	Kv1.5	Hs00266898_S1
KCNA6	Kv1.6	Hs00266903_s1
KCNAB2	Kvβ2	Hs01547935_m1
MYOCD	Myocardin	Hs00538076_m1
PI3KR2	PI3K Regulatory Subunit Beta	Hs00178181_m1
HsRPL18	60 s Ribosomal protein L18	F: aactgatgatgtgcgggttc R: cagctggtcgaaagtgagg Probe: ctgaaggtatgtgcactgcgcgtga

Table M2. Commercial and custom TaqMan assays used.

For the SYBR Green qPCRs, the protocol used is shown in Figure M19.

At the end of the PCR cycling a melting curve was performed to verify the absence of primer dimers and to confirm the specificity of the reaction. The melting curve was generated by increasing the temperature from 60°C to

95 °C one by one degree and acquiring the fluorescent signal at each step so that as the DNA denatures the fluorescence decreases rapidly. A plot of the negative first derivative of the change in fluorescence as a function of the temperature (-dF/dt) shows different peaks corresponding to the melting temperature at which 50% of the DNA is found as single stranded DNA. In specific SYBR Green reactions, this peak must be unique (Figure M20).

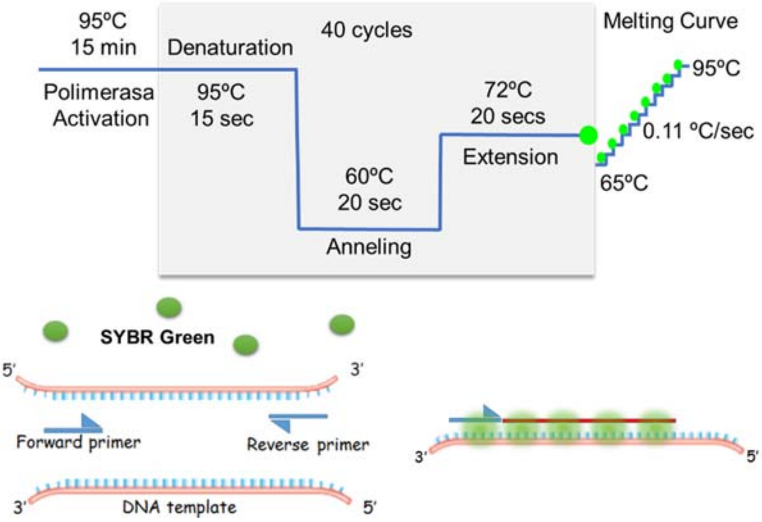
95ºC
15 min
Polimerasa
Activation
Denaturation
95ºC
15 sec
40 cycles
60ºC
20 sec
Anneling
72ºC
20 secs
Extension
Melting Curve
95ºC
0.11 ºC/sec
65ºC
SYBR Green
5'
3'
Forward primer
Reverse primer
3'
DNA template
5'
3'
5'

Figure M19. SYBR Green qPCR protocol, with the green dots indicating fluorescence data acquisition (upper scheme) and SYBR Green action mechanism**.**

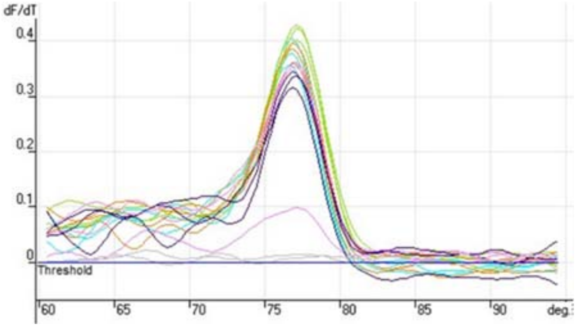

Figure M20. Example of melting curve showing a single peak from specific amplification reaction.

4.4.c. Relative Quantification method

At the beginning of the qPCR reaction, a basal unspecific fluorescence is detected. Setting a threshold over this background signal and within the exponential phase of the amplification curve, we get C_T, which is the cycle number at which the emitted fluorescence surpasses (cuts) the threshold(Figure M21), The C_T value is inversely proportional to the starting amount DNA template (Biermann, 2004).

Comparing the C_T of our target sequence to that of an endogenous control gene (whose expression is not affected by our variable of study) we can now normalize its abundance, as defined by the equation below:

$\Delta CT = Ct\ (_{problem}) - Ct(_{EndC})$

RPL18 gene and SNORD68 were used as mRNA and miRNA endogenous control respectively

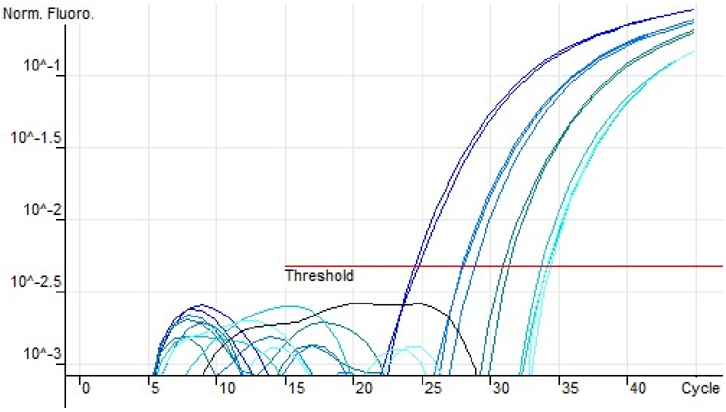

Figure M21. Example of qPCR amplification plot The Y axis is the fluorescence signal in logarithmical scale and the X axis is the cycle number.

In order to perform this normalization the efficiency of the amplification of both, the experimental gene and the endogenous control must be close to 1 and differ less than 10%. To determine the efficiency of the reaction, we performed a PCR with serial dilutions of one sample and obtained the Ct value for each dilution.

Representing Ct against the number of copies of each dilution, we can fit a line to these data and calculate its slope. From this slope, we obtain the efficiency. The efficiency of commercial assays was provided by the manufacturer, and for custom assays we calculate it as shown in Figure M22.

Finally, to calculate the expression levels of the genes and miRNAs of interest the relative quantification method, $2^{-\Delta\Delta Ct}$, was used (Livak & Schmittgen, 2001).

The 2-$^{\Delta\Delta Ct}$ indicates the fold change expression relative to our calibrator (the control group, so that:

$\Delta Ct = Ct_{\text{gene of interest}} – Ct_{\text{Thousekeeping gene}}$

$\Delta\Delta Ct = \Delta Ct_{\text{test grorup}} – \Delta Ct_{\text{control group}}$

All through the work expression data would be represented as fold change or 2-$^{\Delta\Delta Ct}$ or as the relative abundance or $2^{-\Delta Ct}$.

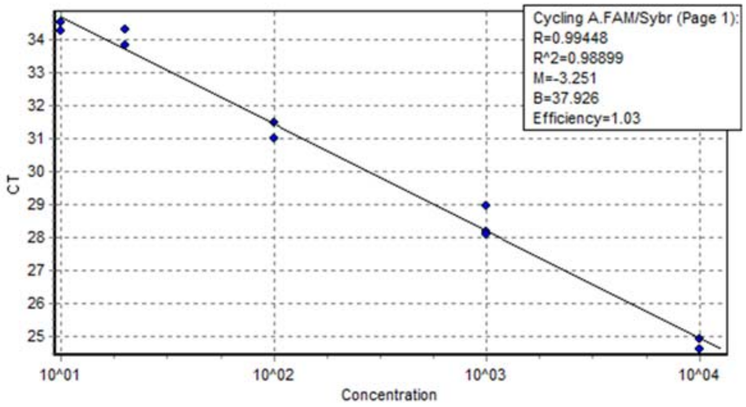

Figure M22. Standard curve of RPL18. (Housekeeping gene). The standard curve shows the Ct on the Y axis and the starting quantity of cDNA template on the X axis. The Slope value is used to calculate the amplification efficiency of the reaction that was 1.03.

4.5. miRNA PCR array

To identify miRNAs that might be altered in T2DM, we used the miScript miRNA PCR Array focused in Human Cardiovascular Disease (Qiagen, NIHS-113Z) which explores the expression of 84 miRNAs known to exhibit altered expression during cardiovascular diseases. The PCR array has a 96 well format (Figure M23), where wells A1 to G12 contained the specific forward primers for each mature miRNA (and the reverse primer is an universal primer included in the reaction mixture, see below). The last row contained the controls: two wells for *C. elegans* miR-39 primers (Ce) that can be used as an alternative data normalization using exogenously spiked miR-39, 5 snoRNA primers used for data normalization using the ΔΔCt method for relative quantification, two miRNA reverse transcription controls for assessment of cDNA synthesis performance and two positive PCR controls.

cDNA was prepared with the previously described miScript II RT kit (Qiagen) using the HiSpec Buffer. The reaction mix contained:

- 1375 µl SYBR Green PCr Mster Mix,
- 275 µl of universal primer (reverse primer),
- 1000 µl of RNase-free water
- 100 µl of cDNA

The total volume of 2750µl, that was split in 27 µl per well. The PCR run was carried out in StepOnePlus™ Real-Time PCR System with the same program described for real-time PCR for SYBR Green assays.

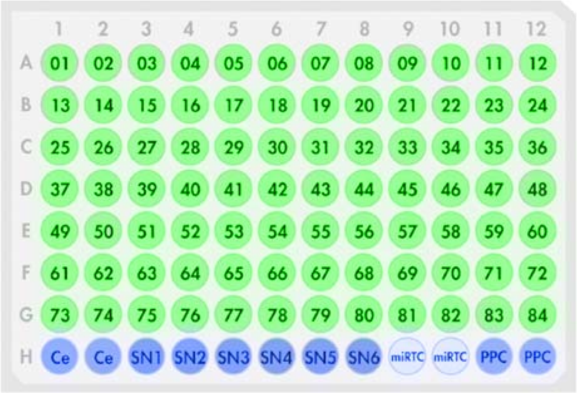
1
2
3
4
5
6
7
8
9
10
11
12
A
B
C
D
E
F
G
H
01 02 03 04 05 06 07 08 09 10 11 12
13 14 15 16 17 18 19 20 21 22 23 24
25 26 27 28 29 30 31 32 33 34 35 36
37 38 39 40 41 42 43 44 45 46 47 48
49 50 51 52 53 54 55 56 57 58 59 60
61 62 63 64 65 66 67 68 69 70 71 72
73 74 75 76 77 78 79 80 81 82 83 84
Ce Ce SN1 SN2 SN3 SN4 SN5 SN6 miRTC miRTC PPC PPC

Figure M23. Plate layout of the miRNA PCR Array. Green wells contain forward primer for each mature miRNA. The blue wells contain qPCR controls: C. elegans miR-39 forward primer,(Ce) snoRNAs (SNx, SNORD61, 68, 72, 95, 96A and RNU6B), miRTC and PPC contain negative and positive PCR controls respectively.

Data analysis was conducted at QIAGEN's Gene Globe Data Analysis Center using the web-based miScript miRNA PCR Array data analysis tool.

5. Protein expression

Protein expression studies were accomplished using western blot, immunofluorescence and immunohistochemistry techniques.

5.1. Western Blot

Western blotting is used to detect proteins that have been separated by gel electrophoresis and transfer to a membrane.

To extract protein from cultured VSMCs and vessel tissue, we used the lysis buffer RIPA, containing 150 mM NaCl, 1% NP-40, 0.5% sodium deoxycholate, 0.1 SDS, 50 mM Tris ph8. Immediately before use, 1X Halt Protease and Phosphatase Inhibitor Cocktail was added to the buffer. For vessels, the buffer was modified to contain 2% SDS.

For lysis of cells, after discarding the culture medium and washing the cells with PBS at 4 ºC, we added a small volume of cold lysis buffer (about 120 μl per 35 mm plate) and mix gently by pipetting up and down a few times taking care of not to make bubbles and let it sit 5 minutes. Next, the lysate was transferred to an Eppendorf tube, and centrifuged at 14.000 g, 10 minutes at 4 ºC to pellet all cellular debris. Finally, we transferred the supernatant with the proteins to a new tube.

For vessel homogenization and lysis, we used liquid nitrogen for freeze the vessels followed by mechanical homogenization with plastic sticks. Then, we added cold lysis buffer (40 μl per 5 cm ring vessel) and mix by pipetting up and down.

Protein samples were prepared with XT Sample buffer (BioRad) and XT Reducing Agent (BioRad) and incubated for 5 minutes at 95ªC. Then, the samples and protein ladder (Precision Plus Protein Standards, Bio-Rad) were loaded in a 10% polyacrylamide gel and Sodium dodecyl sulfate-polyacrylamide gel electrophoresis (SDS-PAGE) was carried out for 2 hours at 100 volts. After that, proteins were transferred to a nitrocellulose membrane, for 2 hours at 350 mA.

Membrane was blocked with 5% non- fat dry milk in TTBS (2.4 g Trizma base, 9 g NaCl, 0.1% Tween-20) for 1 hour. After this, membranes were then incubated with primary antibodies for two hours at RT or overnight at 4ºC, and then with the secondary antibodies (anti-Rabbit HRP and anti-Mouse HRP from Dako, at 1:5000-1:10000 dilution) for 1 hour at RT, both in blocking solution. The primary antibodies employed, and their concentrations are listed below (Table M3).

Proteins were detected by chemiluminescence in a Versa-Doc 5000 (Bio-Rad), following the manufacturer’s instructions for SuperSignal® West Femto Chemiluminescent Substrate (Thermo Scientific). They were quantified using the software Quantity One 4.5.2 (Bio-Rad). The mean background intensity was subtracted to the intensity each band and then, the bands at the expected molecular weight were normalized by that of their loading controls, as previously described (Cidad *et al.*, 2015; Jiménez-Pérez *et al.*, 2016).

5.2. Immunofluorescence

Immunofluorescence was used for protein detection both in cultured VSMCs and in tissue. Cells were seeded in poly-lysine coated crystals and fixed with 4% formaldehyde for 15 minutes. Tissue was deparaffinized and dehydrated as previously described. Then both samples were permeabilized with 0.25%TritonX-100 in PBS for 5 minutes and incubated in blocking solution (0.25% Triton X-100 solution and 1% goat serum) for 2 hours. After that, samples were incubated with the primary antibody for 2-3 hours at RT and then with the secondary antibody conjugated with Alexa Fluor 488 or 594 (Molecular Probes) at 1:1000 for 1-2 hours at RT, both antibodies were prepared in blocking solution. Finally, samples were incubated with Hoechst (1:2000 for 5-30 minutes, for cells or tissues respectively) and mounted with 50% glycerol.

5.3. Immunohistochemistry.

For some antibodies the detection of the proteins in tissue sections was made with 3,3'-Diaminobenzidine (DAB) reagent. This protocol follows the same steps as the immunofluorescence technique with 4 differences.

1. The primary antibody was incubated overnight at 4ºC.
2. The secondary antibodies were conjugated with horseradish peroxidase (HRP) that catalyzed the oxidation of DAB substrate (ThermoFisher Scientific) in the presence of H_2O_2. The oxidized DAB forms a brown precipitate visible using light microscopy. Samples were incubated with DAB substrate for at least 5 minutes or until the color is evident under the microscopy.
3. The nuclei were counterstained with Harris hematoxylin (Bio-Optica) in purple.
4. The samples were dehydrated with Ethanol, cleared with Xylene and the coverslips mounted with Eukitt® (Kindler).

5.4. Antibodies

The primary antibodies used for protein expression are detailed in the following table (TableM3). They include antibodies against several SM contractile proteins as well as antibodies against Kv channels (Kv1.3 and Kv1.5) and against GFP protein. Anti-GFP was used in some cases to identify these ion channels (the fusion proteins).

Target	Source	Catalog #	dilution	Final concentration	technique
Kv1.5	Alomone	APC004	1:30	20 µg/ml	IHC
GFP	NeuroMab	75-131	1:50	20 µg/ml	IHC
Myocardin	Sigma	SAB4200539	1:50	20 µg/ml	IHC
Myosin HCII	Abcam	AB683	1:50	20 µg/ml	IHC
Kv1.3	Alomone	APC-101	1:40	20 µg/ml	IHC
Calponin	Novus	NB110-55650	1:50	20 µg/ml	IHC
SM22	Abcam	ab14106	1:20	20 µg/ml	IHC
COL1A1	SCBT	sc-293182	1:50	2 µg/ml	WB
COL3A1	SCBT	sc-8780-R	1:100	2 µg/ml	WB
Myocardin	Sigma	SAB4200539	1:50	20 µg/ml	IHC
aSMA	Abcam	ab7817	1:50	4 µg/ml	IF
Phospho-ERK1/2	Cell signaling	4370	1:2000	0.5 µg/ml	WB
Phospho insulin receptor β	Cell signaling	3024	1:1000	1 µg/ml	WB
Phospho AKT	Cell signaling	9271	1:1000	1 µg/ml	WB
β tubulin	Sigma	T7816	1:1000	1 µg/ml	WB

Table M3. List of primary antibodies, inmunohistochemestry (IHC), immunofluorescence (IF), western blot (WB).

6. Functional studies

6.1. Proliferation studies

Proliferation studies were performed in primary VSMCs determining the cells entering the S-phase of the cell cycle with the Click-iT® EdU Imaging kit (Invitrogen). This assay is based on the incorporation of 5-ethynyl-2`-deoxyuridine (EdU), a nucleoside analog of thymidine, that is incorporated into the newly synthesized DNA Then the click reaction is produced where azide-Alexa Fluor dye is added and reacts with an alkyne group present in the EdU. This allows fluorescent detection of newly synthesized DNA.

Confluent VSMCs cells were detached with trypsin-EDTA, as described previously and were counted in a Neubauer chamber. Then, 20.000 to 30.000 cells were seeded onto fibronectin coated 12 mm diameter cover slips placed at the bottom of a 4-well plate and incubated for 24 hours in control medium (10% FBS). Next day medium was replaced with serum-free medium and proliferation was induced by addition of PDGF (20 ng/ml) alone or in combination with the indicated blockers for 24 hours. Then, EdU was added to the culture medium for 6 hours, and after that cells were fixed for 15 minutes with 4% formaldehyde, permeabilized with 0.5% TritonX-100 and the Click-iT® reaction was performed following the manufacturer's instructions.

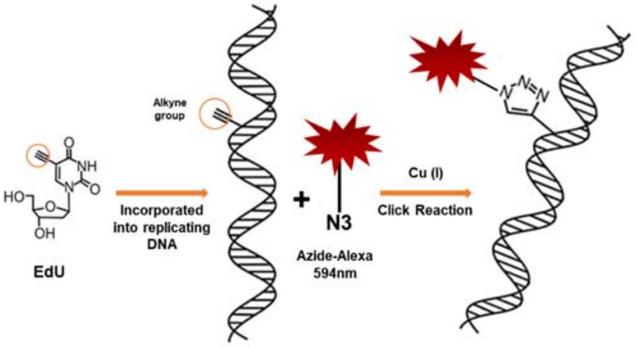

Figure M24. The uridine-modified EdU is incorporated during DNA synthesis. Later on, Alexa Fluor reagents react with the EdU in a quick click chemistry reaction that allows to detect cells that incorporated the EdU.

Finally, cells were incubated with Hoechst (1:3000 in PBS) for 20 minutes at RT, washed with PBS and distilled water and still wet the coverslips were mounted with Vectashield Mounting Medium (Vector Laboratories) to glue the cover slips to a microscope slide, which was sealed with nail polish.

Proliferation was determined as the percentage of EdU positive cells (EdU+) from the total cell number stained with Hoechst. Images were obtained from each sample/condition using the 4Xobjetive and the filters UV-2A (Ex355/50), B-2A (Ex470/40) and G-2A (Ex535/50) from the fluorescence microscope Nikon Eclipse 90i (Nikon). In each sample the incorporation of EdU is obtained from the average of 4 randomly selected fields per coverslips. In the experimental design, we always use triplicates for each individual condition and we always have intra-experimental positive and negative controls. To analyze and quantify the images, ImageJ (Fiji) software was used. When possible, images were analyzed in a blind manner.

6.2. Migration studies

Migration is a cellular process altered in VSMC upon PM which is also relevant for the development of the intimal hyperplasia. In order to study the migration capability of VSMC, we performed 2 different assays: Scratch migration assay and Boyden assay.

6.2.a. Scratch migration assay

The Scratch migration assay involves the creation of a wound or scratch in a cell monolayer, to study the time course of cell invasion to cover the wounded area (Liang *et al.*, 2007).

To carry out the scratch migration assay, once reaching confluence VSMC were incubated with 0%FBS-MEM overnight. Next day, after creating a wound in the cell monolayer with a 10 µl tip, the medium was changed to media with 0.5% FBS alone for positive control or with the indicated blockers. Images of the same area were taken at 0, 4, 6, 8, 12 and 24 hours and analyzed using ImageJ (Fiji) software. To evaluate migration the % of invaded area was calculated as:

$\%\ \text{Invaded Area} = 100 \times (A_{t0} - A_t) / A_{t0}$

Where A_{t0} is the area at the beginning of the assay, and A_t is the area at the indicate time from the beginning of the experiment.

6.2.b. Boyden migration assay

Boyden migration assay explores cell migration and invasion using a chamber with two compartments separated by a porous membrane. Cells are place in the membrane facing the upper compartment and are allowed to migrate through the pores towards the chemotactic agents present in the lower compartment (Figure M25),(Chen, 2005).

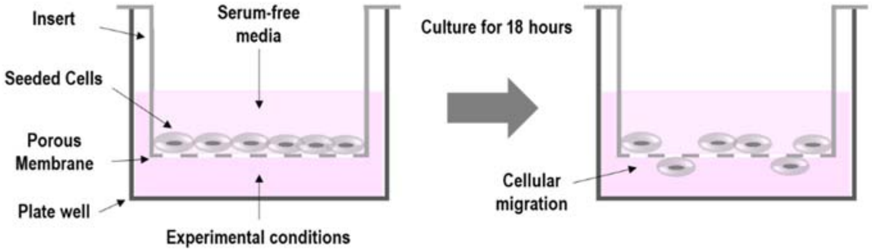

Figure M25. Schematic illustration of the Boyden assay design.

Boyden migration assay was performed using the polycarbonate cell culture inserts of 8 µm pore size (Nunc™, 140629). Around 20,000 VSMCs were seeded in the upper side of the insert placed in 24-well plates with 200 µl of 2% FBS media, and let sit overnight. Next day, the media was replaced with 0%FBS (negative and positive control) or 0%FBS with PAP-1 (experimental condition), and the bottom of the insert was filled with 500 µl of 0% FBS (as negative control), 20% FBS culture medium (as the migration stimulus) and 20% FBS with PAP-1 (as experimental conditions).

Cells were allowed to migrate at 37ºC in 5% CO2 humidified atmosphere for 18 hours. Then the inserts were washed with PBS. The non-migrated cells from the upper side were scraped off with cotton swabs and the inserts were fixed with 4% formaldehyde for 15 minutes. The nuclei of the cells in the bottom side were stained with Hoechst (1:2000) for 5 minutes, and the membrane from the insert was cut off and mounted on a slide. Five randomly selected fields pictures were taken with a LEICA SP5 confocal microscope. Nuclei from migrated cells were counted with ImageJ (Fiji) software.

6.3. Electrophysiological studies

Patch clamp techniques were used to analyze the currents expressed in cultured VSMCs either in control conditions or after viral transduccion of Kv channels.

6.3.a. Voltage-clamp experiments

To explore K currents in VSMC, we use the patch-clamp technique in the voltage-clamp mode. Voltage-clamp can be used in several different configurations (Figure M26). Here we used the whole-cell configuration, in which after sealing the membrane with the pipette tip, we break it. By doing so, we achieve electrical continuity between the recording electrode and the inside of the cell, dialyzing the intracellular medium with the solution in the pipette (internal solution, see composition below). In this configuration, we control V_M with an electronic feedback system that measures the cell membrane potential and compares it with the potential established in the experimental protocol. Differences between both potentials are immediately corrected with an injection of current, that mirrors (with opposite direction) the ionic current that we are registering.

Ionic currents were recorded at room temperature (20–25°C) using this whole-cell configuration. Patch pipettes were made from borosilicate glass (2.0 mm O.D., WPI) and double pulled (Narishige PP-83) to resistances ranging from 4 to 8 MΩ when filled with an internal solution with this composition (in mM): 125 KCl, 4 MgCl2, 10 HEPES, 10 EGTA, 5 MgATP (pH 7.2 with KOH). The composition of the bath solution was (in mM): 141 NaCl, 4.7 KCl, 1.2 MgCl2, 1.8 CaCl2, 10 glucose, and 10 HEPES (pH 7.4 with NaOH).

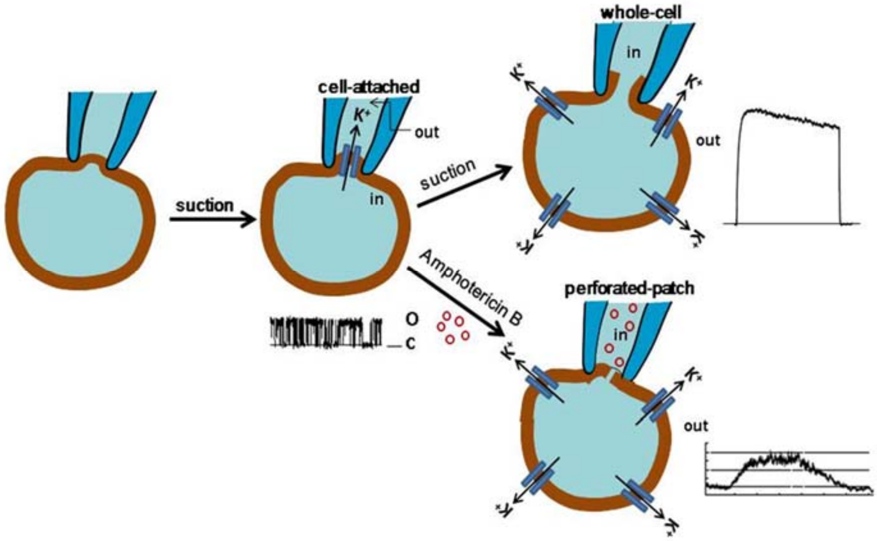

Figure M26. Cell-Attached, Whole-Cell and Perforated-Patch configurations. Once a Gigaohm seal is achieved between the patch pipette and the cell, single channel recordings can be made in the cell-attached mode. If additional suction is applied to the seal, whole-cell is gained. Perforated-patch configuration was obtained by adding amphotericin B to the internal solution and can be used for current-clamp experiments.

Whole-cell currents were recorded using an Axopatch 200 patch clamp amplifier, filtered at 2 kHz (_3 db, 4-pole Bessel filter) and sampled at 10 kHz. When leak subtraction was performed, an online P/4 protocol was used. Recordings were digitized with a Digidata 1200 A/D interface driven by CLAMPEX 8 software (Axon Instruments).

Outward K^+ currents were elicited by 200-800 ms depolarizing pulses from a holding potential of -80mV to +40 mV applied in 10 seconds intervals. In some cells full current/voltage curves were constructed from potentials ranging from -60 to+60 mV in 10mV steps.

Kv1.3 current was defined as the current sensitive to the selective blockers PAP-1 (100 nM) or Margatoxin (10 nM) and Kv1.5 currents were dissected with their sensitivity to DPO (1 μM). In all cases, the effects of the drugs were calculated taken as control the averaged current amplitude before and after drug application.

Electrophysiological data acquisition and part of the analysis were performed with the Clampfit subroutine of the pCLAMP software (Axon Instruments) and with Origin 7.5 software (OriginLab Corp., Northampton, MA, USA).

7. Statistical analyses

Statistical analysis was performed using Origin 7.5 software (OriginLab Corp., Northampton, MA, USA), Microsoft Excel and R software (R foundation for Statistical Computing, Austria). Pooled data were expressed as mean values ± standard error of the mean (SEM) from several different experiments.

For comparisons between two groups with normal distribution, Student's t test, for paired or unpaired data as required, was used. If the data did not follow a normal distribution, a Mann-Whitney-Wilcoxon test was applied.

For comparisons among several groups, one-way ANOVA followed by Tukey’s test was employed in the case of normal distributions and equal variances; alternatively Kruskal-Wallis analysis followed by Dunn’s test was used. Shapiro-Wilk test and Bartlett’s test were used to test normality and homogeneity of variances respectively. Linear correlation between variables was measured with Pearson coefficient.

All through the Results section, p-values < 0.05 were considered as significantly different.

Results

1. Kv1.3 blockade and phenotypic modulation of human vessels

1.1. Characterization of the human vessel organ culture model

We used an *ex vivo* organ culture model to explore the effects of Kv1.3 blockers against restenosis in human vessels. First, we tested the suitability of this model to study phenotypic modulation. We characterize the degree of preservation of tissue architecture after 2 weeks in culture, (in serum-free media, our negative control) and the effect of 20% FBS treatment promoting remodeling and intimal hyperplasia (our positive control). At the end of the 2-week treatment, the vessels were fixed in formaldehyde, embedded in paraffin and cut in 7 µm-thick cross sections. The morphological characterization of these sections was performed by a Masson trichrome stain, which identifies cell nuclei in black, vascular smooth muscle cells in red and collagen fibers in green (Figure R1 A, B). Vascular remodeling was quantified by determining the intima /media ratio (I/M ratio = Intima area/Media area) and the percentage of stenosis (% Stenosis = (Intima area/Intima area+Lumen area)*100), as detailed in the methods section.

Incubation of hMA and hSV with 20% FBS during 2 weeks led to a marked inward remodeling of the vessel, characterized by an increased thickness of intimal and media layers and a concomitant decrease of the lumen area (Figure R1 A and B). As shown in the images, 20%FBS induced neointima formation in hMA and increases the intima layer of hSV. Remodeling was consistently observed in 18 out of 21 hSV and in 18 out of 20 hMA. Both I/M ratio and % stenosis were significantly increased with FBS treatment (Figure R1 C).

Information about the sex of the patients was available for the majority of donors, but due to the small number of female samples, data were analyzed for both sexes together. In the case of hSV, we tried to look for sex differences in the FBS-induced vascular remodeling in organ culture (Figure R2 A and B) and we did not find any significant difference. Nevertheless, the small number of cases and the differences also in age distribution between sexes (Figure R2 C and D) precluded any further analysis.

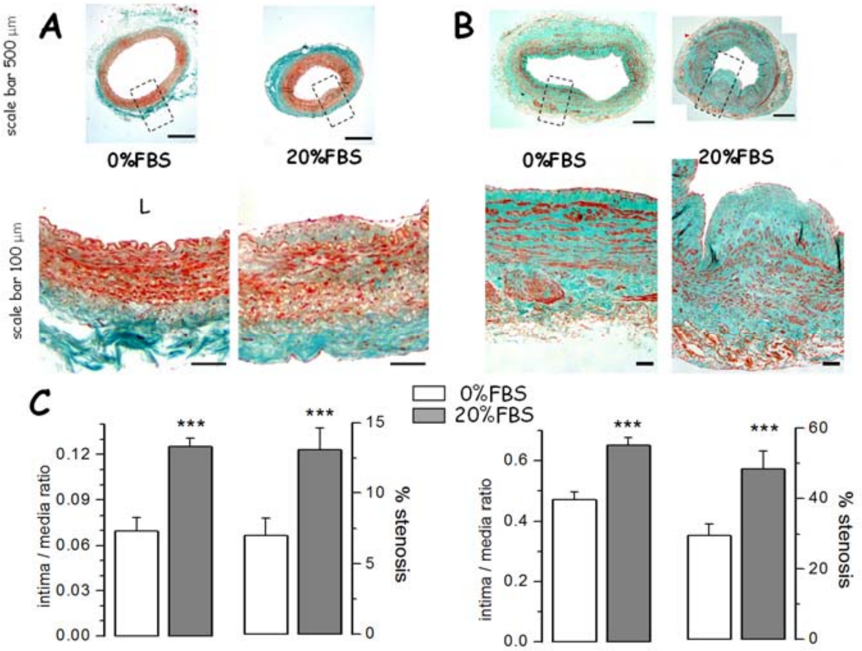
A
B
scale bar 500 µm
scale bar 100 µm
0%FBS
20%FBS
0%FBS
20%FBS
L
C
0%FBS
20%FBS
***
***
***
***
intima / media ratio
0.00
0.03
0.06
0.09
0.12
% stenosis
0
5
10
15
intima / media ratio
0.0
0.2
0.4
0.6
% stenosis
0
20
40
60

Figure R1. Representative microphotographs of hMA (**A**) and hSV (**B**) stained with Masson trichrome after two weeks in organ cultured without (0%FBS) or with 20% FBS. The upper panels show images of the vessel rings (objective 4X, NA=0.13), and a section of the ring (dotted square) is amplified in the lower panels. Scale bars= 500 µm (upper panels) and 100 µm (lower ones). L = lumen side. **C**. Bar graphs representing intima/media ratio and % Stenosis for hMA (left graphs) and hSV (right bar). Mean ± SEM of 18 hMA or 16 hSV. ***P<0.001 for paired data.

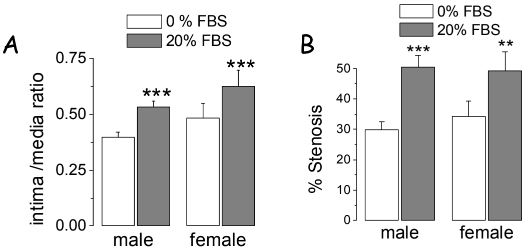

C

human Saphenous Vein		
sex	n	age
male	12 (75 %)	62.75
female	4 (25%)	74.25

human Mammary Artery		
sex	n	age
Male	25 (86.2 %)	69.75
Female	4 (13.8%)	71.5

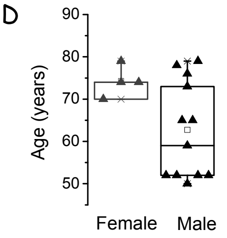

Figure R2. A, B. Analysis of vascular remodeling in male and female hSV. The bar graphs show intima/media ratio (A) and % stenosis (B). Data are Mean ± SEM, male n=12, female =4. ** P<0.01, ***P<0.001 as compared to 0%. **C**. Sex and age distribution (total number of samples and percentages) of the hMA and hSV used in our study. **D**. Box plot showing the age distribution of the male and female hSV samples.

1.2. Effect of Kv1.3 blockers on FBS-induced IH

Next we determined the impact of treatment with Kv1.3 blockers on FBS-induced intimal hyperplasia (IH), using histomorphometric analysis of cross sections of vessels rings. Incubation of hSV or hMA with the selective Kv1.3 blocker PAP-1 (100 nM) significantly reduced FBS-induced intimal hyperplasia (Figure R3 A and B), and had no effect in our negative control (vessels kept in 0%FBS). In this later case, we did not observe any remodeling when compared with control vessels not in organ culture (t=0 condition).

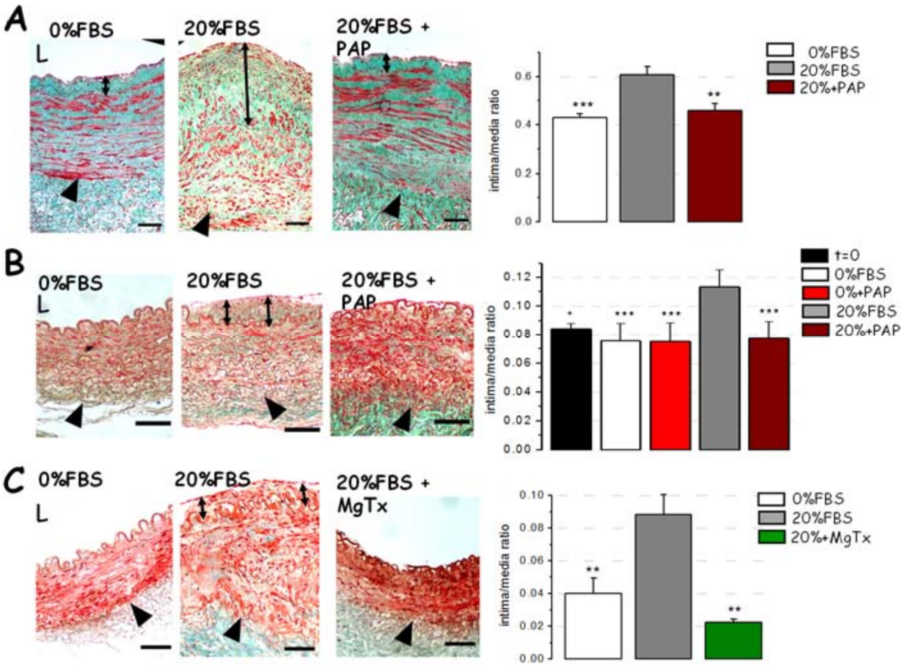
A
0%FBS
L
20%FBS
20%FBS + PAP
intima/media ratio
0.0
0.2
0.4
0.6
***
**
☐ 0%FBS
▨ 20%FBS
■ 20%+PAP
B
0%FBS
L
20%FBS
20%FBS + PAP
intima/media ratio
0.00
0.02
0.04
0.06
0.08
0.10
0.12
*
***
***
***
■ t=0
☐ 0%FBS
■ 0%+PAP
▨ 20%FBS
■ 20%+PAP
C
0%FBS
L
20%FBS
20%FBS + MgTx
intima/media ratio
0.00
0.02
0.04
0.06
0.08
0.10
**
**
☐ 0%FBS
▨ 20%FBS
■ 20%+MgTx

Figure R3. A. Representative microphotographs of cross sections of human saphenous vein (hSV) stained with Mason trichrome. hSV were kept in organ culture for 2 weeks in serum-free conditions (0%FBS), or in the presence of 20% FBS alone or combined with PAP-1 (100 nM). Images were taken with a 10x objective (NA=0.3). L=lumen side. The black arrows indicates the thickness of the intima layer, and the arrowheads the media/adventitia border. The average data (mean ± SEM) of the intima/media ratio obtained in 12 different vessels are represented in the right plot. **B**. Representative microphotrographs of human mammary artery (hMA) in the same experimental condition as hSV. The I/M ratio of hMA not maintained in organ culture (t=0) and PAP-1 treatment in 0% FBS condition is also included in the bars plot, which shows average data of 8-15 arteries. **C**. Representative microphotographs of the effect of margatoxin (MgTx; 10 nM) on 20% FBS-induced remodeling of hMA. Summary data were obtained from 4 arteries. **P*<0.05; ***P*<0.01; ****P*<0.001 with respect to 20% FBS, for paired data. Scale bar=100 µm.

We choose 100nM PAP-1 for our experiments as previous dose-response studies of the effect of PAP-1 in inhibiting proliferation (Cidad *et al.*, 2010), indicated that we can get the maximal effect of PAP-1 at concentrations between 0.1 and 1 µM. At 0,1 µM, PAP-1 inhibited more than 90% of the currents in Kv1.3 transfected HEK cells, but at higuer concentrations (>100nM) PAP-1 is not specific for Kv1.3 channels, and can inhibit other Kv1 channels, importantly Kv1.5.

FBS-induced hMA remodeling was also prevented with 10 nM Margatoxin (MgTx, Figure R3 C), another selective Kv1.3 blocker not structurally related to PAP-1 and 10nM Mgtx have the same effect that 100 nM PAP-1 inhibiting Kv1.3 currents and Kv1.3-induced proliferation (Cidad et al., 2015, Cidad et al 2012). These data suggest that these effects are due to Kv1.3 inhibition.

1.3. Effects of Kv1.3 blockade on the functional characteristics of dedifferentiated VSMCs.

Upon phenotypic modulation (PM), VSMCs dedifferentiate and show proliferative, migratory, and secretory capabilities, which are involved in the process of IH development. In other words, PM of VSMCs is the principal contributor to intimal hyperplasia. As we have seen that Kv1.3 blockers inhibited intimal hyperplasia, we tried to identify which of these processes were affected by Kv1.3 blockade.

1.3.a. Kv1.3 blockers and VSMC proliferation

Proliferation was analyzed in hMA rings kept in culture by counting the number of Hoechst-labeled nuclei in the intima and media layer in 4 sections of 225-µm wide for each sample. The conditions explored were 0% FBS, 20% FBS and 20% FBS+100 nM PAP-1. We found that 20% FBS increased by 40% the number of nuclei in the vessel ring, an effect that was fully abolished with PAP-1.

We also determined proliferation of hMA VSMCs cultures by EdU incorporation, after a 24 h treatment in serum free (SF) conditions or in the presence of 20 ng/ml of PDGF alone or with the Kv1.3 blockers PAP-1 (100 nM) or MgTx (10 nM). We also explored the effect on proliferation of PD98059 20 µM (PD98) which is a potent MEK/ERK inhibitor. All these treatments decreased PDGF-induced proliferation (Figure R4 B). However, when exploring the effect of combining PD98 with PAP-1, it was not additive, which suggests the involvement of the MEK/ERK signaling in Kv1.3-induced proliferation signaling pathway, as previously described in human coronary artery VSMCs (Cidad *et al.*, 2015).

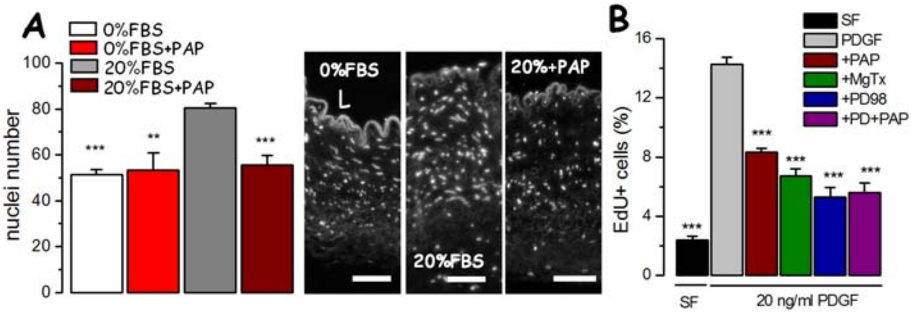

Figure R4. A. Bars plot displays the nuclei number as the mean ± SEM of 4 to 10 arteries in the indicated conditions. Representative images (10x objective) are depicted as an inset (scale bar=100 µm). L=lumen side. ***P*<0.01; ****P*<0.001 with respect to 20% FBS. **B**. Bar graph shows proliferation experiments. Each data bar is the mean ± SEM of 12 to 40 individual determinations obtained in at least 5 independent experiments. ****P*<0.001 with respect to PDGF alone.

1.3.b. Kv1.3 blockers and VSMC migration

Migration of hMA VSMCs was tested only in cultured cells with two different methods: Scratch assay and Boyden assay. In the first one, the invaded area at a given time was determined, whereas in the Boyden assay, the number of cells migrating from the upper to the lower part of a porous membrane placed in a transwell insert were counted.

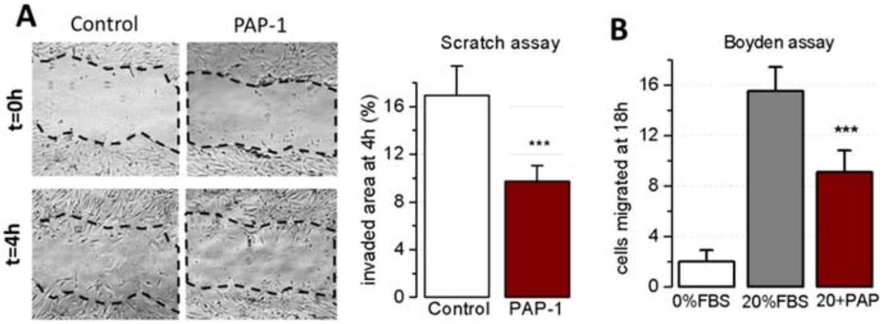

Figure R5. A. Representative examples of a scratch migration assay in control conditions (left) or in the presence of PAP-1 (right). For migration assays a wound was created with a white tip and pictures were taken every 2 hours. Bars plot with the summary data of the percentage of invaded area at 4 h. Each bar is the average ± SEM of 18 individual experiments from 7 different primary VSMC cultures. ***P<0.001. **B**. Data of Boyden chamber migration assay representing the cell number that migrated to the lower side of the chamber after 18 h of treatment. Mean ± SEM, n=9. ***P<0.001 with respect to 20% FBS.

As shown in Figure R5 A, the presence of PAP-1 decreased almost by half the percentage of invaded area at 4h in the scratch assay. A similar effect was observed in the Boyden assay, as there is an almost 50% reduction in the number of cells crossing the transwell insert membrane when PAP-1 was present in the media (Figure R5 B).

1.3.c. Kv1.3 blockers and VSMC secretion

As PM also associates with an increased secretion of ECM proteins, we explored whether Kv1.3 blockers could modulate ECM synthesis. Collagen (particularly types I and III) and elastin are the most abundant proteins in the ECM of the vessel walls (Wagenseil & Mecham, 2009). Upon PM, an increase in collagen synthesis and deposition, particularly collagen I, together with an increased secretion and disorganization of elastin fibers have been reported (Karnik *et al.*, 2003)(Wong *et al.*, 2015). We explored if these changes could be observed in our preparation, and if PAP-1 treatment could show some effect.

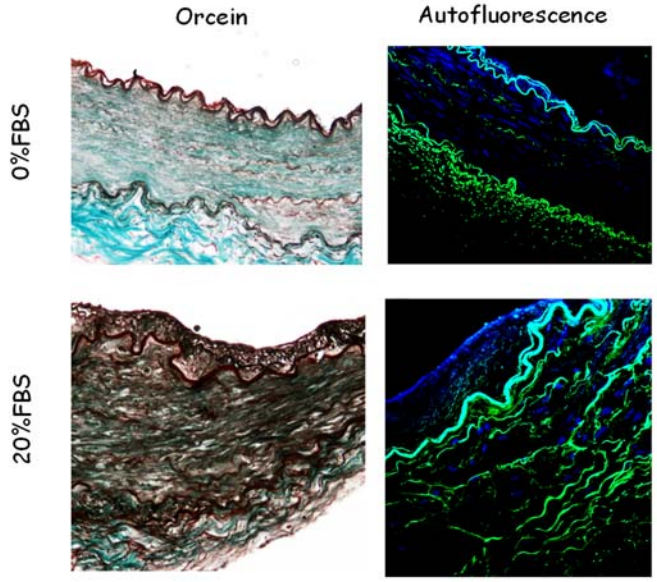

Figure R6. Microphotografs of hMA in organ culture displaying elastin fibers labeling. The lelf panel is hMA sections with orcein stain which colors the elastin fibers in reddish-brown. The right panel shows elastin fibers by its autofluorescence in green.

We took advantage of elastin auto-fluorescence to determine the amount and the degree of integrity of elastic laminae. hMA vessels kept in serum free media shows a well-defined internal and external elastic lamina, and no fluorescence in the intima and media layers. However, 20% FBS induces increased content and disorganization of elastic structure, as described previously. In addition, orcein staining provided a similar pattern of the increased elastin content as can be seen in figure R6. Of interest, the presence of PAP-1 fully prevented 20% FBS induced alterations of elastin (Figure R7 A). In fact, as shown in the microphotographs, elastin structure in vessels with 20% FBS+PAP-1 is not different from the vessels incubated in 0%FBS media.

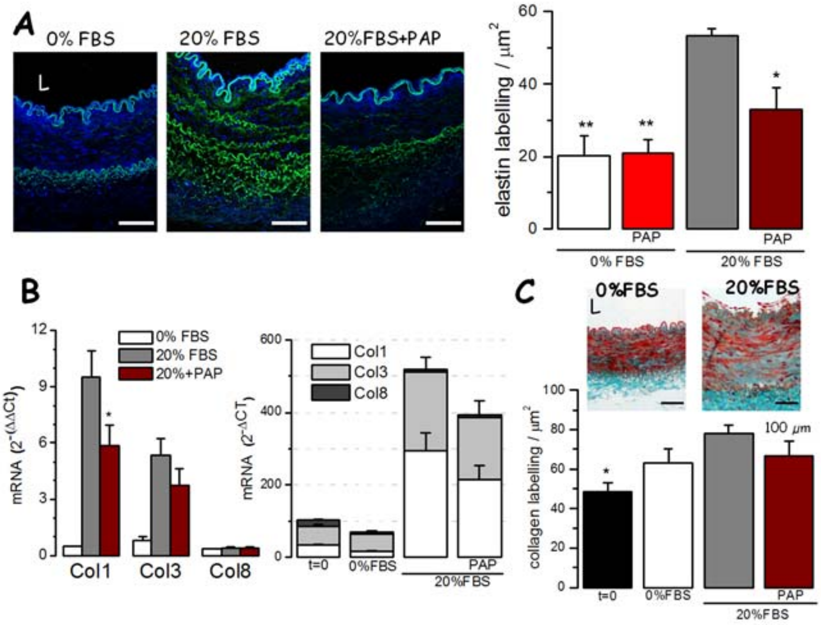

Figure R7. A. Microphotographs of rings from one hMA incubated in the indicated conditions, showing elastic lamina auto-fluorescence (green) and Hoechst stained nuclei (blue). Images were taken with a 20x objective (NA=0.5). Scale bar=100 µm. Bar plot shows elastin quantification from 9 experiments (mean ± SEM; **P*<0.05, ***P*<0.01compared with 20% FBS, paired data. **B**. mRNA expression of COL1A1, COL3A1, and COL8A1 genes was determined in hMA rings in control conditions (t=0) or after 2 weeks in organ culture in the indicated conditions. The left graph shows data normalized to the t=0 condition with the $2^{-\Delta\Delta Ct}$ relative quantification method, where $\Delta\Delta Ct = \Delta Ct_{experimental} - \Delta Ct_{calibrator}$ and the right graph bar is the mRNA amount as $2^{-\Delta Ct} = CtColx - CtRPL18$. Data are mean ± SEM obtained from triplicates of at least 5 different samples. **P*<0.05 compared with 20% FBS. **C**. Collagen content obtained from the Masson trichrome. Representative microphotographs (scale bar=100 µm, 10x objective) and pooled data (mean ± SEM, n=9). **P*<0.05 compared with 20% FBS. L indicates lumen side.

The mRNA levels of the alpha subunit of collagens I and III (COL1A1 and COL3A1) were determined by qPCR, using RPL18 as housekeeping gene. We also measured the mRNA expression levels of collagen VIII (COL8A1), a network-forming collagen type with increased expression in vascular remodeling in atherosclerosis models (Lopes *et al.*, 2013). COL1A1 and COL3A1 expression increased with 20% FBS treatment and was reduced in the presence of PAP-1 (Figure R7 B). On contrast, COL8A1 expression decreased in all experimental conditions; however, collagen mRNA changes were determined by the dominant expression of COL1A1 and COL3A1 (right graph, Figure R7 B).

Masson trichrome stain was also used as a rough estimation of the collagen content in hMA vessels, by quantifying the green stained area of intima and media layers. With this approach, we found that hMA kept in 20% FBS increased collagen content (green color). However, in this case no significant effect of PAP-1 was seen (Figure R7 C).

2. Mechanisms linking Kv1.3/Kv1.5 ratio to phenotypic modulation

2.1. Regulation of the expression of Kv1.3 and Kv1.5 channels upon phenotypic modulation

The previous results prompted us to explore possible mechanisms linking PM to the functional expression of Kv1.3 channels. We first determined the remodeling of Kv1.x expression upon PM, by looking at the mRNA expression of all Kv1 channels in hMA, both in fresh tissue (contractile) and in VSMC culture (proliferative phenotype). As previously described in other preparations (Miguel-Velado *et al.*, 2005; Cidad *et al.*, 2010), our data confirmed the dominant expression of Kv1.5 in contractile phenotype and the switch towards a prominent role of Kv1.3 in dedifferentiated cells. Actually, Kv1.3 is the most abundant Kv1 in proliferative phenotype because all Kv1 channels but Kv1.3 decreased their expression (Figure R8).

Extensive studies and developmental models suggest that myocardin (MYOCD) has a central role in regulating smooth muscle cells (SMCs) phenotype and SMC-specific gene expression via SRF interaction (Miano *et al.*, 2007; Owens, 2007; Talasila *et al.*, 2013). MYOCD expression associates with the contractile SMC phenotype, and its reduced expression or activity during PM is a regulator key of the neointima response. Therefore, we explored whether Kv1.3 and/or Kv1.5 genes could be MYOCD-regulated genes.

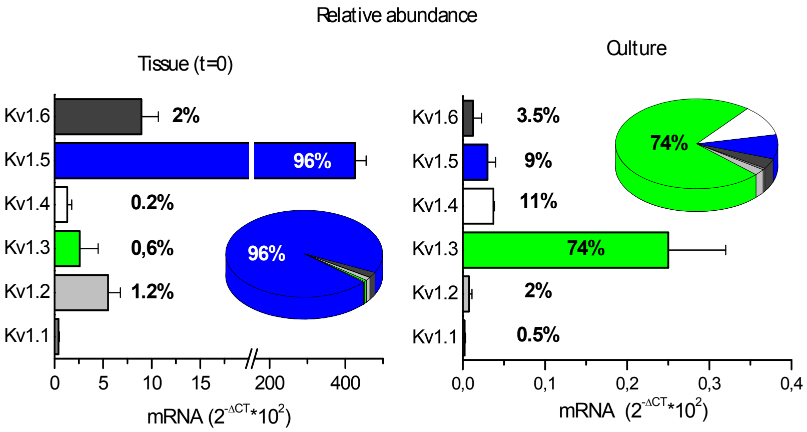

Figure R8. Relative mRNA abundance of the voltage-dependent potassium channel Kv1 family genes in contractile (tissue) and proliferating (culture) vascular smooth muscle from hMA. Expression levels were normalized with respect to RPL18 and expressed as $2^{-\Delta Ct}$, where $\Delta Ct = Ct_{channel} - Ct_{RPL18}$. Each bar is the mean of 4-6 determinations from different donors in triplicate assays. The relative abundance (in %) of each Kv1 member in both conditions is indicated in the bars plot and also illustrated in the pie charts.

First, we determined MYOCD mRNA expression in our experimental conditions. MYOCD mRNA is highly expressed in hMA fresh tissue (t=0), showing a significant decrease after keeping the arterial rings in culture for 2 weeks.

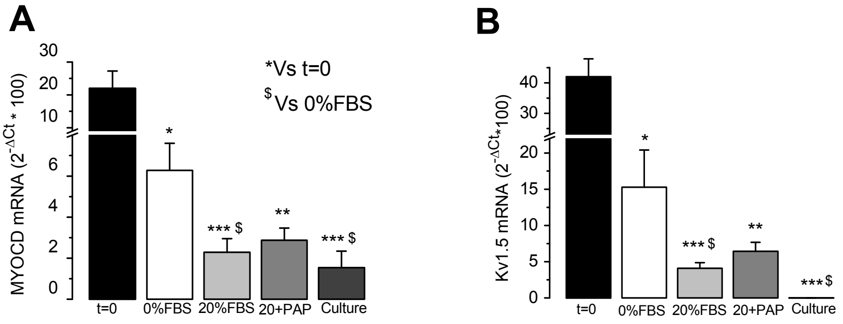

Figure R9. Real-time qPCR with Taqman probes were used to determine mRNA expression of myocardin (**A**) and KCNA5 (the Kv1.5 gene, **B**). In both cases, mRNA abundance is expressed as $2^{-\Delta Ct}$, relative to RPL18. mRNA was obtained from fresh untreated arterial rings (t=0), arterial rings kept 2 weeks in organ culture in the indicated conditions and from cultured hMA VSMCs. In both graphs (PAP=PAP-1 100nM), $^{*}P<0.05$, $^{**}P<0.01$, $^{***}p<0.001$ with respect to untreated tissue (t=0) and \$P<0.05 compared with 0% FBS samples (n=8–10 determinations).

As expected, the decrease is more evident when arterial rings were cultured with 20% FBS. This decrease was similar to that observed in cultured VSMCs (Figure R9 A). Next, we explored the changes in the expression of Kv1.5 channels to investigate whether it could behave as a MYOCD regulated gene. This was a plausible hypothesis as Kv1.5 mRNA levels are high in contractile phenotype and almost undetectable in cultured VSMCs (see Figure R8).

Kv1.5 expression in the same experimental conditions (Figure R9 B) showed the same pattern of expression than MYOCD. In fact, there was a very good correlation between MYOCD and Kv1.5 mRNA expression levels (Figure R10). Calponin (Cnn1) mRNA expression levels were also determined as a positive control of a MYOCD-regulated gene (Chen *et al.*, 2002; Du *et al.*, 2003).

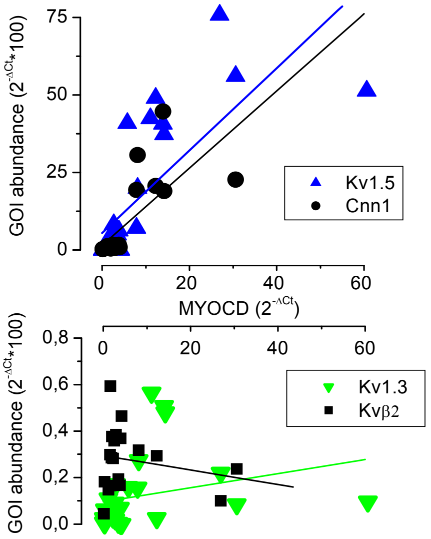

Figure R10. The graphs show the correlation in each sample (n=30 for each data set) between the relative abundance ($2^{-\Delta Ct}$ using RPL18 as a endogenous gene control) of myocardin and the relative abundance of KCNA5 (Kv1.5, blue triangles) and CNN1 (Calponin, black circles, upper plot) or KCNA3 (Kv1.3, green triangles) and KCNAB2 (Kvβ2, black squares, lower graph).The lines show the fit of the data to a linear function. Pearson correlation coefficients were 0.83 (Calponin), 0.765 (Kv1.5), 0.15 (Kv1.3), and −0.19 (KCNAB2).

Figure R10 indicates a positive correlation between MYOCD mRNA expression and either Cnn1 or Kv1.5 mRNA levels. Of interest, this correlation was absent when comparing MYOCD expression with Kv1.3, or with its accessory subunit Kvβ2. Both showed little variation in all conditions tested. Altogether, these data suggest that Kv1.5 mRNA expression (but not Kv1.3) may be regulated by MYOCD.

Finally, we search for the presence of the CArG box regulatory elements in the promoter and 5'UTR sequences of Kv1.5 and Kv1.3 genes, KCNA5 and KCNA3. We studied a 2000 bp region upstream of the ATG with the PROMO 3.0 program of the ALGGEN web (alggen.lsi.upc.es) and in agreement with the literature (Wang *et al.*, 2003; Benson *et al.*, 2011) and with our results, we found two CArG boxes in KCNA5 located from -2 to 8 and from 152 to 162 bp position to the transcriptions start site, but no CArG boxes in KCNA3.

2.2. Effects of manipulating Kv1.3/Kv1.5 expression

2.2.a. Characterization of Kv1. channels overexpression

Kv1.5 channels have been shown to reduce proliferation in heterologous systems. In native VSMC, in the light of the previous findings, we postulate that their downregulation in response to PM may be the trigger for Kv1.3 signaling to proliferation. In other words, we hypothesize that Kv1.5 may inhibit proliferation by occluding Kv1.3 channel signaling. To test this hypothesis, we designed viral vectors to overexpress fluorescently tagged Kv1.3 or Kv1.5 channels, with the idea of exploring whether Kv1.5 overexpression could inhibit Kv1.3-induced proliferation and/or revert PM of VSMCs.

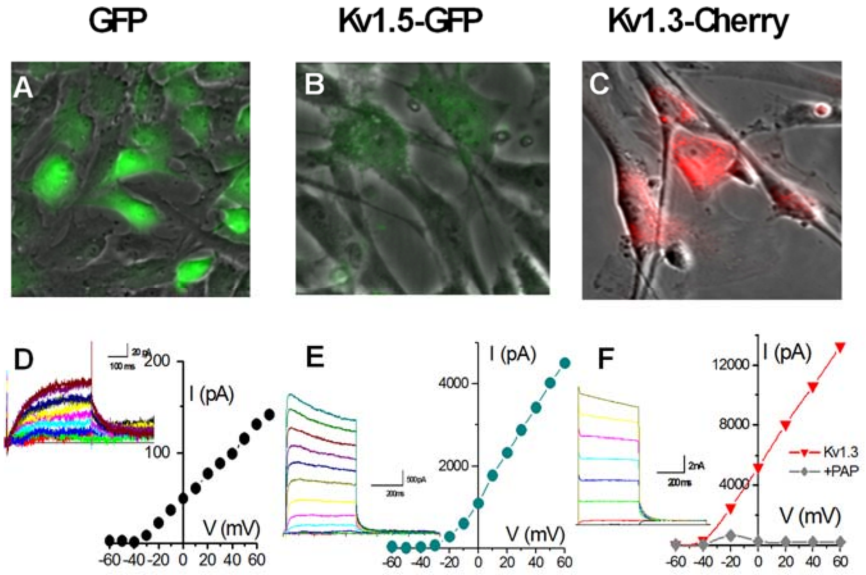

Figure R11. A-C. Microphotographs showing the efficiency of the infections with AAV-GFP (GFP), AAV-Kv1.5 (Kv1.5-GFP), and AAV-Kv1.3 (Kv1.3-Cherry) by direct visualization of the fluorescent tags. **D-F.** Representative current-voltage (I/V) curves obtained in hMA VSMCs infected. Currents were elicited by pulses from −60 to +60 mV in 10 mV steps. The current traces elicited are shown in each case. For Kv1.3, the I/V curve obtained in the presence of PAP-1 (100 nM) is also shown.

The efficiency of infection was tested in hMA and hCA VSMCs in primary cultures. When infecting hMA VSMCs with AAV carrying GFP alone, Kv1.5-GFP or Kv1.3-Cherry, >90% of the cells showed reporter gene expression that could be detected in vivo (Figure R11 A-C) or with GFP immunostaining (not shown).

Electrophysiological studies in these cells demonstrated substantial expression of Kv1.5 or Kv1.3 currents (peak current density at +40 mV was 219.76±36 pA/pF for Kv1.3 and 149.27±25 pA/ pF for Kv1.5 infected cells, versus 8.48±4 pA/pF in non-infected VSMCs or 2.58±2 pA/pF in GFP-infected VSMCs, Figure R11 D-F and Figure R12). Kv1.3 currents were identified by their sensitivity to PAP-1 (as shown in the example of Figure R11 F) and also by their more negative activation threshold (−52.27±1.8 mV) compared with Kv1.5-infected cells (−35.28±2.5 mV, Figure R12 B), as previously described (Jiménez-Pérez *et al.*, 2016).

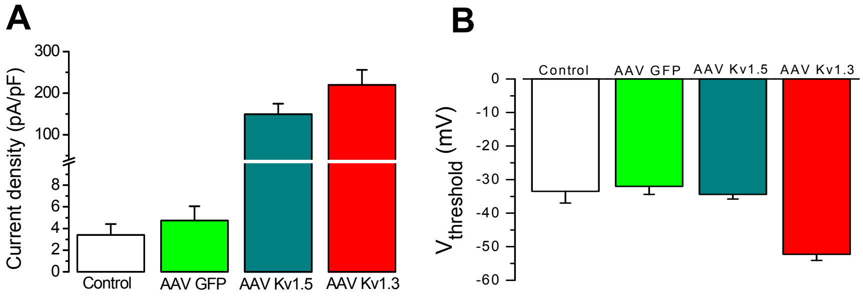

Figure R12. A. Bar plot showing peak current density (pA/pF) at +40mV obtained in control cells or in cells infected with the 3 types of AAV vectors as indicated. N=8–11 cells in each group from at least 3 independent experiments. **B**. Bar plot shows the activation threshold estimated in the same conditions. Only Kv1.3-overexpressing VSMCs showed a shift toward a more negative threshold. Mean ± SEM, n=6-9 cells in each group.

2.2.b. Effects on proliferation of Kv channels overexpression

After these initial controls, we tested if Kv1.3 or Kv1.5 overexpression could affect VSMC migration and proliferation. hMA VSMCs infected with AAV-GFP, AAV-Kv1.3, or AAV-Kv1.5 were incubated for 30 h with PDGF (20 ng/mL) alone or in combination with 100 nM PAP-1. Proliferation rate (calculated as the % of EdU-positive cells) was increased in Kv1.3-infected cells, while Kv1.5 overexpression significantly reduces proliferation rate (Figure R13 A). AAV-GFP infection did not modify proliferation rate (not shown). Moreover, Kv1.5 overexpression abolished the inhibitory effect of PAP-1 treatment, consistent with the hypothesis that Kv1.5 overexpression may be blocking Kv1.3 signaling (see below).

In another set of experiments, we explored the effect of overexpression of the Y447A Kv1.3 mutant (Kv1.3-Y2). This mutant has an alanine in instead the Tyrosine 447, lacking a phosphorylation site required for Kv1.3 induced proliferation.(Jiménez-Pérez *et al.*, 2016), and has been described to abolish Kv1.3-induced proliferation in HEK cells. We confirmed that the increased proliferation rate of hMA VSMCs infected with Kv1.3 could not be reproduced by the Kv1.3-Y2 mutant channel (Figure R13 B).

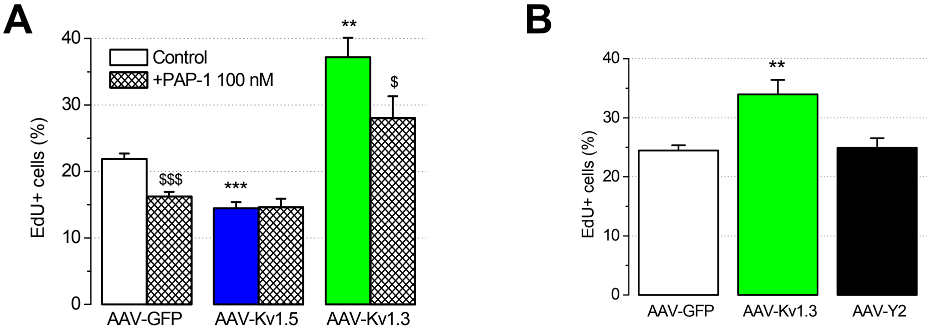

Figure R13. A. Effect of AAV-mediated overexpression on cell proliferation. Each bar is mean ± SEM of 12-25 individual determinations from at least 4 independent experiments. **P<0.01, ***P<0.001 compared with control (GFP); $P<0.05, $$$P<0.001 compared with their own control (PAP-1-untreated VSMCs). **B,** Proliferation rate of VSMCs overexpressing GFP, Kv1.3 or the phosphorylation-defective mutant Kv1.3-Y2 as indicated. N=12–22 independent experiments from 5 -10 different cultures.

The effects on proliferation of AAV-Kv1.5 infections were also reproduced using a lentiviral vector to overexpress Kv1.5 (Lv-Kv1.5; Figure R14). As in the case of AAV-Kv1.5 infected cells, in Lv-Kv1.5-infected cells proliferation was not further inhibited by PAP-1 which did have and inhibitory effect on control, GFP-infected cells.

These data are again consistent with the hypothesis that Kv1.5 inhibits proliferation by occluding Kv1.3. Moreover, we found that treatment with the MEK/ERK inhibitor PD98059 inhibited proliferation to the same level in both GFP and Kv1.5 expressing cells. As Kv1.3 acts through MEK/ERK pathway (Cidad *et al.*, 2015), the lack of an additive effect of PD98059 inhibiting proliferation in Kv1.5 expressing cells gives more support to our hypothesis.

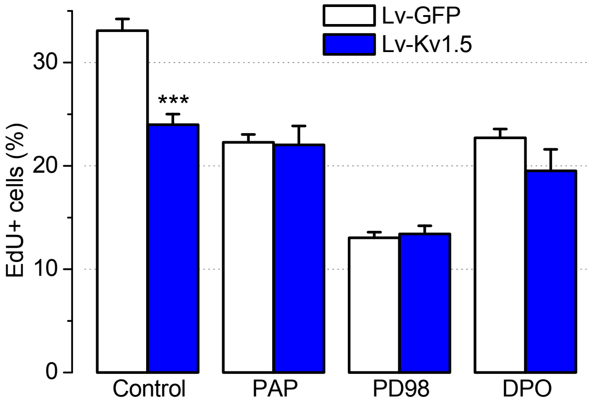

Figure R14. Proliferation rate of human coronary VSMCs infected with lentiviral vectors overexpressing GFP (white bars) or Kv1.5 (Blue bars). Cells were incubated in control media alone or with 100 nM PAP-1 (PAP), 20μM PD98059 (PD98) or 2 μM Diphenyl phosphine oxide-1 (DPO), a Kv1.5 blocker. Data presented as mean ± SEM, n=6-15 data from 3-6 different experiments. ***P<0.001 as compared to Lv-GFP.

Kv1.3 channel is the leading Kv1 in proliferative cells so that Kv1.5 is not able to occlude its proliferative actions. However, Kv1.5 blockade with diphenyl-iodinium (DPO) decreased proliferation in control GFP-infected and did not have additive effect in Lv-Kv1.5 infected cells, showing a pattern similar to PAP-1. These data suggest that DPO is blocking not only Kv1.5 channels but also Kv1.3-containing channels (homo or heterotetrameric).

2.2.c. Effects on migration of Kv channels overexpression

We also explored the effect of AAV infections on hMA VSMCs migration using a scratch assay. The invaded area at different time points (from t=0 to t=24) was explored in control cells (expressing AAV-GFP) or cells overexpressing Kv1.3, Kv1.5 or the Kv1.3 pore mutant (Kv1.3WF).

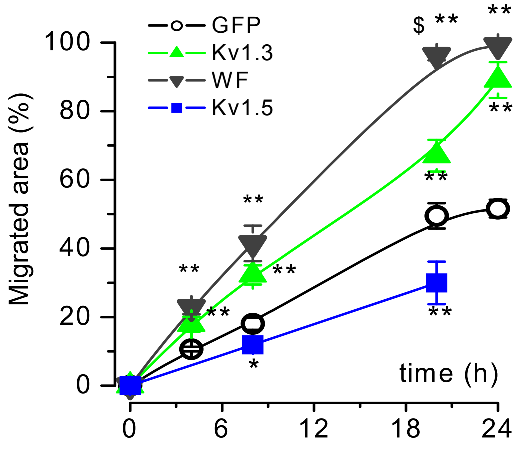

Figure R15. Scratch assay was used to determine the time course of migration of hMA VSMCs overexpressing GFP, Kv1.5, Kv1.3, or a poreless Kv1.3 mutant (WF). Each point is Mean ± SEM, n=4. *$P<0.05$, **$P<0.01$ compared with control, GFP-infected VSMCs; \$$P<0.05$ compared with Kv1.3.

As we can see (Figure R15), Kv1.5 overexpression inhibited cell migration, while Kv1.3 or the non conducting Kv1.3 mutant (WF) highly increased it. The effect of this Kv1.3 pore mutant indicates that K^+ flux through Kv1.3 channel is not needed for Kv1.3-induced VSMCs migration. This observation confirms in a native preparation our previous observation in an heterologous expression system (Cidad *et al.*, 2012).

2.2.d. Effect of Kv1.5 overexpression on intimal hyperplasia

As our data indicated that Kv1.5 overexpression was able to inhibit Kv1.3 effects on VSMC proliferation and migration, we wonder whether Kv1.5 overexpression could also prevent PM. hMA rings in organ culture were infected with AAV-Kv1.5 and AAV-GFP vectors.

Several control experiments were carried out to confirm the efficiency of infection (Figure R16). While direct visualization of GFP fluorescence in live cells or in confocal images of arterial sections showed a very low number of infected cells, suggesting low efficiency, GFP mRNA expression levels were high in all the infected samples, (and absent from non-infected vessels). Finally, immunolabeling of arterial sections with GFP and Kv1.5 antibodies provided a more direct quantification of the degree of expression of the AAV-carried transcripts, confirming a good level of infection of the arterial rings. Figure R16 C shows that GFP Immunolabeling was positive in vessels infected with AAV-GFP and AAV-Kv1.5, whereas Kv1.5 staining was positive only in AAV-Kv1.5-infected vessels, were a large number of cells in the intima and media layer of the vessels were labelled.

After infection for 4 days with AAV-GFP or AAV-Kv1.5, the hMA rings were left for 14 more days in organ culture in 0%FBS and 20% FBS media (alone or in the presence of 100 nM PAP-1). AAV-GFP infected vessels kept in 0%FBS and 20% FBS were used as negative and positive control respectively for IH development.

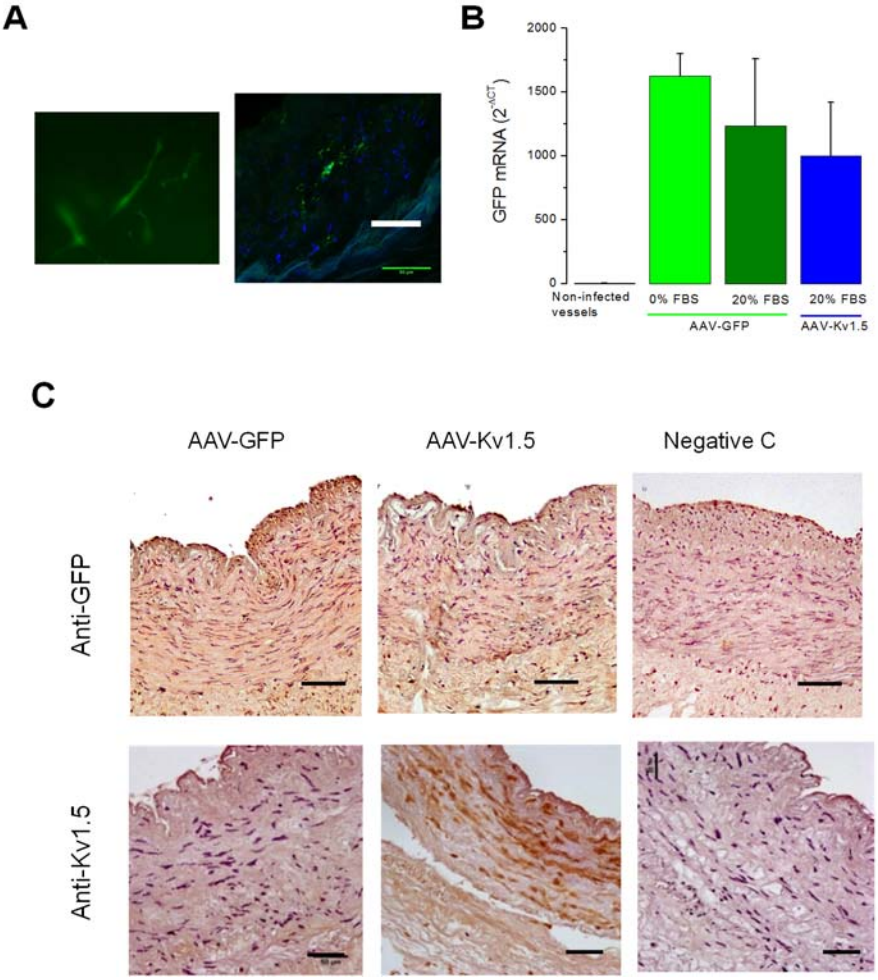
A
B
2000
1500
1000
500
0
GFP mRNA (2^-ΔCT)
Non-infected vessels
0% FBS
20% FBS
20% FBS
AAV-GFP
AAV-Kv1.5
C
AAV-GFP
AAV-Kv1.5
Negative C
Anti-GFP
Anti-Kv1.5

Figure R16. A. Microphotographs showing direct visualization of GFP-labelled cells from arterial rings in organ culture (left image) or with confocal image of a paraffin section of hMA (right image), nuclei labelled with Hoechst (blue); scale bar = 50 µm. **B.** qPCR determination of the relative amount of GFP ($2^{-\Delta Ct}$ using RPL18 as endogenous control gene) in hMA rings non-infected, AAV-GFP infected (kept in 0%FBS or 20%FBS) and AAV-Kv1.5-GFP infected (kept in 20%FBS). Data are Mean ± SEM of 4-5 independent experiments. **C.** Immunohistochemical labelling for GFP (upper panel) or Kv1.5 (lower panel) in paraffin-embedded cross-sections from hMA infected with AAV-GFP (left panel) or AAV-Kv1.5 (middle panel) and kept in organ culture with 20%FBS. Nuclei are counterstained in purple with hematoxylin. Right panel show a negative control (no antibody). 20x objective, scale bar = 100 µm. Data from 4 – 5 determinations.

Histomorphometric analysis of sections of these vessels showed that AAV-Kv1.5 infections prevented 20% FBS-induced remodeling to the same extent as PAP-1 treatment (Figure R17). Moreover, when PAP-1 was present in the Kv1.5 overexpressing vessels the inhibitory effect on

IH development was not additive, confirming that also in organ culture Kv1.5 overexpression and Kv1.3 blockade are acting through a common pathway. The results obtained when determining the I/M ratio were also confirmed when estimating proliferation rate by counting the nuclei present in the intima and media layer of hMA sections stained with Hoechst (Figure R17 B): Kv1.5 overexpression decreased proliferation to the same extent that PAP-1 treatment and the addition of PAP-1 to the AAV-Kv1.5 infected vessels did not have additive effects on proliferation inhibition.

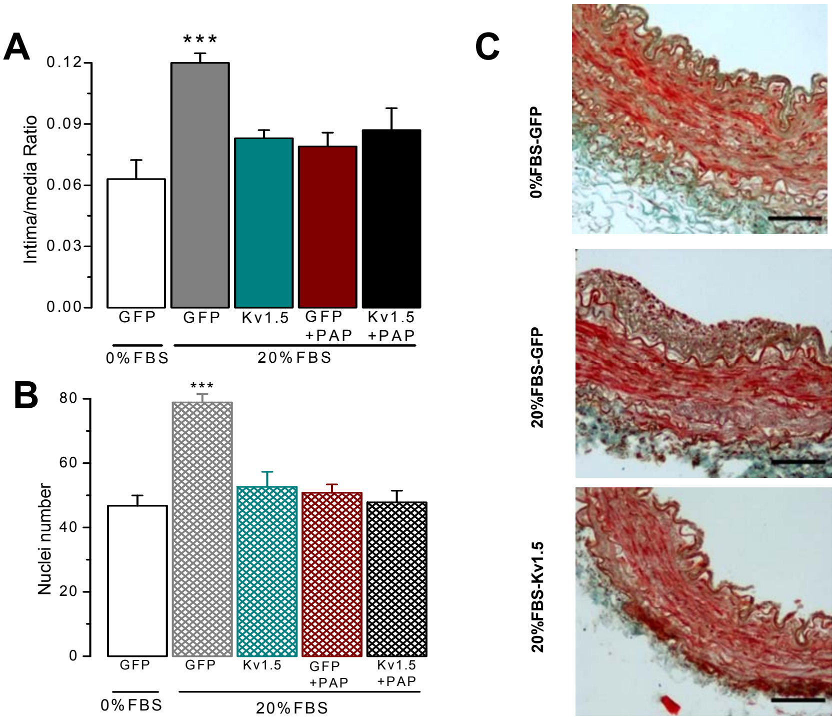

Figure R17. A. Effect of Kv1.5 overexpression on intimal hyperplasia (I/M Ratio) induced by 20% FBS. **B.** Proliferation rate in AAV-Kv1.5- infected hMA rings in organ culture. **C.** Representative microphotographs of hMA sections stained with Masson trichrome in the 3 indicated conditions. Scale bar=100um. Each bar is the mean ± SEM of 3 to 6 experiments,*** P<0.001 compared with 0% FBS-GFP.

2.3. Myocardin as mediator of Kv1.5 effects on PM

The previous set of experiments indicates that Kv1.5 channels expression opposes VSMC dedifferentiation and vessel remodeling. As we have also found that MYOCD mRNA expression correlates with Kv1.5 expression, we tried to explore if, in the context of PM, both observations reflect a causal association. We hypothesize that Kv1.5 could be a MYOCD regulated gene, so that upon PM the decrease of MYOCD expression will determine the observed downregulation of Kv1.5 gene (KCNA5). As a way to demonstrate this hypothesis, we generated a MYOCD knockdown in our organ culture model of IH, using a Lentiviral vector to deliver a Crispr/Cas9 construct against two exons of MYOCD gene (exon1 and exon 10). We infected the hMA rings with this construct (Lv-ccMYOCD) and we use a Lv-GFP vector as control. As before, the hMA rings infected with Lv-GFP and kept in 0%FBS or 20%FBS media were used as negative and positive control for IH, respectively. The vessels infected with Lv-ccMYOCD were kept in 0%FBS media.

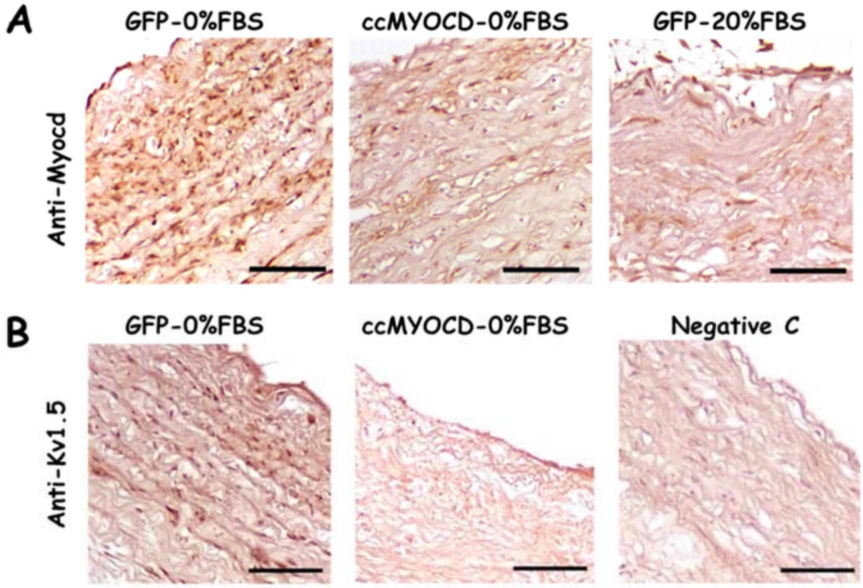

Figure R18. Immunohistochemical labeling for myocardin (upper pannels) and Kv1.5 (lower ones) of cross sections from hMA vessels kept in 0%FBS and infected with Lv-GFP (left) or Lv-ccMYOCD (middle). Positive control for IH are Lv-GFP infected vessels kept in 20%FBS (upper right). Negative control for immnunolabeling are cross sections without primary antibody (lower right). Scale bar 100µm, objective 10x. Data from 2-3 experiments.

Knockdown of myocardin upon Lv-ccMYOCD infection was confirmed by the decreased in MYOCD mRNA expression by qPCR (see below) and the decreased of myocardin protein expression determined by immunohistochemical labeling of cross-sections of the vessels (Figure R18). The expression of myocardin is evident in vessels kept in 0% FBS, but significantly decreased in hMA rings infected with Lv-ccMYOCD even though they are also kept in 0%FBS. In fact the labelling of myocardin in this later case is not different from the observed in vessels maintained in 20% FBS. In support of our hypothesis, immunolabeling with anti-Kv1.5 indicated that Kv1.5 expression followed the same pattern of expression as myocardin (see lower panels of the figure).

To corroborate these findings, and to check myocardin antibodies (Lyu *et al.*, 2019), we also explored expression of other well-known myocardin target genes: myosin heavy chain II (MYHII) and smooth muscle protein 22-alpha (SM22). Immunohistochemical experiments showed that both proteins also decreased their expression upon Lv-ccMYOCD infection or after 20%FBS treatment (Figure R19).

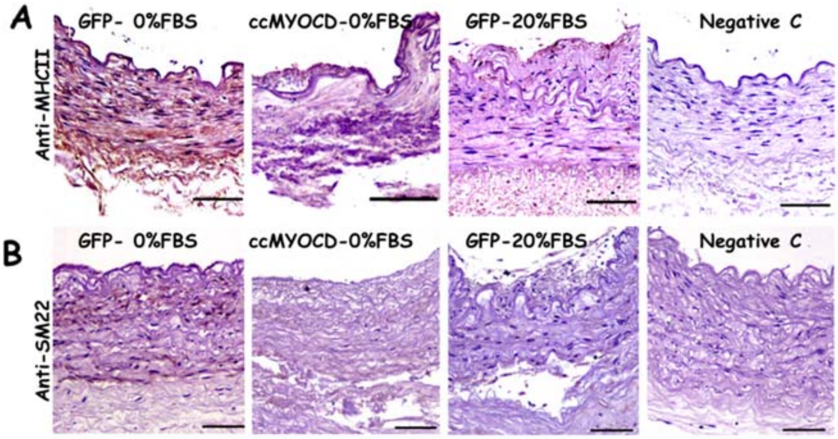

Figure R19. Representative microphotographs showing the labelling of the smooth muscle contractile proteins Myosin heavy chain II (MHCII, upper panels) and SM22 (lower panels) in paraffin-embedded cross-sections of hMA infected with Lv-GFP or the myocardin knock-down Lv-ccMYOCD. Arterial rings were kept in organ culture for 14 days in 0% or 20% FBS as indicated. Right panels show the negative control for each antibody in a GFP-0% FBS sample. 10x objective (NA=0.3), scale bar 100µm. Data from 2- 3 experiments.

The Lv-ccMYOCD construct had two different guides against two exons, 1 and 10,so that additional control experiments to exclude possible off-target effects of this construct were also performed (Figure R20), comparing the effect of our construct with other two vectors targeting each individual MYOCD exon: CRISPR-1 (targeting Exon 1) and CRISPR-10 (against Exon 10). Infected arterial rings were incubated for 7 days, after which mRNA expression of both Kv1.5 and MYOCD was determined. Our data shows that the CRISPR-1 targeting exon 1 was as effective as the ccMYOCD targeting both exons, while the CRISPR-10 had no effect.

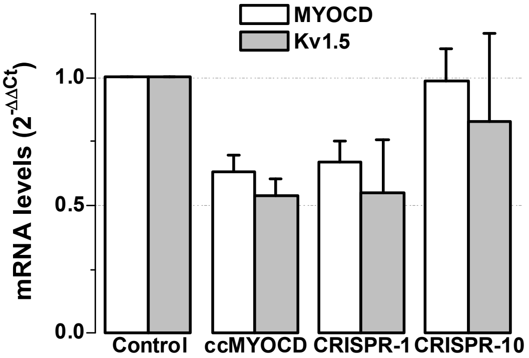

Figure R20. mRNA expression levels of Kv1.5 and Myocardin with the different myocardin knock-down vectors: CRISPR-1 (targeting exon 1), CRISPR-10 (targeting Exon 10), ccMYOCD (targeting both exons). Lv-GFP was used as control. Bar plot shows relative expression ($2^{-\Delta\Delta t}$) of MYOCD (white bars) and Kv1.5 (grey bars) using Lv-GFP as calibrator and RPL18 as the endogenous control gene. n= 4-6 determinations.

After confirming the efficiency of our myocardin knockdown strategy, we used Masson trichrome stain to explored vascular remodeling.

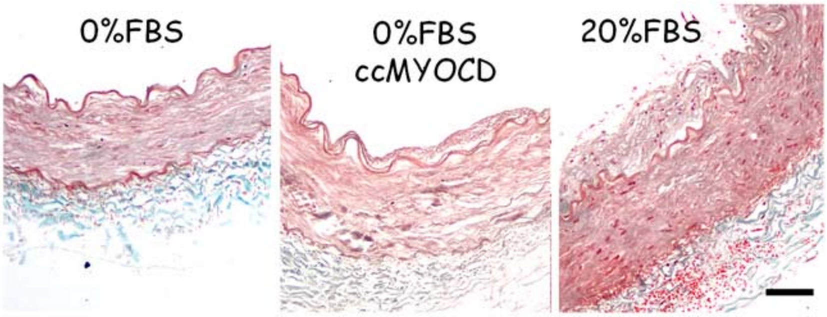

Figure R21. Representative microphotographs with Masson trichrome stain of 0% FBS-Lv-GFP- (left), 0% FBS-Lv-ccMYOCD- (middle) and 20% FBS-Lv-GFP-infected (right) vessels. 10x objective (NA=0.3),scale bar 100 μm. n=3.

We found that hMA vessels infected with ccMYOCD and kept in 0%FBS develop neointima layer, which is also present in the 20%FBS treated vessels, but not in the control rings in 0%FBS (Figure R21). From these sections, I/M ratio was calculated to evaluate the IH in the different experimental conditions. The average data from 3 independent experiments shows a significant increase of I/M ratio in Lv-ccMYOCD-infected vessels in 0%FBS when comparing with control vessels in the same conditions (0%FBS, Figure R22).

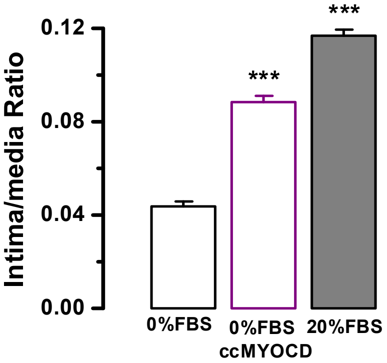

Figure R22. Effect of myocardin knockdown on PM. average data (mean ± SEM) of the I/M ratio obtained in Lv-GFP-infected vessels in 0% FBS or 20% FBS or Lv-ccMYOCD-infected vessels in 0%FBS; n=3.

Finally, in order to confirm a causal relationship between myocardin and Kv1.5, we determined the mRNA expression levels of MYOCD, Cnn1, and endogenous KCNA5 mRNA, comparing vessels infected with Lv-ccMYOCD and AAV-Kv1.5 (MYOCD knockdown and Kv1.5 overexpression), see Figure R23.

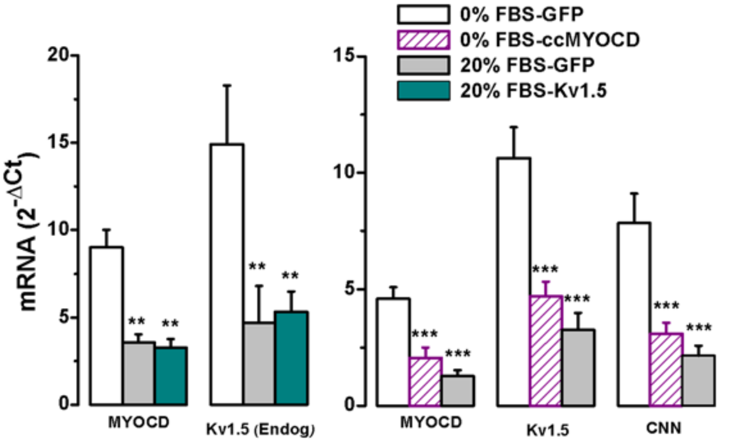

Figure R23. Relative amount of MYOCD or endogenous Kv1.5 mRNA in hMA infected with AAV-GFP (kept in 0% or 20% FBS) or AAV-Kv1.5 (in 20% FBS) was determined by qPCR and expressed as $2^{-\Delta Ct}$ using RPL18 as endogenous control (left plot). The right plot shows mRNA expression of myocardin, Kv1.5, or calponin in hMA infected with Lv-GFP (in 0% and 20% FBS) or Lv-ccMYOCD (in 0% FBS). Mean ± SEM, 3-5 independent experiments. $^{**}P<0.01$, $^{***}P<0.001$ compared to 0% FBS-GFP.

MYOCD expression decreased when arterial rings were cultured in the presence of 20% FBS (grey bars), and was unchanged by Kv1.5 overexpression in AAV-Kv1.5 infected samples (green bars). However, MYOCD knockdown in Lv-ccMYOCD infected rings decreased calponin and Kv1.5 mRNA expression (dashed bars), and also Kv1.5 protein expression as previously described, see Figure R23. In other words, while MYOCD expression is unchanged when Kv1.5 expression is manipulated, Kv1.5 channel expression follows myocardin changes, so that it behaves as a MYOCD-regulated gene.

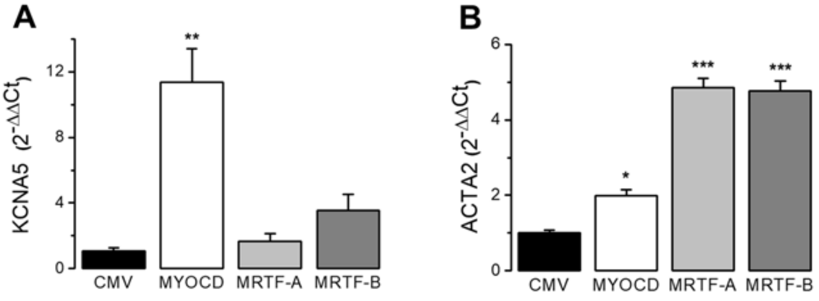

Figure R24. The **A** and **B** panels show the relative mRNA expression of KCNA5 and alpha-actin-2 (ACTA2) respectively by qPCR in human coronary artery smooth muscle cells (hCASMCs) transduced with adenovirus expressing myocardin (ADV-216227), MRTF-A (ADV-21549) or MRTF-B (ADV-215500). Cells infected with control adenovirus, with empty cytomegalovirus promoter (CMV), were used as calibrator. Relative expression was calculated as $2^{-\Delta\Delta Ct}$, data are mean ± SEM of 5 independent transductions.

A further confirmation of our hypothesis was obtained in parallel, complementary experiments in which, using adenoviral vectors to overexpress myocardin or myocardin-related transcription factors A and B (MRTF-A and MRTF-B), we explored the changes in gene expression in hCA VSMCs. We found a significant upregulation of Kv1.5 mRNA (KCNA5), which was only partially reproduced by MRTF-B infection (Figure R24). The expression levels of alpha-actin-2 (ACTA2) mRNA, a known myocardin target, were also determined in the same samples as a positive control. These data demonstrated that Kv1.5 expression is regulated by MYOCD. 3. Expression and functional contribution of Kv1.3 to PM in diseased vessels.

3. Expression and functional contribution of Kv1.3 to PM in diseased vessels

3.1. Effect of Kv1.3 blockers inhibiting phenotypic modulation in T2DM patients

A significant number of patients undergoing vascular surgeries have underlying diseases that worsen the prognosis of the surgery, as they became more susceptible to develop intimal hyperplasia. Essential hypertension, diabetes, metabolic syndrome or obesity are some of these diseases. Here we have focused in a subgroup of this risk populations, the patients with Type 2 diabetes (T2DM). T2DM is one of the most important risk factors for exacerbation of IH. T2DM associates with increased prevalence of coronary artery disease and is an independent risk factor for increased morbidity and mortality. Moreover, it is a recognized risk factor for poor outcome following vascular surgery, with higher morbidity and short- and long-term mortality. Yet up to 25% of patients undergoing coronary revascularization have diabetes, so understanding the dysregulation of the signaling pathways leading to increased restenosis in T2DM patients is of major clinical importance.

Characteristic	Total (n=28)	No-T2DM (n=15)	T2DM (n=13)
Age (yrs) *Mean±SEM*	68.55±1.53	68.44±2.24	68.69±2.13
Gender (%)			
Male	82.14	86.67	76.92
Female	17.86	13.33	23.08
BMI (Kg/m^2) *Mean±SEM*	27.75±0.75	27.87±1.00	27.61±1.17
Blood Pressure (mmHg)			
Systolic	128.72±4.63	127.30±6.70	130.50±6.65
Diastolic	76.33±3.65	79.10±5.57	72.88±4.45
Mean	93.80±3.76	95.17±5.72	92.08±4.89
Glycemia (mg/dl) *M±SEM*	123.85±8.63	102.93±4.27	146.38±15.25**
T2DM treatment (%)			
Diet			15.38
OADs			53.85
Insulin			30.77
CV risk factors (%)			
Hypertension	73.90	54.55	91.60 *
Dyslipemia	73.68	60.00	88.90
Smoking	15.79	20.00	11.11
Previous MI	47.37	30.00	66.66
Previous Angina	68.42	80.00	55.55
Previous stroke	5.56	0.00	11.11
PVD	22.22	0.00	44.44 *

Table R 1. Table summarizing relevant clinical data of the hMA donors. . **BMI** :body mass index = weight (kg)/[height (cm)]^2, **OADs**: oral antidiabetic drugs, **MI** myocardial infarction, **PVD** peripheral vascular disease.

As we have access to clinical data from the hMA donors, we segregated the population in two groups, T2DM and no-T2DM (control) and summarized the most relevant clinical information in table R1 As shown in this table,T2DM and no-T2DM groups show no differences in age, BMI (body mass index), dyslipemia, smoking, previous myocardial infarction, angina and stroke. T2DM group shows higher glycaemia ($p< 0.009$, t-test), and higher incidence of hypertension and peripheral vascular diseases ($p<0.04$Fisher exact test) when comparing with non-T2DM patients

Thus, we aimed to explore if we can find differences in remodeling between these two groups, T2DM and no-T2DM (control), in our *in-vitro* model and to determine if Kv1.3 blockade could represent an effective strategy to prevent restenosis in this population. First we determined Kv1.3 mRNA expression levels. Kv1.3 channel expression was significantly more abundant in T2DM hMA (Figure R25). *A priori*, this data suggests that not only Kv1.3 could be a valid therapeutical target in these patients, but also that it may have a more important role in remodeling of T2DM vessels.

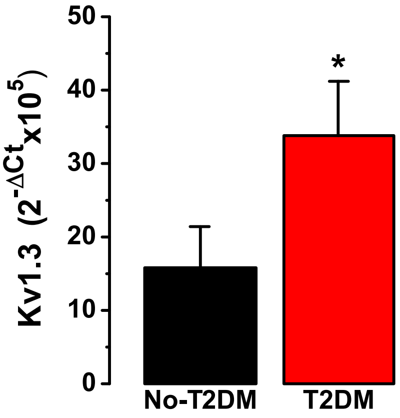

Figure R25. Bar graph displaying mRNA Kv1.3 relative abundance (normalized to RPL18) in contractile VSMCs from hMA. .Data are mean ± SEM of 4-6 individual determinations in triplicate. $*P<0.05$ compared to non-diabetic samples.

3.1.a. Differences in IH in non-T2DM and T2DM vessels

In the clinics, prevention of IH after percutaneous interventions with stent implantation is addressed by the use of drug eluting stents containing tacrolimus (taxol) or sirolimus or everolimus (derivatives of rapamycin). In order to propose an alternative therapy we will need to prove its superior efficacy compared with current treatments. Accordingly, we decided to explore the effect of the Kv1.3 blocker PAP-1 in parallel to the effect of the mTOR inhibitor everolimus, which is the gold standard in the clinics (Byrne *et al.*, 2008; Stefanini & Holmes, 2013).

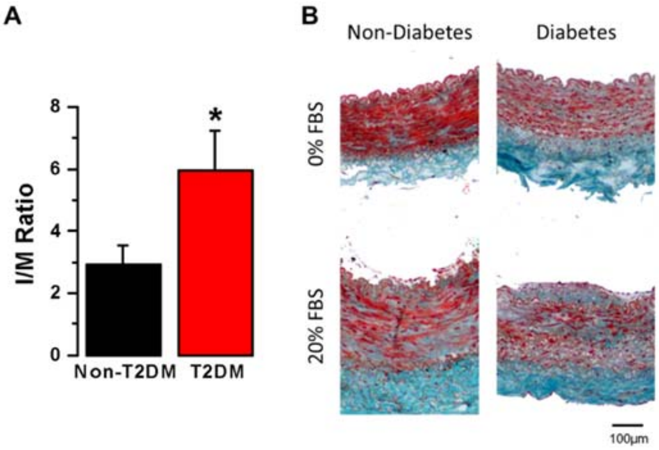

Figure R26. A, Bar graph showing intima/media ratio of hMA vessels kept in 2 weeks-organ culture with 20%FBS. Data from 15 different vessels (9 from non-diabetic and 6 from diabetic donors).* P<0.05. **B**. Representative microphotographs of hMA with Masson trichrome. 10x objective, scale bar=100 µm.

First we explored the possible differences in remodeling between vessels from T2DM and non-T2DM. hMA were kept in organ culture in the presence of 20%FBS, and after two weeks, intima/media ratio (I/M) was measured in several samples of both groups. The average I/M ratio values obtained in the T2DM (5.94 ±1.28) were significantly larger than in non-T2DM (2.9 ± 0.63), indicating that, as expected from previous data in the literature, also in our IH model T2DM vessels show increased remodeling (Figure R26).

3.1.b. Effects of Kv1.3 blockers preventing IH in T2DM vessels

Once demonstrated that T2DM vessels develop more IH, we asked about the effect of Kv1.3 blockade on 20%FBS-induced IH in both groups. We used PAP-1 treatment in vessels kept in organ culture with 20% FBS, and we also explored in parallel the effects of the mTOR inhibitor everolimus. Both PAP-1 and everolimus show an inhibitory effect on T2DM vessel remodeling of comparable magnitude. However, while PAP-1 blockade also reduced I/M ratio in non-T2DM vessels, everolimus treatment was without effect in this group (Figure R27).

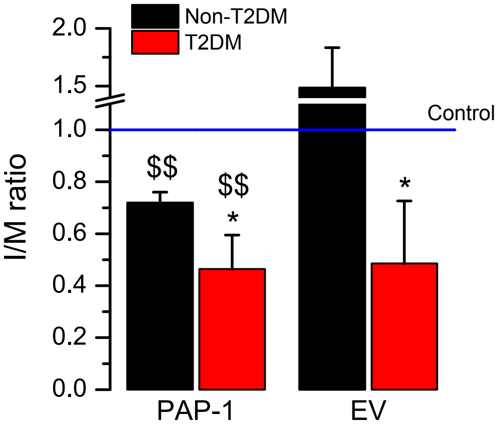

Figure R27. Bar graph shows the intima to media ration in the presence of 100 nM PAP-1 and 1nM Everolimus (Ev) in non-T2DM and T2DM hMAs after 2 weeks-organ culture with 20%FBS, normalized to the remodeling observed in control samples (incubated with 20%FBS alone, blue line). *P<0.05 compared to Non-T2DM samples. $$p<0.01 compared to control. N=3-7 arteries for each group.

3.1.c. Kv1.3 blockers in T2DM proliferation and migration

To gain further insight in the processes underlying IH that can be differentially regulated in T2DM and non-T2DM vessels, we next explored the effect of PAP-1 and everolimus on proliferation and migration of primary VSMCs cultures obtained from T2DM and non T2DM patients.

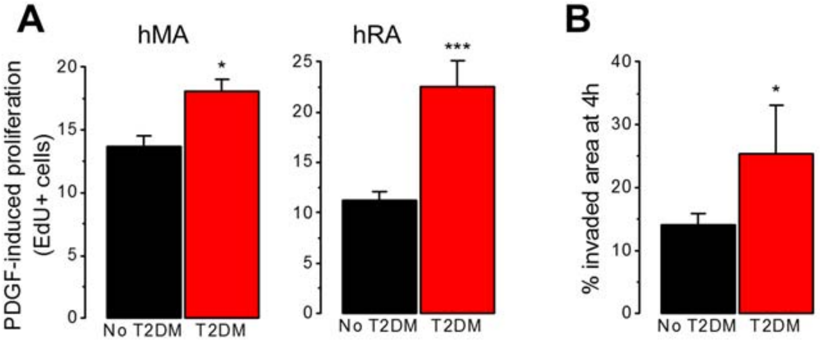

Figure R28. A. Average proliferation rates (mean ±SEM) of non-T2DM and T2DM VSMCs cultures obtained from human mammary and renal arteries (hMA and hRA). EdU+ cells were determined after 6h incubation in the presence of PDGF, and the proliferation obtained in the absence of PDGF was substracted. N= 17-22 determinations from at least 4 different cultures. .**B,** Migration rate of non-T2DM and T2DM VSMCs expressed as % of invaded area in scratch assays from 6-18 independent assays. *P<0.05, *** P<0.001 compared to non-T2DM samples.

First, we determined whether the differences in IH development observed in organ culture between non-T2DM and T2DM are also present when determining the basal rate of proliferation and migration in non-T2DM and T2DM VSMC cultures. We found that T2DM VSMCs from hMA (and also from renal arteries, hRA) showed higher rates of PDGF-induced proliferation, with a very consistent pattern in both cases. Proliferation rates were obtained from 8-12 different assays from at least 4 different patients in each group. Also, in the wound healing assays used to determine migration, T2DM cells showed increased invasion rates, significantly different from non-T2DM (Figure R28).

Next, we compared the magnitude of the inhibition of these responses (migration and proliferation) in the presence of PAP-1 or everolimus. EdU incorporation assays indicated that both drugs were able to reduce VSMC proliferation. We did not observe differences in the case of PAP-1, but 10 pM everolimus inhibited a larger fraction of PDGF-induced proliferation in non-T2DM samples (Figure R29).

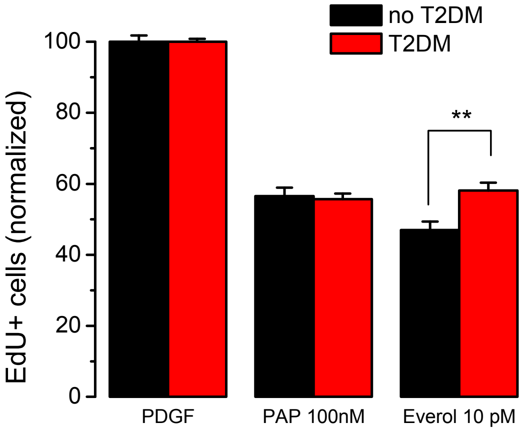

Figure R29. EdU incorporation assay in hMA VSMCs from non-T2DM or T2DM patients. The plot shows the mean ± SEM of 20-50 individual determinations from at least 10 independent experiments in each group and using cell lines from at least 4 different patients. **P<0.01, compared to non-T2DM samples.

Finally, we explored the effect of PAP-1 and everolimus on migration with a scratch assay. When comparing non-T2DM and T2DM VSMCs, we found that PAP-1 was able to inhibit migration in both groups, albeit to a higher extent in T2DM VSMCs. On contrast, everolimus only inhibited migration in T2DM samples (Figure R30).

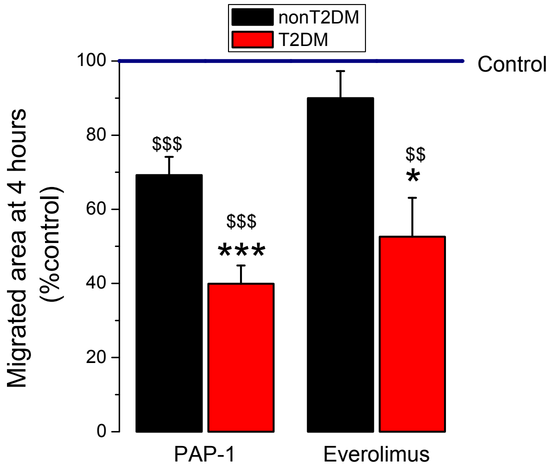

Figure R30. Bar graph showing PAP-1 and everolimus effect inhibiting migration. Data is normalized to control migration (in the absence of drugs, blue line) in each individual experiment. N=5-16 experiments. *P<0.05, ***P<0.001 compared to non-T2DM samples, $$P<0.01, $$$ P<0.001 compared to control.

3.1.d. Kv1.3-induced remodeling and T2DM signaling in VSMC

So far, our data indicated that Kv1.3 expression is increased in T2DM vessels, and Kv1.3 blockers are more effective inhibiting FBS-induced intimal hyperplasia in T2DM vessels, suggesting a larger contribution of Kv1.3 to vessel remodeling in T2DM patients. In addition, Kv1.3 blockade with PAP-1 is also more efficient inhibiting T2DM VSMCs migration. In order to get more insight into the possible associations between Kv1.3 signaling and T2DM in VSMCs, we seek to explore if it could be a cross talk of the signaling pathways involved in Kv1.3-induced proliferation (mainly the MEK/ERK pathway, see (Cidad *et al.*, 2012) and in T2DM (mainly PI3K/AKT pathway).

Therefore, we explored the levels of expression and activity of key proteins involved in these two signaling pathways. In particular, we looked at the expression of phosphorylated-insulin receptor (pIR) and phosphorylated-AKT (pAKT) to determine the effect of T2DM. Western blot analysis indicated that T2DM VSMCs have decreased expression of pAKT and pIR when comparing with non-T2DM VSMCs, indicating that PI3K pathway is less active in diabetic VSMCs (Figure R31).

As previous work from our lab have stated that Kv1.3 channel exerts its actions through MEK/ERK signaling pathway (Cidad *et al.*, 2015), we determined by western blot the amount of phosphorylated ERK (p-ERK). T2DM VSMCs showed more expression of p-ERK protein than non-T2DM VSMC, suggesting that T2DM samples have more activated the

MAPK pathway, which is consistent with the proposed increased contribution of Kv1.3 channels in this group.

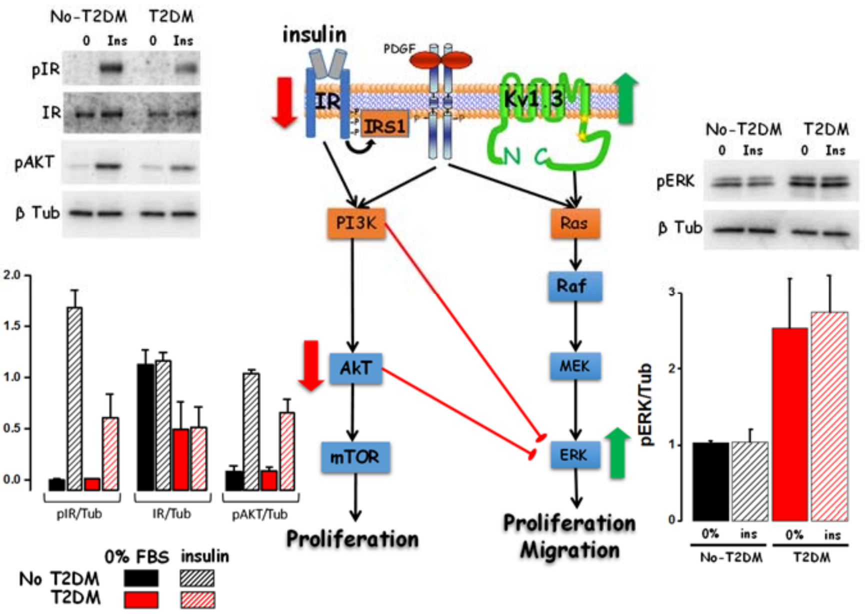

Figure R31. Representative western blotting of phosphorylated insulin receptor (pIR), phosphorylated AKT (pAKT) and phosphorylated ERK (pERK) from T2DM and non-T2DM cultured VSMC obtained from renal or mammary arteries as indicated, and incubated for 10 min with or without insulin or PDGF. The scheme shows the simplified view of the signaling pathways activated by insulin or PDGF and also the pathway modulated by Kv1.3.

In any case, the differences observed between T2DM and non-T2DM point towards epigenetic changes induced by T2DM and still remaining in VSMC cultures, which we decided to investigate in more detail.

3.2. Differential miRNA expression profile in T2DM vessels.

microRNAs have emerged as molecules that can regulate the expression of many proteins by repressing its expression. Using a miRNA qPCR array focused in cardiovascular disease, we screened the expression of 84 mature miRNAs, in order to get more insight into the mechanism involved in PM in T2DM patients. miRNA expression profile was studied in hMA VSMC from tissue (contractile phenotype) and VSMCs culture (proliferative phenotype). A table containing the name (ID) of the miRNA, Ct, $2^{-(\Delta Ct)}$, fold change and fold regulation of the 84 miRNA is provided in Annex 1 and Annex 2. A pool of 2-3 samples for each condition (non-T2DM and T2DM, tissue and culture) was used for each array. The miRNA showing significant changes in expression between non-T2DM and T2DM samples were validated by qPCR in the same individual samples that were pooled for the array as well as in VSMC samples from other patients.

3.2.a. miRNAs profile in T2DM contractile VSMC

The miRNA array profile in contractile VSMC (hMA tissue) showed consistent expression of 73 out of 84 miRNAs (Figure R32).

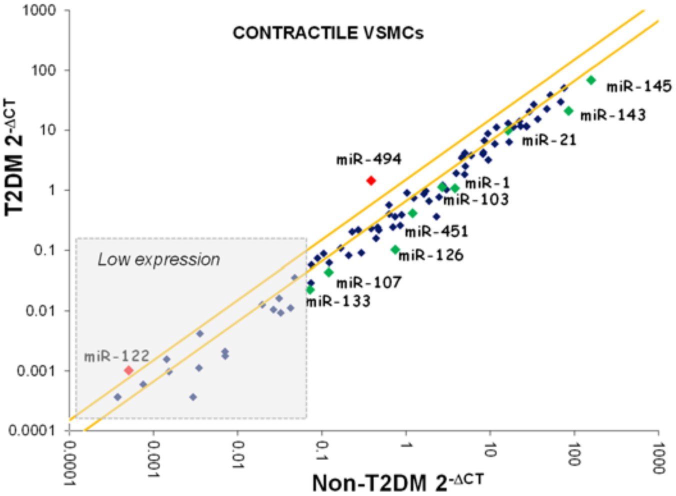

Figure R32. Scatter plot displays miRNA expression in contractile VSMC (hMA tissue) from T2DM vs non-T2DM patients. The most dramatic changes for either upregulation (red) and downregulation (green), more than 1.5 fold changes and meeting other criteria (see text) are also identified Data were obtained from miRNA array using a pool of 3 different patients for each group, in triplicate determinations.

After analyzing which one of those showed consistent changes when comparing T2DM versus non-T2DM samples, we focused on the ones that meet more than one of the following criteria: 1) showing large fold changes (over 1.5-2 fold times), 2) presenting reasonable high expression levels and 3) previously reported as relevant in PM or diabetes.

To identify the differences in expression of these miRNAs we represented miRNA expression levels (normalize to endogenous control) of contractile VSMCs from T2DM patients versus non-T2DM patients in a scatter plot. In Figure R32, the data points within the two yellow lines shows miRNAs with no changes in T2DM patients (i.e., expression differences <1.5 fold change with respect to non-T2DM). Outside this area we plotted the miRNAs with fold change >1.5, the most upregulated are highlighted in red and in green the most downregulated.

With the aforementioned criteria, we selected miR-1, miR-21, miR-103, miR-107, miR-126, miR-133, miR-143 and miR-145, and their changes in expression were validated by qPCR of individual samples, using both the VSMCs of the microarrays and VSMCs form other patients. The differences in expression of all but miR-21 were validated by qPCR. Also, with the exception of miR-1, which showed increased expression by qPCR in T2DM tissues (while presenting downregulation in the miRNA array), all the others showed a downregulation in T2DM that was confirmed by qPCR. (Figure R33).

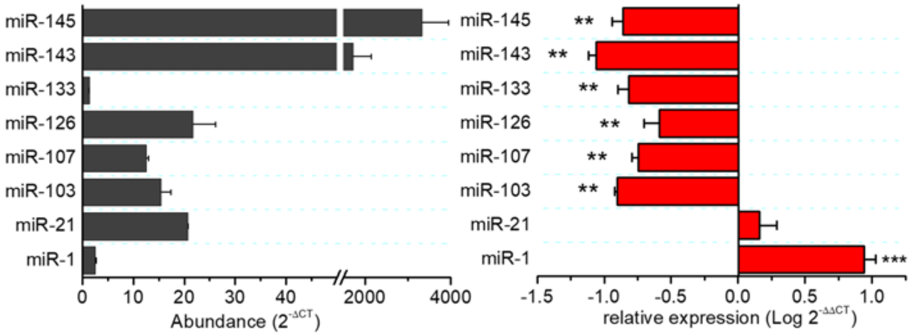

Figure R33. qPCR validations of selected miRNA in contractile VSMCs. Left plot shows the relative abundance ($2^{-\Delta CT}$) using SNORD68 as endogenous control of the indicated miRNAs in non-T2DM VSMCs. Right plot shows the relative expression (Log $2^{-\Delta\Delta CT}$) in T2DM VSMCs using the non-T2DM as calibrator. Mean ± SEM, triplicates of 3-4 different patients. **P<0.01, *** P<0.001 compared to non-T2DM samples.

3.2.b. miRNAs profile in T2DM dedifferentiated VSMC

The same study was carried out in cultured VSMCs (proliferative phenotype) from non-T2DM and T2DM patients, and the results are presented in the same way: a scatter plot of the miRNA array and the data from the qPCR validation (Figure R34 and Figure R35) In this case 71 out of the 84 miRNAs explored were expressed in VSMCs, and less variations in expression were found, as shown in Figure R34, were most of the data points fall within the two yellow lines. Following similar criteria than before, we selected miR-1, miR-122, miR-126, miR-182 and miR-451 for validation with qPCR.

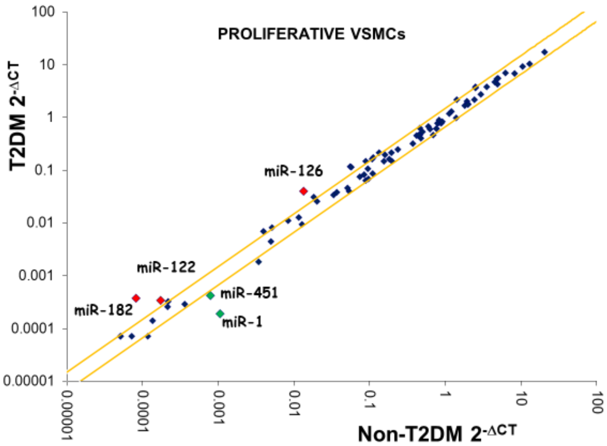

Figure R34. Scatter plot shows miRNA expression in T2DM versus non-T2DM cultured VSMC obtained from microarrays of miRNA. The largest changes in expression are labelled and colored as in Figure R30. Data are obtained from pooled data from 2 different patients in each group.

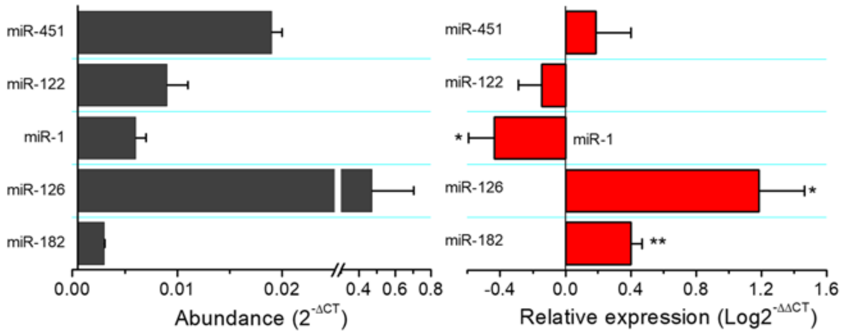

Figure R35. qPCR validations of selected miRNA in cultured VSMCs. Left plot shows the relative abundance ($2^{-\Delta CT}$) using SNORD68 as endogenous control, in non-T2DM VSMCs. Right plot shows the relative expression (Log $2^{-\Delta\Delta CT}$) in T2DM VSMCs using the non-T2DM as calibrator All data is presented as mean ± SEM. *P<0.05, **P<0.01, compared to non-T2DM samples Data are triplicates of 3-4 different patients**.**

The results of these validation (Figure R35) confirmed the upregulation of miR-126 and miR-182 and the downregulation of miR-1 in T2DM dedifferentiated VSMC, while the changes in expression of miR-122 and miR-451 did not reach statistical significance. The low expression levels of these two miRNAs, and the smaller fold change observed in the miRNA array could contribute to this lack of confirmation.

3.2.c. miR-126 origin in non-T2DM and T2DM samples.

The results of this initial screening attracted our attention to miR-126 for several reasons: 1) miR-126 is the most heavily downregulated miRNA in T2DM tissue (i.e. contractile VSMC); 2) miR-126 shows the opposite change, a significant upregulation in T2DM dedifferentiated cells (cultured VSMCs) see Figure R36. miR-126 showed high expression levels in both preparations (tissue and cell culture) which suggest a potentially important role and facilitates the study of expression changes. In addition, data in the literature links miR-126 with vascular pathologies and with T2DM, and several proteins of the insulin signaling pathways such as insulin receptor substrate 1 (IRS-1), PI3K and AKT are known miR-126 targets (Zampetaki *et al.*, 2010; Zhou *et al.*, 2013).

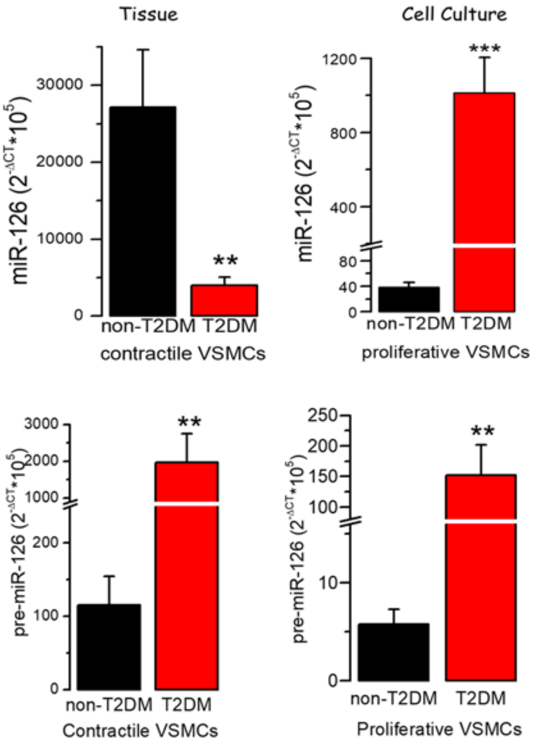

Figure R36. The upper bar graphs show miR-126 abundance in VSMCs in contractile (tissue, left) and proliferative phenotype (cell culture, right) from hMA VSMCs. SNORD68 was used as housekeeping control. Each bar is mean ±SEM of 7-10 meassures from 5 non-T2DM patients and 6 T2DM patients. The lower plots show the abundance of pre-miR-126 in the same conditions and samples. $^{**}P<0.01$;$^{***}P<0.001$ compared to non-T2DM samples.

However, miR-126 has been described as an endothelial miRNA, secreted by EC and internalized by VSMCs, to regulate VSMC gene expression and function in a paracrine fashion (Wang *et al.*, 2008; Zhou *et al.*, 2013), although our data suggested that miR-126 could also be expressed in VSMC. In order to discern the source of miR-126, EC or VSMC, we explored the presence and the expression levels of miR-126 precursor (pre-miR-126) in our VSMC samples. Using probes that identify both pri-miR-126 and pre-miRNA-126, we analyzed their expression in contractile and proliferative VSMCs (i.e. arterial tissue and cultured VSMCs) in non-T2DM and T2DM. We found that VSMC do express miR-126 by itself as we found expression of pre-miR-126. Of interest, pre-miR-126 expression was significantly upregulated in all T2DM samples (Figure R37). This results suggested that the presence of EC could have an effect on the final concentration of miR-126, at least in T2DM patients. To explore this, we analyze expression of pre-miR-126 and miR-126 in contractile VSMC alone or with EC tissue. Figure R37 shows that EC have no effect on non-T2DM patients, but in the case of T2DM it seems that mir-126 is produced at increased rate in VSMCs to be secreted and internalized by EC.

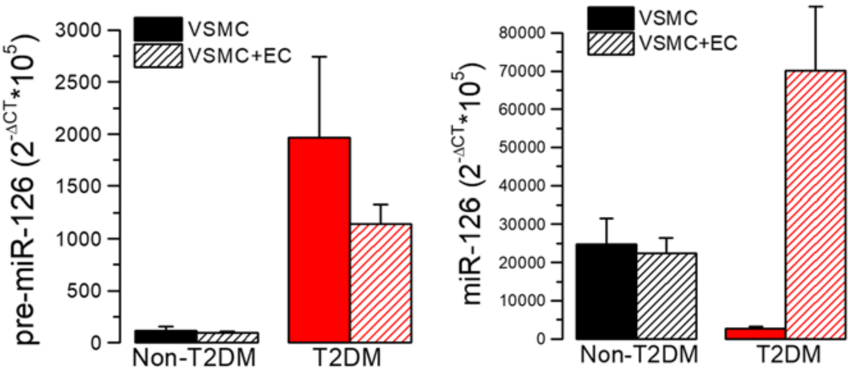

Figure R37. Relative abundance ($2^{-\Delta CT}$) of pre-miR-126 and miR-126 in hMA tissue from non-T2DM patients (black bars) or T2DM patiens (red bars). Determinations were made using either VSMC alone (i.e., the media layer, solid bars) or VSMC+EC (media+intima layers, stripped bars). Each bar is the average from 5-6 different patients.

3.2.d. Functional contribution of miR-126 to PM in T2DM.

We focus on analyzing if the changes in miR-126 observed in cultured VSMCs from T2DM could explain some of the functional changes observed previously, and for that purpose we used miRNA mimics transfection to force increased expression of miR-126.

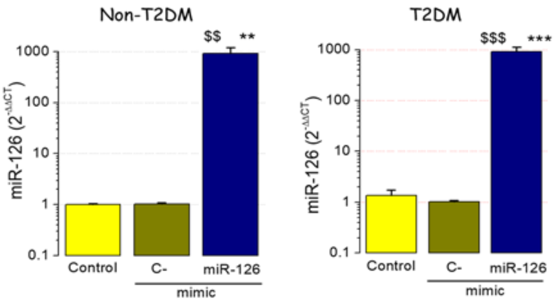

Figure R38. miR-126 expression in non-T2DM and T2DM cells transfected with mimic C- and mimic miR-126. Control cells were mock-transfected. Data is expressed with the $2^{-\Delta\Delta CT}$ method using SNORD 68 as housekeeping and mimic C- as calibrator. Each bar is mean ± SEM of 3-4 experiments **P<0.01, ***p<0.001 compared with mimic C-; $$, $$$, compared with control.

VSMCs from non-T2DM and T2DM patients were transfected with the miR-126 mimic or a mimic negative control (mimic C-). Also a parallel control of mock transfected cells was used. The validation of this procedure was carried out by qPCR, to confirm the changes in miR-126 expression in transfected cells (Figure R38).

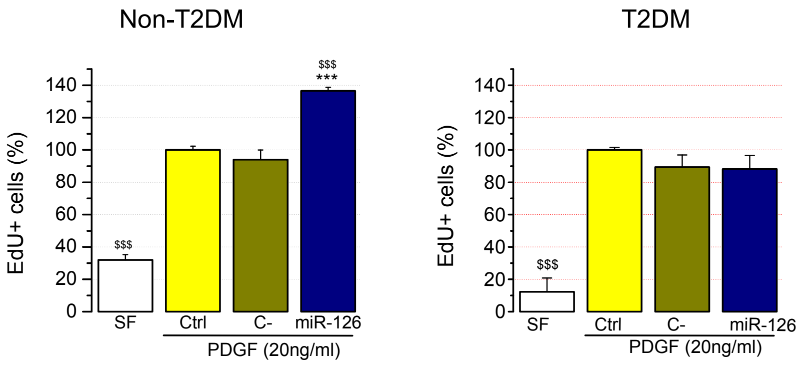

Figure R39. Proliferation assay data of non-T2DM and T2DM cells in the indicated conditions: SF (serum free, negative control), Ctrl or PDGF alone (positive control), PDGF + C- (negative mimic), PDGF + miR-126 (mimic miR-126). All data is represented as mean ± SEM from 7-10 determinations from 4 sets of experiments. . *P<0.05, ** P<0.01 and ***P<0.001 compared to mimic C-. $$$P<0.001 compared to Ctrl PDGF 20 ng/ml.

When using mimic C- as calibrator, we did not find any significant changes compared to mock transfected cells, excluding unspecific effects, but we did confirm miR-126 overexpression at very high levels and with no difference in both non-T2DM and T2DM VSMCs

While the degree of overexpression of mir126 was comparable in both groups, proliferation studies in these same VSMC cultures using EdU incorporation showed that while non-T2DM VSMCs miR-126 mimic transfection increased the proliferation rate by 56% with respect to mimic C-, it has no effect on T2DM VSMCs proliferation. (Figure R39).

Similar results were obtained when exploring the effect of miR126 overexpression in migration rate using the wound healing assay. miR-126 mimic increased migration in non-T2DM by 55% (compared to migration rate of the mimic C- transfected cells). As mentioned (see Figure R28), the basal migration rate of T2DM VSMC was higher, and it was unaffected by miR126 mimic transfection. (Figure R40)

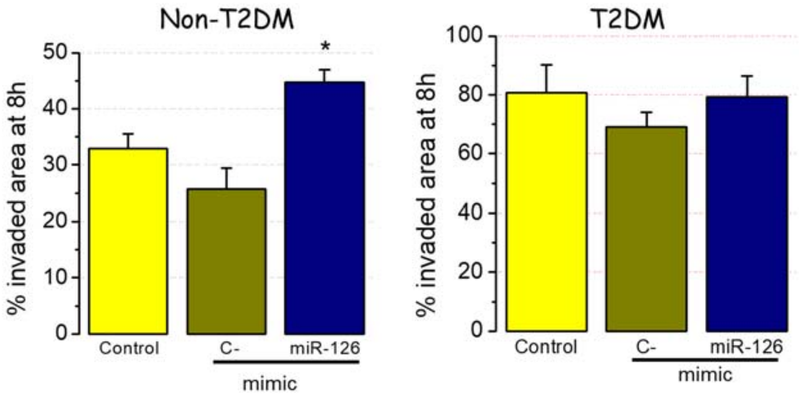

Figure R40. Migration rate was expressed as % of invaded area 8 hours after performing a scratch in confluent VSMCs. The experiments were carried out in mock-transfected (Control) or cells transfected with mimic C- or miR-126 as indicated. Each bar is mean ± SEM of 6-8 determinations from 3–4 independent experiments. *P<0.05 compared to mimic C- condition.

In the light of these results, we tried to determine possible mir126 target genes that could be involved in these effects of miR-126 in proliferation and migration of non-T2DM VSMCs. We analyzed the expression of some of the already described miR-126 target genes which are related to VSMC differentiation and/or T2DM.

	$2^{-\Delta\Delta CT}$	
Gene	**mimic C-**	**mimic miR-126**
KCNA3	1.02±0.10	0.70±0.05
MEK1	1.01±0.08	0.95±0.11
MEK2	1.03±0.09	1.21±0.27
FOXO3	1.02±0.06	0.77±0.06
SPRED1	1.01±0.05	0.96±0.15
AKT1	1.01±0.04	0.74±0.07
AKT2	1.01±0.04	0.62±0.07 ***
IRS1	1.00± 0.03	0.95±0.25
PI3KR2	1.00±0.02	0.44±0.12 ***

Table R2. Relative expression of miR-126 target genes in non-T2DM VSMCs upon mimic C- or miR-126 mimic transfection.

Among those, we determined the mRNA expression levels of SPRED1, FOXO3, PI3KR2, IRS1, AKT1 and AKT2. In addition, we explored changes in other genes related to MEK/ERK signaling, including MEK1, MEK2 and KCNA3 (Table R2).From all these genes, only AKT2 and PI3KR2 show a consistent and significant decrease of their expression upon miR-126 mimic transfection in non-T2DM VSMC in culture. However, in T2DM VSMCs, no changes in the mRNA expression of these two genes (PI3KR2 and AKT2) were observed in cells transfected with miR-126 mimics (Figure R41).

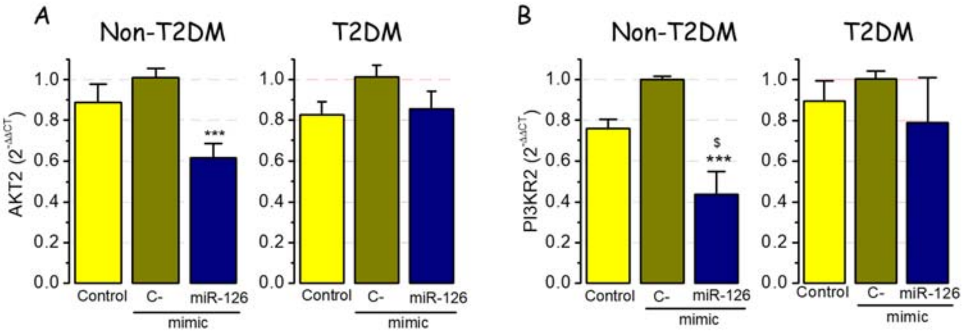

Figure R41. AKT2(A) and PI3KR2 (B) gene expression obtained from non-T2DM and T2DM VSMC transfected with mimic C- and mimic miR-126. Data is represented as $2^{-\Delta\Delta CT}$ using mimic C- as calibrator. ***$P<0.001$ compared to mimic C- condition. \$ $p<0.05$ compared to Control, n= 3-4 independent experiments.

3.3. Role of Kv1.3 in IH in a cardiovascular risk mice model.

3.3.a. Creating a mice model of vascular risk factors: BPH/HFD

Vascular risk factors (VRF) like hyperglycemia, insulin resistance, obesity and hypertension worsen the prognostic of patients undergoing vascular surgeries. Therefore, in order to get insight into the mechanisms and the response to treatment of IH lesions in the presence of these risk factors, we pursue to develop a mouse model with some of these risk factors.

Hypertensive (BPH) mice strain have mild essential hypertension comparable to the most common hypertension that afflict population We fed BPH mice with high fat diet (HFD) for 24 weeks to increase their cardiovascular risk and we monitored weight gain, blood pressure and metabolic parameters such as blood glucose levels and glucose and insulin tolerance tests. For some of these parameters, we also compared the normotensive controls of BPH, the BPN strain (Blood Pressure Normal).

Weight gain: The weight increase was evident (see Figure R42 A). Compared with BPH mice fed with standard diet (BPH/SD), BPH mice fed with high fat diet (BPH/HFD) increased their weight by 36% at 12 week and 21% at 24 week of HFD.

Blood Pressure: The Blood pressure was measured at week 12 and 24. HFD did not modified the already high values of blood pressure in BPH mice (Figure R42 B and C).

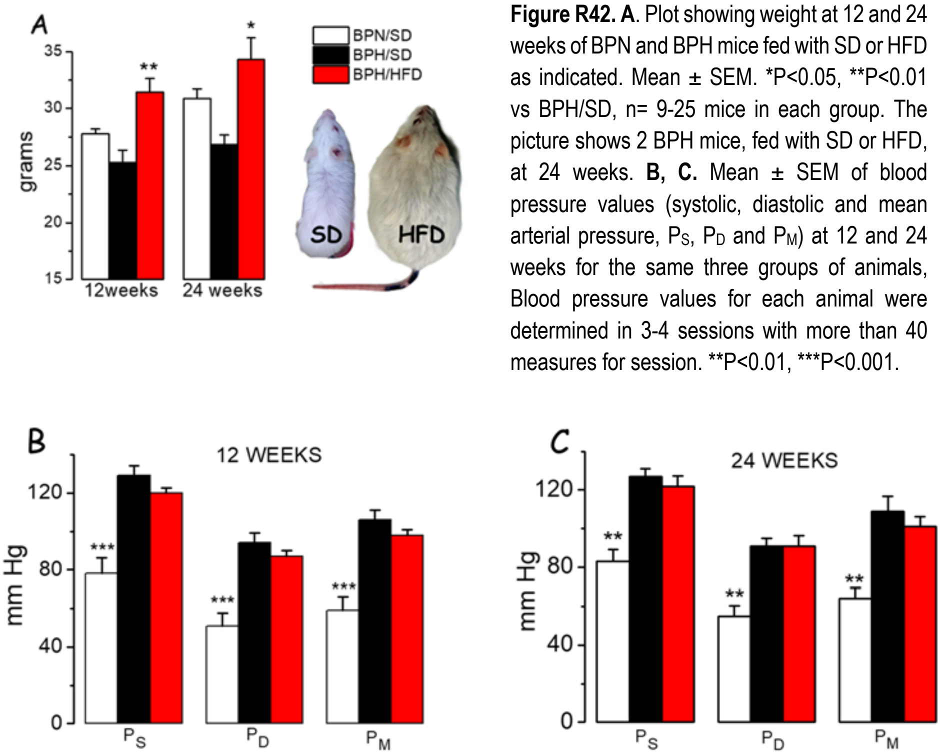

Figure R42. A. Plot showing weight at 12 and 24 weeks of BPN and BPH mice fed with SD or HFD as indicated. Mean ± SEM. *P<0.05, **P<0.01 vs BPH/SD, n= 9-25 mice in each group. The picture shows 2 BPH mice, fed with SD or HFD, at 24 weeks. **B, C.** Mean ± SEM of blood pressure values (systolic, diastolic and mean arterial pressure, P_S, P_D and P_M) at 12 and 24 weeks for the same three groups of animals, Blood pressure values for each animal were determined in 3-4 sessions with more than 40 measures for session. **P<0.01, ***P<0.001.

Glucose metabolism: Fasting blood glucose was determined after 18-hours fasting from a blood sample from the tail vein. Glucose levels were significantly increased in mice fed with HFD when comparing with BPH/SD mice (Figure R43), although the increase was moderate.

Both BPH/HFD and BPH/SD mice were subjected to a glucose tolerance test (ipGTT). After a load injection of glucose in fasting animals, blood glucose was determined every 20 minutes to explore glucose clearance time course. Figure R44 portrays the ipGTT curves obtained at 12 and 24 weeks of HFD. At 12 weeks, BPH/HFD mice have a higher peak of blood glucose concentration after glucose injections and needed more time to level the blood glucose. A similar behavior was observed at 24 weeks. These data indicate that BPH/HFD mice become glucose intolerants within 12 weeks of HFD. The same results can be obtained when ipGTT curves are represented as the area under the curve (lower plots).

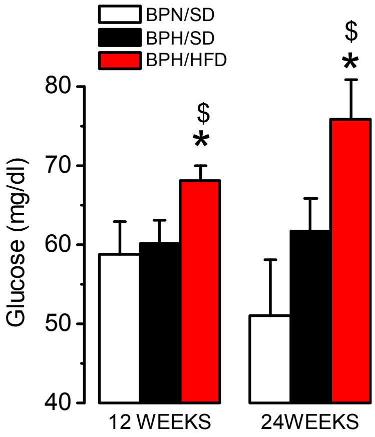

Figure R43. Fasting blood glucose determined at 12 weeks and 24 weeks from the beggining of HFD, after 18h fasting, and using a blood drop from the tail vein. Data is mean ± SEM of 4 BPN/SD, 9 BPH/SD and 25 BPH/HFD mice at 12 weeks and 4 BPN/SD, 5 BPH/SD and 16 BPH/HFD mice at 24 weeks. *P<0.05 vs BPH/SD and $ P<0.05 vs BPN/SD.

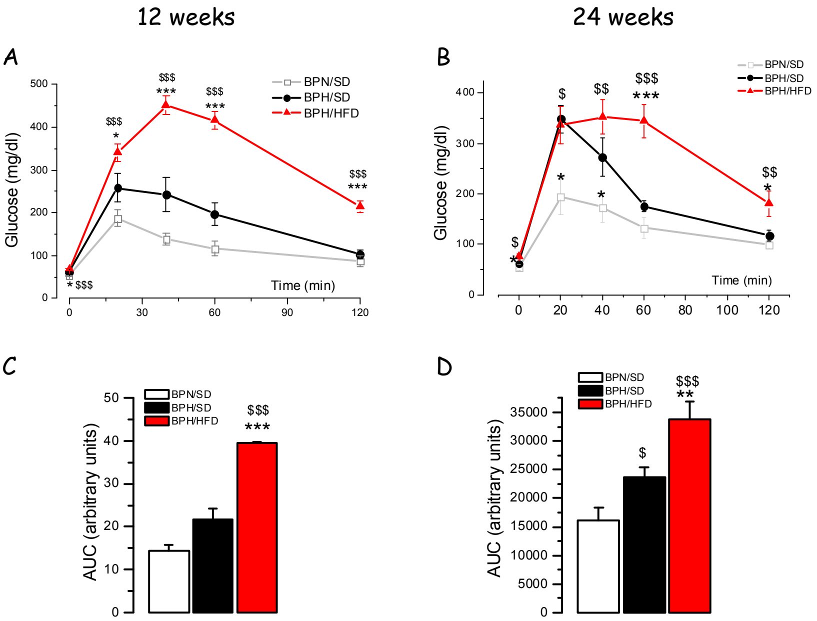

Figure R44. A, ipGTT at 12 week (BPN/SD=4, BPH/SD n=9, BPH/HFD n=25) and **B,** ipGTT at 24 weeks (BPN/SD=4, BPH/SD n=5, BPH/HFD n=16). The graphs show the time course of blood glucose level after an intraperitoneal glucose injection in fasting animals. **C,** and **D,** Area under the curve of the ipGTT at 12 and 24 weeks, *P<0.05, **P< 0.01, *** p<0.001 vs BPH/SD and $; $$, $$$ vs BPN/SD.

Finally, we also performed intraperitoneal insulin tolerance test (ipITT, Figure R45). Non-fasting animals were injected with insulin and the blood glucose level were measured at time 0 and every 20 minutes after the insulin injection. The ipITT curve shows that HFD increased insulin resistance in BPH mice comparing with BPH/SD, as glucose levels are not decreased at the level of BPH/SD or BPN mice.

Altogether our data indicate that BPH mice on HFD develop metabolic syndrome, becoming obese and showing high basal glucose, glucose intolerance and insulin resistance, while remaining hypertensive.

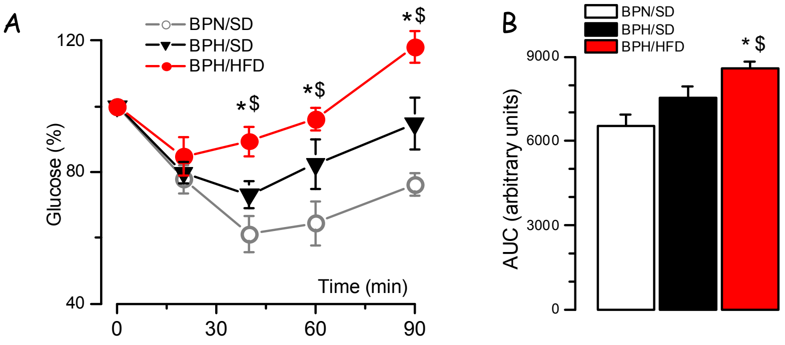

Figure R45. A. Line graph illustrates the changes in blood glucose (100% is glucose at t=0) after a load of insulin, in the 12 week group of animals. **B.** Bar graph plot of the area under the curve. *P<0.05 vs BPH/SD, $P<0.05 vs BPN. BPN/SD n=3, BPH/SD n=10, BPH/HFD n=16.

3.3.b. Characterization of vascular remodeling in BPH/HFD.

Our next goal was to generate an in-vivo IH model in these mice with VRF, using a carotid artery ligation lesion model, but previously we investigated the changes that HFD produced in carotid artery of BPH mice.

The right and left carotid arteries emerges from the aortic arch. Both carotid arteries run along the trachea, and distally are divided in internal and external carotid arteries. The tunica media of the carotid artery is well defined by a prominent internal and external elastic lamina. In addition, a third elastic lamina in the middle of the tunica media was evident. The tunica adventitia is rich in collagen fibers. Histomorphometric analysis of carotid arteries (Figure R46) showed that HFD per se produce inward remodeling, with a decrease of the total area of the vessel and a concomitant increase of the wall thickness in BPH/HFD mice.

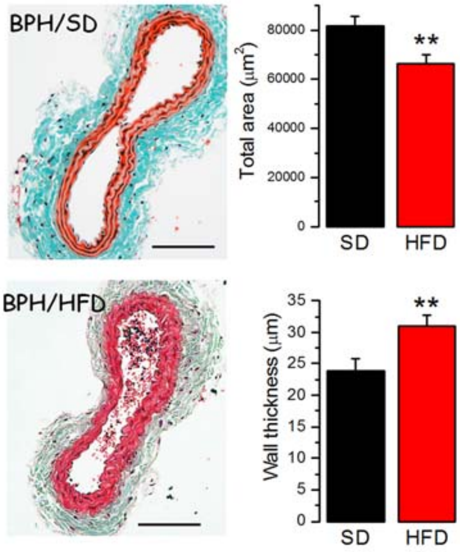

Figure R46. Representative microphotographs of carotid arteries stainined with Masson trichrome, 20x objetive. Scale bar 50μm. The bar plots represent mean ± SEM of total area (calculated from the perimeter of the external elastic lamina) and wall thickness (obtained from the wall and lumen radius, see Table M1). N= 10 BPH/SD and 11 BPH/HFD mice. **P < 0.01.

The inward remodeling of carotid arteries in HFD led to an increased wall thickness that could be due to either an increase in the number of VSMC or an increased in their size and tone. Quantification of the number of VSMC in the media layer showed no differences with BPH/SD arteries, suggesting the absence of VSMCs proliferation. Besides, the wall area of the carotid artery did not change in BPH/HFD animals (i.e., remodeling is not hypertrophic). The second option was the existence of a hypercontractile state of VSMCs. We used several approaches to investigate this hypothesis:

1. We analyzed the ***nuclei shap***e. In normal conditions, VSMCs have fusiform or spindle-shaped nuclei embedded within the muscle fibers, so that when VSMCs contracts the nuclei shape is squeezed and shortened following the cell shape (Skinner & Johnson, 2017). We studied the nuclei shape by measuring the length of both axis in Hoechst labelled nuclei of carotid arteries cross-sections. The nuclei aspect ratio (AR, long diameter/short diameter) was used to represent the shape, so that AR = 1 indicated a perfectly round nuclei shape while increasing AR values indicated more elongated nuclei. While BPH/SD VSMC showed elongated nuclei, VSMC from BPH/HFD mice have more rounded nuclei, implying an increased basal tone (Figure R47).

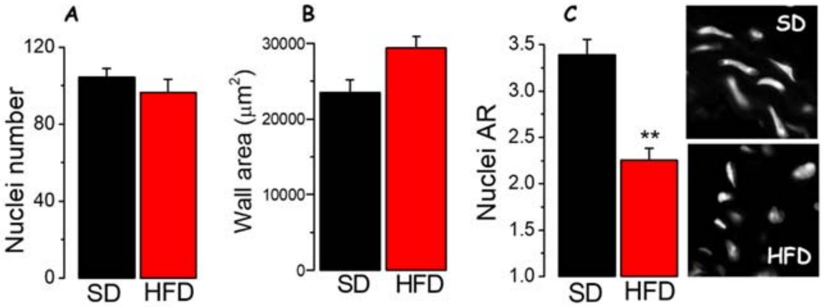

Figure R47. A. Bar plot showing nuclei number in 122 µm-width sections of the carotid artery wall with Hoechst nuclei labeling. **B.** Wall area calculated as total vessel area (from perimeter of external elastic lamina) – lumen area. **C.** Bar plots displaying nuclei aspect ratio (AR) defined as long/short axis, and representative microphotographs of VSMC nuclei from SD and HFD carotid arteries with Hoechst stain, objective 40x, scale bar= 10µm**.** All plots are mean ± SEM, n=4-6 arteries. **P<0.01.

2. We explored the ***expression of contractile markers***. We looked at the mRNA and protein expression of contractile proteins such as calponin (CNN1). Figure R48 shows increased CNN1 immunolabeling (with DAB or fluorescence) in the tunica media of carotid arteries from BPH/HFD mice. In agreement with this, CNN1 mRNA expression is also significantly increased in mesenteric arteries from in HFD mice). These observation support the conclusion that inward vascular remodeling observed in BPH/HFD is built upon an increased basal contractile state of the VSMCs in the media layer.

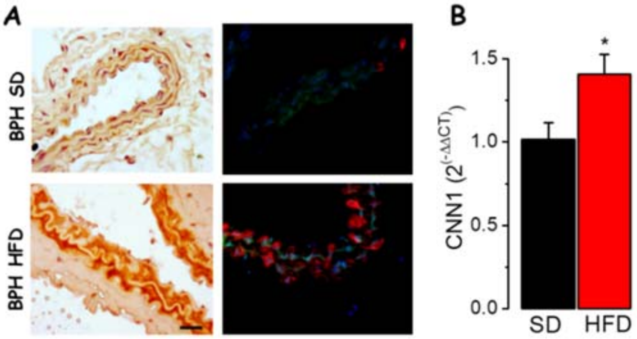

Figure R48. A. DAB immunohistochemistry and Alexa 594 immunofluorescence for calponin in 7µm carotid cross sections from BPH/SD or BPH/HFD as indicated. Scale bar 25 µm and 40x magnification**. B.** CNN1 relative mRNA expression levels using RPL18 as housekeeping and BPH/SD as calibrator. N=4; *P<0.05.

3.3.c. Kv1.3 and Kv1.5 expression in BPH/HFD mice VSMCs.

We have previously proposed that the Kv1.3/Kv1.5 ratio can be used to define VSMC phenotype (Cidad *et al.*, 2012, 2015). To explore whether HFD determines a change in VSMC phenotype, we analyzed mRNA expression of Kv.1.3 and Kv1.5 channel in SD and HFD mesenteric arteries. Although both channels increased their expression upon HFD, the upregulation was more pronounced for Kv1.3 gene (KCNA3) so that there is a significant increase in the Kv1.3/Kv1.5 ratio in HFD (Figure R49 A). At least for Kv1.3, the changes in mRNA expression parallel changes in protein expression, as shown in immunohistochemistry experiments in cross sections from paraffin embedded carotid arteries, whereas changes in Kv1.5 were not evident (Figure R49 B).

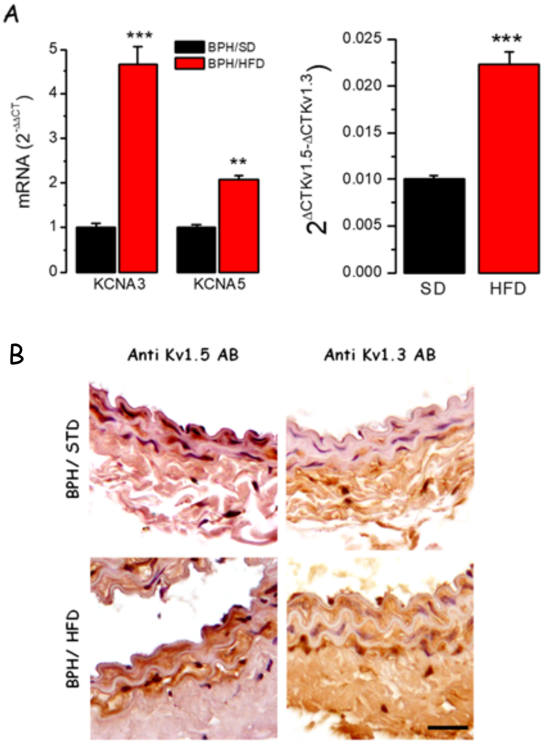

Figure R49. A, The bars plot in the left showing Kv1.3 and Kv1.5 mRNA relative expression as $2^{-\Delta\Delta Ct}$, using RPL18 as endogenous control and BPH/SD as calibrator. The right graph shows the Kv1.3 to Kv1.5 ratio obtained form the expression data, using the expression $2^{\Delta CtKv1.5-\Delta CtKv1.3}$ as indicated. Data are mean ± SEM from a pool of 5 to 8 mice. $^{**}P<0.01$, $^{***}P<0.001$ versus BPH/SD group. **B.** Representative microphotographs of DAB immunolabeling of 7μm cross sections from paraffin embedded carotid arteries. Primary antibody (1:50) was incubated overnight at 4ºC. Nuclei were labelled in purple with Harris hematoxylin. Pictures were taken with 40X magnification. Scale bar 25μm.

If the Kv1.3/Kv1.5 truly reflects the degree of VSMC dedifferentiation, the changes in HDF will suggest a change towards a more dedifferentiated phenotype, which could indicate that VSMCs from HFD animals should be more prone to PM in the presence of triggering factors. At some point, this observation parallels the data from T2DM hMA vessels, where we also found increased Kv1.3 expression (see data from previous section), and could add to the idea that our animal model reproduces some of the changes observed in vessels from T2DM human patients.

3.3.d. Characterization of intimal hyperplasia in BPH/HFD

Carotid ligation in BPH/SD mice

Carotid ligation was used to study IH in our mice model. Both males and females BPH mice underwent right carotid ligation surgery and were kept in the animal house for 4 weeks.

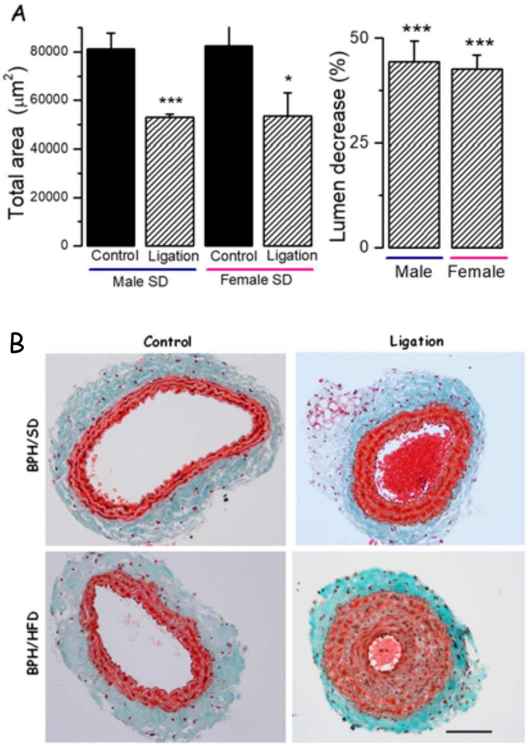

Figure R50. A Bar graphs representing the mean ±SEM of total area of the vessel calculated from the external elastic area perimeter (left) and the % Stenosis estimated as lumen decrease of ligated vessels. Data from 5 males and 6 females BPH/SD *p<0.05 and ***p<0.001 vs the corresponding control, the unligated vessels **B.** Representative images of control and ligated vessels from BPH mice fed with SD or HFD. Right carotid arteries were ligated and contralateral arteries were used as controls. Vessel were harvested four weeks after surgery, embedded in paraffin to obtain 7 µm cross section and stained with Masson trichrome to perform histomorphometic analysis. 20x objective. Scale bar 100 µm.

Histomorphometric analysis showed that carotid ligation induced inward remodeling, with a marked decrease of the total area of the vessel (Figure R50 A). The increased thickness of the wall in ligated arteries is mainly due to the development of a neointima lesion that determines a significant reduction of the lumen (see upper panels of Figure R50 B). No gender-related differences in remodeling were found, so data are presented together from now on.

Carotid ligation in BPH/HFD mice

After characterization of the lesion in control (BHP/SD) mice, we ligated the right carotid of BPH mice 4 weeks before the end of the HFD treatment.. A summary of all remodeling descriptors comparing SD and HFD animals is provided in TableR3.

	SD control **N = 9**	**SD Ligation** **N = 9**	**HFD control** **N = 11**	**HFD Ligation** **N = 9**
Total area (µm^2)	81,94±3,77	53,34±4,045***	66,36±3,53++	72,2940±7,31
Wall area (µm^2)	21,62±2,37	31,94±2,83***	26,85±2,552	60,406±9,18**, ++
Intima area (µm^2)	0	3,37 ± 1,87	0	25,675±6,90***, ++
Wall thickness (µm)	23.86±1.9	67.72±6.68***	31.07±1.66+	89.37±14.37***, ++
Lumen area (µm^2)	51,765±4,50	21,40±1,64**	47,181±6,06	11,888±2,60***, ++
I/M ratio	0	0.10±0.05	0	0.73±0.15***, ++
% Stenosis	0	10.19±4.52	0	56.10±11.16***, ++
Lumen decrease (%)	0	43.41±2.69***	0	73.67±6.35***, ++

Table R3. Summary table of vascular remodeling descriptors of carotid ligation in BPH/SD and BPH/HFD.

Carotid ligation led to neointima formation, increasing wall thickness and decreasing lumen area, as shown in the microphotographs in (Figure R50 B lower panels and Figure R51). However, in this case the total area of the vessel was not altered with ligation, probably because HFD per se had already decreased it (as shown in the bar plot in Figure R46). The VSMC that migrated to the neointima are dedifferentiated cells, as evidenced by the lack of staining with smooth muscle differentiation markers such as the contractile protein SM22 (Figure R51)

As evidenced in the images of Figure R50 B, the extent of IH induced by carotid ligation seemed larger in BPH/HFD animals. Neointima was quantified by analyzing the intima to media ratio (I/H ratio) and the percentage of lumen decrease upon ligation, and both parameters were significantly increased in BPH/HFD arteries (Figure R52). That is, our mice model also developed more neointima, which again parallels the higher IH of T2DM hMA in organ culture (see section 3a).

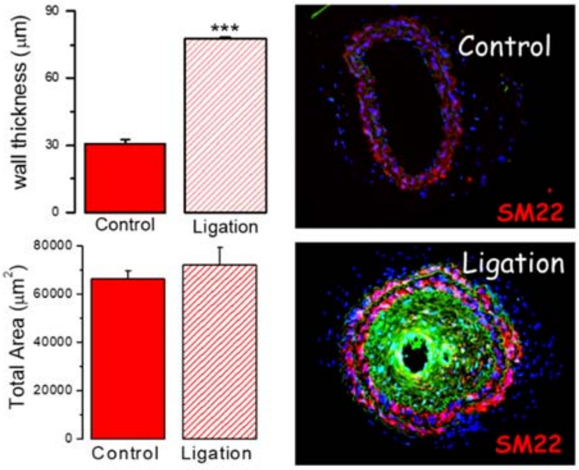

Figure R51. Average wall thickness (upper) and total area (lower) from 9 BPH/HFD arteries in each group. Microphotographs shows SM22 labeling (in red) in control and ligated arteries Autofluorescence of elastic lamina is shown in green. The sections are from the same arteries shown in Figure R50, to illustrate the limit between media layer (SM22 positive) and intima layer (SM22 negative).

Expression of Kv1.3 channels in BPH/HFD ligated vessels

In addition, DAB immunohistochemistry using anti-Kv1.3 antibodies showed that not only control BPH/HFD arteries had increased immunostaining, as indicated above, but also that upon carotid ligation there is a larger increase of the labelling in these channels (Figure R53). This finding is not surprising, as neointima formation depends on VSMC dedifferentiation. Besides, the higher levels of Kv1.3 channel expression in the vascular lesion in BPH/HFD mice suggest that Kv1.3 blockers might represent an even better therapy for prevention of IH in these animals than in the control ones (Cidad *et al.*, 2014).

Figure R52. Bar plots representing intima to media ratio (left) of ligated carotid arteries, and lumen decrease % (right). Both values were used to compare remodeling of ligated artery between BPH/SD and BPH/HFD Analysis was performed in 3 different cross section per mouse (BPH/SD n=9 and BPH/HFD n=9). **p<0.01 vs BPH/SD animals.

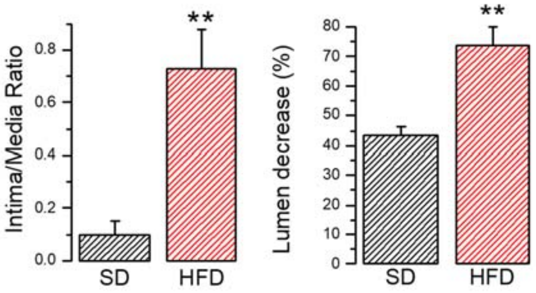

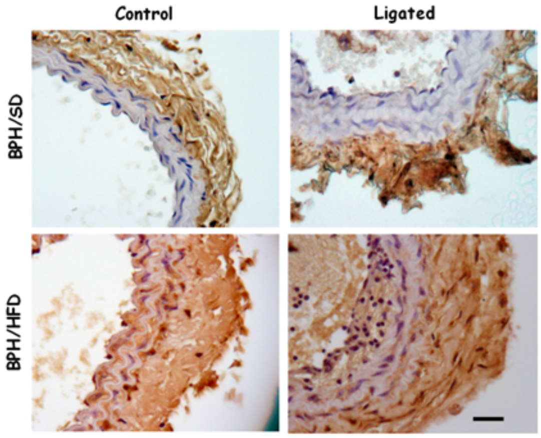

Figure R53. Immunohistochemistry of 7 μm cross sections of paraffin embedded carotid arteries from BPH/SD and BPH/HFD mice, with and without ligation. Sections were incubated with anti-Kv1.3 channel antibodies and developed with DAB. Microphotographs were taken with 40x magnification. Scale bar 25μm.

3.3.e. Effect of Kv1.3 blockers preventing IH in BPH/HFD mice.

We next explored the effects of treatment with Kv1.3 blockers for prevention of IH in these mice using either, minipumps for systemic drug delivery, or local application of PAP-1 with an ELR-biocompatible polymer in animals with carotid ligation. First, we studied the effectiveness of this treatment in BPH/SD mice, comparing with the application of the mTOR inhibitor everolimus.

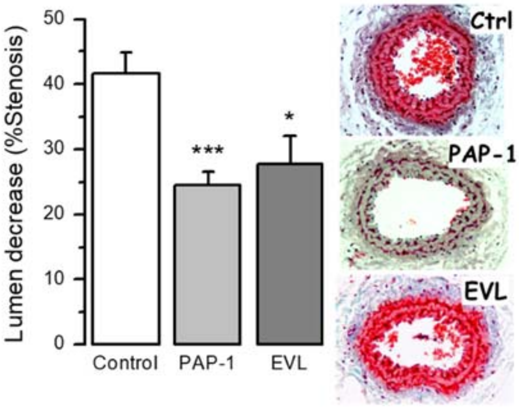

Figure R54. Effect of PAP-1 and Everolimus delivered with minipumos in vascular remodeling. Bar plot showing mean ± SEM of the lumen decrease of ligated carotid arteries with the labeled tretament. Histomorphometric analysis was performed in 7μm parrfin embeded cross sections stained with Masson trichrome Microphotograhs are representative examples of the data. 20x objective. Data from 5 to 11 BPH/SD mice for each group. *p<0.05, ***p<0.001 versus control.

Our data (Figure R54) demonstrated that both treatments decreased in a significant way the vessel stenosis induced by carotid ligation, albeit PAP-1 treatment seemed to be more potent and consistent in all treated animals. The effects of PAP-1 inhibiting remodeling was explored both in male and female BPH mice, and both using the systemic or local application, and again no sex related differences were observed when studying the effects of PAP-1 and the different routes of administration (Table R4).

Table R4. Summary of the effects of PAP-1 in remodeling in the different conditions tested.

	Wall area (μm2)		**Lumen decrease (%Stenosis)**
	Control	**Ligated**	**Ligated**
Male	23,02 ± 1,46	34,22 ± 1,79	44.69 ± 5.92
Female	22,75 ± 3,92	31,25 ± 3,55	39.19 ± 3.25
Polymer control	28,48 ± 3,32	34,15 ± 2,24	37.94 ± 9.07
Polymer PAP-1	34,08 ± 4,10	29,20 ± 1,13	21.33 ± 2.25
mini Pump control	22,30 ± 3,21	36,76 ± 6,24	42.03 ± 4.46
mini Pump PAP-1	24,12 ± 3,58	23,22 ± 2,05	27.83 ± 2.67

Next, we determined the effect of local application of PAP-1 on the remodeling after carotid ligation in BPH/HFD mice.

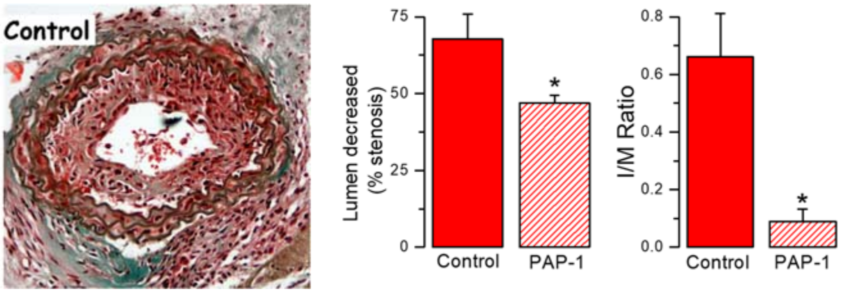

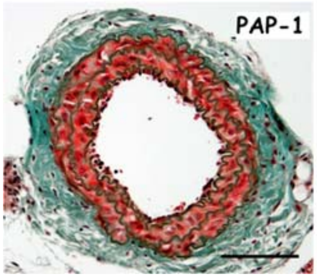

Figure R55. Microphotographs of ligated carotid without treatment (control) and ligated carotid treated with PAP-1 *in-situ.* Pictures taken with 20x magnification, scale bar 100 μm. Bar plots displays Lumen decrease (left) and intima to media ratio (right). Data from 9 control BPH/HFD and 5 PAP-1 BPH/HFD; *p<0.05 compared to control.

As shown in Figure R55 the degree of stenosis and the intima/media ratio were significantly decreased in the PAP-1-treated animals.

However, no differences in the effect of PAP-1 were observed when comparing SD and HFD vessels (the percentage of inhibition of lumen stenosis with PAP-1 was of 41±4.7% and 37±3.5% in SD and HFD mice respectively).

Notwithstanding, additional beneficial effects of PAP-1 were evident in the HFD mice. Local application of PAP for 4 weeks reverted the weight increase of these animals, in spite of showing no differences in food intake. This effect of PAP seems to be specific of the HFD model, as no differences in weight gain were observed in BPH/SD during PAP-treatment (Figure R56). More interestingly, PAP-1 treatment fully reverted insulin resistance of BPH/HFD diet

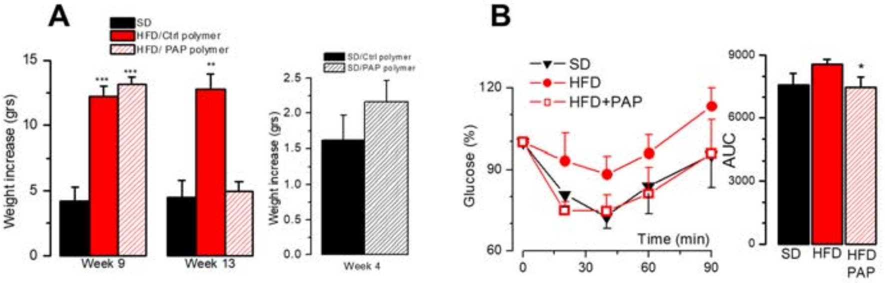

Figure R56. A. Bar plots shows the weight gain of BPH with SD or HFD before (week 9), or after carotid ligation and 4-weeks treatment with vehicle or PAP-1 (week 13). The middle graph shows the effect on weight gain of 4-weeks PAP-1 treatment in BPH/SD animals after carotid ligation. Mean ± SEM, n=5-6 mice per group. **P< 0.01; *** P< 0.001 versus SD group. **B.** Insulin tolerance test showing the changes in blood glucose (as % of control at t=0) after a load of insulin in non-fasting animals. Right bar depicts the area under the curve of ipITT. *P<0.05 vs HFD.

Discussion

The main goal of this work was to explore the link between Kv1.3 channels and VSMC phenotypic switch and the mechanisms by which Kv1.3 blockers inhibit intimal hyperplasia development. The fact that we used human vessels and human VSMCs cultures represents a relevant added value to our work, as we are exploring the functional expression of Kv1.3 channels and the effects of the blockers in the same vessels used for angioplasty in the clinics. Our work allowed to support several relevant conclusions: We demonstrate that Kv1.3 channels have a relevant contribution to IH in human vessels, through an indirect mechanism that involves myocardin-dependent Kv1.5 channel downregulation upon PM. In addition, we studied the contribution of Kv1.3 channels to PM in T2DM human vessels and in an *in-vivo* animal model with vascular risk factors, and we conclude that Kv1.3 blockers represent an anti-restenosis therapy even more effective in these vessels with underlying diseases, paving the way for the use of Kv1.3 channels as targets for the prevention of intimal hyperplasia in these vulnerable populations.

1. Contribution of Kv1.3 channel to IH in human vessels

Cardiovascular diseases (CVD) are the number one cause of death globally, according to the World Health Organization (WHO). Coronary artery disease is the most common CVD. The development of bypass surgery (CABG) and catheter-based endovascular interventions such as PTA has represented a huge therapeutical improvement, but a limitation of these procedures is restenosis of the target vessel, due to excessive activation of the vessel repair mechanisms. The use of drug-eluting stents releasing anti-proliferative drugs such as rapamycin and placlitaxel has decreased the incidence of restenosis. However, their lack of specificity with the subsequent failure of healing (Lüscher *et al.*, 2007) calls for the development of newer agents and polymers for stent coverings. In this scenario, we propose a novel strategy (the use of Kv1.3 channel blockers). The efficacy of this approach has been previously tested in animal models of lesion. Yet, it is well known that these models have many limitations: they are not restenosis models, neointima formation is not always associated with lumen narrowing, rodent vessels do not behave like human vessels and healthy vessels do not behave like diseased vessels, because of differences in cell cycle regulation between dedifferentiated VSMCs in the lesion and normal VSMCs (O'Sullivan *et al.*, 2003; Calvert & Bennett, 2009).

With this background, we explored the efficacy of Kv1.3 blockers in human vessels. We used 20% FBS to trigger vascular remodeling in hMA and hSV in organ culture. These vessels are donated by patients undergoing CABG, so that they are from patients with CVD, and most of them have other associated risk factors: overweight (BMI 27.75 ± 0.75), T2DM, hypertension and/or dyslipidemia (Table R1). We used the organ culture of vessel rings, that has many advantages over cell culture, as it maintains tissue architecture, cell to cell interactions, extracellular matrix and cell morphology (Deng *et al.*, 2014). Many studies have shown that organ culture of intact blood vessels is a good model for the phenotypic changes that occurs in VSMC during vascular remodeling, (Hansen-Schwartz *et al.*, 2008; Johnsson *et al.*, 2008; Deng *et al.*, 2014).

We demonstrated that Kv1.3 blockade prevents vascular remodeling with two structurally different Kv1.3 blockers MgTx blocks Kv1.3 currents acting as an open channel blocker, while PAP-1 is able to bind to the open channels but has higher affinity for inactivated Kv1.3 channels, that upon PAP-1 binding are stabilized in this inactivated, non-conducting state. However, our previous work demonstrated that in addition to these effects, both drugs are able to modulate the voltage-sensing mechanism of Kv1.3 channels, as they inhibited gating charge movements. (Cidad *et al.*, 2012). This finding explains why both MgTx and PAP-1 are able to block the proliferation mediated but Kv1.3 channels but also by mutant, non-conducting channels (Kv1.3WF).

Kv1.3 blockade inhibits neointima formation in human vessels by reducing VSMC proliferation, migration and ECM production. This characterization of the effects of Kv1.3 blockers was carried out in the organ culture and when possible, also confirmed in cultured VSMC obtained from these same vessels. This was true for the study of cell proliferation and migration.

However, the study of the ECM composition and the changes upon PM or in response to the treatment was only possible in the organ culture. Regarding this aspect, our study provided some clear conclusions but also left some unanswered questions.

The extracellular matrix of the vessel wall gives structure and define the mechanical properties that are critical for proper function o the vascular system. In addition, ECM provides signals that induce, define and stabilize VSMC phenotypes. (Wagenseil & Mecham, 2009). We study the principal vascular ECM components (collagen I, collagen III, collagen VIII, and elastin) and its modulation in response to vessel remodeling and upon Kv1.3 blockade. Collagens I and III are the most abundant collagens in the arteries, collagen I helps to give structure to the artery and collagen III gives elasticity. For this reason, under physiological conditions, collagen III is predominant in the vascular system (Plenz *et al.*, 2003), and this is what we found in our vessel samples, at least in control conditions (t=0), although collagen I proportion is higher than previously described and shows the largest increases upon PM (see Figure R7). Nevertheless, a shift toward a higher proportion of type I collagen has been observed in atherosclerotic lesions, indicating decreased vascular elasticity.

Considering that our vessel samples come from an aged group of people that undergoes vascular surgery, most likely associated to atherosclerotic lesions, our finding of an imbalance towards more collagen I expression is what should be expected.

Interestingly, western blot demonstrated that VSMCs with contractile phenotype express Collagen type III in the canonical isoform while VSMCs from cell culture have a smaller, mature isoform 2 of Collagen III (Figure D1). This isoform 2 is the results of alternative splicing of COL3A1 (https://www.uniprot.org/), and its expression in dedifferentiated VSMCs may indicate a different functional role, as smaller collagen III might not fulfil the functions of the canonical collagen III, yet more research is needed to confirm or discard this assumption.

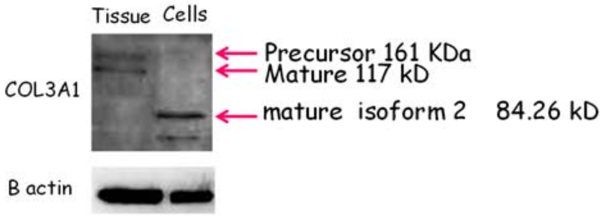

Figure D1. Western blot of lysates of VSMCs from hMA tissue (t=0) and VSMC from cell culture. Beta actin was used as control.

Collagen VIII is a net forming collagen that is characteristic from dedifferentiated VSMCs and helps to cell migration (Plenz *et al.*, 2003). In contrast to these studies, we found that collagen VIII expression decreased during vessel organ culture. However, most of the data supporting this prominent role of collagen VIII in vascular remodeling have been obtained n the context of inflammatory lesions associated to atherosclerotic plaque formation, which may differ from the conditions of our experimental design (Plenz *et al.*, 2003). In addition, several studies identify α1 type VIII collagen mRNA overexpression after balloon injury in rat carotid arteries (Bendeck *et al.*, 1996; Sibinga *et al.*, 1997). These studies in vivo are more similar to our model, and the authors showed that collagen VIII expression at mRNA and protein levels is coincident with SMC migration, concluding that it may serve as a useful tag to identify migrating SMCs and/or play an important functional role in mediating SMC migration. In agreement with this interpretation, the expression of the collagen VIII by western blot was increased at 1, 2, and 4 days after injury, but not at any subsequent time; In fact at longer times post injury there is even a decrease compared to control tissue (Bendeck *et al.*, 1996). It is possible that in our model, after two weeks of treatment, the migratory response associated to collagen VIII overexpression is already over, and consequently we are looking at the downregulation phase.

The changes in elastin upon PM and the effect of PAP-1 treatment in them are a clear-cut result of our work. Elastin is the principal ECM component of the tunica media. The protein product of the elastin (ELN) gene is synthesized by the VSMC and secreted as a monomer tropoelastin which is crosslinked and organized into elastin polymers that form concentric rings of elastic lamellae around the arterial lumen. Each elastic lamina alternates with rings of VSMCs and provides elasticity and helps the vessel structure (Karnik *et al.*, 2003). Taking advantage of elastin auto fluorescence, we found out that vessel organ culture augmented elastin quantity and disorganization of elastin. In fact, literature states that elastic lamina is necessary to control VSMCs proliferation, migration and maintaining a dedifferentiated state (Karnik *et al.*, 2003; Wise & Weiss, 2009); therefore fragmented and disorganized elastin might facilitated neointima formation by VSMC dedifferentiation and proliferation and migration from the tunica media to the tunica intima. Kv1.3 blockade was able to revert elastin disorganization and thus decreasing IH, suggesting that Kv1.3 has an important role in altering the structure of the vascular wall through modifying the ECM to ease neointima formation and vascular remodeling.(Hinek & Rabinovitch, 1993).

IH is a complex process that involves multiple cell types (not only VSMCs) and multiple processes (not only proliferation). This could explain why the current treatments using anti-proliferative drugs have limited success in preventing restenosis after vascular surgery. Using the same human vessels that are commonly used for coronary angioplasty, we demonstrate here that local Kv1.3 channel blockade is an efficient strategy to prevent vascular remodeling. This approach inhibits neointima formation by reducing VSMC proliferation and migration and ECM production. It is likely that it could also reduce remodeling by acting on other targets aside from VSMCs. Kv1.3 blockers modulate the immune responses (Feske *et al.*, 2015) have anti-inflammatory effects by inhibiting migration, proliferation, and NOS expression in macrophages,(Vicente *et al.*, 2003) and can exert antithrombotic effects (McCloskey *et al.*, 2010). Thus, by targeting several biological processes involved in restenosis (inhibiting PM of VSMCs, decreasing fibrosis, inflammation, and platelet aggregation), Kv1.3 inhibitors could represent good candidates for the prevention of unwanted remodeling in human vessels.

2. Kv1.5 as a novel myocardin-regulated contractile marker

Another major finding of our work is the identification of at least one mechanism associating the functional expression of Kv1.3 channels to PM. We provide evidence suggesting that MYOCD-dependent expression of Kv1.5 channels, via modulation of the Kv1.3/Kv1.5 ratio in VSMCs, underlies the changes in the functional contribution of Kv1.3 channels to PM. Besides, we demonstrated that Kv1.5 channels inhibit vascular remodeling by occluding Kv1.3 activity as overexpression of Kv1.5 inhibits IH in human vessels at the same levels of PAP-1 and the use of both therapies (PAP-1 and Kv1.5 overexpression) do not have additive effects. We propose that upon PM reduction of Kv1.5 uncovers Kv1.3-dependent signaling pathways leading to proliferation and migration.

These coordinated changes in Kv channel expression have been already reported in other vascular and non-vascular preparations associated to a proliferative/activated phenotype. In particular, downregulation of Kv1.5 channels often associates with Kv1.3 upregulation in proliferating cells (Kotecha & Schlichter, 1999; Vautier *et al.*, 2004; Cidad *et al.*, 2015). Based on these observations, we proposed that the relative amount of these 2 channels (Kv1.3/Kv1.5 ratio) could represent the master switch determining the Kv1 channel effect on proliferation. In fact, even though in some preparations Kv1.3 mRNA expression increased upon PM (Cidad *et al.*, 2010), our more consistent finding in all human and mouse vascular beds explored is a dramatic decrease of Kv1.5 expression upon PM or in response to mitogens, most often with no significant changes in Kv1.3 expression (Cidad *et al.*, 2012, 2015).

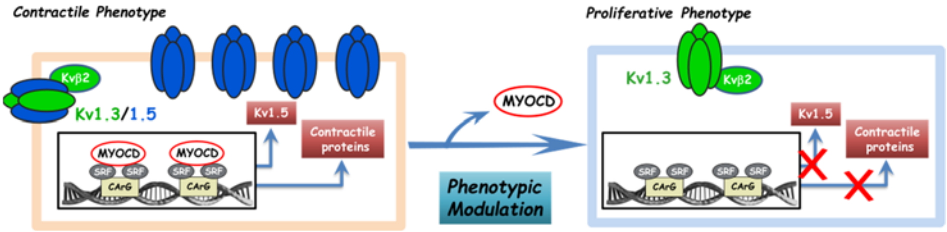
Contractile Phenotype
Kvβ2
Kv1.3/1.5
Kv1.5
Contractile proteins
MYOCD
MYOCD
SRF
SRF
SRF
SRF
CArG
CArG
MYOCD
Phenotypic Modulation
Proliferative Phenotype
Kv1.3
Kvβ2
Kv1.5
Contractile proteins
SRF
SRF
SRF
SRF
CArG
CArG

Figure D2. Proposed model for the effect of myocardin on VSMC Kv1.5 channels and its role in PM (modified from Arevalo-Martínez et al 2019)

Here, we confirmed this notion in organ culture experiments of human vessels. There is a clear inverse relationship between Kv1.5 mRNA levels and PM; in fact, we show for the first time that Kv1.5 expression is regulated by myocardin. We demonstrated that myocardin knockdown decreased expression of Kv1.5 and myocardin overexpression increases it, while Kv1.5 overexpression inhibits PM without affecting myocardin expression (Figures R18-24). Altogether, these data indicated that not only there is a correlation between myocardin and Kv1.5 expression levels but also that Kv1.5 expression is regulated by myocardin, confirming our hypothesis that Kv1.5 is another SM-specific differentiation marker, in the same way as other contractile proteins.

Indeed, when we leveraged publicly accessible human RNA-Seq data (https://gtexportal.org) for correlation analysis, highly significant correlations were found in several tissues including the coronary artery. In addition, Kv1.5 expression shows a very high expression in heart and arteries (https://gtexportal.org/home/gene/KCNA5) and seems to be mainly located in cardiac and smooth muscle. Figure D3 plots some of these correlations.

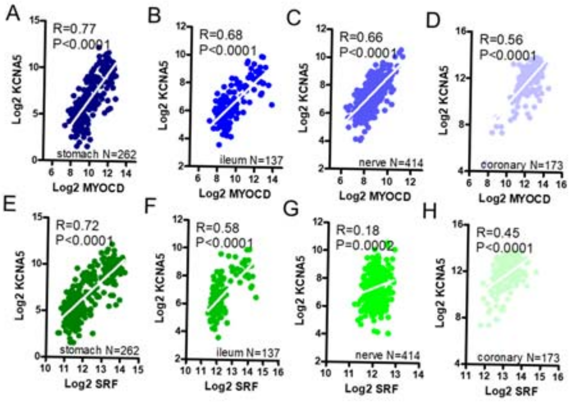

Figure D3. KCNA5 correlates with MYOCD and SRF at the mRNA level across human tissues. RNA-Seq data was downloaded from the GTExPortal.org and normalized Correlations were tested in stomach (N=262), ileum (N=137), tibial nerve (N=414), and coronary artery (N=173) using Log2 transformed expression data P-values, and Spearman Rho values are given in the panels (A through D). Straight white lines represent best linear fits.

To explore other potential candidates for the mechanism(s) responsible of Kv1.5 downregulation during PM, we also looked at SRF and KLF4 mRNA expression, but we found no changes in their expression in our experimental conditions. More work will be required to address this question by exploring other potential candidates.

2.1. Mechanisms of Kv1.5 antiproliferative effects

Two alternative mechanisms could explain the observed Kv1.5-mediated inhibition of PM: 1) activation of antiproliferative signaling pathways or 2) prevention of Kv1.3-induced proliferation. Heterologous expression of Kv1.5 in HEK cells inhibits proliferation, supporting the first option (Cidad *et al.*, 2012; Jiménez-Pérez *et al.*, 2016). However, this may not be the case in native systems, where Kv1.3 and Kv1.5 are likely to form heteromultimeric channels, as has been described for several Kv1 channels (Sobko *et al.*, 1998; Plane *et al.*, 2005; Pannasch *et al.*, 2006).

Here, we demonstrate that Kv1.5 overexpression inhibits PM both in organ culture and in cultured VSMCs. In both preparations, the effects of Kv1.5 overexpression can be reproduced with Kv1.3 blockade, and the 2 effects are non-additive. The interference of Kv1.5 with the proproliferative signaling pathways activated by Kv1.3 protein is the simplest explanation for these data.

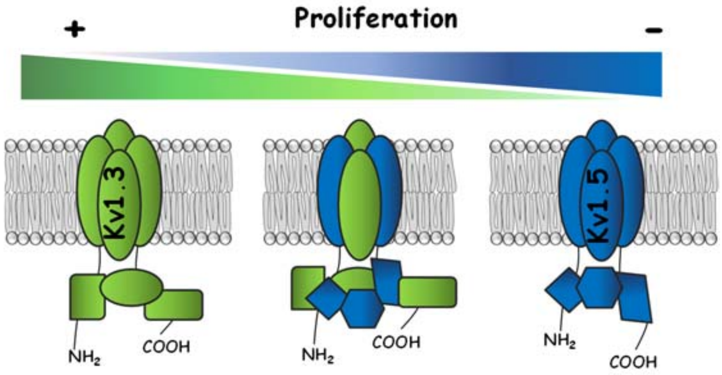

Figure D4. Proposed mechanism for Kv1.5 antiproliferative effects. Kv1.3 and Kv1.5 form heteromultimeric channels in VSMCs. In contractile VSMCs, Kv1.5 is the dominant channel, inhibiting Kv1.3 signaling to proliferation. Kv1.5 downregulation upon PM releases this inhibition and allows Kv1.3 effects on proliferation. (Modified from (López-López *et al.*, 2018))

Kv1.5 channel seems to occlude the activity of Kv1.3, which is explained because:

1) We can only see Kv1.3-induced proliferation in the absence of Kv1.5 channels,

2) Kv1.3 channels expression does not change with PM, but due to their low expression in contractile VSMC they are most likely part of heteromultimeric with Kv1.5 channel
3) Kv1.5 overexpression inhibits proliferation to the same extent that PAP-1, and the effects are not additive.

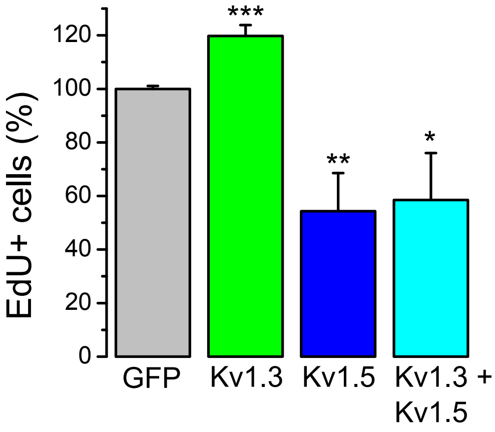

Figure D 5 The bar plot shows the mean ± SEM of 3 different sets experiments using human renal artery VSMCs transduced with AAV-Kv1.5, AAV-Kv1.3 or a mixture of both * P<0.05, ** p<0.01 and *** P<0.001 vs GFP.

4) Preliminary experiments, with overexpression of Kv1.3, Kv1.5 or Kv1.3+Kv1.5 channel together in cultured VSMCs, show that proliferation was reduced when both channels are overexpressed together (see figure D5). These data suggest that Kv1.5 channel has a dominant effect

Although it could also be that Kv1.5 per se had an antiproliferative effect (which we have not explored in native VSMCs), the hypothesis of a physical occlusion of Kv1.3 by Kv1.5 overexpression fits better with these latter observations and results.

2.2. Mechanisms of Kv1.3-pro-proliferative effects

Our results with adenoviral expression of mutant Kv1.3 channels in VSMCs provided some other relevant conclusions about the mechanisms involved in Kv1.3-induced proliferation in these cells. When exploring the possible contribution of Kv1.3 channels to proliferation, we can think of two possible scenarios, which are not mutually exclusive. In one hand, VSMCs could be using Kv1.3 channels to regulate resting V_M (and hence cell cycle), as ion fluxes through the channels could induce these changes. In this hypothesis Kv1.3 channels will be acting as effectors or these changes. In the other hand, Kv1.3 function in VSMC could be to serve as sensors of changes in membrane potential, acting as a signaling molecule connecting bioelectrical signals with intracellular pathways. In the first option we will need the channel to conduct, but in the second one K^+ fluxes through Kv1.3 channels will not be necessary for the effect on proliferation.

Both modes of operation have been confirmed for Kv1.3-induced proliferation in different cells (Pérez-García *et al.*, 2018). In heterologous systems, we demonstrated that K^+ fluxes through Kv1.3 channel are not required for proliferation, but the response needs a voltage-dependent conformational change of the channel.

We explored here whether this result in HEK cells overexpressing WT Kv1.3 or mutant channels can be extrapolated to the native system. The effect of overexpression of the pore-mutant, non-conducting Kv1.3 channel (Kv1.3WF) indicates that, also in VSMCs, K^+ fluxes are not required for Kv1.3-induced proliferation. We found and increase proliferation rate in these cells that was even higher that the observed when overexpressing the WT Kv1.3 channel.

Moreover, we also tried to confirm in the native system another observations regarding the mechanism of Kv1.3-induced proliferation that had been obtained in heterologous expression systems. It has been reported that phosphorylation of at least two individual sites in the C-terminal region of the channel could recapitulate Kv1.3-induced proliferation, as their individual mutation to alanine abolished the effect (Jiménez-Pérez *et al.*, 2016). Here, we found that while overexpression of WT Kv1.3 channels increased VSMCs proliferation, overexpression of one of these phosphorylation-deficient channel Kv1.3Y2 did not change proliferation rate (Figure R13), confirming also in native cells the requirement for interaction of Kv1.3 protein with other partners (via phosphorylation of the channel) to activate proliferation. Altogether, our data suggest that there is a specific requirement for Kv1.3 channel protein to facilitate proliferation, which does not depend on ion fluxes through the channel. The nature of these interacting proteins and the detailed molecular mechanisms activating Kv1.3-induced proliferation await future research.

3. Effect of Kv1.3 blockers on remodeling in T2DM

Type 2 diabetes (T2DM) represents the dark side of restenosis, as these patients have more aggressive forms of vascular disease and worse outcomes, with exacerbated restenosis after vascular surgery. For that reason, in the last part of this thesis, we sought to investigate the effect of Kv1.3 blockers for the prevention of IH in T2DM vessels.Using human mammary artery samples from T2DM patients we have explored the contribution of Kv1.3 inhibitors to vessel remodelling in organ culture and to migration and proliferation of VSMCs in primary culture. Most of T2DM patients also have underlying diseases that might alter the response of treatments restenosis, so that the clinical information obtained from the hMA donors was important to get a better understanding of the results. The table R1 summarized the most important clinical aspect of the non-T2DM and T2DM patients. Overall, this information suggests that our T2DM and non-T2DM samples came from a homogeneous population where T2DM was the main difference between both groups, and hence the factor determining the differences in the contribution of Kv1.3 to vessel remodeling and VSMCs migration and proliferation. In addition, we have created a mouse model of T2DM to explore the in vivo effects of this treatment in order to predict the clinical outcomes. Our results that Kv1.3 blockers such as PAP-1 are well-suited strategies for the prevention of IH in T2DM patients, because not only they have a direct effect inhibiting PM of VSMCs, but also show additional indirect benefits improving the metabolic profile and decreasing associated risk factors.

One interesting observation we made is that not only T2DM vessels show differences in remodelling and in the response to Kv1.3 blockers, but also that these differences persisted in cultured VSMC and remained after many passages that is suggestive of metabolic memory in VSMC form T2DM patients. Uncontrolled hyperglycemia leaves an early imprint on vascular cells, so that its deleterious effects persist long time after effective glycemic control (Holman *et al.*, 2008; Intine & Sarras, 2012), and for that reason we explored the contribution of miRNAs to diabetes epigenetic signature in human VSMCs.

Using a cardiovascular miRNA array, we identified several miRNAs differentially expressed in arterial samples and VSMCs from T2DM patients. Among those, we further characterize the role of miR-126, which was differentially expressed in T2DM contractile and proliferative VSMCs but in opposite directions. We found that mir-126 is increased in VSMCs of T2DM patients and contributes to the metabolic memory of these cells after hyperglycemic episodes, representing a novel target for control of epigenetic modifications in the T2DM population.

3.1. Effect of Kv1.3 blockers in T2DM vessels

T2DM human vessels develop higher IH that those vessels from non-T2DM patients, thus reproducing in the organ culture model the poorer outcomes of T2DM patients undergoing vascular surgeries and the higher incidence of restenosis in this population. The higher levels of Kv1.3 in T2DM vessels, which suggest a larger role of Kv1.3 channel during vascular remodeling in T2DM patients, fit with the idea of the pro-proliferative role of these channels. Of course many other factors must be contributing to the different response to T2DM vessels after surgery, but our observation provides a rational support for the observation that Kv1.3 blockade was more effective in decreasing IH in T2DM vessels. We tested in parallel the effect of everolimus, as it is the gold standard treatment in the clinics. To our surprise, EVL only was able to decrease IH in T2DM vessels in organ culture. As the effects of EVL are mediated through the inhibition of mTORC-1, these data indicate that mTORC-1 activity may be enhanced in T2DM vessels. This conclusion is supported by data form the literature. It has been reported an increased activity of mTOR signaling in several tissues of animal models of T2DM, due to increased levels of circulating insulin, amino acids, and pro-inflammatory cytokines. Also, the increased mTOR signaling contributes to peripheral insulin resistance due to enhanced feedback inhibition of PI3K/AKT signaling (Khamzina *et al.*, 2005; Saxton & Sabatini, 2017). Basal increased activity of mTOR might help to understand the effect of EVL on IH in T2DM vessels. However, we do not have an explanation for the lack of effect of EVL in non-T2DM vessels, which was unexpected.

When exploring the effect of these two drugs on proliferation and migration of VSMCs in culture, we found that PAP-1 and EVL were able to decrease proliferation in both groups, and in this case the effect of EVL was larger in non-T2DM cells. However, PAP-1 and EVL treatments in migration scratch assays paralleled the data obtained from those treatments in IH induced in vessels organ culture. This suggest, that migration exerts a larger effect than proliferation during IH formation so that it could represent the limiting factor for the development of restenosis. In the case of EVL in non-T2DM patients, the lack of effect of EVL in VSMCs migration translates in the lack of effect on IH formation, in spite of the clear inhibition of VSMC proliferation.

3.2. Signaling pathways affected by T2DM in VSMCs

The vascular remodeling observed in T2DM patients was still present in VSMC cultures obtained from T2DM vessels, indicating the presence of hyperglycemia-induced epigenetic changes inducing metabolic memory in those cells. As previously described, VSMCs PM is mediated through activation of key signaling pathways, most importantly the PI3K/AKT and the MAPK/ERK pathways, and this later one is involved in Kv1.3 signaling to proliferation (Cidad *et al.*, 2015). On the other hand, T2DM has been associated with marked reductions of insulin-stimulated IRS-1 phosphorylation and IRS-1-associated PI3K activity in VSMCs. (Sandu *et al.*, 2000). In fact, PI3K–dependent pathways represent a major branch of insulin signaling regulating metabolic functions, whereas Ras/MAPK pathways are involved in promoting mitogenic and growth effects of insulin. In the vasculature hyperinsulinemia associated with T2DM will overdrive unaffected MAPK–dependent pathways, leading to an imbalance between PI3K and MAPK–dependent functions (Kim *et al.*, 2006) which could explain enhanced PM in these patients.

To explore this possibility, we checked the expression of some of the elements of these two signaling pathways in VSMCs form T2DM and non-T2DM patients. We found that T2DM cultures have decreased PI3K/AKT activity and increased ERK1/2 phosphorylation, suggesting that T2DM changes where still present in VSMC cultures (Figure R31).

Of interest, these changes in the activity of the signaling pathways in T2DM VSMCs were confirmed with the effects of the two anti-restenotic drugs used. The data obtained with PAP-1, which shows an overall increased potency in T2DM vessels and VSMCs fully agrees with the increased activity of the MAPK/ERK pathway in these cells. In the other hand, the differential effect of everolimus inhibiting IH in T2DM vessels, indicates that in spite of the decreased PI3K/AKT activity, T2DM cells might have an increased have mTORC1 activity.

A complex disease such as T2DM exemplifies this apparent paradox of high mTORC1 activity coexisting with decreased insulin signaling. mTORC1 integrates signals arising from nutrients, energy, and growth factors (Zoncu *et al.*, 2011). T2DM is a chronic disease that is generally hastened by long-term overfeeding and insulin resistance, two conditions leading to increased mTORC1 activation.

Overfeeding causes abnormally high levels of glucose and amino acids in the blood which trigger insulin release by the pancreas. In turn, chronically high nutrients and insulin lead to sustained mTORC1 activation, which desensitizes the cell to insulin through a series of inhibitory loops converging onto the IR (Figure D6). In this way mTORC1 overactivity worsens the metabolic alterations and its aberrant activation in several tissues may contribute to the pathogenesis of T2DM (Zoncu *et al.*, 2011). This overactivity of mTORC1 has been described in several tissues (liver, skeletal muscle, adipose tissue) which do not include VSMC, but our data suggest that this may be the case.

The ability to sustain these complications in the absence of hyperglycemia (hereafter referred to as the metabolic memory state) invokes a role for the epigenome in perpetuating diabetic complications. Epigenetic mechanisms include post-translational histone modifications, changes in chromatin access through DNA methylation, and changes in regulation of gene expression through non-coding micro-RNAs.

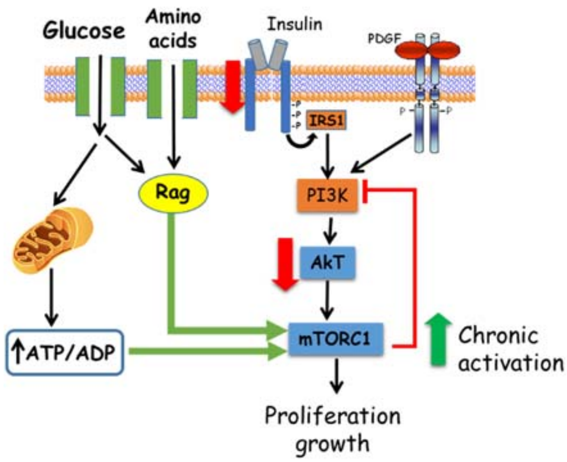

Figure D6. Modulation of mTORC1 in T2DM tissues. There is an increased mTORC1 activity in spite of the reduced insulin signaling. The figure shows the e main mechanisms of activation of mTORC1 (RTKs, nutrients and metabolic state), and also the negative feedback loops that regulate RTK-IRS1/2-PI3K, that contributes to worsen T2DM. Red arrows indicated the pathways downregulated in T2DM.

4. T2DM-associated miRNA profile in VSMCs: miR-126

There are many recent studies devoted to explore contribution of miRNAs in the development of vasculoproliferative diseases and also in the detrimental vascular phenotype associated to diabetes (Zampetaki *et al.*, 2010; Reddy *et al.*, 2016; Togliatto *et al.*, 2018; Torella *et al.*, 2018). However, the outcome of these studies identifies a diverse group of potentially relevant miRNAs, suggesting that exacerbation of the synthetic/proliferative phenotype of VSMCs in T2DM is mediated by a miRNA signature. The concerted action of these dysregulated miRNAs contributes to the multifactorial vascular response in diabetes. Nevertheless, the use in these studies of different species and/or different animal models of diabetes could represent a confounding factor which has not been addressed.

To overcome some of these problems, here we studied the differential expression of and array of miRNAs in human T2DM VSMCs from contractile and proliferative phenotype. Our results showed changes in a different set of miRNAs in each VSMC phenotype, and from all of them we focused in particular in miR-126.

In this part of the discussion, we will try to put together the main findings of some of these papers focused on miRNAs related to cardiovascular complications of T2DM, pointing out the differences in experimental design, that could led to the different conclusions, and also when possible the identification of our target miR-126 in these other studies.

Next, we will focus on discuss the changes in the expression of miR-126 in T2DM VSMC and their functional implications in our preparation.

4.1. miRNA profile in T2DM vessels

Our miRNA PCR Array focused in Human Cardiovascular Disease provided several miRNAs differentially regulated in T2DM VSMCs, both in contractile and proliferative phenotype (i.e. cells from the media layer of the vessels and cultured VSMC respectively). Some of these miRNAs differentially expressed in T2DM have been previously described in other preparations, although there is a huge variability in the results provided. This plethora of altered miRNAs most likely indicates that the T2DM phenotype of VSMCs associated to restenosis and vasculoproliferative diseases is mediated by multiple miRNAs whose contemporary or sequential dysregulation act together to provide the multifactorial vascular response observed. On top of this, the huge differences in the experimental design and the methodological approach also contribute to the dispersion of the results. We have identified some of these differences in the experimental model or the design of these studies:

1. Some of the studies, devoted to identification of biomarkers for risk stratification or prognosis, only explore circulating miRNAs, but not the expression and/or function of these miRNAs in vascular cells (Zampetaki *et al.*, 2010; Olivieri *et al.*, 2015; Barutta *et al.*, 2017) reviewed in (Banerjee *et al.*, 2017). These kind of studies are centered on the identification of biomarkers of T2DM vascular complications. It should be reminded that plasma miRNAs may not necessarily reflect local tissue levels. ***Neverthelss, in all the aforementioned studies the lost of miR-126 is consistently identified as a consistent, robust biomarker of cardiovascular risk in T2DM.***

2. Some studies used high-throughput miRNA sequencing in VSMCs or vessels from models of T2DM. However, most of these studies used animal models of disease, and either vessel or cultured VSMCs from these models, (but not both) to explore the impact of PM in T2DM. For example:

a. Redy et al (Reddy *et al.*, 2016) identifies miR-504 upregulation in RNA-seq from db/db VSMC in culture. We did not explore this miRNA in our array, but interestingly, ***their study also identified the up-regulation of miR-126 in these db/db VSMCs***.

b. Torella et al (Torella *et al.*, 2018) explores with RNA-seq the miRNA profile in vessels of T1DM model (using STZ-treated rats) and T2DM model (using Zucker rats) two days after carotid lesion. They found a set of 6 miRNAs dysregulated in both T1DM and T2DM models, some of them also confirmed in atherosclerotic plaques from diabetic patients. 5 out of these 6 miRNAs (miR-29c, miR-199a, miR-195, miR140 and miR-25) were also included in our study, and also downregulated in T2DM tissues. The only upregulated miRNA (miR-204) was not included in our study. They reproduced their main changes (concomitant up regulation of miR-204 and downregulation of miR-29c in an in vitro model of DM, cultured VSMC treated with high glucose and high insulin. However, none of these miRNAs hem showed significant changes in our cultured VSMCs, suggesting important differences in the model. ***Again, miR-126 in this study showed no changes in injured T1DM but a very large decrease in T2DM.***

4.2. miR-126 role in vascular diseases and T2DM

In spite of the enormous differences in the reported data regarding vascular miRNAs and T2DM, in most of the studies using high-throughput miRNA techniques agree in the importance of miR-126. The data of this thesis underwrite this finding, as we found that miR-126 is differentially expressed in T2DM both in contractile and dedifferentiated phenotype, being in both preparations one of the miRNAs showing a larger fold-regulation together with abundant expression. However, some of our results do not fit the previous data regarding miR-126 origin and function in vessels in general an in the context of T2DM in particular. Some of these mismatches are discussed here.

4.2.a. miR-126 origins.

miR-126 is considered an endothelial miRNA, but we see expression and regulation in VSMC preparations Data in the literature links miR-126 with vascular pathologies and with T2DM. miR-126 plays a central role in endothelial cells homeostasis and induces angiogenesis during embryogenesis and tissue repairs. (Chistiakov *et al.*, 2016). In VSMCs, miR-126 serves as a paracrine mediator secreted by endothelial cells to acts on VSMC and modulate its gene expression and function towards atherogenic phenotype, acting as a key mediator to increase VSMC turnover (Wang *et al.*, 2008; Kuhnert *et al.*, 2008). A role for miR-126 in IH has been proposed, but while some studies showed that systemic depletion of miR-126 in mice inhibits neotintimal lesion formation induced by carotid artery ligation (Zhou *et al.*, 2013), other authors stated that endothelial miR-126 reduce vascular remodeling (Jansen *et al.*, 2017; Izuhara *et al.*, 2017).

Even thought, miR-126 has been described as an endothelial miRNA, we found its expression in VSMCs and confirmed it VSMCs origin by looking for the expression of miR-126 precursor. We found that miR-126 is produced and expressed in VSMCs and its production was augmented in T2DM cells from contractile and proliferative phenotype (see Figure R36). This observation is relevant because it indicates that T2DM induced increased production (and expression) of miR-126, which is in contrast with the consistently lower levels of plasmatic miR-126 has been associated to T2DM patients (Zampetaki *et al.*, 2010) and to T2DM animal models (Venkat *et al.*, 2019). However, as indicated before, plasma miRNA levels do not necessarily reflect tissue levels. The higher miR-126 expression found in VSMC T2DM cells does not imply a higher circulating levels, as miR126 could remain in VSMCs (as it seems to be the case in cultures) or being secreted from VSMC to EC (as we propose in the case of contractile VSMCs).

To confirm this later hypothesis, we explored pre-miR-126 and miR-126 expression in VSMC+EC tissue to test if secretion of miR-126 from VSMC to EC could be taking place (Figure R37).

In the case of non-T2DM, we did not find differences between VSMC alone and VSMC+ EC tissue, thus implying that in our preparation (hMA) miR-126 expression is taking place almost exclusively in VSMC (even though miR-126 is considered an endothelial miRNA). On the other hand, in T2DM samples miR-126 expression increases more than 50 times when comparing VSMC alone versus VSMC+EC. However, the expression of the precursors is the same, confirming its VSMC origin.

From these data we can conclude that VSMC from hMA are the cells producing and expressing miR-126. In non-T2DM vessels, this miR-126 remains mostly in the VSMC. However, upon T2DM, there is a marked increase in miR-136 production (more than 40 times increase in pre-miR-126 levels), and in this situation miR-126 is secreted from VSMC to ECs. As circulating miR-126 levels are consistently downregulated in DM patients, we assume that this miR-126 secreted from VSMC and internalized in ECs is not released to circulation but it has a functional role in these ECs. Yet, it will be necessary to explore the circulating miR-126 levels in our patients to confirm this extent.

4.2.b. miR-126 targets and effects on VSMCs

Our data with miR-126 gain of function experiments in cultured VSMC form non-T2DM and T2DM provides very clear-cut results regarding the role of miR-126 in both groups. In both cases we got comparable levels of overexpression of miR-126. However, while miR-126 overexpression augments proliferation and migration rates in non-T2DM cells, it did not have any effect on the T2DM. We have previously found that T2DM VSMCs showed higher rates of migration and proliferation than non-T2DM VSMCs (Figure R26). Here we demonstrated that in this regard miR-126 overexpression can confer the “diabetic” phenotype to non-T2DM cells. We explore the changes in the expression of known miR-126 targets to identify the molecular mechanisms involved in this effect of miR-126 in non-T2DM cells. Of all the described targets, we only found changes in two, AKT-2 and PI3K regulatory subunit 2 (PI3KR2). The expression of these two genes decreased upon miR-126 expression but only in non-T2DM VSMCs. These results fit nicely with the reported downregulation of the PI3K/AKT pathway described upon T2DM and reported in our preparation, confirming that miR-126 can induce the T2DM phenotype.

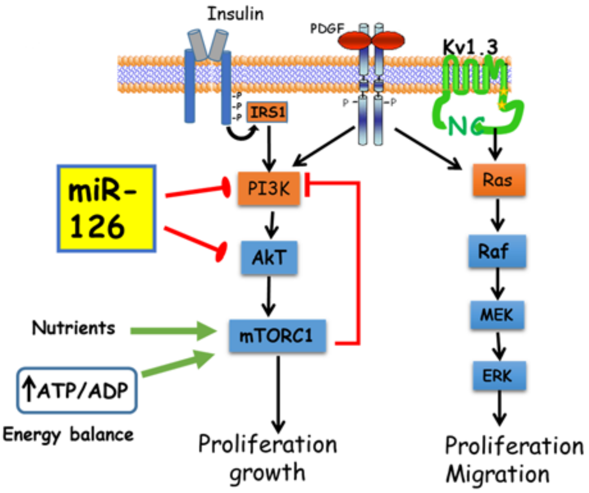

Figure D7. Signaling pathways affected by miR-126 overexpression in non-T2DM VSMCs See text for more details.

There are many other targets of miR-126 that we could not confirm in our cells (see Table R2). Clearly, both miRNA targets and miRNA effects are tissue specific. In that regard, it is likely that this specificity can explain most of the differences in the function of miR-126 between our preparation (where miR-126 is acting on VSMCs) and previously described ones (mostly ECs miR-126 functions). EC miR126 has been proposed to increase atherogenesis (Zhou *et al.*, 2013), VSMCs turnover during angiogenesis (Kuhnert *et al.*, 2008), or decrease proliferation and migration in VSMCs (Jansen *et al.*, 2017). In all cases, these effects of miR-126 were mediated by target genes that were not affected in our preparation, including FOXO3, IRS-1, Sprouty-related protein (SPRED1) or EGF-like domain-containing protein 7 (EGFL7) among others.

4.2.c. miR-126 effects on VSMCs and in vitro T2DM models

T2DM cells behave differently to non-T2DM when cultured in the same conditions suggesting that cells need to be in a diabetic environment quite a time before becoming T2DM cells. Therefore, in vitro models of T2DM, such as cells kept with high glucose (25 mM) and high insulin (200 nM) (Torella *et al.*, 2018) might not necessarily transform cells into T2DM cells, or allow to extrapolate regulatory mechanisms.

Our data suggest that miR-126 could be involved in the metabolic memory of T2DM cells. We hypothesize that cells cultured under “diabetic conditions” do not recapitulate the characteristics of cells harvested from T2DM patients, our model of in vitro T2DM. To get some insight, we tested the expression of miR-126 from non-T2DM VSMCs cultured in high glucose (22mM).

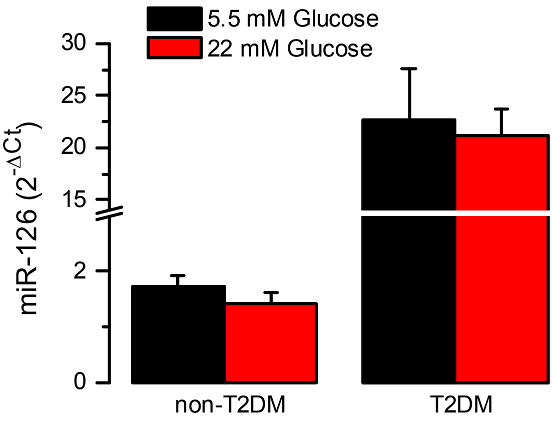

Figure D8. Mean ±SEM of miR-126 expression level normalized to SNORD 68. VSMCs were incubated with high glucoses concentration for 48 hours. Data from 3 different experiments in each group.

Our preliminary data showed these culture conditions did not change the expression levels of miR-126 (Figure D8), confirming the lack of parallelism between both models.

5. Vascular remodeling in T2DM-like animal models

5.1. Development of a VRF mouse model.

We developed an animal model with VRF to have an *in-vivo* model that could mimic the diseased background of patients undergoing vascular surgeries that will allow to test the effect of Kv1.3 blockers. Previous work from or lab, have demonstrated that Kv1.3 blocker reduce vascular remodeling in *in vivo* animal models, however this was tested on healthy animal without any other pathologies (Cidad *et al.*, 2014). With the idea of getting a model that closely mimicked T2DM, including other common associated pathologies of this population (see Table R1) we fed hypertensive mice with HFD and within 12 weeks, we obtained obese, glucose intolerant and insulin resistant animals.

HFD induce obesity which is one of the greatest risk factors linked to T2DM in the population (Yeadon, 2015), in fact almost all of our T2DM donors were overweight. We selected HFD to induce overweight and T2DM in BPH mice because it stablished the proper etiological and pathological development of the diseases as it occurs in human patients. Limitations of HFD is that it requires months of feeding to achieve the full spectrum of T2DM symptoms and also different mouse strain presents variable responses to HFD. For instance, C57Bl/6J mouse strain is among the most sensitive to HFD and develop severe obesity, liver inflammation and liver steatosis. Contrary to C57Bl/6J, BALBc gain less weight and are more susceptible to liver steatosis(Jovicic *et al.*, 2015; Heydemann, 2016).

Genetic mice models for T2DM model like the homozygous ob/ob and the db/db mutations were the earliest diabetic mouse models characterized. Leptin is a hormone that regulate appetite, and mutations in either the leptin gene (ob/ob) or its receptor (db/db) induce unregulated feeding (hyperpagia), resulting in subsequent obesity and frank diabetes. However, ob/ob and db/db mice have diabetes at 4 weeks of age (O’brien *et al.*, 2014; Yeadon, 2015) which do not resembles the gradually onset of the pathology like in T2DM human patients.

BPH strain have hypertension mediated by sympathetic activity. In addition, BPH mice presents metabolic differences when comparing with BPN mice. BPH mice have lower body weight (Schlager *et al.*, 1979), increased locomotor activity (McGuire *et al.*, 2007), higher metabolic rate (Jackson *et al.*, 2014), and abnormal thermoregulation (Malo *et al.*, 1989). Here, we found that BPH male mice have a tendency to develop glucose intolerance and insulin resistance with aging, which represents new evidence for more metabolic irregularities.

We concluded that BPH/HFD developed **pre-diabetes** within 12 weeks as these mice became glucose intolerant, showed insulin resistance and became obese, although basal glycemia was only moderately increased. We also fed BPN mice with HFD, but in this case we did not observe any metabolic change, not even overweight after 24 weeks (Figure D9). BPN mice is a clear example of a HFD-resistant strain.

To our delight, BPH/HFD model also resembled the data observed in T2DM human vessels with regards to the increased expression of Kv1.3. channels mRNA and protein. We found both a higher Kv1.3 expression and also a higher Kv1.3 to Kv15 ratio, both suggestive (according to our hypothesis) of a change towards a more dedifferentiated phenotype. In fact, we confirmed that VSMCs from BPH/HFD are prone and more susceptible to increased remodeling, as carotid ligation resulted in more neointima formation in BPH/HFD than in BPH/SD mice

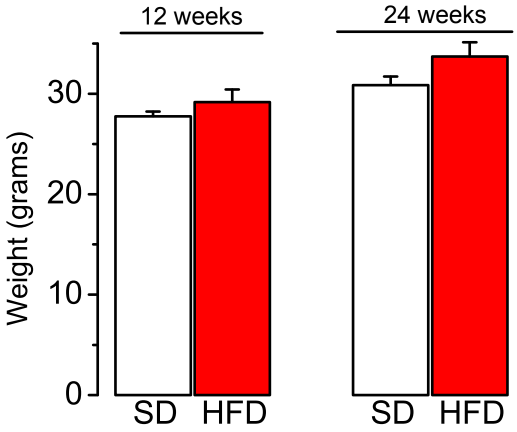

Figure D9. Weight of BPN mice with standard and HFD at 12 and 24 weeks. Data displayed as mean ± SEM of 4–7 mice.

5.2. Effects of Kv1.3 blockers in remodeling in mice models

Carotid ligation was used as to induce IH in mice because it’s an easy and reproducible technique. Before performing carotid ligation in our

VRF mice model (BPH/HFD), we tested the kind of vascular remodeling in our mice strains. The vascular remodeling upon carotid ligation depends of the mice strain. For instance, in C57BL/6J, A/J or AKR/J ligation produce inward remodeling, in BALB/cJ and FVB/NJ produce abundantly neointima formation while in SM/J strain carotid ligation do not induce intimal hyperplasia (Harmon *et al.*, 2000). We demonstrated that BPH strain develop inward remodeling with little neointima formation upon right carotid ligation. In BPH/HFD, ligation produced a large neointima formation and hypertrophy of the vascular wall. The large IH in BPH/HFD mice was expected as it has been described also in the genetic models of T2DM, such as ob/ob mice (Liu *et al.*, 2018).

Next we explored the effects of PAP-1 in vivo both in the control animals (Ligated BPH/SD) and the T2DM-like ones (BPH/HFD mice). PAP-1 treatment decreased the vascular remodeling upon carotid ligation.

Our data demonstrated that PAP-1 has good efficiency in preventing IH and vascular remodeling not only in healthy vessels but also in vessels with diseased backgrounds (BPH/HFD). These data correlate with these from human vessels in organ culture. Besides, the decrease of IH upon Kv1.3 blockade shows no gender differences and no differences between systemic (mini-pump) and *in-situ* drug delivery (ELR-polymer).

In addition, in the case of the SD animals, we also compared the effect of PAP-1 and everolimus and even though we do not have a large n, our data suggest that PAP-1 is at least as efficient as EVL in preventing IH, and probably even more, as the effects were larger and more homogeneous in the PAP-1 treated animals.

More interestingly, additional systemic beneficial effects of PAP-1 were evident in the HFD mice. PAP-1 treatment decreased weight gain and improved insulin sensitivity in BPH mice with HFD. This effect of PAP was observed even in the case of *in-situ* drug administration, at the carotid ligation, and seems to be specific of the HFD model, as no differences in weight gain were observed in BPH/SD during the 4 weeks of PAP-treatment. More interestingly, PAP-1 treatment fully reverted insulin resistance of BPH/HFD diet.

Several hypothesis can be put forward to explain these positive effects of Kv1.3 blockade, on top of the local effects on vessel remodeling:

1. It has been shown that Kv1.3 channel are also expressed in postganglionic sympathetic neurons, where they can influence the

functions of sympathetic activity that regulates body weight and energy homeostasis. (Doczi *et al.*, 2008).

2. Besides, Kv1.3 channel activity has been associated to insulin resistance (Choi & Hahn, 2010), an effect which could explain the reversion of the ipITT curve in PAP-1 treated mice.

It has been reported that the use of Kv1.3 blockers such as ShK-186 counteracts the negative effects of increased caloric intake in mice fed a diet rich in fat and fructose. These changes mimic the effects of Kv1.3 gene deletion, and, as in our case, the blocker did not alter weight gain in mice on a chow diet, suggesting that the obesity-inducing diet enhances sensitivity to Kv1.3 blockade (Upadhyay *et al.*, 2013). Among the proposed mechanisms for this effect are the activation of brown adipose tissue, (leading to increase energy expenditure with no change in caloric intake), and the obesity-induced increased Kv1.3 expression in the live, which seems to be responsible of the differential effect on weight gain between obese and lean animals.

Altogether, our data supports that Kv1.3 blockers such as PAP-1 could represent a good therapy against vascular restenosis in human patients, and especially for patients with underlying diseases as T2DM or metabolic syndrome. Yet, more studies are necessary to completely understand the signaling pathways associated to Kv1.3 and Kv1.5 channels, and their dysregulation in T2DM patients. Finally, although our data identified changes in miR-126 expression as relevant for the establishment of the VSMC diabetic phenotype, more research will be needed to determine the molecular interactions and the crosstalk between miR-126 modulated pathways and Kv1.3 signaling pathways in T2DM VSMCs.

Conclusions

1. ***Kv1.3 channel contributes to vascular remodeling and intimal hyperplasia in human vessels***. Kv1.3 channels represent a promising therapeutical target against vascular remodeling in human vessels, as the use of Kv1.3 blockers prevents this remodeling by inhibiting VSMCs proliferation, migration and extracellular matrix secretion.

~~2.~~ ***The increased functional contribution of Kv1.3 upon phenotypic modulation is a consequence of the myocardin-dependent downregulation of Kv1.5 channels*****.**

3. ***Kv1.5 channel is a myocardin-regulated VSMC contractile gene***. We observed a perfect correlation between expression levels of Kv1.5 and myocardin mRNA in VSMCs from tissue, organ culture and cell culture. Moreover, K1.5 expression is downregulated upon myocardin knock down and upregulated by myocardin overexpression, while Kv1.5 overexpression does not change myocardin expression.

4. ***Kv1.5 overexpression inhibited human vessels remodeling by hampering Kv1.3-induced migration and proliferation, as the effects of Kv1.5 overexpression and Kv1.3 blockade are not additive.*** We propose that the presence of Kv1.5 in heterotetrameric Kv1 channels occludes Kv1.3 signaling pathways leading to proliferation. Strategies directed to block Kv1.5 downregulation could also represent an efficient approach for the prevention of restenosis after vascular surgeries.

5. ***The vessels from T2DM patients in organ culture show increased remodeling and higher expression of Kv1.3 channels***. In agreement with this observation, Kv1.3 blockers are more effective inhibiting IH in T2DM vessels, indicating that they could represent a better therapy for the prevention of restenosis in this vulnerable population.

6. ***The differences in remodeling in T2DM vessel reflect hyperglycemia-induced epigenetic changes***. Increased remodeling of T2DM vessels correlates with an increased rate of migration and proliferation of diabetic VSMCs in culture**.** In addition, the effect of Kv1.3 blockers and mTOR blockers on both cultured VSMCs and vessels in organ culture suggest a larger contribution of VSMC migration to intimal hyperplasia.

7. ***T2DM VSMCs show decreased activity of the PI3K/AKT pathway and increased activity of the MAPK/ERK pathway.*** As Kv1.3 effects on proliferation are mediated by ERK activation, these changes in the signaling of T2DM cells can help to explain the increased contribution of Kv1.3 channels activity to vascular remodeling in diabetic patients.

8. ***Differential expression of miRNAs in non-T2DM and T2DM contractile and proliferative VSMCs identified miR-126 as the most significant misregulated miRNA in both preparations*.** miR-126 expression is decreased in T2DM contractile VSMC and upregulated in T2DM cultured VSMCs.

9. ***The study of the expression of miR-126 precursors indicates that VSMCs do express miR-126 and that its production is upregulated in T2DM cells in both phenotypes***. In cultured VSMC this increased miR-126 remains in the cells while in the contractile VSMCs miR-126 is secreted to endothelial cells.

10. ***The increase of miR-126 contributes to the metabolic memory of T2DM VSMCs cultures.*** Overexpression of miR-126 increases migration and proliferation rate of non-T2DM cultures but was without effect in T2DM cells. In addition, miR-126 decreased PI3KR2 and AKT2 mRNA expression only in non-T2DM VSMCs.

11. ***We obtained an animal model that parallels the characteristics of T2DM human vessels.*** After 12 weeks of HFD, BPH mice showed obesity, insulin resistance and glucose intolerance. In

addition, BPH/HFD showed increased Kv1.3 expression and augmented vascular remodeling upon carotid ligation.

12. ***Kv1.3 blockers showed better results in the prevention of IH in diseased vessels compared to healthy vessels.*** In our in vivo model Kv1.3 blockers inhibited IH in both control and BPH/HFD mice to a similar extent. However, Kv1.3 blockade showed additional benefits in our disease model, improving insulin sensitivity and normalizing weight of BPH/HFD. Our data indicated that Kv1.3 channels represent a promising therapeutical target against vascular remodeling with higher impact in diseased vessels.

References

Albinsson S & Sessa WC (2011). Can microRNAs control vascular smooth muscle phenotypic modulation and the response to injury? *Physiol Genomics* **43,** 529–533.

Alexander MR & Owens GK (2012). Epigenetic Control of Smooth Muscle Cell Differentiation and Phenotypic Switching in Vascular Development and Disease. *Annu Rev Physiol* **74,** 13–40.

Althoff TF & Offermanns S (2015). G-protein-mediated signaling in vascular smooth muscle cells — implications for vascular disease. *J Mol Med* **93,** 973–981.

Aranda Jr. JM & Hill J (2000). Cardiac Transplant Vasculopathy. *Chest* **118,** 1792–1800.

Aurnhammer C, Haase M, Muether N, Hausl M, Rauschhuber C, Huber I, Nitschko H, Busch U, Sing A, Ehrhardt A & Baiker A (2012). Universal Real-Time PCR for the Detection and Quantification of Adeno-Associated Virus Serotype 2-Derived Inverted Terminal Repeat Sequences. *Hum Gene Ther Methods* **23,** 18–28.

Bagmet AD (2002). Vascular Remodeling and Apoptosis in Health and Disease. *Kardiologiya* **42,** 83–86.

Banerjee J, Nema V, Dhas Y & Mishra N (2017). Role of MicroRNAs in Type 2 Diabetes and Associated Vascular Complications. *Biochimie* **139,** 9–19.

Barutta F, Bruno G, Matullo G, Chaturvedi N, Grimaldi S, Schalkwijk C, Stehouwer CD, Fuller JH & Gruden G (2017). MicroRNA-126 and micro-/macrovascular complications of type 1 diabetes in the EURODIAB Prospective Complications Study. *Acta Diabetol* **54,** 133–139.

Beech DJ (2007). *Ion channel switching and activation in smooth-muscle cells of occlusive vascular diseases*. Available at: www.biochemsoctrans.org.

Bendeck MP, Regenass S, Tom WD, Giachelli CM, Schwartz SM, Hart C & Reidy MA (1996). Differential expression of alpha 1 type VIII collagen in injured platelet-derived growth factor-BB--stimulated rat carotid arteries. *Circ Res* **79,** 524–531.

Beneit N, Fernández-García CE, Martín-Ventura JL, Perdomo L, Escribano, Michel JB, García-Gómez G, Fernández S, Díaz-Castroverde S, Egido J, Gómez-Hernández A & Benito M (2016). Expression of insulin receptor (IR) A and B isoforms, IGF-IR, and IR/IGF-IR hybrid receptors in vascular smooth muscle cells and their role in cell migration in atherosclerosis. *Cardiovasc Diabetol*; DOI: 10.1186/s12933-016-0477-3.

Benson CC, Zhou Q, Long X & Miano JM (2011). Identifying functional single nucleotide polymorphisms in the human CArGome. *Physiol Genomics* **43,** 1038–1048.

Berridge MJ (2014). *Cell Signalling Biology*. Portland Press Ltd.

Bhattacharyya A, Lin S, Sandig M & Mequanint K (2014). Regulation of vascular smooth muscle cell phenotype in three-dimensional coculture system by Jagged1-selective Notch3 signaling. *Tissue Eng Part A* **20,** 1175–1187.

Biermann C (2004). PCR Primer: A Laboratory Manual. Second Edition. Edited by Carl W Dieffenbach and Gabriela S Dveksler. *Q Rev Biol* **79,** 204–205.

Brown A, Reynolds LR & Bruemmer D (2010). Intensive glycemic control and cardiovascular disease: An update. *Nat Rev Cardiol* **7,** 369–375.

Byrne RA, Mehilli J, Iijima R, Schulz S, Pache J, Seyfarth M, Schomig A & Kastrati A (2008). A polymer-free dual drug-eluting stent in patients with coronary artery disease: a randomized trial vs. polymer-based drug-eluting stents. *Eur Heart J* **30,** 923–931.

Calvert PA & Bennett MR (2009). Restenosis revisited. *Circ Res* **104,** 823–825.

Cavalli G & Heard E (2019). Advances in epigenetics link genetics to the environment and disease. *Nature* **571,** 489–499.

Chang S, Song S, Lee J, Yoon J, Park J, Choi S, Park JK, Choi K & Choi C (2014). Phenotypic modulation of primary vascular smooth muscle cells by short-term culture on micropatterned substrate. *PLoS One*; DOI: 10.1371/journal.pone.0088089.

Chen H-C (2005). Boyden chamber assay. *Methods Mol Biol* **294,** 15–22.

Chen J, Kitchen CM, Streb JW & Miano JM (2002). Myocardin: A Component of a Molecular Switch for Smooth Muscle Differentiation. *J Mol Cell Cardiol* **34,** 1345–1356.

Chen J, Yin H, Jiang Y, Radhakrishnan SK, Huang ZP, Li J, Shi Z, Kilsdonk EPC, Gui Y, Wang DZ & Zheng XL (2011). Induction of MicroRNA-1 by myocardin in smooth muscle cells inhibits cell proliferation. *Arterioscler Thromb Vasc Biol* **31,** 368–375.

Chen R & Chung SH (2014). Binding modes of two scorpion toxins to the voltage-gated potassium channel kv1.3 revealed from molecular dynamics. *Toxins (Basel)* **6,** 2149–2161.

Chistiakov DA, Orekhov AN & Bobryshev Y V. (2016). The role of miR-126 in embryonic angiogenesis, adult vascular homeostasis, and vascular repair and its alterations in atherosclerotic disease. *J Mol Cell Cardiol* **97,** 47–55.

Choi BH & Hahn SJ (2010). Kv1.3: A potential pharmacological target for diabetes. *Acta Pharmacol Sin* **31,** 1031–1035.

Cidad P, Jiménez-Pérez L, García-Arribas D, Miguel-Velado E, Tajada S, Ruiz-McDavitt C, López-López JR & Pérez-García MT (2012). Kv1.3 channels can modulate cell proliferation during phenotypic switch by an ion-flux independent mechanism. *Arterioscler Thromb Vasc Biol* **32,** 1299–1307.

Cidad P, Miguel-Velado E, Ruiz-McDavitt C, Alonso E, Jiménez-Pérez L, Asuaje A, Carmona Y, García-Arribas D, López J, Marroquín Y, Fernández M, Roqué M, Pérez-García MT & López-López JR (2015). Kv1.3 channels modulate human vascular smooth muscle cells proliferation independently of mTOR signaling pathway. *Pflugers Arch Eur J Physiol* **467,** 1711–1722.

Cidad P, Moreno-Domínguez A, Novensá L, Roqué M, Barquín L, Heras M, Pérez-García MT & López-López JR (2010). Characterization of ion channels involved in the proliferative response of femoral artery smooth muscle cells. *Arterioscler Thromb Vasc Biol* **30,** 1203–1211.

Cidad P, Novensà L, Garabito M, Batlle M, Dantas AP, Heras M, López-López JR, Pérez-García MT & Roqué M (2014). K+Channels Expression in Hypertension After Arterial Injury, and Effect of Selective Kv1.3 Blockade with PAP-1 on Intimal Hyperplasia Formation. *Cardiovasc Drugs Ther*; DOI: 10.1007/s10557-014-6554-5.

Coetzee WA, Amarillo Y, Chiu J, Chow A, Lau D, McCormack T, Moreno H, Nadal MS, Ozaita A, Pountney D, Saganich M, Vega-Saenz de Miera E & Rudy B (1999). Molecular diversity of K+ channels. *Ann N Y Acad Sci* **868,** 233–285.

Cooper ME (2009). Metabolic memory: implications for diabetic vascular complications. *Pediatr Diabetes* **10,** 343–346.

Davids MS (2017). Targeting BCL-2 in B-cell lymphomas. *Blood* **130,** 1081–1088.

Davis-Dusenbery BN, Wu C & Hata A (2011). Micromanaging vascular smooth muscle cell differentiation and phenotypic modulation. *Arterioscler Thromb Vasc Biol* **31,** 2370–2377.

Davis BN, Hilyard AC, Lagna G & Hata A (2008). SMAD proteins control DROSHA-mediated microRNA maturation. *Nature* **454,** 56–61.

Deng CY, Yang H, Kuang SJ, Rao F, Xue YM, Zhou ZL, Liu XY, Shan ZX, Li XH, Lin QX, Wu SL & Yu XY (2014). Upregulation of 5-hydroxytryptamine receptor signaling in coronary arteries after organ culture. *PLoS One*; DOI: 10.1371/journal.pone.0107128.

Dhaliwal A & Thohan V (2006). Cardiac allograft vasculopathy: the Achilles' heel of long-term survival after cardiac transplantation. *Curr Atheroscler Rep* **8,** 119–130.

Dhalla NS, Nagano M & Ostadal B (2011). *Molecular Defects in Cardiovascular Disease*. Springer.

Doczi MA, Morielli AD & Damon DH (2008). Kv1.3 channels in postganglionic sympathetic neurons: expression, function, and modulation. *Am J Physiol Regul Integr Comp Physiol* **295,** R733–R740.

Du KL, Ip HS, Li J, Chen M, Dandre F, Yu W, Lu MM, Owens GK & Parmacek MS (2003). Myocardin Is a Critical Serum Response Factor Cofactor in the Transcriptional Program Regulating Smooth Muscle Cell Differentiation. *Mol Cell Biol* **23,** 2425–2437.

Eckel RH, Grundy SM & Zimmet PZ (2005). The metabolic syndrome. *Lancet* **365,** 1415–1428.

Fadool DA, Tucker K, Perkins R, Fasciani G, Thompson RN, Parsons AD, Overton JM, Koni PA, Flavell RA & Kaczmarek LK (2004). Kv1.3 channel gene-targeted deletion produces "Super-Smeller Mice" with altered glomeruli, interacting scaffolding proteins, and biophysics. *Neuron* **41,** 389–404.

Fergus DJ, Martens JR & England SK (2003). Kv channel subunits that contribute to voltage-gated K+ current in renal vascular smooth muscle. *Pflugers Arch Eur J Physiol* **445,** 697–704.

Feske S, Wulff H & Skolnik EY (2015). Ion Channels in Innate and Adaptive Immunity. *Annu Rev Immunol* **33,** 291–353.

Fish JE, Santoro MM, Morton SU, Yu S, Yeh R-F, Wythe JD, Ivey KN, Bruneau BG, Stainier DYR & Srivastava D (2008). miR-126 Regulates Angiogenic Signaling and Vascular Integrity. *Dev Cell* **15,** 272–284.

Garcia-Calvo M, Leonard RJ, Novick J, Stevens SP, Schmalhofer W, Kaczorowski GJ & Garcia ML (1993). Purification, characterization, and biosynthesis of margatoxin, a component of Centruroides margaritatus venom that selectively inhibits voltage-dependent potassium channels. *J Biol Chem* **268,** 18866–18874.

Gibson WT & Hayden MR (2007). Mycophenolate mofetil and atherosclerosis: Results of animal and human studies. In *Annals of the New York Academy of Sciences*, pp. 209–221. Blackwell Publishing Inc.

Grundy SM, Cleeman JI, Daniels SR, Donato KA, Eckel RH, Franklin BA, Gordon DJ, Krauss RM, Savage PJ, Smith SC, Spertus JA & Costa F (2005). Diagnosis and Management of the Metabolic Syndrome. *Circulation* **112,** 2735–2752.

References

Haeussler M, Schönig K, Eckert H, Eschstruth A, Mianné J, Renaud J-B, Schneider-Maunoury S, Shkumatava A, Teboul L, Kent J, Joly J-S & Concordet J-P (2016). Evaluation of off-target and on-target scoring algorithms and integration into the guide RNA selection tool CRISPOR. *Genome Biol* **17,** 148.

Haglund K, Rusten TE & Stenmark H (2007). Aberrant receptor signaling and trafficking as mechanisms in oncogenesis. *Crit Rev Oncog* **13,** 39–74.

Hansen-Schwartz J, Ansar S & Edvinsson L (2008). Cerebral vasoconstriction after subarachnoid hemorrhage--role of changes in vascular receptor phenotype. *Front Biosci* **13,** 2160–2164.

Harmon KJ, Couper LL & Lindner V (2000). Strain-dependent vascular remodeling phenotypes in inbred mice. *Am J Pathol* **156,** 1741–1748.

He G-W (1999). Arterial Grafts for Coronary Artery Bypass Grafting: Biological Characteristics, Functional Classification, and Clinical Choice. *Ann Thorac Surg* **67,** 277–284.

Heldin C & Westermark B (1999). *Mechanism of Action and In Vivo Role of Platelet-Derived Growth Factor*. Available at: www.physiology.org/journal/physrev.

Heydemann A (2016). An Overview of Murine High Fat Diet as a Model for Type 2 Diabetes Mellitus. *J Diabetes Res* **2016,** 2902351.

Hinek A & Rabinovitch M (1993). The ductus arteriosus migratory smooth muscle cell phenotype processes tropoelastin to a 52-kDa product associated with impaired assembly of elastic laminae. *J Biol Chem* **268,** 1405–1413.

Holman RR, Paul SK, Bethel MA, Matthews DR & Neil HAW (2008). 10-year follow-up of intensive glucose control in type 2 diabetes. *N Engl J Med* **359,** 1577–1589.

Hopkins BD, Hodakoski C, Barrows D, Mense SM & Parsons RE (2014). PTEN function: the long and the short of it. *Trends Biochem Sci* **39,** 183–190.

House SJ, Potier M, Bisaillon J, Singer HA & Trebak M (2008). The non-excitable smooth muscle: Calcium signaling and phenotypic switching during vascular disease. *Pflugers Arch Eur J Physiol* **456,** 769–785.

Huang PL (2009). A comprehensive definition for metabolic syndrome. *DMM Dis Model Mech* **2,** 231–237.

Hui DY (2008). Intimal Hyperplasia in Murine Models. *Curr Drug Targets* **9,** 251–260.

Ibraheem D, Elaissari A & Fessi H (2014). Gene therapy and DNA delivery systems. *Int J Pharm* **459,** 70–83.

Intine R V. & Sarras MP (2012). Metabolic memory and chronic diabetes complications: Potential role for epigenetic mechanisms. *Curr Diab Rep* **12,** 551–559.

Ip JH, Fuster V, Badimon L, Badimon J, Taubman MB & Chesebro JH (1990). Syndromes of accelerated atherosclerosis: Role of vascular injury and smooth muscle cell proliferation. *J Am Coll Cardiol* **15,** 1667 LP – 1687.

Izuhara M, Kuwabara Y, Saito N, Yamamoto E, Hakuno D, Nakashima Y, Horie T, Baba O, Nishiga M, Nakao T, Nishino T, Nakazeki F, Ide Y, Kimura M, Kimura T & Ono K (2017). Prevention of neointimal formation using miRNA-126-containing nanoparticle-conjugated stents in a rabbit model ed. Pintus G. *PLoS One* **12,** e0172798.

Jackson KL, Nguyen-Huu TP, Davern PJ & Head GA (2014). Energy metabolism in BPH/2J genetically hypertensive mice. *Hypertens Res* **37,** 413–421.

Jackson WF (2000). Ion Channels and Vascular Tone. *Hypertension* **35,** 173–178.

Jansen F, Stumpf T, Proebsting S, Franklin BS, Wenzel D, Pfeifer P, Flender A, Schmitz T, Yang X, Fleischmann BK, Nickenig G & Werner N (2017). Intercellular transfer of miR-126-3p by endothelial microparticles reduces vascular smooth muscle cell proliferation and limits neointima formation by inhibiting LRP6. *J Mol Cell Cardiol* **104,** 43–52.

Jeremy JY & Thomas AC (2010). Animal Models for Studying Neointima Formation. *Curr Vasc Pharmacol* **8,** 198–219.

Ji R, Cheng Y, Yue J, Yang J, Liu X, Chen H, Dean DB & Zhang C (2007). MicroRNA expression signature and antisense-mediated depletion reveal an essential role of MicroRNA in vascular neointimal lesion formation. *Circ Res* **100,** 1579–1588.

Jiménez-Pérez L, Cidad P, Álvarez-Miguel I, Santos-Hipólito A, Torres-Merino R, Alonso E, de la Fuente MÁ, López-López JR & Pérez-García MT (2016). Molecular Determinants of Kv1.3 Potassium Channels-induced Proliferation. *J Biol Chem* **291,** 3569–3580.

Jiménez Pérez L (2015). *The role of Kv1.3 channels in cell proliferation: mechanisms and molecular determinants* (thesis). Universidad de Valladolid. Available at: http://uvadoc.uva.es/handle/10324/16072 [Accessed March 31, 2020].

Johnsson E, Maddahi A, Wackenfors A & Edvinsson L (2008). Enhanced expression of contractile endothelin ET(B) receptors in rat coronary artery after organ culture. *Eur J Pharmacol* **582,** 94–101.

Johnstone T & Veves A (2005). *Diabetes and Cardiovascular Disease*, second. Humana Press Inc.

Jorgensen C, Darré L, Vanommeslaeghe K, Omoto K, Pryde D & Domene C (2015). In silico identification of PAP-1 binding sites in the Kv1.2 potassium channel. *Mol Pharm* **12,** 1299–1307.

Jovicic N, Jeftic I, Jovanovic I, Radosavljevic G, Arsenijevic N, Lukic ML & Pejnovic N (2015). Differential Immunometabolic Phenotype in Th1 and Th2 Dominant Mouse Strains in Response to High-Fat Feeding ed. Nerurkar P V. *PLoS One* **10,** e0134089.

Karnik SK, Brooke BS, Bayes-Genis A, Sorensen L, Wythe JD, Schwartz RS, Keating MT & Li DY (2003). A critical role for elastin signaling in vascular morphogenesis and disease. *Development* **130,** 411–423.

Kasza A (2013). Signal-dependent Elk-1 target genes involved in transcript processing and cell migration. *Biochim Biophys Acta - Gene Regul Mech* **1829,** 1026–1033.

Khamzina L, Veilleux A, Bergeron S & Marette A (2005). Increased Activation of the Mammalian Target of Rapamycin Pathway in Liver and Skeletal Muscle of Obese Rats: Possible Involvement in Obesity-Linked Insulin Resistance. *Endocrinology* **146,** 1473–1481.

Kim J, Montagnani M, Koh KK & Quon MJ (2006). Reciprocal relationships between insulin resistance and endothelial dysfunction: molecular and pathophysiological mechanisms. *Circulation* **113,** 1888–1904.

Koeppen, Bruce M, Stanton & Bruce A (2018). *Berne and Levy Physiology*.

Köhler R, Wulff H, Eichler I, Kneifel M, Neumann D, Knorr A, Grgic I, Kämpfe D, Si H, Wibawa J, Real R, Borner K, Brakemeier S, Orzechowski HD, Reusch HP, Paul M, Chandy KG &

Hoyer J (2003). Blockade of the intermediate-conductance calcium-activated potassium channel as a new therapeutic strategy for restenosis. *Circulation* **108,** 1119–1125.

Kotecha SA & Schlichter LC (1999). A Kv1.5 to Kv1.3 Switch in Endogenous Hippocampal Microglia and a Role in Proliferation. *J Neurosci* **19,** 10680 LP – 10693.

Krauss G (2014). *Biochemistry of Signal Transduction and Regulation*. Available at: www.ebook3000.com.

Kuhnert F, Mancuso MR, Hampton J, Stankunas K, Asano T, Chen C-Z & Kuo CJ (2008). Attribution of vascular phenotypes of the murine Egfl7 locus tothe microRNA miR-126. *Development* **135,** 3989–3993.

Kumar A & Lindner V (1997). Remodeling With Neointima Formation in the Mouse Carotid Artery After Cessation of Blood Flow. *Arterioscler Thromb Vasc Biol* **17,** 2238–2244.

Ledoux J, Werner ME, Brayden JE & Nelson MT (2006). Calcium-Activated Potassium Channels and the Regulation of Vascular Tone. *Physiology* **21,** 69–78.

Levick JR (2013). *An Introduction to Cardiovascular Physiology*. Elsevier Science. Available at: https://books.google.es/books?id=nL_dAgAAQBAJ.

Liang CC, Park AY & Guan JL (2007). In vitro scratch assay: A convenient and inexpensive method for analysis of cell migration in vitro. *Nat Protoc* **2,** 329–333.

Lindner V, Fingerle J & Reidy MA (1993). Mouse model of arterial injury. *Circ Res* **73,** 792–796.

Liu R, Chen B, Chen J & Lan J (2018). Leptin upregulates smooth muscle cell expression of MMP-9 to promote plaque destabilization by activating AP-1 via the leptin receptor/MAPK/ERK signaling pathways. *Exp Ther Med* **16,** 5327–5333.

Livak KJ & Schmittgen TD (2001). Analysis of Relative Gene Expression Data Using Real-Time Quantitative PCR and the 2−ΔΔCT Method. *Methods* **25,** 402–408.

Lopes J, Adiguzel E, Gu S, Liu S-L, Hou G, Heximer S, Assoian RK & Bendeck MP (2013). Type VIII Collagen Mediates Vessel Wall Remodeling after Arterial Injury and Fibrous Cap Formation in Atherosclerosis. *Am J Pathol* **182,** 2241–2253.

López-López JR, Cidad P & Pérez-García MT (2018). Kv channels and vascular smooth muscle cell proliferation. *Microcirculation*; DOI: 10.1111/micc.12427.

Lüscher TF, Steffel J, Eberli FR, Joner M, Nakazawa G, Tanner FC & Virmani R (2007). Drug-eluting stent and coronary thrombosis: biological mechanisms and clinical implications. *Circulation* **115,** 1051–1058.

Lyu Q, Dhagia V, Han Y, Guo B, Wines-Samuelson ME, Christie, K. C, Yin Q, Slivano OJ, Herring P, Long X, Gupte SA & Miano JM (2019). 乳鼠心肌提取 HHS Public Access. *Physiol Behav* **176,** 139–148.

MacK CP (2011). Signaling mechanisms that regulate smooth muscle cell differentiation. *Arterioscler Thromb Vasc Biol* **31,** 1495–1505.

Malo D, Schlager G, Tremblay J & Hamet P (1989). Thermosensitivity, a possible new locus involved in genetic hypertension. *Hypertension* **14,** 121–128.

Mann MJ, Whittemore AD, Donaldson MC, Belkin M, Conte MS, Polak JF, Orav EJ, Ehsan A, Dell'Acqua G & Dzau VJ (1999). Ex-vivo gene therapy of human vascular bypass grafts with E2F decoy: the PREVENT single-centre, randomised, controlled trial. *Lancet* **354,** 1493–1498.

Matsushita T, Elliger S, Elliger C, Podsakoff G, Villarreal L, Kurtzman GJ & Iwaki Y (1998). Adeno-associated virus vectors can be efficiently produced without helper virus. 938–945.

McCloskey C, Jones S, Amisten S, Snowden RT, Kaczmarek LK, Erlinge D, Goodall AH, Forsythe ID & Mahaut-Smith MP (2010). Kv1.3 is the exclusive voltage-gated K+ channel of platelets and megakaryocytes: Roles in membrane potential, Ca2+ signalling and platelet count. *J Physiol* **588,** 1399–1406.

McGuire JJ, Van Vliet BN, Giménez J, King JC & Halfyard SJ (2007). Persistence of PAR-2 vasodilation despite endothelial dysfunction in BPH/2 hypertensive mice. *Pflugers Arch Eur J Physiol* **454,** 535–543.

Mehta D, Angelini GD & Bryan AL a. J (1996). Experimental models of accelerated atherosclerosis syndromes. *Int J Cardiol* **56,** 235–257.

Miano JM (2003). Serum response factor: toggling between disparate programs of gene expression. *J Mol Cell Cardiol* **35,** 577–593.

Miano JM, Long X & Fujiwara K (2007). Serum response factor: Master regulator of the actin cytoskeleton and contractile apparatus. *Am J Physiol - Cell Physiol* **292,** 70–81.

Miguel-Velado E, Moreno-Domínguez A, Colinas O, Cidad P, Heras M, Pérez-García MT & López-López JR (2005). Contribution of Kv channels to phenotypic remodeling of human uterine artery smooth muscle cells. *Circ Res*; DOI: 10.1161/01.RES.0000194322.91255.13.

Mohrman DE & Heller LJ (2006). *Cardiovascular Physiology 8/E*. McGraw-Hill Education. Available at: https://books.google.es/books?id=hbEJAgAAQBAJ.

Morla AO & Mogford JE (2000). Control of Smooth Muscle Cell Proliferation and Phenotype by Integrin Signaling through Focal Adhesion Kinase. *Biochem Biophys Res Commun* **272,** 298–302.

Murphy GJ & Angelini GD (2004). Side Effects of Cardiopulmonary Bypass: *J Card Surg* **19,** 481–488.

Nelson MT & Quayle JM (1995). Physiological roles and properties of potassium channels in arterial smooth muscle. *Am J Physiol Physiol* **268,** C799–C822.

Neylon CB (2002). Potassium channels and vascular proliferation. *Vascul Pharmacol* **38,** 35–41.

Noble A (2005). *The Cardiovascular System*. Elsevier Churchill Livingstone. Available at: https://books.google.es/books?id=AchqAAAAMAAJ.

O'Brien KD, Allen MD, McDonald TO, Chait A, Harlan JM, Fishbein D, McCarty J, Ferguson M, Hudkins K & Benjamin CD (1993). Vascular cell adhesion molecule-1 is expressed in human coronary atherosclerotic plaques. Implications for the mode of progression of advanced coronary atherosclerosis. *J Clin Invest* **92,** 945–951.

O'brien PD, Sakowski SA & Feldman EL (2014). Mouse models of diabetic neuropathy. *ILAR J* **54,** 259–272.

O'Shea PM, Griffin TP & Fitzgibbon M (2017). Hypertension: The role of biochemistry in the diagnosis and management. *Clin Chim Acta* **465,** 131–143.

References

O'Sullivan M, Scott SD, McCarthy N, Figg N, Shapiro LM, Kirkpatrick P & Bennett MR (2003). Differential cyclin E expression in human in-stent stenosis smooth muscle cells identifies targets for selective anti-restenosis therapy. *Cardiovasc Res* **60,** 673–683.

Olivieri F, Spazzafumo L, Bonafè M, Recchioni R, Prattichizzo F, Marcheselli F, Micolucci L, Mensà E, Giuliani A, Santini G, Gobbi M, Lazzarini R, Boemi M, Testa R, Antonicelli R, Procopio AD & Bonfigli AR (2015). MiR-21-5p and miR-126a-3p levels in plasma and circulating angiogenic cells: relationship with type 2 diabetes complications. *Oncotarget* **6,** 35372–35382.

Onuki Y, Bhardwaj U, Papadimitrakopoulos F & Burgess DJ (2008). A Review of the Biocompatibility of Implantable Devices: Current Challenges to Overcome Foreign Body Response. *J Diabetes Sci Technol* **2,** 1003–1015.

Owens GK (2007). Molecular control of vascular smooth muscle cell differentiation and phenotypic plasticity. *Novartis Found Symp* **283,** 173-174,238-241.

Owens GK, Kumar MS & Wamhoff BR (2004). Molecular regulation of vascular smooth muscle cell differentiation in development and disease. *Physiol Rev* **84,** 767–801.

Pannasch U, Färber K, Nolte C, Blonski M, Yan Chiu S, Messing A & Kettenmann H (2006). The potassium channels Kv1.5 and Kv1.3 modulate distinct functions of microglia. *Mol Cell Neurosci* **33,** 401–411.

Pearson G, Robinson F, Beers Gibson T, Xu BE, Karandikar M, Berman K & Cobb MH (2001). Mitogen-activated protein (MAP) kinase pathways: regulation and physiological functions. *Endocr Rev* **22,** 153–183.

Pérez-García MT, Cidad P & López-López JR (2018). The secret life of ion channels: Kv1.3 potassium channels and proliferation. *Am J Physiol - Cell Physiol* **314,** C27–C40.

Plane F, Johnson R, Kerr P, Wiehler W, Thorneloe K, Ishii K, Chen T & Cole W (2005). Heteromultimeric Kv1 channels contribute to myogenic control of arterial diameter. *Circ Res* **96,** 216–224.

Plenz GAM, Deng MC, Robenek H & Völker W (2003). Vascular collagens: spotlight on the role of type VIII collagen in atherogenesis. *Atherosclerosis* **166,** 1–11.

Plumb DC (2008). *Veterinary Drug Handbook Sixth Edition*, sixth edit.

Po S, Roberds S, Snyders DJ, Tamkun MM & Bennett PB (1993). Heteromultimeric assembly of human potassium channels: Molecular basis of a transient outward current? *Circ Res* **72,** 1326–1336.

Prattichizzo F, Giuliani A, De Nigris V, Pujadas G, Ceka A, La Sala L, Genovese S, Testa R, Procopio AD, Olivieri F & Ceriello A (2016). Extracellular microRNAs and endothelial hyperglycaemic memory: a therapeutic opportunity? *Diabetes, Obes Metab* **18,** 855–867.

Reaven PD, Emanuele N V., Wiitala WL, Bahn GD, Reda DJ, McCarren M, Duckworth WC & Hayward RA (2019). Intensive glucose control in patients with type 2 diabetes - 15-year follow-up. *N Engl J Med* **380,** 2215–2224.

Reddy MA, Das S, Zhuo C, Jin W, Wang M, Lanting L & Natarajan R (2016). Regulation of vascular smooth muscle cell dysfunction under diabetic conditions by MIR-504. *Arterioscler Thromb Vasc Biol* **36,** 864–873.

Roque M, Fallon JT, Badimon JJ, Zhang WX, Taubman MB & Reis ED (2000). Mouse model of femoral artery denudation injury associated with the rapid accumulation of adhesion molecules on the luminal surface and recruitment of neutrophils. *Arterioscler Thromb Vasc Biol*; DOI: 10.1161/01.ATV.20.2.335.

Ross MH & Pawlina W (2007). *Histologia: Texto Y Atlas*. Médica Panamericana. Available at: https://books.google.es/books?id=NxYmIRZQi2oC.

Rovner AS, Murphy RA & Owens GK (1986). Expression of smooth muscle and nonmuscle myosin heavy chains in cultured vascular smooth muscle cells. *J Biol Chem* **261,** 14740–14745.

Sandu O a, Ragolia L & Begum N (2000). Diabetes in the Goto-Kakizaki Rat Is Accompanied Muscle Cell Relaxation. *Diabetes*.

Sanjana NE, Shalem O & Zhang F (2014). Improved vectors and genome-wide libraries for CRISPR screening iPipet : sample handling using a tablet. *Nat Publ Gr* **11,** 783–784.

Saxton RA & Sabatini DM (2017). mTOR Signaling in Growth, Metabolism, and Disease. *Cell* **168,** 960–976.

Schlager G (1981). Longevity in spontaneously hypertensive mice. *Exp Gerontol* **16,** 325–330.

Schlager G, Freeman R & Sustarsic SS (1979). Brain catecholamines and organ weight of mice genetically selected for high and low blood pressure. *Experientia* **35,** 67–69.

Schlager G & Sides J (1997). Characterization of hypertensive and hypotensive inbred strains of mice. *Lab Anim Sci* **47,** 288–292.

Schmauss D & Weis M (2008). Cardiac allograft vasculopathy: recent developments. *Circulation* **117,** 2131–2141.

Schmitz A, Sankaranarayanan A, Azam P, Schmidt-Lassen K, Homerick D, Ansel W & Wulff H (2005). Design of PAP-1, a Selective Small Molecule Kv1.3 Blocker, for the Suppression of Effector Memory T Cells in Autoimmune Diseases. *Mol Pharmacol*1254–1270.

Sibinga NE, Foster LC, Hsieh CM, Perrella MA, Lee WS, Endege WO, Sage EH, Lee ME & Haber E (1997). Collagen VIII is expressed by vascular smooth muscle cells in response to vascular injury. *Circ Res* **80,** 532–541.

Siegel G, Walter A, Schnalke F, Schmidt A, Buddecke E, Loirand G & Stock G (1991). Potassium channel activation, hyperpolarization, and vascular relaxation. *Z Kardiol* **80 Suppl 7,** 9–24.

Skinner BM & Johnson EEP (2017). Nuclear morphologies: their diversity and functional relevance. *Chromosoma* **126,** 195–212.

Skyler JS, Bergenstal R, Bonow RO, Buse J, Deedwania P, Gale EAM, Howard B V, Kirkman MS, Kosiborod M, Reaven P, Sherwin RS, American Diabetes Association, American College of Cardiology Foundation & American Heart Association (2009). Intensive glycemic control and the prevention of cardiovascular events: implications of the ACCORD, ADVANCE, and VA diabetes trials: a position statement of the American Diabetes Association and a scientific statement of the American College of Cardiology Foundation and the American Heart Association. *Circulation* **119,** 351–357.

Sobko A, Peretz A, Shirihai O, Etkin S, Cherepanova V, Dagan D & Attali B (1998). Heteromultimeric Delayed-Rectifier K&lt;sup&gt;+&lt;/sup&gt; Channels in Schwann Cells: Developmental Expression and Role in Cell Proliferation. *J Neurosci* **18,** 10398

LP – 10408.

Solanes N, Rigol M, Castellà M, Khabiri E, Ramírez J, Segalés J, Roqué M, Agustí E, Pérez-Villa F, Roig E, Pomar JL, Sanz G & Heras M (2004). Cryopreservation alters antigenicity of allografts in a porcine model of transplant vasculopathy. *Transplant Proc* **36,** 3288–3294.

Solanes N, Rigol M, Ramírez J, Segalés J, Roqué M, Marimon JM, Pérez-Villa F, Roig E, Sanz G & Heras M (2005). *Histological Basis of the Porcine Femoral Artery for Vascular Research*. Available at: www.blackwell-synergy.com.

Somlyo AP & Avril B (1994). Signal transduction and regulation in smooth muscle. *Nature* **372,** 231–236.

Somlyo AP & Somlyo A V. (2003). Ca2+ sensitivity of smooth muscle and nonmuscle myosin II: Modulated by G proteins, kinases, and myosin phosphatase. *Physiol Rev* **83,** 1325–1358.

Stefanini GG & Holmes DR (2013). Drug-eluting coronary-artery stents. *N Engl J Med* **368,** 254–265.

Talasila A, Yu H, Ackers-Johnson M, Bot M, van Berkel T, Bennett MR, Bot I & Sinha S (2013). Myocardin regulates vascular response to injury through miR-24/-29a and platelet-derived growth factor receptor-β. *Arterioscler Thromb Vasc Biol* **33,** 2355–2365.

Testa R, Bonfigli AR, Prattichizzo F, La Sala L, De Nigris V & Ceriello A (2017). The “Metabolic Memory” Theory and the Early Treatment of Hyperglycemia in Prevention of Diabetic Complications. *Nutrients*; DOI: 10.3390/nu9050437.

Thiriet M (2013). *Tissue Functioning and Remodeling in the Circulatory and Ventilatory Systems*. Springer New York, New York, NY. Available at: http://link.springer.com/10.1007/978-1-4614-5966-8.

Togliatto G, Dentelli P, Rosso A, Lombardo G, Gili M, Gallo S, Gai C, Solini A, Camussi G & Brizzi MF (2018). PDGF-BB carried by endothelial Cell-derived extracellular vesicles reduces vascular smooth muscle cell apoptosis in diabetes. *Diabetes* **67,** 704–716.

Torella D, Iaconetti C, Tarallo R, Marino F, Giurato G, Veneziano C, Aquila I, Scalise M, Mancuso T, Cianflone E, Valeriano C, Marotta P, Tammè L, Vicinanza C, Sasso FC, Cozzolino D, Torella M, Weisz A & Indolfi C (2018). MiRNA regulation of the hyperproliferative phenotype of vascular smooth muscle cells in diabetes. *Diabetes* **67,** 2554–2568.

Tykocki NR, Boerman EM & Jackson WF (2017). Smooth muscle ion channels and regulation of vascular tone in resistance arteries and arterioles. *Compr Physiol* **7,** 485–581.

Upadhyay SK, Eckel-Mahan KL, Mirbolooki MR, Tjong I, Griffey SM, Schmunk G, Koehne A, Halbout B, Iadonato S, Pedersen B, Borrelli E, Wang PH, Mukherjee J, Sassone-Corsi P & Chandy KG (2013). Selective Kv1.3 channel blocker as therapeutic for obesity and insulin resistance. *Proc Natl Acad Sci U S A*; DOI: 10.1073/pnas.1221206110.

Vautier F, Belachew S, Chittajallu R & Gallo V (2004). Shaker-type potassium channel subunits differentially control oligodendrocyte progenitor proliferation. *Glia* **48,** 337–345.

Venkat P, Cui C, Chopp M, Zacharek A, Wang F, Landschoot-Ward J, Shen Y & Chen J (2019). MiR-126 mediates brain endothelial cell exosome treatment–induced neurorestorative effects after stroke in type 2 diabetes mellitus mice. *Stroke* **50,** 2865–2874.

Vicente R, Escalada A, Coma M, Fuster G, Sánchez-Tilló E, López-Iglesias C, Soler C, Solsona C, Celada A & Felipe A (2003). Differential Voltage-dependent K+ Channel Responses during Proliferation and Activation in Macrophages. *J Biol Chem* **278,** 46307–46320.

Villa-Pérez P, Cueto M, Díaz-Marrero A, Lobatón C, Moreno A, Perdomo G & Cózar-Castellano I (2017). Leptolide Improves Insulin Resistance in Diet-Induced Obese Mice. *Mar Drugs*; DOI: 10.3390/md15090289.

Vinué Á & González-navarro H (2015). Chapter 17 Glucose and Insulin Tolerance Tests in the Mouse. **1339,** 247–254.

Vlodaver Z, Wilson RF & Garry DJ (2012). *Coronary Heart Disease: Clinical, Pathological, Imaging, and Molecular Profiles*. Springer US. Available at: https://books.google.es/books?id=xQn3CLFv0Q8C.

Wagenseil JE & Mecham RP (2009). Vascular Extracellular Matrix and Arterial Mechanics. *Physiol Rev* **89,** 957–989.

Wallner M, Meera P & Toro L (1996). Determinant for β-subunit regulation in high-conductance voltage-activated and Ca2+-sensitive K+ channels: An additional transmembrane region at the N terminus. *Proc Natl Acad Sci* **93,** 14922–14927.

Wamhoff BR, Bowles DK & Owens GK (2006). Excitation-transcription coupling in arterial smooth muscle. *Circ Res* **98,** 868–878.

Wang D-Z, Chang PS, Wang Z, Sutherland L, Richardson JA, Small E, Krieg PA & Olson EN (2001). *Activation of Cardiac Gene Expression by Myocardin, a Transcriptional Cofactor for Serum Response Factor*.

Wang S, Aurora AB, Johnson BA, Qi X, McAnally J, Hill JA, Richardson JA, Bassel-Duby R & Olson EN (2008). The Endothelial-Specific MicroRNA miR-126 Governs Vascular Integrity and Angiogenesis. *Dev Cell* **15,** 261–271.

Wang Z, Wang D-Z, Pipes GCT & Olson EN (2003). Myocardin is a master regulator of smooth muscle gene expression. *Proc Natl Acad Sci* **100,** 7129–7134.

Wickenden AD (2002). K+ channels as therapeutic drug targets. *Pharmacol Ther* **94,** 157–182.

Wise SG & Weiss AS (2009). Tropoelastin. *Int J Biochem Cell Biol* **41,** 494–497.

Wong CY, Rothuizen TC, de Vries MR, Rabelink TJ, Hamming JF, van Zonneveld AJ, Quax PHA & Rotmans JI (2015). Elastin is a Key Regulator of Outward Remodeling in Arteriovenous Fistulas. *Eur J Vasc Endovasc Surg* **49,** 480–486.

Yeadon J (2015). choosing-among-type-ii-diabetes-mouse-models @ www.jax.org. Available at: https://www.jax.org/news-and-insights/jax-blog/2015/july/choosing-among-type-ii-diabetes-mouse-models#.

Zampetaki A, Kiechl S, Drozdov I, Willeit P, Mayr U, Prokopi M, Mayr A, Weger S, Oberhollenzer F, Bonora E, Shah A, Willeit J & Mayr M (2010). Plasma MicroRNA profiling reveals loss of endothelial MiR-126 and other MicroRNAs in type 2 diabetes. *Circ Res* **107,** 810–817.

Zhang MJ, Zhou Y, Chen L, Wang YQ, Wang X, Pi Y, Gao CY, Li JC & Zhang LL (2016). An overview of potential molecular mechanisms involved in VSMC phenotypic modulation. *Histochem Cell Biol* **145,** 119–130.

Zhou J, Li YS, Nguyen P, Wang KC, Weiss A, Kuo YC, Chiu JJ, Shyy JY & Chien S (2013). Regulation of vascular smooth muscle cell turnover by endothelial cell-secreted microRNA-126 role of shear stress. *Circ Res* **113,** 40–51.

Zimin PI, Garic B, Wulff H & Zhorov BS (2009). Mapping the Binding Site of the Alkoxypsoralen PAP-1 in the Voltage-Gated K+ Channel Kv1.3. *Biophys J* **96,** 176a.

Zoncu R, Efeyan A & Sabatini DM (2011). MTOR: From growth signal integration to cancer, diabetes and ageing. *Nat Rev Mol Cell Biol* **12,** 21–35.

Resumen

Introducción

Las células de músculo liso vascular (VSMCs) en su estado maduro presentan un fenotipo diferenciado o contráctil cuya principal función es la contracción para regular el diámetro de los vasos y por tanto el flujo sanguíneo a los distintos tejidos. Sin embargos, estas células conservan su plasticidad y capacidad de cambiar su fenotipo a uno desdiferenciado o proliferativo en un proceso que se conoce como modulación fenotípica (PM). Este proceso implica cambios coordinados en el patrón de expresión génico de las VSMCs.

Estudios previos de nuestro laboratorio, asociaron la PM con cambios en la expresión de los canales de potasio dependientes de voltaje, Kv1.3 y Kv1.5. El canal Kv1.5 es el canal de la familia Kv1 más abundante en las VSMCs con fenotipo contráctil; mientras que el Kv1.3 es el más expresado en el fenotipo desdiferenciado. Estos trabajos demostraron que la expresión funcional de Kv1.3 contribuye a la PM, ya que el bloqueo del canal inhibe la migración y proliferación celular. Además, encontramos que el aumento de la actividad de Kv1.3 durante la PM es consecuencia de la disminución de la expresión de Kv1.5, por lo que se estableció que los cambios en el ratio Kv1.3/Kv1.5 permitían definir el fenotipo de las VSMCs.

La PM es un proceso necesario en situaciones fisiológicas como angiogénesis o reparación de lesiones, sin embargo, determinados factores (físicos, mecánicos, inmunológicos o inflamatorios) pueden desencadenar una respuesta patológica que se manifiesta con una reducción de la luz del vaso como sucede durante la hiperplasia de la íntima (IH). La IH es el engrosamiento de la de túnica íntima del vaso como consecuencia de los mecanismos de reparación vascular en los que participan la migración y proliferación de las VSMCs. La hiperplasia de la íntima es una complicación frecuente de las cirugías vasculares como bypass coronario, trasplantes de órganos y angioplastia, ya que puede llegar a generar oclusión de los vasos y es la causa principal del fracaso de estas cirugías. Esta patología se ve agravada en pacientes con factores de riesgo adicionales como la diabetes. Los pacientes diabéticos presentan mayor prevalencia de enfermedad vascular, una mayor respuesta oclusiva después de las cirugías vasculares y por tanto un peor pronóstico en estas intervenciones.

Objetivo

El objetivo de este trabajo es explorar la eficacia del bloqueo del Kv1.3 para prevenir la hiperplasia de la íntima en vasos sanguíneos humanos y los mecánicos que vinculan el cambio del ratio Kv1.3/Kv1.5 con la modulación fenotípica. Además, exploramos si el aumento de remodelado vascular que se observa en diabetes se asocia con el aumento de expresión del Kv1.3 para determinar si el uso de bloqueantes del Kv1.3 pueden mejorar el pronóstico de cirugías vasculares en estos grupos de pacientes con más riesgo.

Material y Métodos

Para abordar los objetivos de esta Tesis se han utilizado distintas preparaciones de estudio que incluyen modelos humanos *in-vitro* como el cultivo de órgano y el cultivo primario de VSMCs y modelos de ratón *in-vivo.* Para caracterizar estos modelos y sus respuestas se han empleado técnicas de biología celular, funcional y molecular.

Los modelos *in-vitro* humanos se llevan a cabo con muestras de arterias mamarias humanas (hMA), vena safena humana (hSV) y arteria renal humanas (hRA) pertenecientes a la colección COLMAH (COLección de Muestras Arteriales Humanas). Las muestras de vasos humanos fueron obtenidas de pacientes sometidos a cirugía de bypass coronario (para las hMA y hSV) o nefrectomía (hRA) junto con el correspondiente consentimiento informado de cada paciente. Las muestras vasculares se emplearon para realizar cultivo de órgano, para obtener cultivo primario de VSMCs y para llevar a cabo estudios de expresión génica y proteica.

El cultivo de órgano se utilizó para estudiar el remodelado vascular. Los anillos vasculares se incubaron durante 2 semanas en cultivo y se estudiaron los efectos del bloqueo del canal Kv1.3 (con PAP-1 o Margatoxina), de la sobreexpresión del canal Kv1.5, y del *knock-down* de la miocardina (cofactor de transcripción regulador del fenotipo contráctil) sobre la hiperplasia de la íntima. Además, el cultivo primario de las VSMCs se utilizó para explorar los efectos de estos tratamientos sobre los procesos de migración y proliferación celular.

Se generó un modelo de animal con de factores de riesgo vascular administrando una dieta alta en grasa a ratones hipertensos

(BPH/HFD). Los animales además de hipertensión presentaban, obesidad, intolerancia a la glucosa y resistencia a la insulina. La ligadura de carótida se realizó para generar un modelo *in-vivo* de hiperplasia de la íntima en animales control (BPH) y animales con riesgo de enfermedad vascular(BPH/HFD). En este modelo se estudió el efecto del bloqueo del canal Kv1.3 sobre la hiperplasia de la íntima inducida por la lesión.

La hiperplasia de la íntima tanto en vasos humanos como de ratón se exploró mediante análisis histomorfométrico de cortes de anillos vasculares teñidos con la tinción tricrómica de Masson. La caracterización de los cambios de expresión asociados al cambio fenotípico y a los factores de riesgo vascular se llevó a cabo mediante estudios de expresión a nivel de proteína mediante *western blot*, inmunohistoquímica e inmunocitoquímca y a nivel de mRNA y de microRNA mediante *qPCR*.

Resultados

Los resultados obtenidos en la caracterización del modelo humano de hiperplasia de la íntima mostraron que el bloqueo farmacológico del canal Kv1.3 redujo la IH inducido por 20% FBS en vasos sanguíneos humanos en cultivo de órgano mediante la inhibición de la proliferación, la migración y la secreción de matriz extracelular. Los efectos de los bloqueantes del Kv1.3 se reprodujeron con la sobreexpresión del canal Kv1.5 y estos efectos no fueron aditivos. El *knock-down* de la miocardina en esta preparación redujo la expresión de KV1.5 e indujo la hiperplasia de la íntima mientras que la sobrexpresión de Kv1.5 inhibió la IH sin afectar la expresión de miocardina. Además, la sobrexpresión de miocardina aumentó la expresión de Kv1.5 en VSMCs.

Cuando se agruparon y analizaron las muestras vasculares según su origen, pacientes diabéticos o no diabéticos, se encontró que la IH en respuesta a 20% FBS fue mayor en las muestras de diabéticos en cultivo de órgano, que la expresión del canal Kv1.3 era también mayor en estos vasos y consecuentemente el bloqueante PAP-1 fue más eficiente previniendo la IH en vasos diabéticos. También encontramos que la proliferación y la migración fue mayor en células en cultivo procedentes de diabéticos. El hecho de que las diferencias entre los cultivos de células procedentes de diabéticos y no diabéticos se persistieran en el tiempo, a pesar de haber estado en las mismas condiciones de cultivo durante varios meses, se atribuyó a la memoria metabólica.

Para explorar posibles mecanismos epigenéticos responsables de la memoria metabólica de las VSMCs de diabéticos, estudiamos los cambios de expresión de microRNAs asociados a enfermedades vasculares utilizando *qPCR arrays*. Centramos nuestro estudio en el miR126 que aumentó su expresión en VSMCs diabéticas con fenotipo proliferativo. La sobreexpresión de mir126 en VSMCs no diabéticas aumentó la migración y proliferación celular pero no tenía ningún efecto sobre las VSMCs diabéticas.

Finalmente, en nuestro modelo de ratón con factores de riesgo vascular (BPH/HFD) encontramos un mayor remodelado vascular y una mayor expresión del canal Kv1.3 en la arteria carótida en comparación con los ratones BPH con dieta estándar (controles). Además, tras la cirugía de ligadura de carótida los BPH/HFD desarrollan más hiperplasia de la íntima que sus controles. El bloqueo de canal Kv1.3 resultó más eficaz para reducir la IH tras la ligadura de las carótidas en vasos enfermos. Además, encontramos que el bloqueo del canal Kv1.3 tiene otros efectos beneficiosos sobre el animal como la disminución de la ganancia de peso y el aumento de la sensibilidad a la insulina en los ratones BPH/HFD.

Conclusiones

Las enfermedades cardiovasculares representan la causa número uno de muerte a nivel mundial según la Organización Mundial de la Salud (WHO). El desarrollo de cirugías como bypass coronario y angioplastias representan una mejora para los pacientes con enfermedades vasculares, pero una limitación de estas cirugías es el desarrollo de hiperplasia de la íntima en los vasos tratados, debido a la activación exacerbada de mecanismos de reparación. En la actualidad existen tratamientos para evitar este problema, pero los tratamientos no son específicos de las VSMCs e impiden la correcta reendotelización y reparación de la capa íntima del vaso. Por esta razón, aquí proponemos una nueva diana terapéutica más específica y eficaz en la prevención del remodelado vascular, el canal Kv1.3.

Los resultados de este trabajo demostraron que el bloqueo del canal Kv1.3 reduce el remodelado vascular y la hiperplasia de la íntima en vasos humanos en cultivo de órgano. Los datos mostraron que el bloqueo del canal previene el remodelado vascular al disminuir la proliferación, migración y secreción de matriz extracelular de las VSMCs.

Los resultados de expresión mostraron que el aumento de contribución funcional de Kv1.3 a la modulación fenotípica es consecuencia de la disminución de la expresión de Kv1.5. Observamos que la expresión del canal Kv1.5 está regulada por miocardina, la expresión de KV1.5 disminuyó con el *knock-down* de miocardina y aumentó con la sobreexpresión de miocardina. Estos resultados permiten considerar al canal Kv1.5 como un nuevo marcador de fenotipo contráctil de las VSMCs, ya que la miocardina es un conocido cofactor de transcripción regulador de la expresión de los genes contráctiles en músculo liso. Por otro lado, observamos que la sobreexpresión del canal Kv1.5 inhibió el remodelado vascular al ocluir la actividad del canal Kv1.3. Este trabajo propone que la disminución de la expresión del canal Kv1.5 deja en libertad al canal Kv1.3 para ejercer su función en las VSMCs con fenotipo desdiferenciado.

Nuestros datos muestran también que el canal Kv1.3 se expresa más en vasos de pacientes diabéticos y el bloqueo del canal reduce de forma más eficiente la hiperplasia de la íntima en cultivo de órgano de vasos de pacientes diabéticos. La proliferación y migración es mayor en VSMCs de diabéticos indicando que conservan memoria metabólica y cambios epigenéticos asociados a la exposición a hiperglicemia. Entre los posibles cambios epigenéticos, encontramos que la diabetes induce cambios en el perfil de expresión de los miRNA. Nuestros resultados destacan los cambios en la expresión de miR-126 que está aumentada en el fenotipo proliferativo de VSMCs de pacientes diabéticos.

Finalmente, en este trabajo hemos generado un modelo de ratón que presenta a nivel vascular características similares a los vasos de humanos diabéticos, ratones BPH sometidos a una dieta alta en grasa (HFD). Encontramos que los vasos del modelo BPH/HFD presentan un mayor remodelado vascular, la expresión del Kv1.3 es mayor y tras la ligadura de la carótida, desarrolla más hiperplasia de la íntima que sus controles (BPH con dieta estándar). El bloqueo de Kv1.3 mostró mayor eficacia en la prevención de la hiperplasia de la íntima en los vasos enfermos y además mejoró otros factores de riesgo metabólico del modelo BPH/HFD.

Nuestros datos en conjunto señalan al canal KV1.3 como una nueva y prometedora diana terapéutica para prevenir el remodelado vascular tras cirugía vascular, especialmente en vasos enfermos.

Annex

Table I. miRNA qPCR array data of VSMCs from hMA tissue.

						comparing to non-T2DM	
Well	Mature ID	average Ct		$2^{-\Delta CT}$		T2DM	T2DM
		non-T2DM	T2DM	non-T2DM	T2DM	Fold Change	Fold Regulation
A01	hsa-let-7a-5p	18.75	19.23	29.06	20.57	0.71	-1.41
A02	hsa-let-7b-5p	20.39	20.45	9.37	8.83	0.94	-1.06
A03	hsa-let-7c-5p	21.29	21.53	5.01	4.18	0.83	-1.20
A04	hsa-let-7d-5p	21.41	21.8	4.61	3.46	0.75	-1.33
A05	hsa-let-7e-5p	20.05	20.09	11.84	11.29	0.95	-1.05
A06	hsa-let-7f-5p	19.37	20.07	18.93	11.50	0.61	-1.65
A07	hsa-miR-1-3p	22.18	23.43	2.70	1.12	0.41	-2.41
A08	hsa-miR-100-5p	20.11	21.01	11.36	5.97	0.53	-1.90
A09	hsa-miR-103a-3p	22.02	23.55	3.01	1.03	0.34	-2.92
A10	hsa-miR-107	26.66	28.11	0.12	0.04	0.36	-2.79
A11	hsa-miR-10b-5p	24.68	25.79	0.48	0.22	0.46	-2.19
A12	hsa-miR-122-5p	34.56	33.54	0.00	0.00	1.99	1.99
B01	hsa-miR-124-3p	31.75	31.49	0.00	0.00	1.18	1.18
B02	hsa-miR-125a-5p	18.57	18.83	32.90	27.15	0.83	-1.21
B03	hsa-miR-125b-5p	17.51	18.7	68.64	29.75	0.43	-2.31
B04	hsa-miR-126-3p	24.03	26.88	0.75	0.10	0.14	-7.31
B05	hsa-miR-130a-3p	22.71	24.2	1.88	0.66	0.35	-2.86
B06	hsa-miR-133a-3p	27.4	29.07	0.07	0.02	0.31	-3.23
B07	hsa-miR-133b	27.37	28.68	0.07	0.03	0.40	-2.53
B08	hsa-miR-140-5p	21.3	22.71	4.96	1.84	0.37	-2.70
B09	hsa-miR-142-3p	30.76	32.48	0.01	0.00	0.30	-3.36
B10	hsa-miR-143-3p	17.19	19.2	85.61	20.99	0.25	-4.08
B11	hsa-miR-144-3p	32.02	35	0.00	0.00	0.12	-8.02
B12	hsa-miR-145-5p	16.31	17.5	158.39	68.29	0.43	-2.32
C01	hsa-miR-146a-5p	28.62	29.54	0.03	0.02	0.52	-1.92
C02	hsa-miR-149-5p	27.35	27.7	0.08	0.06	0.77	-1.30
C03	hsa-miR-150-5p	28.17	30.06	0.04	0.01	0.26	-3.78

C04	hsa-miR-155-5p	27.11	27.34	0.09	0.07	0.84	-1.19
C05	hsa-miR-15b-5p	23.57	23.73	1.03	0.91	0.88	-1.14
C06	hsa-miR-16-5p	20.37	21.91	9.46	3.21	0.34	-2.95
C07	hsa-miR-17-5p	23.84	25.53	0.85	0.26	0.30	-3.28
C08	hsa-miR-181a-5p	24.8	26.24	0.44	0.16	0.36	-2.77
C09	hsa-miR-181b-5p	23.79	24.94	0.88	0.39	0.44	-2.26
C10	hsa-miR-182-5p	32.97	33.6	0.00	0.00	0.64	-1.57
C11	hsa-miR-183-5p	33.06	32.91	0.00	0.00	1.09	1.09
C12	hsa-miR-185-5p	25.87	27.19	0.21	0.08	0.39	-2.54
D01	hsa-miR-18b-5p	26.87	27.09	0.10	0.09	0.85	-1.18
D02	hsa-miR-195-5p	19.55	20.92	16.78	6.38	0.38	-2.63
D03	hsa-miR-199a-5p	22.41	25.04	2.30	0.37	0.16	-6.31
D04	hsa-miR-206	25.38	27.04	0.29	0.09	0.31	-3.21
D05	hsa-miR-208a-3p	28.01	28.4	0.05	0.04	0.75	-1.33
D06	hsa-miR-208b-3p	35	35	0.00	0.00	0.98	-1.02
D07	hsa-miR-21-5p	19.59	20.29	16.32	9.86	0.60	-1.66
D08	hsa-miR-210-3p	29.29	29.88	0.02	0.01	0.65	-1.54
D09	hsa-miR-214-3p	22.18	23.31	2.71	1.22	0.45	-2.23
D10	hsa-miR-22-3p	21.68	23.49	3.82	1.07	0.28	-3.57
D11	hsa-miR-221-3p	22.91	23.8	1.63	0.87	0.53	-1.88
D12	hsa-miR-222-3p	22.83	23.63	1.72	0.98	0.57	-1.76
E01	hsa-miR-223-3p	25.74	25.88	0.23	0.20	0.89	-1.12
E02	hsa-miR-224-5p	26.19	26.78	0.17	0.11	0.65	-1.53
E03	hsa-miR-23a-3p	17.37	17.91	75.79	51.18	0.68	-1.48
E04	hsa-miR-23b-3p	17.92	18.31	51.78	38.75	0.75	-1.34
E05	hsa-miR-24-3p	18.42	19.65	36.73	15.40	0.42	-2.39
E06	hsa-miR-25-3p	23.31	24.02	1.23	0.75	0.60	-1.65
E07	hsa-miR-26a-5p	18.05	19.08	47.15	22.74	0.48	-2.07
E08	hsa-miR-26b-5p	18.85	20.07	27.08	11.51	0.43	-2.35
E09	hsa-miR-27a-3p	18.87	20.03	26.84	11.80	0.44	-2.27
E10	hsa-miR-27b-3p	19.1	20.03	22.92	11.77	0.51	-1.95
E11	hsa-miR-29a-3p	19.58	19.88	16.39	13.07	0.80	-1.25

E12	hsa-miR-29b-3p	22.31	23.96	2.47	0.77	0.31	-3.19
F01	hsa-miR-29c-3p	19.13	19.77	22.31	14.14	0.63	-1.58
F02	hsa-miR-302a-3p	33.99	34.31	0.00	0.00	0.79	-1.27
F03	hsa-miR-302b-3p	35	35	0.00	0.00	0.98	-1.02
F04	hsa-miR-30a-5p	20.58	21.59	8.19	4.01	0.49	-2.04
F05	hsa-miR-30c-5p	20.56	21.48	8.31	4.32	0.52	-1.92
F06	hsa-miR-30d-5p	21.64	22.64	3.93	1.93	0.49	-2.03
F07	hsa-miR-30e-5p	21.28	22.25	5.06	2.53	0.50	-2.00
F08	hsa-miR-31-5p	30.75	32.73	0.01	0.00	0.25	-4.02
F09	hsa-miR-320a	20.52	20.84	8.51	6.75	0.79	-1.26
F10	hsa-miR-328-3p	25.5	25.78	0.27	0.22	0.81	-1.23
F11	hsa-miR-342-3p	24.29	24.39	0.63	0.57	0.92	-1.09
F12	hsa-miR-365b-3p	21.04	21.66	5.95	3.82	0.64	-1.56
G01	hsa-miR-378a-3p	26.64	27.58	0.12	0.06	0.51	-1.95
G02	hsa-miR-423-3p	24.28	24.9	0.63	0.40	0.64	-1.57
G03	hsa-miR-424-5p	28.56	30.35	0.03	0.01	0.28	-3.51
G04	hsa-miR-451a	23.35	24.87	1.20	0.41	0.34	-2.93
G05	hsa-miR-486-5p	25	25.7	0.38	0.23	0.60	-1.66
G06	hsa-miR-494-3p	24.99	23.06	0.39	1.44	3.74	3.74
G07	hsa-miR-499a-5p	31.79	33.39	0.00	0.00	0.33	-3.07
G08	hsa-miR-7-5p	28.85	30.16	0.03	0.01	0.40	-2.53
G09	hsa-miR-92a-3p	21.39	21.73	4.68	3.64	0.78	-1.29
G10	hsa-miR-93-5p	24.05	25.05	0.74	0.36	0.49	-2.03
G11	hsa-miR-98-5p	24.73	25.64	0.46	0.24	0.52	-1.91
G12	hsa-miR-99a-5p	24.13	25.63	0.70	0.24	0.35	-2.88
H01	cel-miR-39-3p	35	35	0.00	0.00	0.98	-1.02
H02	cel-miR-39-3p	34.26	35	0.00	0.00	0.59	-1.70
H03	SNORD61	23.24	23.78	1.30	0.88	0.67	-1.48
H04	SNORD68	21.33	20.84	4.86	6.74	1.39	1.39
H05	SNORD72	29.9	29.5	0.01	0.02	1.31	1.31
H06	SNORD95	22.22	22.17	2.64	2.68	1.02	1.02
H07	SNORD96A	24.16	23.97	0.68	0.77	1.13	1.13

H08	RNU6-6P	20.83	21.3	6.87	4.90	0.71	-1.40
H09	miRTC	22.31	22.06	2.47	2.88	1.17	1.17
H10	miRTC	22.37	22.34	2.37	2.38	1.00	1.00
H11	PPC	19.88	19.8	13.27	13.81	1.04	1.04
H12	PPC	20.33	20.32	9.76	9.64	0.99	-1.01

Table 1. miRNA qPCR array data of VSMCs from cell culture.

Well	Mature ID	average Ct		$2^{-\Delta CT}$		comparing to non-T2DM	
						T2DM	T2DM
		non-T2DM	T2DM	non-T2DM	T2DM	Fold Change	Fold Regulation
A01	hsa-let-7a-5p	18.45	19.13	4.86	4.30	0.89	-1.13
A02	hsa-let-7b-5p	19.79	20.23	1.92	2.01	1.05	1.05
A03	hsa-let-7c-5p	21.99	22.35	0.42	0.46	1.10	1.10
A04	hsa-let-7d-5p	22.17	22.86	0.37	0.33	0.88	-1.14
A05	hsa-let-7e-5p	19.73	20.38	2.00	1.81	0.90	-1.11
A06	hsa-let-7f-5p	19.88	20.49	1.80	1.68	0.93	-1.07
A07	hsa-miR-1-3p	30.61	33.58	0.00	0.00	0.18	-5.54
A08	hsa-miR-100-5p	17.69	18.46	8.25	6.85	0.83	-1.20
A09	hsa-miR-103a-3p	21.01	21.55	0.82	0.80	0.97	-1.03
A10	hsa-miR-107	25.63	26.1	0.03	0.03	1.03	1.03
A11	hsa-miR-10b-5p	24.94	25.86	0.05	0.04	0.75	-1.33
A12	hsa-miR-122-5p	33.23	32.76	0.00	0.00	1.97	1.97
B01	hsa-miR-124-3p	28.93	30.33	0.00	0.00	0.54	-1.86
B02	hsa-miR-125a-5p	19.45	20.1	2.44	2.20	0.90	-1.11
B03	hsa-miR-125b-5p	17.04	17.85	12.89	10.42	0.81	-1.24
B04	hsa-miR-126-3p	26.95	25.87	0.01	0.04	2.99	2.99
B05	hsa-miR-130a-3p	23.88	23.74	0.11	0.18	1.56	1.56
B06	hsa-miR-133a-3p	32.91	33.14	0.00	0.00	1.21	1.21
B07	hsa-miR-133b	34.5	35	0.00	0.00	1.00	1.00
B08	hsa-miR-140-5p	24.23	25.19	0.09	0.06	0.73	-1.37
B09	hsa-miR-142-3p	32.17	32.96	0.00	0.00	0.82	-1.22
B10	hsa-miR-143-3p	21.27	22.34	0.69	0.47	0.67	-1.49
B11	hsa-miR-144-3p	35	35	0.00	0.00	1.42	1.42
B12	hsa-miR-145-5p	20.25	21.24	1.39	1.00	0.71	-1.40
C01	hsa-miR-146a-5p	23.38	23.59	0.16	0.20	1.23	1.23
C02	hsa-miR-149-5p	26.37	26.51	0.02	0.03	1.28	1.28
C03	hsa-miR-150-5p	32.88	32.8	0.00	0.00	1.50	1.50

C04	hsa-miR-155-5p	25.03	25.66	0.05	0.05	0.92	-1.09
C05	hsa-miR-15b-5p	21.86	22.32	0.46	0.47	1.03	1.03
C06	hsa-miR-16-5p	20.46	20.87	1.21	1.29	1.07	1.07
C07	hsa-miR-17-5p	23.08	24	0.20	0.15	0.75	-1.33
C08	hsa-miR-181a-5p	21.13	21.93	0.76	0.62	0.81	-1.23
C09	hsa-miR-181b-5p	21.12	21.94	0.76	0.61	0.80	-1.24
C10	hsa-miR-182-5p	34.31	32.61	0.00	0.00	4.62	4.62
C11	hsa-miR-183-5p	35	35	0.00	0.00	1.42	1.42
C12	hsa-miR-185-5p	24.1	25.1	0.10	0.07	0.71	-1.41
D01	hsa-miR-18b-5p	23.92	24.77	0.11	0.09	0.79	-1.27
D02	hsa-miR-195-5p	21.08	21.6	0.79	0.78	0.99	-1.01
D03	hsa-miR-199a-5p	21.86	21.91	0.46	0.63	1.36	1.36
D04	hsa-miR-206	27.01	27.95	0.01	0.01	0.74	-1.36
D05	hsa-miR-208a-3p	27.16	27.53	0.01	0.01	1.10	1.10
D06	hsa-miR-208b-3p	35	35	0.00	0.00	1.42	1.42
D07	hsa-miR-21-5p	16.38	17.11	20.43	17.50	0.86	-1.17
D08	hsa-miR-210-3p	24.92	24.34	0.06	0.12	2.12	2.12
D09	hsa-miR-214-3p	21.8	22.55	0.48	0.40	0.85	-1.18
D10	hsa-miR-22-3p	20.22	20.11	1.42	2.18	1.53	1.53
D11	hsa-miR-221-3p	19.42	19.3	2.49	3.82	1.53	1.53
D12	hsa-miR-222-3p	19.42	19.36	2.49	3.66	1.47	1.47
E01	hsa-miR-223-3p	33.78	35	0.00	0.00	0.61	-1.65
E02	hsa-miR-224-5p	23.65	23.44	0.13	0.22	1.64	1.64
E03	hsa-miR-23a-3p	17.34	18.03	10.51	9.24	0.88	-1.14
E04	hsa-miR-23b-3p	19.18	19.79	2.94	2.72	0.93	-1.08
E05	hsa-miR-24-3p	18.57	19	4.49	4.71	1.05	1.05
E06	hsa-miR-25-3p	23.42	23.98	0.16	0.15	0.96	-1.04
E07	hsa-miR-26a-5p	19.74	20.42	1.99	1.76	0.89	-1.13
E08	hsa-miR-26b-5p	20.91	21.6	0.88	0.78	0.88	-1.14
E09	hsa-miR-27a-3p	18.91	19.32	3.54	3.78	1.07	1.07
E10	hsa-miR-27b-3p	20.56	20.99	1.12	1.19	1.06	1.06
E11	hsa-miR-29a-3p	18.1	18.44	6.22	6.93	1.11	1.11

E12	hsa-miR-29b-3p	24.21	23.98	0.09	0.15	1.66	1.66
F01	hsa-miR-29c-3p	18.41	18.78	4.99	5.49	1.10	1.10
F02	hsa-miR-302a-3p	28.71	28.39	0.00	0.01	1.78	1.78
F03	hsa-miR-302b-3p	28.35	28.18	0.01	0.01	1.59	1.59
F04	hsa-miR-30a-5p	21.48	21.8	0.59	0.68	1.14	1.14
F05	hsa-miR-30c-5p	21.9	22.35	0.45	0.46	1.04	1.04
F06	hsa-miR-30d-5p	22.82	23.24	0.24	0.25	1.06	1.06
F07	hsa-miR-30e-5p	21.74	22.12	0.50	0.54	1.09	1.09
F08	hsa-miR-31-5p	18.46	18.78	4.84	5.47	1.13	1.13
F09	hsa-miR-320a	20.86	21.48	0.92	0.84	0.92	-1.09
F10	hsa-miR-328-3p	26.51	26.26	0.02	0.03	1.69	1.69
F11	hsa-miR-342-3p	24.49	24.97	0.07	0.07	1.01	1.01
F12	hsa-miR-365b-3p	20.99	21.39	0.83	0.90	1.07	1.07
G01	hsa-miR-378a-3p	27.63	27.71	0.01	0.01	1.34	1.34
G02	hsa-miR-423-3p	23.08	23.43	0.20	0.22	1.11	1.11
G03	hsa-miR-424-5p	24.12	24.47	0.10	0.11	1.12	1.12
G04	hsa-miR-451a	31.04	32.44	0.00	0.00	0.54	-1.85
G05	hsa-miR-486-5p	28.39	29.03	0.00	0.00	0.91	-1.10
G06	hsa-miR-494-3p	24.86	24.37	0.06	0.11	1.99	1.99
G07	hsa-miR-499a-5p	33.56	34.01	0.00	0.00	1.04	1.04
G08	hsa-miR-7-5p	25.49	25.95	0.04	0.04	1.03	1.03
G09	hsa-miR-92a-3p	21.41	21.95	0.63	0.61	0.98	-1.03
G10	hsa-miR-93-5p	23.18	23.85	0.18	0.16	0.89	-1.12
G11	hsa-miR-98-5p	24.31	24.81	0.08	0.08	1.00	-1.00
G12	hsa-miR-99a-5p	23.94	23.85	0.11	0.16	1.51	1.51
H01	cel-miR-39-3p	35	34.94	0.00	0.00	1.48	1.48
H02	cel-miR-39-3p	35	33.66	0.00	0.00	3.59	3.59
H03	SNORD61	22.1	23.2	0.39	0.26	0.66	-1.52
H04	SNORD68	19.04	19.86	3.23	2.60	0.81	-1.24
H05	SNORD72	26.39	26.35	0.02	0.03	1.46	1.46
H06	SNORD95	19.54	20.22	2.28	2.02	0.88	-1.13
H07	SNORD96A	20.61	21	1.09	1.18	1.08	1.08

H08	RNU6-6P	18.08	18.75	6.27	5.60	0.89	-1.12
H09	miRTC	22.22	22.22	0.36	0.51	1.42	1.42
H10	miRTC	22.26	22.4	0.35	0.45	1.29	1.29
H11	PPC	19.31	19.41	2.67	3.54	1.32	1.32
H12	PPC	19.8	20	1.91	2.35	1.23	1.23

∆Ct : Ct(Gene Of Interest) – average Ct(HouseKeepingGene)

Fold change is the normalized mRNA expression in each T2DM group divided the normalized miRNA expression in the non-T2DM sample.

Fold regulation represents fold-changes results in a biologically meaningful way.

Fold changes values less than one indicate a down-regulation, and the fold-regulation is the negative inverse of the fold change. Fold change and fold-regulation values greater than 2 are indicated in red: fold changes values less than 0.5 and fold-regulation values less than -2 are indicated in blue.